WESTERN SYDNEY
UNIVERSITY

An investigation into the breakdown products of cuprizone and the inflammatory role of RAW 264.7 macrophages in an *in vitro* culture system

Melissa Catherine Zenkis

Supervisor: A/Prof David Anthony Mahns

Co-Supervisor: A/Prof Peter Shortland

Co-Supervisor: Dr Sabine Christine Ingrid Piller

Co-Supervisor: Dr David Grant Harman

A thesis presented to the Western Sydney University

in fulfilment of the requirements for the degree of

Master of Philosophy (Medicine)

Dedication

I dedicate this thesis to my beloved Grandpa, Kevin Seth Beauchamp.

Acknowledgements

"One of the greatest values of mentors is the ability to see ahead what others cannot see and to help them navigate a course to their destination" (John C Maxwell).

I extend my sincerest appreciation to the following individuals, which have all played an important part in the completion of this thesis. I wish to thank my primary supervisor Associate Professor David Anthony Mahns, for providing me with immense support during the entirety of my degree. Also, for kindly equipping me with the necessary resources and invaluable insights to be able to undertake the experiments.

I would also like to express my deepest gratitude to one of my co-supervisors, Dr Sabine Christine Ingrid Piller, for supporting me timelessly through my cell culture work, Western Blots and helping me with analysis and future experimental directions. Her mentorship throughout my degree has been an inspiration. Dr Piller has taught me to be critical, analytical, and conscientious towards my own work and fine details. She has also pushed me to always strive to find more efficient and appropriate research measures to produce credible and reliable research. Stating "for every question answered you will always have more questions", Dr Piller helped me realise the reality of science with the issue of not being able to solve all the questions. For all of this Dr Piller, I am grateful.

I would also like to give a special mention to my other co-supervisors' Associate Professor Peter Shortland and Dr David Grant Harman. Thank you Dr Harman, for assisting me with solubility of the drugs used in the experiments, as well as the overall assistance in the chemical aspect of my research. Associate Professor Peter Shortland, thank you for the critical feedback, constant thought-provoking questions, and knowledge, which helped direct my research.

On a personal level, I would not have been able to complete this Master's degree without the immense support from my Mum and Dad (Sharon and Peter), my siblings (Amanda and Michael) and my fiancé Andre. You have all helped motivate me and reinforced to me that you can do anything when you put your mind to it.

Statement of Authentication

The work presented in this thesis is, to the best of my knowledge and belief, original except as acknowledged in the text. I hereby declare that I have not submitted this material, either in full or in part, for a degree at this or any other institution.

Melissa Catherine Zenkis

Table of Contents

List of Tables

List of Figures and Illustrations

Abbreviation Pages

Abbreviation	Full Term
ABTS	2,2′-Azino-bis (3-ethylbenzthiazoline-6-sulfonic acid)
aDMA	Asymmetric Dimethylarginine
AdoHcy	S-adenosylhomocysteine
AdoMet	S-adenosylmethionine
ANOVA	Analysis of Variance
APCs	Antigen Presenting Cells
ASYM24	Anti-Dimethyl-Arginine Antibody, Asymmetric
ATP	Adenosine Triphosphate
BBB	Blood Brain Barrier
BCA	Bicinchoninic Acid
BMDM	Bone Marrow Derived Macrophage
BrdU	5-Bromo-2'-Deoxyuridine
BSA	Bovine Serum Albumin
C	Complement
CAPS	Cryopyrin-Associated Periodic Syndrome
CASPASE	Cysteine-Aspartic Protease
CASP1	Caspase 1
CNS	Central Nervous System
CDL	Cortical Demyelinating Lesion
CPZ	Cuprizone
CSF	Cerebrospinal Fluid
DNA	Deoxyribonucleic acid
DF	Dilution Factor
DMEM	Dulbecco's Modified Eagle's Medium
DTT	Dithiothreitol
EAE	Experimental Autoimmune Encephalomyelitis
EBV	Epstein Barr Virus
ELISA	Enzyme-Linked Immunosorbent Assay
ETC	Electron Transport Chain

ER	Endoplasmic Reticulum
ExAP	ExtrAvidin Alkaline Phosphatase
FCS	Fetal Calf Serum
FI	Fluorescence Intensity
g	Gravitational Force
GAPDH	Glyceraldehyde-3-Phosphate Dehydrogenase
GSDMD	Gasdermin D
GFP	Green Fluorescent Protein
HHV-6A	Human Herpes Virus 6A
HRP	Horseradish Peroxidase
HSP	Heat Shock Protein
ICE	IL-1β Converting Enzyme
IFN-γ	Interferon Gamma
IGF-1	Insulin-Like Growth Factor-1
IL	Interleukin
IRAK	Interleukin 1 Receptor Associated Kinase
kDa	Kilo Dalton
KO	Knockout
L	Litre
LBP	Lipopolysaccharide Binding Protein
LFA-1	Lymphocyte Function Associated Antigen 1
LPS	Lipopolysaccharide
mg	Milligram
mL	Millilitre
mM	Millimolar
MMA	Monomethylarginine
MNGC	Multinucleated Giant Cell
MRI	Magnetic Resonance Imaging
mRNA	Messenger Ribonucleic Acid
MS	Multiple Sclerosis
MTB	Mycobacterium Tuberculosis
MWT	Molecular Weight

MyD88	Myeloid Differentiation 88
n	Nano
NAT	N-acetyltransferase
NO	Nitric Oxide
NOS-2	Nitric Oxide Synthase 2
NLRP3	Nod-Like Receptor Protein 3
ng	Nanogram
nm	Nanometre
ODH	Oxalyldihydrazide
OPC	Oligodendrocyte Precursor Cell
OMV	Outer Membrane Vesicle
PBS	Phosphate Buffered Saline
PBMC	Peripheral Blood Mononuclear Cell
PCR	Polymerase Chain Reaction
pg	Picogram
PPMS	Primary Progressive Multiple Sclerosis
PreOLG	Oligodendrocyte Precursor
PRMS	Progressive Relapsing Multiple Sclerosis
PRMT	Protein Arginine Methyltransferase
PVDF	Polyvinylidene Difluoride
RRMS	Relapsing Remitting Multiple Sclerosis
sDMA	Symmetric Dimethylarginine
SDS	Sodium Dodecyl Sulfate
SPMS	Secondary Progressive Multiple Sclerosis
solTNF	Soluble Tumour Necrosis Factor
SVZ	Subventricular Zone
SYM10	Anti-Dimethyl-Arginine Antibody, Symmetric
TB	Tuberculosis
TIR	Toll-Interleukin-1-Receptor
TG2	Tissue Transglutaminase 2
TLR	Toll Like Receptor
TMB	Tetramethyl-benzidine

tmTNF	Transmembrane Tumour Necrosis Factor
TNF-α	Tumour Necrosis Factor Alpha
TRIF	Toll-Interleukin-1-Receptor Domain-Containing Adapter-Inducing IFN-β
U	Units
v	Volume
VCAM-1	Vascular Cell Adhesion Molecule 1
VLA-4	Very Late Activation Antigen 4
VZV	Varicella Zoster Virus
WB	Western Blot
µg	Microgram
µm	Micrometre
µM	Micro Molar
°C	Degrees Celcius

Abstract

The cuprizone mouse model is commonly used to study axonal demyelination/remyelination events that are associated with diseases such as multiple sclerosis (MS). The aetiology of MS remains unclear, but this inflammatory condition involves the crosstalk between neuronal and immune cells. Cuprizone (CPZ) is a reversible demyelinating, toxic, copper-chelating drug that inhibits cell growth and promotes oligodendrocyte death. RAW 264.7 macrophages are innate immune cells that were used in this thesis due to their role in demyelinating diseases.

In *vivo*, following oral ingestion, CPZ is hydrolysed by the acid in the stomach to form the breakdown products, cyclohexanone and oxalyldihydrazide. This thesis tested the hypothesis that one of the breakdown products of CPZ, oxalyldihydrazide, is responsible for the release of pro-inflammatory cytokines, altered morphology and viability of RAW 264.7 macrophages. This hypothesis was tested using enzyme-linked immunosorbent assays (ELISAs) for tumour necrosis factor alpha (TNF-α), interleukin 1 beta (IL-1β) and the viability of the cells through the Trypan blue assay. Furthermore, it was hypothesised that protein arginine methylation would change based on the activation status of the RAW 264.7 cells, which was tested using Western blotting.

Optimisation of the protocol of activating the RAW 264.7 macrophages was conducted, using different concentrations of cells and fetal calf serum (FCS) to be able to clearly observe the morphology of the cells under the light microscope. RAW 264.7 cells when activated for 6, 12, 18 and 24-hour time points showed drastic changes in the cellular morphology when activated with lipopolysaccharide (LPS) and interferon gamma (IFN-γ). Significant differences in the live and total cell numbers between the activated and non-activated RAW 264.7 macrophages were observed at the 24-hour time point.

RAW 264.7 macrophages exposed to increasing amounts of cyclohexanone and oxalyldihydrazide showed reduced cell numbers, compared to the controls. The cell numbers were drastically reduced when cells were treated with oxalyldihydrazide or cyclohexanone, when the RAW 264.7 macrophages were re-activated with LPS and IFN-γ during the drug treatment (after 12 hours activation). Increased IL-1β concentrations were produced by re-activated cells treated with higher concentrations of cyclohexanone/oxalyldihydrazide.

Cyclohexanone, compared to oxalyldihydrazide treated cells, produced larger quantities of TNF-α. The effect on cell numbers and the cytokine production of drug treated RAW 264.7 macrophages were a concentration and activation-dependent response.

RAW 264.7 macrophages exposed to cyclohexanone or oxalyldihydrazide had a swollen morphology. Interestingly, treatment of the cells with cyclohexanone and oxalyldihydrazide resulted in the formation of multinucleated cells in a dose-dependent manner. This observation to date has not been documented in CPZ treated cells or mice. Furthermore, morphological changes such as elongation and blebbing of the RAW 264.7 macrophages treated with cyclohexanone or oxalyldihydrazide were observed. Further analysis is required to identify the mechanism(s) responsible for these changes.

Due to the role of protein arginine methyltransferases in inflammation and demyelination being unresolved, Western blots were performed on the total cell lysates of the RAW 264.7 cells, which demonstrated the asymmetrical and symmetrical di-methylation of cellular proteins in resting non-activated and activated RAW 264.7 cells. Protein bands indicative of increased protein arginine methylation were observed in activated macrophages.

This thesis is important due to the lack of research investigating the roles of the specific breakdown products of CPZ and their effects on cellular viability, morphology, and cytokine production in RAW 264.7 macrophages. This thesis provides methodological considerations that should be acknowledged when optimising protocols in all aspects of cell culture work, when working with immune cells. Pyroptosis was identified as a potential explanation of the collective data obtained in this thesis including the morphological changes and cytokine production in the RAW 264.7 macrophages. This cellular death pathway could be attributed to the apparent toxic nature of CPZ and an overreactive immune system in some disease states. Further cellular work and animal studies are required to discern the effect of the breakdown products of CPZ, which should be compared to human glial cells from MS patients. Such comparative studies will assist in understanding the pathological events associated with demyelination, which could identify more therapeutic targets for numerous demyelinating diseases.

1.0 Introduction

Advancements in scientific research have allowed the scientific field to discover numerous previously unknown facets of a plethora of diseases. It is in this section of this thesis that the CPZ demyelination/remyelination model will be introduced, focusing on the hypothesised mechanisms and comparison to an alternate model that is used within a laboratory environment for demyelinating diseases. Specifically, MS will be addressed, as the CPZ model is commonly used for this demyelinating disease. Comparisons between macrophages and microglia will be discussed and their immunological roles including their activation and associated cytokine release. Protein arginine methylation as an important post-translational modification will be explored due to the recent spark of research interest in numerous diseases and immunological responses.

1.1 *Cuprizone*

CPZ is a copper-chelating agent that ultimately leads to demyelination in specific areas within the brain, including the corpus callosum (Zhen et al. 2017). The CPZ model has been widely regarded as a white matter demyelination model. However, Goldberg et al. (2015) observed almost complete demyelination in C57BL/6J mice treated with CPZ in grey matter regions of the brain including the cortex, the lateral aspect of the caudoputamen and the substantia innominate. CPZ is used to study demyelination and remyelination, which is symptomatic in numerous neuroinflammatory diseases (Torkildsen et al. 2008). Carlton (1966) was the first to discover the detrimental effects of CPZ on mice. His experiments showed that feeding of 0.5% CPZ was extremely toxic, leading to the development of microscopic lesions, demyelination, weakness, oedema and inhibitory effects on growth (Carlton 1966). Mice that are treated with CPZ show changes in behaviour, impaired motor skills and mood (Vega-Riquer et al. 2019). Young mice fed with CPZ display oligodendrocyte death and subsequent demyelination. However, four days after withdrawal from CPZ, remyelination is evident (Torkildsen et al. 2008).

Lucchinetti et al. (2000) described CPZ-induced lesions in mice, to have a similar pathological pattern to type 3 and 4 lesions in MS patients. Lucchinetti et al. (2000) characterised 4 different

patterns of demyelination within MS patients. Patterns I and II show extensive T-lymphocyte and macrophage inflammation, with immunoglobin G only residing in type II lesions. Patterns III and IV resembled virus or toxin induced demyelination rather than autoimmunity. Both Type III and IV patterns have T lymphocyte and macrophage infiltrates, with the complete absence of complement and immunoglobins. Type III have extensive oligodendrocyte loss at the active plaque border and pattern IV is defined by substantial oligodendrocyte death (Lucchinetti et al. 2000).

The chemical structure of CPZ is shown in Figure 1. CPZ is a condensation product of oxalyldihydrazide and cyclohexanone. CPZ has a molecular weight (MWT) of 278.45008g/mol and has a molecular formula of $C_{14}H_{22}N_4O_2$ (Vega-Riquer et al. 2019). CPZ has been widely used as an oral agent that induces central demyelination in rodents (Sen et al. 2019). This toxin-based model is necessitated in a laboratory environment to produce neuroinflammation within rodents that has numerous pathological features similar to human MS (Toomey et al. 2021). Research on the breakdown and synthesis of CPZ is immature, as well as the action of CPZ on isolated/cultured cells. Given that orally administered CPZ must traverse the acidic environment of the stomach before being absorbed, this raises the possibility that it may well be hydrolysis products of CPZ rather than CPZ itself inducing the associated demyelination.

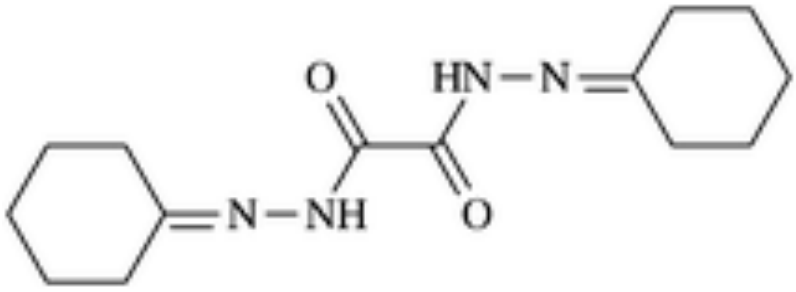

Figure 1: Chemical structure of CPZ (Muniz-Miranda et al. 2008).

1.1.1 Mechanism of Action of CPZ

The mechanism to which CPZ induces demyelination has not been delineated. One mechanism that has been postulated to cause demyelination from CPZ is through the interruption of the cell cycle. The cell cycle is divided into five distinct phases: G0 (resting phase), G1 (preparatory phase), S (DNA replication), G2 (gap phase), and M (cell division phase) (Mi et al. 2016). Within the brain, oligodendrocyte derive from local oligodendrocyte precursor cells (OPCs) in the brain parenchyma as well as the cell precursors in the subventricular zone (SVZ) (Gonzalez-Perez & Alvarez-Buylla 2010). The SVZ is where multipotential cells proliferate into neurons and glial cells (Gonzalez-Perez & Alvarez-Buylla 2010). Mi et al. (2016) using double labelling of 5-Bromo-2'-deoxyuridine (BrdU) and Ki-67 which is a marker of proliferation, found a decrease in the $BrdU^{+}/Ki67^{-}$ cells in the anterior SVZ, pertaining to the CPZ treatment inhibiting the potential precursor cells from exiting the cell cycle. The inhibition of OPCs from exiting the cell cycle hinders them from differentiating and maturing into post-mitotic, mature oligodendrocyte. OPCs left in a non-proliferative state leads to apoptosis and hence halts the myelination process (Mi et al. 2016).

Although the exact mechanism of action of CPZ is not fully understood, based on the copper-chelating properties of CPZ, it is postulated that the pathogenesis of CPZ is due to the inhibition of mitochondrial enzymes dependent on copper, specifically cytochrome oxidase and monoamine oxidase (Venturini 1973). Varhaug et al. (2020) found mitochondrial dysfunction may extend to the neurons, as mice exposed to CPZ had decreased levels of cytochrome oxidase in Purkinje neurons. This study demonstrated that CPZ impacts oligodendrocytes, other glial cells and neurons resulting in demyelination and cytotoxicity.

1.1.2 **Breakdown Products of CPZ**

Metabolised at a low pH, CPZ is hydrolysed into two breakdown products, namely cyclohexanone and oxalyldihydrazide. Cyclohexanone is a 6-carbon ring with a chemical formula of $C_6H_{10}O$, has a MWT of 98.16g/mol, and has an aromatic smell resembling acetone. It has a boiling temperature of 155.65°C and a freezing temperature of -32.1°C. It is a colourless to yellow viscous liquid (Wypych 2008). The chemical structure of cyclohexanone is shown in Figure 2. Oxalyldihydrazide is a pale yellow to white solid that has a molecular formula of $C_2H_6O_2$. Oxalyldihydrazide has a melting point of 242-244°C. The chemical structure is shown in Figure 3. Oxalyldihydrazide has a MWT of 118.09g/mol (Dhananjaya et al. 2012).

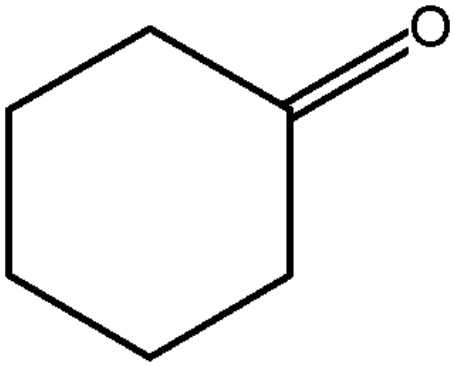

Figure 2: Chemical structure of cyclohexanone (Wypych 2008).

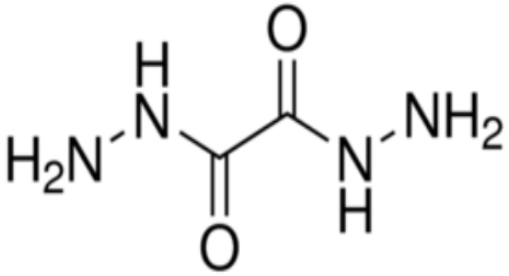

Figure 3: Chemical structure of oxalyldihydrazide (Merck 2021).

1.1.3 Comparison of the CPZ Model with the EAE Model

The CPZ and experimental autoimmune encephalomyelitis (EAE) models of demyelination/remyelination have been created largely on the basis of the two competing theories of MS; the 'outside-in' and 'inside-out' theories (Sen et al. 2019). The inside-out model explores the notion that axonal degeneration in the CNS results in the activation of the systemic/adaptive immune cells. Comparatively, the outside-in model refers to the induction of an anti-myelin autoimmune response created by the peripheral immune system, with T cells being the major driver of this response (Sato et al. 2015).

EAE favours the outside-in model, as mice are exposed to a myelin antigen either actively or passively (Sato et al. 2015). The EAE model encompasses both the immunopathological and neuropathological aspects of MS including demyelination, inflammation and gliosis (Constantinescu et al. 2011). In the active EAE model, mice are immunised subcutaneously with myelin antigen containing Freund's adjuvant and inactivated *mycobacterium tuberculosis*. The EAE induction is further induced through the intravenous injection of pertussis toxin by breaching the blood brain barrier (BBB)(Goverman & Stromnes 2006). The passive EAE model, EAE is induced by adoptive transfer of T cells isolated from active EAE mice that have been sensitised with myelin antigens (Stromnes & Goverman 2006). Mannara et al. (2012) found that passive/adoptive transfer of EAE in C57/BL6 mice showed symptoms on day 10, with 100% of incidence reached at day 14. Whereas active EAE symptoms appeared on day 10, with 100% incidence reached by day 15. After the aforementioned periods for passive and active induction of EAE, mice develop motor deficits and associated symptoms. Kalyvas and David (2004) used a 0-5 scoring method of EAE with 0- showing no disease, 1-tone decrease in the tail, 2- mild hindlimb weakness, 3- severe hindlimb weakness, 4- hindlimb paralysis and 5- hindlimb and forelimb paralysis or death. However, this scale of EAE is not universal.

Comparatively, CPZ is a model of toxic demyelination that focuses on the apoptosis of the innate (microglia and astrocytes) and adaptive (T and B cell mediated responses) oligodendrocytes immune system which subsequently causes demyelination. This inside-out model shows patterns of demyelination and spontaneous remyelination; however during CPZ treatment no paralysis occurs (Martinez & Peplow 2020; Skripuletz et al. 2008). The EAE and CPZ models are both rodent models assist in the testing of different molecular aspects that may contribute to MS in humans. Both these models only capture a small aspect of the processes

associated with MS, as both models have their limitations in modelling human MS (Martinez & Peplow 2020; Skripuletz et al. 2008).

1.2 *Myelination and Demyelination*

1.2.1 **Myelination**

Myelin is formed by two different subsets of glial cells: known as oligodendrocytes in the CNS and Schwann cells in the peripheral nervous system (Coggan et al. 2015). Myelination is a process required for the optimal development and functioning of the CNS. It involves the process of protein and lipid assembly into the oligodendrocytes membrane which surrounds and insulates axons (Podbielska et al. 2013). Oligodendrocytes contain a large number of mitochondria to ensure a reliance of high efficiency glycolytic processes that maximise adenosine triphosphate (ATP) products (Meyer & Rinholm 2021). Oligodendrocytes consume glucose and lactate to be able to support the intense energy-consuming process of myelination. It is approximated that $3.3x10^{23}$ ATP molecules are required for the synthesis of just one gram of myelin from oligodendrocytes (Rosko et al. 2019). Myelin sheaths act as an electrical insulation that improves the conduction velocity of action potentials (Coggan et al. 2015). The myelin sheath allows for the process of saltatory conduction of action potentials at the Nodes of Ranvier, regions of localised high densities of sodium ion (Na^+) channels (Traka et al. 2015). Saltatory conduction allows for quicker and more reliable propagation of signals in comparison to unmyelinated axons of the same cross-sectional size (Stiefel, Torben-Nielsen & Coggan 2013; Traka et al. 2015).

1.2.2 **Demyelination**

Myelin is prone to metabolic and autoimmune damage (Matsushima & Morell 2001). This damage to the myelin sheath can have a domino effect on the whole body (Stiefel, Torben-Nielsen & Coggan 2013). Demyelination occurs when there is myelin loss, although there is relative preservation of axons (Love 2006). Demyelination occurs when diseases cause the destruction of the myelin sheath or destruction of oligodendrocytes (Love 2006). Demyelination is a process that is a pathological hallmark in numerous CNS diseases including inflammatory demyelinating diseases such as MS, acute-disseminated encephalomyelitis, acute haemorrhagic leucoencephalitis, acquired metabolic demyelination, central pontine myelinolysis and extrapontine myelinolysis (Kamil et al. 2019; Love 2006). All of these

diseases create a significant burden on the global economy, with the prognosis being poor for the patients affected by the majority of these diseases (Kamil et al. 2019).

1.2.3 Multiple Sclerosis

MS is a neurological, inflammatory disease of the CNS (Ghasemi, Razavi & Nikzad 2017). This debilitating disease affects both physical and cognitive abilities (Ghasemi, Razavi & Nikzad 2017). MS is a neurodegenerative disease classified as an autoimmune disease, where the immune system attacks the myelin sheath (Steinman 2014). Myelin destruction and damage results in axonal damage which may cause focal sensory loss, paraesthesia, muscular weakness and sometimes even paralysis (Love 2006; Steinman 2014). The aetiology of MS remains poorly understood. The diagnosis of MS is based on medical history and neurological assessment utilising MRI, lumbar puncture, CSF and blood analysis (Ghasemi, Razavi & Nikzad 2017).

1.2.3.1 Epidemiology and Symptoms

MS is the most common demyelinating CNS disease, with the mean onset occurring around 30 years of age (Rejdak, Jackson & Giovannoni 2010). In 2013, approximately 2.3 million individuals were affected by MS worldwide, with the incidence of MS in females being higher than in males (Koriem 2016). It was originally hypothesised that MS was confined to white matter; however, lesions have been found in the grey matter of the cortex and in deep grey matter structures (van Munster et al. 2015). MS has extensive heterogeneity in terms of the symptoms experienced by patients including weakened reflexes, muscle spasms, un-coordination, bowel or bladder dysfunction, unilateral vision loss and ataxia due to cerebellar lesions (Brownlee et al. 2017; Koriem 2016; Loma & Heyman 2011).

1.2.3.2 Forms of MS

MS can be classified into four different forms: relapsing remitting MS (RRMS), secondary progressive MS (SPMS), primary progressive MS (PPMS) and progressive relapsing MS (PRMS) (Loma & Heyman 2011). RRMS is the most common form of MS, which accounts for 85-90% of cases (Brownlee et al. 2017). This form of MS is characteristic of periods of neurological decline for at least 24 hours, followed by remission (Brownlee et al. 2017; Loma & Heyman 2011). After 10 to 15 years, the disease can progress to SPMS from RRMS (Lassmann & Bradl 2017). PPMS is observed in 10-15% of patients and is seen in elderly

patients more often than RRMS (Lassmann & Bradl 2017). PPMS is distinguishable by a marked progressive decline in neurological function over time and is found to be more resistant to pharmacological treatments used for other sub forms of MS (Brownlee et al. 2017; Goldenberg 2012). PRMS is a rare form of MS, where symptoms worsen overtime, characterised by no periods of remission (Goldenberg 2012).

1.2.3.3 Hypotheses Underlying the Pathology of MS

The aetiology of this neurological inflammatory disease remains uncertain. It has been postulated to be a multifactorial disease that involves genetics, vitamin deficiencies and infectious agents (Ghasemi, Razavi & Nikzad 2017). Vitamin D deficiency is a major research area with increasing evidence to suggest it as a causative factor of MS, due to its anti-inflammatory effects on the innate and adaptive immune system (Miclea et al. 2020). Ramagopalan et al. (2009) identified an MHC vitamin D response element in the HLA-DRB1 promoter region, providing a plausible link between MS susceptibility genes and vitamin D in MS. B cells transfected with *HLA-DRB1*15* gene promoter demonstrated a higher expression when stimulated with 1-, 25 dihydroxvitamin D3, which was not found when there was the deletion of the VDRE. Infections that have been associated with the MS include *Chlamydia pneumoniae*, *Helicobacter pylori*, and *Staphylococcus aureus* (Marrodan et al. 2019). Ivanova et al. (2015) revealed a higher presence of intrathecal antibodies of *Chlamydia pneumoniae* in the CSF of MS patients compared to the controls. However, due to the heterogenous nature of MS, it is not surprising that no consensus has currently been reached regarding the pathogenesis and primary progression of the disease (Meca-Lallana et al. 2021).

There are numerous hypotheses underlying the cause(s) of MS including immune-mediated and viral hypotheses (Fierz 2017; Prat & Antel 2005). The viral interaction hypothesis insinuates the infection of Human Herpes Virus 6A (HHV-6A) and Epstein Barr Virus (EBV) as the underlying pathological basis for the development of lesions in MS patients (Fierz 2017). The premise behind the viral hypothesis is the B-cell transformation into intrathecal B cells in the brain (Fierz 2017). Bjornevik et al. (2022) demonstrated the high prevalence of MS associated with EBV using longitudinal analysis. There was a 32-fold risk of developing MS after an infection with EBV. In addition to this, the Varicella Zoster Virus (VZV) has been postulated to play a role in the development of MS. It is thought to be a host-viral immune interaction. Sotelo and Corona (2011) conducted a study on peripheral blood mononuclear cells

(PBMC) of MS patients, which supports the viral interaction hypothesis. The study shows 82% of the MS patients that had their blood taken within the first week of acute relapse were positive for VZV Deoxyribonucleic acid (DNA), in contrast to the healthy controls and patients in remission, whom all came back negative (Sotelo & Corona 2011). Another study conducted by Sotelo, Ordoñez and Pineda (2007) showed the presence of VZV DNA in the PBMCs of 95% of patients with relapsing MS, 17% of MS patients in remission and all the controls were negative. Interestingly, using real time polymerase chain reaction (PCR) the high levels of VZV DNA in the first week of relapse had gradually reduced until disappearing after a two-month period. This has been postulated to cause the etiopathogenesis of MS due to the DNA found at the beginning of the active infection and not during remission in RRMS (Sotelo & Corona 2011).

The immune-mediated disease hypothesis perceives an auto-reactive immune system as the causative agent of pathological hallmarks of MS. This subsequently results in an inflammatory cascade that causes detrimental injury to previously healthy myelin and axons (Prat & Antel 2005). This mechanism of immune-mediated disease could pertain to the immune system destroying the myelin sheath, or the failure of the oligodendrocytes to produce new myelin (Koriem 2016). The adaptive immune system, especially lymphocytes, have been extensively recognised to play a role in the pathogenesis of MS (Manoj & Yong 2016). However, research of innate myeloid antigen presenting cells (APCs), including monocytes, macrophages, dendritic cells and microglia as a pathological hallmark of MS has not been so extensively researched (Manoj & Yong 2016).

1.3 *Macrophages and Microglia*

1.3.1 **Background on Macrophages**

Peripheral macrophages have an integral role in the restoration of homeostasis after an inflammatory event has occurred (Rahat, Ebitterman & Elahat 2011). Macrophages are innate immune cells that are present in every tissue in the human body (Watanabe et al. 2019). They play numerous immunological roles including phagocytosing bacteria, secreting pro-inflammatory cytokines and eliminating damaged cells through programmed cell death (Hirayama, Iida & Nakase 2017). Macrophages have a plethora of roles in the human body, from development, repair, and homeostasis. Resident macrophages also play a role as sentinels during tissue homeostasis where they adapt to different tissue physiological states and pathological insults (Wynn, Chawla & Pollard 2013). Macrophage's reparative function and ability to maintain homeostasis is imperative, as diseases such as fibrosis, obesity, and cancer emerge when deregulation of macrophages occur (Wynn, Chawla & Pollard 2013). Subsequently, this has led to the emergence of macrophages becoming prominent pharmacological therapeutic targets (Merly & Smith 2017).

Progenitor cells reside in the adult bone marrow that develop into monocytes through the process of three distinct divisions into monoblasts, promonocytes and monocytes (Duque & Descoteaux 2014; Gordon & Taylor 2005). Monocytes reside in the bone marrow for approximately 24 hours and contribute to 1-6% of the total circulating peripheral leukocyte population in a healthy adult (Duque & Descoteaux 2014; Gordon & Taylor 2005). After 24 hours in the bone marrow, blood monocytes are subsequently released into the bloodstream and are further differentiated into macrophages when they permeate tissue capillary walls, where they are recruited to damaged tissue (Sieweke & Allen 2013; Zhang, Goncalves & Mosser 2008). Differentiation into macrophages is determined by the pathogen associated pattern recognition receptors (Geissmann et al. 2010). When monocytes are differentiated into macrophages morphological changes that occur include a five to ten fold increase in cell size, an increase in phagocytic capacity and organelle complexity (Duque & Descoteaux 2014; Sieweke & Allen 2013).

Macrophages can be classified as either M1 'classically activated' (inflammatory) macrophages which release pro-inflammatory cytokines, or M2 'alternatively activated' (anti-inflammatory) macrophages which release molecules such as IL-4, IL-10 and IL-13 (David &

Kroner 2011). There are numerous ways to distinguish M1 versus M2 macrophages, including the cytokines release and surface markers. M1 macrophages are associated with the secretion of pro-inflammatory cytokines IL-1β and TNF-α. M1 cells also expresses CD86 and CD16/32 surface markers whereas M2 are identified via the expression of mannose receptor (CD206) and enzyme arginase 1 (Arg1) (Rawji & Yong 2013). However, over numerous years the M1/M2 polarisation paradigm has been criticised for the oversimplification of the macrophages function, as more research suggests that the M1/M2 classification is extremes of a continuum of macrophage polarisation (Nahrendorf & Swirski 2016; Palma et al. 2018). This is a research field that has been studied in cancer research, where there has been evidence of a phenotypic switch that occurs in M1 macrophages to a M2 phenotype when there is interaction with tumour cells, causing immunosuppressive effects. M1 can switch to M2 and *vice versa* based on environmental changes, infection and inflammation (Boutilier & Elsawa 2021).

1.3.2 **Background on Microglia**

Microglia are the true CNS parenchymal macrophages, constituting 10% of the cells that reside within the CNS (Aguzzi, Barres & Bennett 2013). Like macrophages, microglia are activated via pathological stimuli and have a prominent immune role and function in the maintenance of homeostasis (Casano & Peri 2015). This is maintained through phagocytosis in response to pathogenic sources, as well as the mediation of the neuroinflammatory response through the release of pro-inflammatory cytokines including: IFN-γ, IL-1β and IL-6 (Shigemoto-Mogami et al. 2014). Microglial immunological functions are integral as the release of microglial associated pro-inflammatory cytokines is required for the enhancement of oligodendrogenesis and neurogenesis (Shigemoto-Mogami et al. 2014).

The current hypothesis of how microglia arise is through primitive haematopoiesis in the yolk sac of an embryo. From the yolk sac, the primitive macrophages travel to the developing neural tube, which gives rise to microglia (Alliot, Godin & Pessac 1999). Alternatively, Ginhoux et al. (2010) observed using fate mapping analysis that adult microglia in mice emanate from primitive myeloid progenitors that emerge before embryonic day 8. Ameboid-shaped microglia play an integral role in phagocytosis during the embryonic period and the population becomes reduced after postnatal stages (Nakajima & Kohsaka 2001). Their morphology reverts to a ramified ‘resting microglia’, which comprises of a small cell body and processes that branch out (Aguzzi, Barres & Bennett 2013; Nakajima & Kohsaka 2001). Even during this resting

state, the microglia contain highly motile processes which constantly scan and monitor the microenvironment of the CNS and respond to injury appropriately (Casano & Peri 2015; Nimmerjahn, Kirchhoff & Helmchen 2005). In the event of injury/disease, microglia transform into an 'activated' ameboid shape, where the size of the cell body increases and the branched processes retract (Nakajima & Kohsaka 2001).

1.3.3 **Role of Macrophages/Microglia in CNS Dysfunction**

Macrophages are suggested to have a dual role in MS by contributing to the formation of lesions and damage to axons, but also by assisting in repair (Vogel et al. 2013). Dysfunction of the CNS has been associated with inflammatory mediators, but the exact role of how macrophages cause axonal loss remains largely unknown (Hendriks et al. 2005). Microglia are thought to initiate the onset of EAE, whereas the influx of monocytes and macrophages of a peripheral origin have a role in the progression of the disease (Nally, Santi & Mccoy 2019). The neurodegenerative pathway associated with the activation of macrophages is illustrated in Figure 4. It is hypothesised that the balance between M1 and M2 phenotypes of macrophages/microglia has an important role in MS, as M1 are activated early in MS and M2 have a role in tissue repair and the resolution of inflammation (Chu et al. 2018).

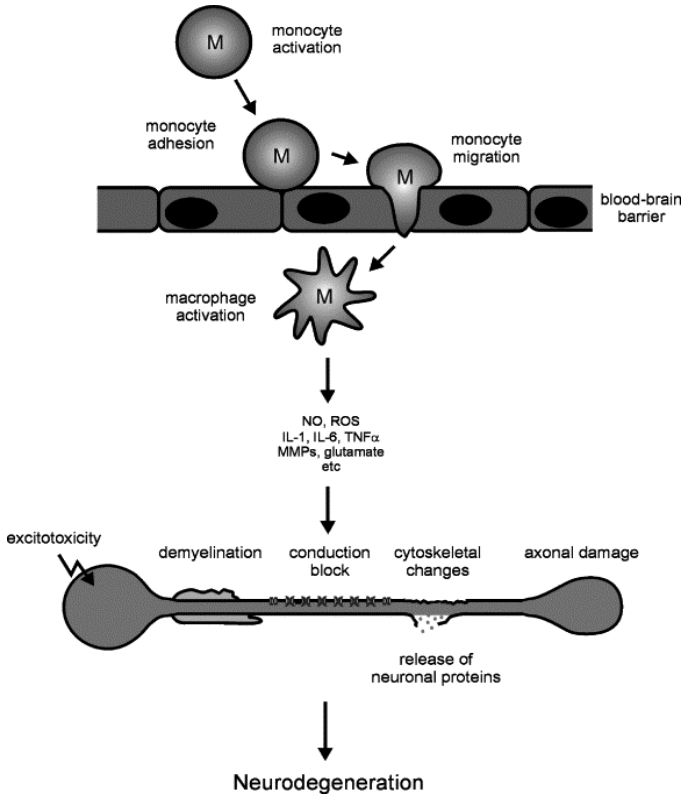

Figure 4: Schematic drawing of macrophage contribution to the progression of MS (Hendriks et al. 2005).

Activated macrophages are usually viewed as detrimental in MS patients. Macrophages contribute to approximately 50% of the infiltrating cells in the CNS of animals in the EAE model (Huitinga et al. 1990). This alludes to macrophages being one of the driving forces in the pathogenesis of EAE and potentially MS. Microglia have also been found to play a role in MS; however, whether they are neuroprotective or neurotoxic, or both, is still unclear (Wang et al. 2019). Microglial activation is found in the earliest stage of lesion formation. Microglial nodules, which are found in normal-appearing white matter, are characterised by having no leukocyte infiltration and demyelination. These microglial nodules may eventuate into active and cortical demyelinating lesions (CDL) (Singh et al. 2013).

The antigen presenting roles microglia and macrophages play an imperative role in maintaining the innate immunity (Gaudino & Kumar 2019). There is inevitable cross talk between microglia and macrophages, and their activation that causes the release of cytokines and growth factors (Chastain et al. 2011). The inflammatory cascade formed by macrophages/microglia may play a role in demyelination and exacerbate the cytotoxic nature of CPZ. Macrophages and microglia share numerous surface markers and functions (Shen et al. 2018). However, microglia and bone marrow derived macrophages (BMDM) are classified as two distinct myeloid populations (Aguzzi, Barres & Bennett 2013). Both microglia and macrophages play a pertinent role in the defence against pathogens in the CNS; however, under certain conditions the CNS inflammation can persist and subsequently lead to the development of autoimmunity (Chastain et al. 2011). This can cause damage to oligodendrocytes and myelin leading to the development of demyelinating diseases including MS (Chastain et al. 2011).

1.4 *RAW 264.7 Cells (Macrophages)*

RAW 264.7 macrophages are a cell line transformed by the Abelson leukemia virus, which originates from BALB/c mice, catalog number TIB- 71™ (ATCC 2022). RAW 264.7 macrophages are an effective cell line for modelling macrophages (Taciak et al. 2018). This cell line is increasingly used as a macrophage/monocyte model within laboratories to predict *in vivo* effects of numerous drug treatments. Experimentation on RAW 264.7 cells closely resembles the *de novo* response in humans, making them a suitable cell line for bio-medical research (Merly & Smith 2017).

The BBB acts as a preventative barrier that restricts the entry of blood borne immune cells into the CNS of healthy individuals. However, in CNS demyelinating diseases, such as MS, the compromise in BBB leads to leukocyte infiltration (McMahon, Suzuki & Matsushima 2002). However, the BBB is not disrupted using CPZ even though there is an immense inflammatory response (McMahon, Suzuki & Matsushima 2002). Studies have shown that the lack of T-cell recruitment in the CNS with CPZ treatment is thought to be associated with the atrophy of the thymus which matures and differentiates T-cells (Almuslehi et al. 2020; Sen et al. 2019).

McMahon, Suzuki and Matsushima (2002) used both flow cytometry and green fluorescent protein (GFP) positive bone marrow transplanted mice, to illustrate that peripheral macrophages migrate to the brain when treated with CPZ, despite the presence of an intact BBB. Interestingly, the population of resident microglia outnumbered the peripheral macrophages, suggesting a potential role in demyelination or remyelination. Peripheral macrophages were found to specifically accumulate in the corpus callosum, fornix and basal ganglia. Based on a staining myelin basic protein (MBP) (a marker for demyelination) the GFP^+ cells were present in all areas of the demyelination (McMahon, Suzuki & Matsushima 2002).

There are numerous difficulties in mouse models including identifying resident microglia and differentiating them from macrophages based on the similarities in morphology and shared surface markers (Shen et al. 2018; Tanaka 2020). Hence, in this thesis the RAW 264.7 macrophage cell line was used to test the action of CPZ breakdown products on the macrophage/microglia for the first time. Using this cell line has the advantage of studying the

effects of the breakdown products in a well characterised and well-studied cell line to identify and better understand the molecular pathways resulting from the breakdown products of CPZ.

1.5 *Activation of RAW 264.7 Cells with LPS and IFN-γ*

LPS, also known as endotoxin, is a molecule found on the outer membrane of gram-negative bacteria (Meng & Lowell 1997). It has been widely demonstrated *in vitro* to activate macrophages (Meng & Lowell 1997). There are two associated stages/signals for the classical activation of murine macrophages. The first signal is the priming step, this is achieved by IFN-γ, and the second stimulation step occurs with a toll like receptor (TLR) such as LPS (Mosser & Zhang 2008).

LPS consists of an O-specific polysaccharide, a non-repeating core oligosaccharide and a hydrophobic moiety also known as lipid A (Raetz & Whitfield 2002). LPS is secreted from the bacterial membrane in the form of outer membrane vesicles (OMVs) (Ryu et al. 2017). The activation of macrophages by LPS is summarised in Figure 5. Initially LPS binds to the LPS binding protein (LBP), a 60 kilo dalton (kDa) glycoprotein, has a high affinity with LPS, which facilitates the transfer of the complex to the CD14 cell surface receptor (Hailman et al. 1994). LPS subsequently binds to CD14, which is a pathogen recognition receptor that is a 55kDa glycoprotein anchored to the plasma membrane via a phosphatidylinositol linkage (Hamann et al. 2002; Kielian & Blecha 1995; Wright et al. 1990). The binding site of CD14 attaches to LPS located at the N-terminal hydrophobic pocket of CD14 monomers (Płóciennikowska et al. 2015). CD14 consequently delivers LPS to the TLR4-MD2 complex; simultaneously CD14 also has a role in increasing the sensitivity detection of LPS (Hailman et al. 1994) .

TLR4 is a very particular type of TLR, as it neccessitates an accessory protein, MD2, to capture its ligand. MD2 is also used by LPS to bury its hydrophobic component (Hailman et al. 1994). The attachment of TLR4 to MD2 forms dimers of the TLR4-MD2 complex. The dimerisation of TLR4 assists in the formation of two adaptor protein complexes: Toll interleukin 1 receptor (TIR) domain containing adaptor protein (TIRAP)/ myeloid differentiation 88 (MyD88) and Toll-IL-1R domain containing adaptor inducing IFN-β-related adaptor molecule (TRAM)/TIR domain-containing adaptor inducing IFN-β (TRIF) to the TIR domain. TRIF has the role of inducing the activation of IFN regulatory factor 3 transcription factors, which activate IFNs as shown in Figure 5 (Płóciennikowska et al. 2015). MyD88 has the role of activativing

Interleukin 1 receptor associated kinase (IRAK) 4 and IRAK-2 to form a myddosome (Płóciennikowska et al. 2015). The formation of this unique complex subsequently triggers the early activation of the NFκB and MAP kinases, as well as the secretion of a plethora of cytokines including TNF-α, IL-1β, and IL-6 (Hamann et al. 2002; Kagan & Medzhitov 2006; Płóciennikowska et al. 2015).

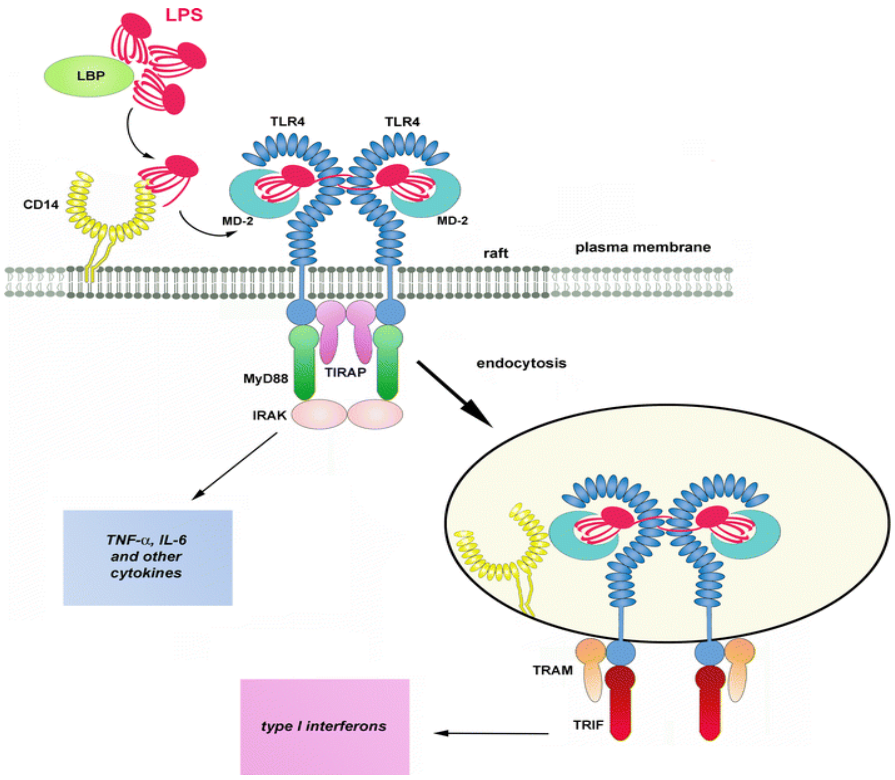

Figure 5: Macrophage activation through LPS via TLR4.

LBP promotes LPS monomers to CD14, this process transfers LPS to the TLR4/MD2 complex. Formation of the dimerised complex produces a multimolecular complex in a myddosome at the TIR domain of TL4, formed by TIRAP, MyD88, and IRAK kinases. This complex formation leads to production of pro-inflammatory cytokines, including TNF-α and IL-6. TRAM and TRIF adaptors are recruited to TLR4 following endocytosis, to initiate a signalling pathway that has a role in controlling the production of type 1 interferons (Płóciennikowska et al. 2015).

Wright et al. (1990) demonstrated the functional receptor importance of CD14 for the production of cytokines by culturing human blood for 16 hours with LPS. The cultured human blood produced TNF-α. When the culture was pre-treated with a CD14 monoclonal antibody blocking agent, this almost completely inhibited the synthesis and release of TNF-α. Interestingly, macrophages treated with phosphatidylinositol-specific phospholipase C removed 70% of cell surface CD14 (Wright et al. 1990). This could be a potential therapeutic target for individuals suffering from septic shock and potentially other diseases such as MS where TNF-α plays a pathological role (further discussed in section 1.6.3).

Experimentally, the activation of RAW 264.7 cells via LPS reproduces the activation of an immune response *in vitro*, through a wide variety of signals including the release of cytokines (Hortelano et al. 2000). Specific cytokines that are secreted by macrophages when activated by an inflammatory stimulus include IL-1, IL-6, IL-8, and IL-12 (Beutler 1999). Activated macrophages are known to be imperative immune effector cells that play a vital role in the body's host defence system (Mosser & Zhang 2008). A myriad of important roles are regulated by macrophages including phagocytosis of pathogens, secretion of chemokines, cytokines, growth factors and removal of necrotic cells (Rahat, Ebitterman & Elahat 2011). Inflammation is an essential process that is primarily mediated by macrophages; they are known as 'phagocytic cells' as they engulf pathogens they encounter (Duque & Descoteaux 2014). However, the inflammatory response involves the coordination of cell types that include monocytes, neutrophils, natural killer cells, T cells, B cells, mast cells and others (Chen et al. 2018).

Macrophages have a role in expressing enzymes involved in the inflammatory process including nitric oxide synthase 2 (NOS-2), cyclooxygenase-2 and the synthesis of reactive oxygen intermediates (ROI), in the ultimate aim to reduce inflammation (Hortelano et al. 2000). The increased release of nitric oxide (NO) due to the overexpression of NOS-2, results in the synthesis of mitochondrial mediators which activate caspases. These events result in apoptosis, which is seen as physiologically relevant by reducing inflammatory stress (Hortelano et al. 2000). Conversely, although inflammation has an integral role in maintaining homeostasis, an overreactive immune system in response to LPS could potentially lead to an increased release of pro-inflammatory cytokines. This may lead to septic shock, causing injury to tissues, organ failure or inherently death (Beutler & Rietschel 2003).

1.6 *Cytokines*

Cytokines are small low MWT proteins that bind to specific receptors that act as messengers to other inflammatory molecules through a signalling cascade (Duque & Descoteaux 2014). Furthermore, cytokines have a role in the regulation of ions, genes and transcription factors (Duque & Descoteaux 2014). Cytokines are produced by a plethora of cell types, with the most abundant being T helper cells and macrophages (Zhang & An 2007). There are both pro-inflammatory and anti-inflammatory cytokines. Pro-inflammatory cytokines are involved in the positive feedback mechanism of the immune and inflammatory response. Examples of pro-inflammatory cytokines include IL-1 (α and β), IL-6 and TNF-α. Whereas, anti-inflammatory cytokines have a role in regulating anti-inflammatory responses. Examples of anti-inflammatory cytokines include IL-4, IL-10, IL-11 and IL-13 (Zhang & An 2007).

1.6.1 **1L-1β**

IL-1β is a pro-inflammatory cytokine that belongs to the IL-1 super family, which comprises of 11 members (Dinarello 2018). This family of cytokines has been highly linked to damaging inflammation, but also has a role in the increased resistance to pathogens (Dinarello 2018). IL-1β is classified as a pyrogen that has a prominent role in the immunity in response to stress and infections. Dendritic cells, natural killer cells and epithelial cells secrete IL-1β, with monocytes and macrophages being the main producers of IL-1β (Duque & Descoteaux 2014). IL-1β is the most extensively studied member of the IL-1 family. It is produced as a 37kDa inactive zymogen, pro 1L-1β, which accumulates in the cytosol, until it is processed and cleaved by the inflammasome activated caspase-1 (Takeuchi & Akira 2010). Within the CNS, IL-1 has a role in the inflammatory cascade involved in neuronal degeneration (Álvarez, van Der Goot & Muñoz-Fernández 2013). IL-1 initiates the production of IL-6 which stimulates inducible NOS2 activity (Álvarez, van Der Goot & Muñoz-Fernández 2013).

IL-1β has been acknowledged as a potential cytokine underlying the pathophysiology of numerous CNS disorders including MS. Mason et al. (2001) studied the effect of CPZ on adult C57BL/6 mice. There was a drastic accumulation of IL-1β in the CC of wild type (WT) mice after 3 weeks of exposure to CPZ, compared to the control mice. Levels of IL-1β continued to increase for 6 weeks until the CPZ treatment was terminated, whilst the IL-1β mRNA reduced to control levels. Insulin like growth factor (IGF-1) showed the same trends as IL-1β; however,

the increased expression rose until week 7, during the remyelination phase (Mason et al. 2001). Interestingly, *IL-1β*$^{-/-}$ mice did not remyelinate properly compared to the wild-type mice, due to the lack of IGF-1. This could indicate that IL-1β has a role in remyelination via the induction of IGF-1 (Mason et al. 2001).

1.6.2 **IL-18**

IL-18 is a part of the IL-1 superfamily; however, it is unique as it induces the production of IFN-γ, but it is not a pyrogen (Duque & Descoteaux 2014). IL-18 has an integral role in the host defence mechanism when invaded by pathogens. IL-18 is part of the innate immune response that has pleiotropic functions including the induction of IFN-γ (Yasuda, Nakanishi & Tsutsui 2019). Similarly, to IL-1β, IL-18 begins as an inactive pro-IL-18, this inactive precursor lacks signal peptides (Dinarello et al. 2013; Yasuda, Nakanishi & Tsutsui 2019). Pro-IL-18 is processed by intracellular cysteine-aspartic protease (caspase) -1 (CASP1) into an active cytokine (Dinarello et al. 2013). IL-18 is regulated through the IL-18 binding protein (IL-18BP).

1.6.3 **TNF-α**

TNF-α is a potent pro-inflammatory cytokine that is produced by a myriad of cells within the body (Flynn et al. 1995). Within the periphery, TNF-α is produced by macrophages, lymphocytes, natural killer cells and dendritic cells (Kemanetzoglou & Andreadou 2017). TNF-α is produced by numerous cell types in the CNS including, microglia, neurons and astrocytes (Kemanetzoglou & Andreadou 2017). TNF-α has a multitude of roles including inflammation, apoptosis, immunity and cell proliferation (Micheau & Tschopp 2003). TNF-α is a cytokine that spikes early upon infection or exposure to bacterial-derived LPS (Feldmann et al. 1994). It is acknowledged that TNF-α is an older terminology, as TNF-β is now referred to as lymphotoxin α, which was first described in 1968 (Williams & Granger 1968). For consistency in this thesis, the old nomenclature of TNF-α has been used.

1.6.3.1 TNF-α Receptors

TNF-α as its precursor form is a 26kDa transmembrane TNF-α (tmTNF) protein, which is characteristic of a cell to cell interactive response (Perez et al. 1990). The 17kDa soluble TNF-α (solTNF) acts remotely from the TNF-α producing cells (Perez et al. 1990). TNF-α converting enzyme (TACE) has the role of cleaving tmTNF, which subsequently releases a soluble TNF-α cytokine. TNF-α binds to two different receptors: TNF receptor 1 (TNFR1) and TNF receptor 2 (TNFR2) (Parameswaran & Patial 2010). TNFR1 is expressed in a plethora of mammalian tissues, conversely, TNFR2 is expressed predominately in immune cells, neurons and endothelial cells (Kemanetzoglou & Andreadou 2017; Parameswaran & Patial 2010). Within the CNS resident phagocytic cells, microglia express TNFR1 and TNFR2, whereas oligodendrocytes and astrocytes predominately express TNFR1. TNFR1 signals through the solTNF and tmTNF, however it has a larger affinity with solTNF, whereas TNFR2 activation occurs only through tmTNF (Grell et al. 1998; Pegoretti et al. 2018). TNFR1 has a role in mediating the caspase associated apoptosis, whilst TNFR2 has a protective role for cells through the Phosphoinositide-3-kinase (PI3K-Akt)/protein kinase B signalling (Pegoretti et al. 2018).

Arnett et al. (2001) showed the dual role of TNF-α. This was seen as TNF-α $^{-/-}$ mice portrayed a statistically significant reduction in the extent of oligodendrocyte loss and demyelination compared to the controls after 3.5 weeks of CPZ treatment. Further analysis of the TNF-α

receptors revealed the importance of TNFR2, not TNFR1, for oligodendrocyte regeneration, as TNFR1$^{-/-}$ mice showed the same extent of remyelination as the wild-type controls, whereas the TNFR2$^{-/-}$ displayed the delayed remyelination that occurred in TNF-α$^{-/-}$ mice (Arnett et al. 2001). This portrays that TNF-α accelerates the demyelination process but is required in the CNS for remyelination to occur. This led to the potential therapeutic target of TNF-α. Some of the TNF-α blockers that are used for the treatment of autoimmune diseases include infliximab, etanercept, adalimumab, PEGylated certolizumab, and golimumab (Pegoretti et al. 2018).

However, controversial studies have been conducted by Mi et al. (2016) who studied the functions of TNFR2 in microglia and macrophages, using conditional knock out (KO) in an EAE mouse model. Microglial TNFR2 KO caused an increased progression of EAE and demyelination, whereas, the KO of TNFR2 in macrophages reduced the immune cell influx and suppressed EAE (Mi et al. 2016). This study raises several important issues including the different responses in macrophages and microglial cells, the importance of the signalling of cytokines and their receptors in various diseases, and the differences in the currently used MS models. Combined these important issues, further support that the molecular mechanism of CPZ breakdown products needs to be studied in a well characterised cell line such as the RAW 264.7 macrophages as undertaken in this thesis.

TNF-α also referred to as cachexin, is known to injure oligodendrocyte (Kim et al. 2011). The major receptor associated with the pathological effects of oligodendrocyte death and demyelination is TNFR1 (Kim et al. 2011). Akassoglou et al. (1998) discovered the importance of the TNFR1 in terms of its inflammatory and cytotoxic effects on the CNS. This is evident as the inflammatory and cytotoxic effects of TNF were absent with TNFR1 KO mice (Akassoglou et al. 1998). Furthermore, in more simplified terms, TNF-α has cytotoxic effects on the CNS. This occurs through LPS causing the activation of the microglia, which causes the subsequent release of TNF-α. Once OPCs come in contact with astrocytes, this causes TNF-α to trigger cell death via the TNFR1 (Kim et al. 2011). TNF-α may also have a direct influence on the astrocytes, which affect the pre-OLGs through a cell to cell mechanism (Kim et al. 2011). Thus, more studies on the effects of blocking TNFR1 would be valuable and potentially identify a therapeutic target for MS patients.

TNF-α plays a role in the process underlying demyelination in MS. However, when administering anti-TNF-α treatments to MS patients, adverse effects including the exacerbation of the disease were observed (Hiltbrunner et al. 1999). A double blind, placebo-controlled Lenercept study conducted by Hiltbrunner et al. (1999) conveyed that patients treated with the prototype TNF-α blocker Lenercept exhibited worse symptoms of MS compared to the control, as well as adverse side effects including headaches, nausea and pain in the abdomen.

1.6.3.2 The Cytotoxic and Diagnostic Nature of TNF-α

The role of unregulated TNF-α in the pathogenesis of MS is evident as TNF-α is found in the CSF of MS patients and the accumulated levels correlate with the severity of the disease and BBB damage (Sharief & Hentges 1991). Sharief and Hentges (1991) conducted a 24-month prospective study, determining the TNF-α levels in patients with chronic progressive MS and stable MS. 53% of the patients with chronic progressive MS had high levels of TNF-α in the CSF, where the levels of TNF-α were not raised in patients that had stable MS. This study highlights the likely potent inflammatory effect of TNF-α in MS and its potential use in prognosis.

TNF-α is a cytokine that is produced by activated microglia (Guadagno et al. 2013). Activated microglia could also have a potential neurotoxic effect through releasing and metabolising glutamate (Centonze et al. 2009). In MS lesions, there is an increase in the microglial metabotropic glutamate receptor 2 (mGluR2), which increases TNF- α release and neurotoxicity (Centonze et al. 2009). This has detrimental effects including 'A1' reactive astrocyte dysfunction, which affects oligodendrocytes and neurons (Centonze et al. 2009). After noxious stimulation or injury to the nerves, astrocytes undergo a process known as reactive astrogliosis. The astrocytes differentiate into either reactive or scar forming astrocytes. The classification of reactive astrocytes is by their function, A1 largely revolving around the secretion of neurotoxins and A2 astrocytes which promote repair (Li et al. 2019). A study conducted by Probert et al. (1995) supports the cytotoxic nature of TNF-α. The study involved transgenic (Tg6074) mice overexpressing TNF-α, this resulted in subsequent demyelination, with histopathological analysis showing demyelination localised to the white matter of the medulla oblongata and cervical spinal cord. Furthermore, astrogliosis and microgliosis in the

CNS were evident in the transgenic mice. The transgenic mice developed random seizures, cerebellar impairments resulting in mortality (Probert et al. 1995)

The CPZ model and the subsequent demyelination that occurs, is a consequence of a local inflammation process which activates microglia and causes the infiltration of macrophages and cytokines when the treatment is longer than 3 weeks (Biancotti, Kumar & de Vellis 2008). Biancotti, Kumar and de Vellis (2008) using real time PCR found increased mRNA levels of IL-1β and TNF-α in mice brains after the first week of CPZ treatment. TNF-α mRNA concentration elevated after three weeks of treatment and IL-1β after four weeks of CPZ treatment. The elevation of these pro-inflammatory cytokines is relevant as the three to four-week period was characterised by predominant demyelination (Biancotti, Kumar & de Vellis 2008).

There are numerous cytokines that play an integral role in the innate immune response when exposed to pathogens. However, for this thesis ELISAs for IL-1β and TNF-α were explored based on their pro-inflammatory roles and previous research linking these cytokines with demyelination and MS as outlined above/in this section 1.6

1.7 *Protein Arginine Methylation*

Protein arginine methylation is a type of post translational modification, where arginine nitrogen atoms are modified to contain methyl groups (Blanc & Richard 2017). This form of Post translational modification occurs as frequently as phosphorylation and ubiquitination (Larsen et al. 2016). Larsen et al. (2016) using high resolution mass spectrometry discovered a total of 8030 sites for arginine methylation within 3300 human proteins that were found in 293 embryonic kidney cells. Protein arginine methylation serves integral roles in the body including mRNA splicing, cellular proliferation, protein-protein interaction and myelogenesis (Kim et al. 2016). There has been increased interest in protein arginine methyltransferases (PRMTs) as therapeutic targets, as the overexpression of these enzymes is often seen in cancer, inflammatory and neurodegenerative diseases (Basavarajappa & Subbanna 2021; Kim et al. 2016; Yang & Bedford 2012).

PRMTs are known to have a role in the methylation of arginine residues that have vital roles in the maintenance of homeostasis within the body (Kim et al. 2016). Protein arginine methylation is an emerging research area in numerous human diseases including MS (Webb & Guerau-de-Arellano 2017). Numerous methylation changes have been identified in diseased states but the reasons for why this occurs is unknown. However, it has been postulated to be because of genetic changes, or dysregulation of methylation pathway genes (Webb & Guerau-de-Arellano 2017). More research into the changes in protein arginine methylation could provide more targets for therapeutic and pharmacological interventions for MS and other diseases.

1.7.1 **Types of Methylated Arginine Residues**

PRMTs transfer a methyl group from S-adenosylmethionine (AdoMet) to the arginine guanidine nitrogen atoms, which are converted to S-adenosylhomocysteine (AdoHcy) (Blanc & Richard 2017; Zakrzewicz et al. 2012). There are three types of methylated arginine residues, asymmetric dimethylarginine (aDMA), symmetric dimethylarginine (sDMA) and monomethylarginine (MMA) (Yang & Bedford 2012). Asymmetric di-methylation occurs when two methyl groups are transferred to the guanidine group on one of the terminal nitrogen atoms (Yang & Bedford 2012). Symmetric di-methylation occurs when one methyl group is placed onto each of the terminal ends of the nitrogen atoms (Yang & Bedford 2012). Figure 6 illustrates the formation of MMA, sDMA, aDMA (Zakrzewicz et al. 2012).

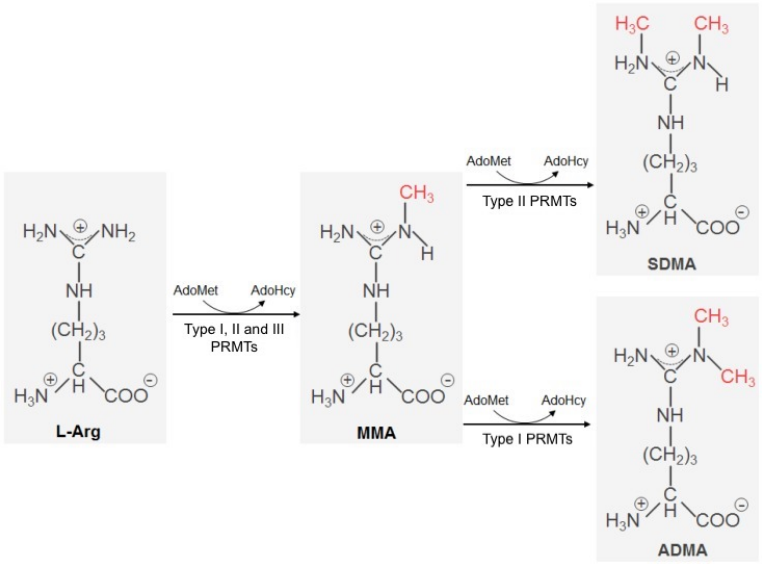

Figure 6: Diagram of the mechanism of action of protein arginine methylation via PRMTs Adapted from (Zakrzewicz et al. 2012).

1.7.2 **Characterisation of PRMTs**

The PRMT family members have many commonalities; however, they do contain differing roles and distribution patterns (Wei et al. 2014). PRMTs are categorised into different enzymes, and there are currently ten mammalian PRMTs (Bedford 2007). Mammalian PRMTs are classified into 3 types, dependent on their catalytic activity. PRMT1 is the type I enzyme mainly responsible for asymmetric di-methylation. Other type I PRMTs include PRMT 2,3,4,6 and 8. PRMT5 is the primary type II enzyme required for symmetric di-methylation (Wei et al. 2014; Yang & Bedford 2012). The one PRMT classified as a type III enzyme is PRMT7, which only catalyses the formation of MMA (Zurita-Lopez et al. 2012). PRMT9 symmetrically di-methylates arginine residues; similar to PRMT5 it contains an ancestrally duplicated methyltransferase domain (Hadjikyriacou et al. 2015). The methylation transfer activity of PRMT10 has not yet been shown experimentally but is based on sequence homology only (Wei et al. 2014).

1.7.3 **The Role of PRMTs in Inflammation and Disease**

PRMT1, PRMT4, PRMT5 and PRMT6 are known to have a role in inflammation, specifically modulating transcriptional factors and cofactors required for the inflammatory process to occur (Kim et al. 2016). PRMT1 is the most commonly expressed PRMT, with approximately 85% of PRMT activity seen in mouse hepatic tissue (Kim et al. 2016). PRMT1 has a role in the asymmetrical di-methylation and mono-methylation of histone 4 (Kim et al. 2016).

PRMT5 is found to have a role in the regulation of T cell response. Webb et al. (2017) investigated the role of PRMT5 in the activity of T helper type 1 cells. In this study, PRMT5 was blocked with a novel PRMT5 inhibitor, which resulted in the blockade of PRMT5 resulted in the suppression of T cell response, inflammation and clinical disease in the EAE mouse model (Webb et al. 2017). The dysregulation of PRMT5 causes tumour cell growth and PRMT5 overexpression is seen in diseases including leukemia, lymphoma, lung cancer, colorectal cancer and breast cancer (Chen et al. 2017).

Further investigation into the role of PRMTs in the cell cycle and diseases states is necessary for the development of therapeutic targets, which may provide more efficacy in drug treatments (Raposo & Piller 2018). Additionally, further insight into the pathogenesis of certain diseases may evolve, when more knowledge on the impact of PRMTs on cellular regulation, homeostasis and inflammation is known.

2.0 Hypothesis and Aims

As stated in section 1.0, while oral CPZ is used as a model to induce demyelination in mice, mimicking the pathological hallmark of MS, no studies so far have been conducted on the two breakdown products of CPZ to identify the molecular pathways and cellular effects of each individual breakdown product of CPZ. Therefore, the null hypothesis was that neither of the breakdown products of CPZ contributes to the cytotoxicity in RAW 264.7 macrophages. The alternate hypothesis was that oxalyldihydrazide, one of the two breakdown products of CPZ, is the major contributor to this effect in RAW 264.7 macrophages. This hypothesis was based on a previous study highlighting the correlation between mixed sensorimotor neuropathy and treatment with isoniazid (Mandel 1959). This hypothesis was drawn due to the chemical similarities in the hydrazide part of isoniazid and oxalyldihydrazide.

The major aim of this thesis was to determine the cellular effects of the two breakdown products of CPZ, cyclohexanone and oxalyldihydrazide, in RAW 264.7 macrophages, including the effects on cell viability, cytokine production and arginine di-methylation of cellular proteins.

The specific aims were to

Optimise a tissue culture protocol to test the effects of the CPZ breakdown products in activated and non-activated RAW 264.7 macrophages. Activation was achieved with LPS and IFN-γ in media with heat inactivated fetal calf serum supplementation.

Determine the effect of the two CPZ breakdown products on cell viability of activated and non-activated RAW 264.7 macrophages, quantified by the Trypan blue assay.

Determine the effect of the two CPZ breakdown products on the cytokine production including TNF-α and IL-1β in activated and non-activated RAW 264.7 macrophages, using ELISA kits.

Investigate whether activation of RAW 264.7 macrophages affects the arginine di-methylation of cellular proteins.

3.0 Materials

3.1 *Chemicals/Materials*

RAW 264.7 cells were kindly provided by the School of Medicine at Western Sydney University at a passage number of 18 (ATCC catalog number TIB-71). Cyclohexanone and oxalyldihydrazide was also provided by the School of Medicine which was purchased from Sigma Aldrich. Chemicals and Materials used in this study and their suppliers are listed in Table 1.

Table 1: List of Chemicals and Materials

Chemical/Material	***Supplier***
ABTS Liquid Substrate	Sigma-Aldrich Australia
Alkaline phosphatase blue membrane substrate solution	Sigma-Aldrich Australia
Bis(cyclohexanone) oxalydihyrazone	Sigma-Aldrich Australia
Cyclohexanone 99.8%	Sigma-Aldrich Australia
Dimethyl sulphoxide (DMSO) hybrid-max ®	Sigma-Aldrich Australia
DMEM- High glucose with 4500 milligrams (mg)/Litre (L) glucose, sodium, pyruvate and sodium bicarbonate, without L-Glutamine, liquid sterile-filtered 500mL	Sigma-Aldrich Australia
Ethanol (100%)	Chem-Supply
ExtrAvidin-Alkaline Phosphatase	Sigma-Aldrich Australia
Dulbecco's Phosphate buffered saline	Sigma-Aldrich Australia

Halt Protease Inhibitor Cocktail (100x)	ThermoFisher (Catalog # 78430)
IFN-γ	Sigma-Aldrich Australia
Invitrogen Alamar blue- cell viability reagent	Thermo Fisher Scientific
Invitrogen IL-1 beta mouse ELISA Kit	Invitrogen
L-Glutamine Solution 200 millimolar (mM)	Sigma-Aldrich Australia
LPS	Sigma-Aldrich Australia
Methanol	Sigma-Millipore Australia
Mini-protean precast gradient gels (4-20%) (10)	Bio-Rad
Mini-protean precast gradient gels (4-20%) (15)	Bio-Rad
Mouse IL-1β ELISA Kit Catalog #: BMS6002	Invitrogen
Oxalyldihydrazide 98%	Sigma-Aldrich Australia
Penicillin-Streptomycin Solution Stabilised	Sigma-Aldrich Australia
Peprotech Development kit Standards ABTS EDK Murine TNF-alpha Catalog #:900-K54 Lot # 0718054	Peprotech
Sodium dodecyl sulfate (SDS)	Sigma-Millipore Australia
Tetramethyl-benzidine (TMB) Substrate solution (IL-1β ELISA)	Invitrogen
Trypan blue solution (0.4%)	Sigma-Aldrich Australia
Tween20	Sigma-Aldrich Australia

3.2 *Buffers*

Buffers used in this study and their composition are listed in Table 2.

Table 2: List of Buffers

Buffer	***Composition***
10x Phosphate buffered saline (PBS)	14.4mM KH2PO4, 1370mM NaCl, 27mM KCL, 81mM Na2HPO4.2, adjusted to pH of 7.4 using HCl or NaOH.
1 x PBS	100mL of 10x PBS 900mL of milliQ water
10x Tris glycine transfer buffer	1.92M Glycine and 250mM of Tris
10x Tris-glycine Sodium dodecyl sulfate (SDS) running buffer	1.92M Glycine, 250mM of Tris and 1% of SDS
1x Tris glycine transfer buffer	70% water, 20% methanol and 10% 10x tris-glycine transfer buffer
Assay Buffer (IL-1β ELISA)	20x pre-prepared assay buffer concentrate diluted into 1x solution using distilled water
Bicinchoninic acid colour reagent	1:50 $CuSO_4$ (copper sulfate): Bicinchoninic acid
Biotin conjugate (IL-1β ELISA)	1:100 dilution biotin conjugate solution :1x assay buffer
Block buffer (TNF-α ELISA)	1% Bovine serum albumin (BSA) in PBS
Diluent (TNF-α ELISA)	0.05% Tween-20, 0.1% BSA in PBS
DMEM	Heat inactivated FCS 10% volume/volume (v/v), penicillin 1000U/mL, streptomycin 0.1mg/mL and 2mM L-glutamate
ExtrAvidin-Alkaline Phosphatase (ExAP)	1:5000 ExAP: PBS-T

IL-1β mouse standard	Reconstituted in 400µL of deionised water
Phosphate buffered saline and Tween 20 (PBS-T)	1x PBS (as shown above), Tween 20 (0.01% v/v)- 1000mL of 1x PBS and 1mL of Tween
PI Lysis buffer	1:100 Pierces buffer (25mM Tris-HCl pH7.4, 150mM NaCl, 1mM EDTA, 1% NP-40, 5% glycerol in PBS).
Reducing Sample Buffer	1:5 dilution (0.5M Tris, 10% v/v Glycerol, 0.028M SDS, 4% v/v β- Mercaptoethanol and 0.00015M Bromophenol blue in Milli-Q Water.
Skim milk blocking buffer	5% w/v skim milk powder in PBS-T
Streptavidin HRP (IL-1β ELISA)	1:200 dilution Streptavidin HRP solution: 1x assay buffer (1x)
Wash buffer (TNF-α ELISA)	0.05% Tween-20 in 1x PBS
Wash Buffer (IL-1β ELISA)	20x Wash Buffer concentrate (pre-prepared) diluted to 1x Wash Buffer using distilled water

3.3 *Equipment*

A list of all equipment used in this study is shown in Table 3.

Table 3: List of Equipment

Equipment	***Use***
Adhesive Film	TNF-α and IL-1β assay
Allegra X-30R Centrifuge	General use
BIO-RAD Mini-Protein tetra system	Western Blotting
BIO-RAD Power Pac HC	Wester Blotting
BODEO Germany Hemocytometer	Cell viability Trypan blue and cell counts
CovaLink Covalent Binding 96 well plate	TNF-α assay
FLUOstar Optima Spectrophotometer	BCA Assay
FLUOstar Omega multi-mode microplate reader	ELISAs
GelmanSciences Biosafety Cabinet	Cell Culture
Greiner cell scrapers	Cell Culture
Greiner Flat bottom 24 well plates	Cell Culture and Alamar blue assay
Greiner Flat Bottom 96 well plates	BCA assay and cell culture
Greiner T25 Cell Culture Flask	Cell Culture

Equipment	*Use*
Greiner T75 Cell Culture Flask	Cell Culture
HERA Cell Incubator	Cell Culture
Labec Water Bath	General use
Olympus CKX53 Microscope	General use
Owl-HEP-1 Semi-Dry Blot System	Thermo Scientific
POLARstart omega plate reader spectrophotometer	Alamar blue Assay
Ratek Dry Block Heater	Western Blotting and general use
Ratek Medium Rocking Platform Mixer	Western Blotting
Sigma-Aldrich Acrodisc syringe filters 0.45µm pore size	Cell drug treatment
Stuart SSM1 Orbital shaker	TNF-α and IL-1β assay
Thermo scientific -20°C freezer	General use
Thermo scientific -80°C freezer	General use
Thermo scientific Nunc-Immuno Wash 8	TNF-α and IL-1β assay
Vortex Genie-2	General use
Luminoptic ISH500 eyepiece camera	Cell Morphology and Trypan Blue assay

3.4 *Antibodies*

All antibodies used in this study are shown in Table 4.

Table 4: List of Antibodies

Antibody	***Primary or Secondary***	***Dilution***	***Supplier***	***Product number***
Anti-Rabbit IgG (whole molecule) biotin antibody produced in goat)	Secondary	1:2500	Sigma-Millipore Australia	B7389
Anti-dimethyl-Arginine Antibody, Asymmetric (ASYM24)	Primary	1:1000	Sigma-Millipore Australia	07-414
Anti-Beta Tubulin	Primary	1:500	Abcam	AB168
Anti-GAPDH antibody	Primary	1:1000	Sigma-Millipore Australia	ABS16
Anti-PRMT1	Primary	1:500	Sigma-Millipore Australia	07-404
Anti-PRMT5	Primary	1: 1000	Sigma-Millipore Australia	07-405
Anti-dimethyl-Arginine Antibody, Symmetric (SYM10)	Primary	1:1000	Sigma-Millipore Australia	07-414

4.0 Methods

4.1 *Cell Passaging*

The RAW 264.7 macrophage cell line from the American Type Culture Collection was provided by the School of Medicine at Western Sydney University, at passage number 18. The RAW 264.7 cells were cultured in Dulbecco's Modified Eagle's Medium (DMEM) supplemented with heat inactivated fetal calf serum (FCS). The FCS was heat inactivated by placing it in a water bath set at 57 degrees Celcius (°C) for 30 minutes. Substances added to the DMEM were the 10% v/v of the heat inactivated FCS, penicillin 1000U/mL, streptomycin 0.1mg/mL, and 2mM L-glutamate. The cells were incubated at 37 °C and 5% CO_2. Approximately every 3-4 days once reaching 80-85% confluency which was estimated by visual inspection using a light microscope. The media was removed using a pipette and the cells were washed using 5mL of sterile PBS twice. The cells were resuspended into 12mL of 10% FCS DMEM and using a cell scraper, adherent cells were removed and transferred into 3x T75 flasks (1:3 confluent cells: fresh DMEM). Another 6mL of fresh 10% DMEM was applied to each T75 flask and cells were maintained at 37°C and 5% CO_2. Cells were harvested and seeded at $0.5x10^6$ cells per well into four 24 well plates for the activation and drug treatment with cyclohexanone and oxalyldihydrazide.

Observations were also made on the change in colour of the media before and after passaging of the cells (as shown in Figure 7A and 7B, respectively). The DMEM contains phenol red, which is widely used in cell culture work as a pH indicator (Liu et al. 2013). This is a helpful observational measure of cell growth and metabolites (Liu et al. 2013). This is evident as the phenol red is pink in colour at normal physiological pH of (7.3-7.4). Phenol red turns to a yellow colour, which is indicative of an acidic environment, a pH that is lower than 7. The colour then turns to a bright pink when the pH is alkaline, above 8.2 (Liu et al. 2013). The change in media colour to a yellow colour is illustrated in Figure 7B.

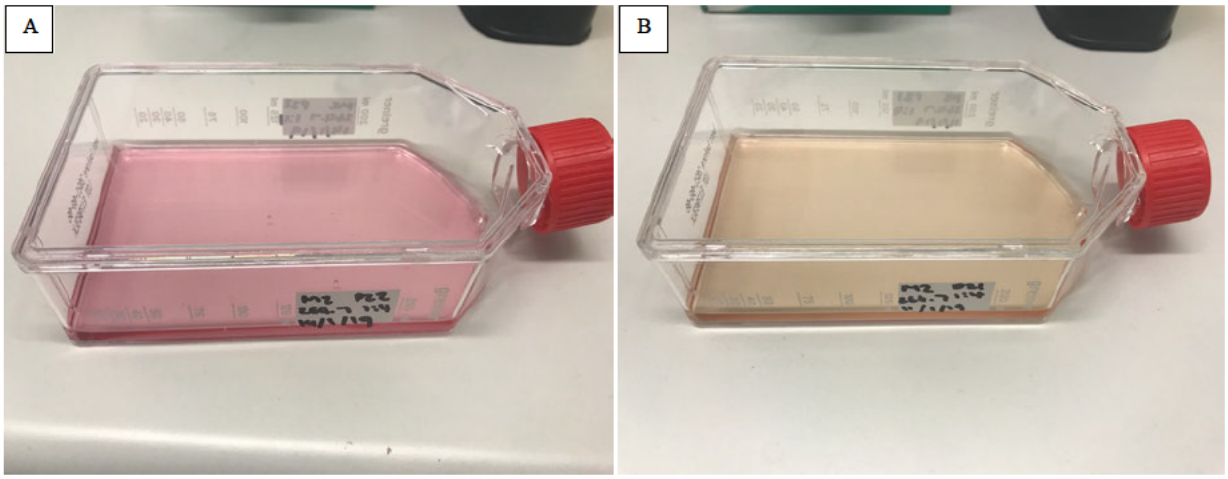

Figure 7: Change in media colour after passaging and incubation of RAW 264.7 cells.
A) T75 flask showing media colour after passaging the cells. B) Media colour after 3-4 days incubation.

FCS is commonly used in cell culture work, to ensure optimal growth of the cells. FCS contains the necessary supplements for cells, specifically growth factors however, FCS does contain complement proteins and inhibitory growth factors, which are the targets of heat inactivating FCS (Rahman et al. 2011). At the beginning of the experiments 0.1% and 10% FCS were used for cell culture work. The lower amount of FCS was used to prevent the FCS from interfering with the activity of the macrophages, as higher concentrations of FCS correlate with a higher probability of endotoxin (LPS) contamination (Kirikae et al. 1997). Furthermore, medium starvation plays a role in the activation process of macrophages with LPS and IFN-γ. Williams et al. (2016) displayed that mice macrophages exposed to no FCS had an adherent phenotype and had an up-regulated pro-inflammatory response of the cells when incubated with LPS, compared to the cells suspended in serum.

Heat inactivation of FCS was used during these experiments due to its influence on the haemolytic activity of FCS. Complement (C) proteins as C1, 2,7 and 8 are heat labile and are considered vital in order to inactivate serum inhibitory factors (Triglia & Linscott 1980). The need to inhibit the C systems is important for immunological assays, as the proteins of the C system play a pivotal role in activating the immune system (Rahman et al. 2011). The presence of FCS in the media has many drawbacks and can lead to serious misinterpretations in immunological studies (Arora 2013). Whilst most cell culture work does not require the use of heat inactivated serum; it is important to use heat inactivated serum when experimenting with or testing immune cells that need to be activated for the experimental protocol.

4.2 *Cell Harvesting (optimisation)*

Cells adhere at the bottom of either the wells or cell culture flask through cell adhesion proteins, specifically fibronectin and vitronectin (Brown et al. 2007). These cell adhesion molecules bind to heterodimeric transmembrane proteins called integrins (Brown et al. 2007). Trypsin is a proteolytic enzyme that is widely used within cell culture work, as it disrupts the adherent proteins. Trypsin removes cells from the cell culture flask by cleaving of the C-terminal side of arginine and lysine amino acids, leaving the associated remnant peptides (Olsen, Ong & Mann 2004). Trypsin is known to be a convenient method of removing adherent cells, as they can then be used for further experimentation or subculture.

Trypsin has been used previously in experiments when harvesting the RAW 264.7 cells (Zong et al. 2012). Figure 8 illustrates the difference in the adherent cells after using 1x trypsin, incubated at 37°C and 5% CO_2 for 15 minutes, compared to the volume of cells remaining after using a cell scraper. A larger number of cells remained adherent to the bottom of the 24 well plate when using trypsin (Figure 8A and B) compared to the cell scraper (Figure 8C and D). Note that a pipette tip was used to scrape the cells (as shown by the lines indicated by the red arrow in Figure 8B), due to the high volume of cells left in the wells.

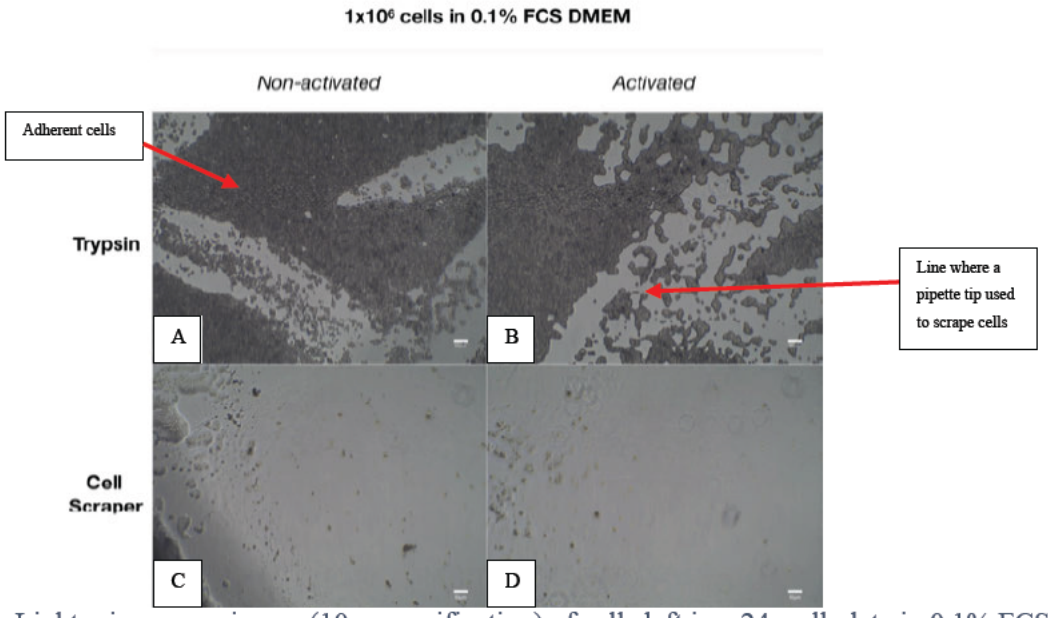

Figure 8: Light microscopy image (10x magnification) of cells left in a 24 well plate in 0.1% FCS. A) Remaining cells after trypsinising adhered cells activated for 6 hours. Red arrow indicates adherent cells. B) Cells after trypsinising cells activated for 24 hours. Red arrow indicates the line where a pipette tip was used to scrape the adherent cells. C) Cells after using a cell scraper to remove cells activated for 6 hours. D) Remaining cells after using a cell scraper to remove cells activated for 24 hours. Scale bar indicates 50μm.

Figure 9 illustrates the left-over cells that are visible by the human eye and camera lens shown in the top row of the 24 well plate. Comparing the two approaches in detaching the adherent 264.7 cells, trypsin was less effective, consequently a cell scraper was used for all subsequent experiments.

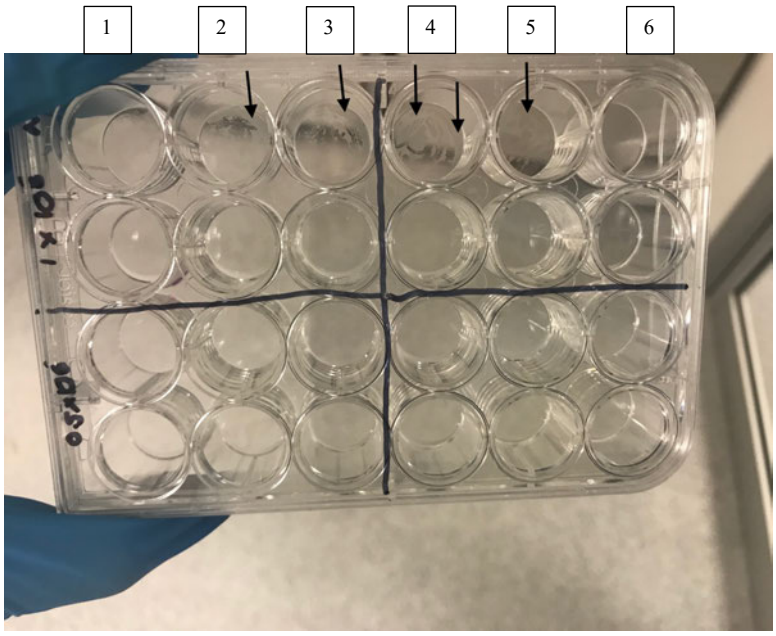

Figure 9: Photo of leftover RAW 264.7 cells after trypsinisation.
The black arrows indicate adhered cells at the bottom of the wells, which are cloudy, opaque in nature.

For the conducted experiments, the following protocol was used once the cells reached around 80-85% confluency. The media was removed using a pipette into a falcon tube and the flask was washed using 5mL of sterile PBS twice. The adherent cells were detached using the cell scraper and pipetted into a falcon tube. The cells were centrifuged at 400 x gravitational force (g) for 5 minutes and the supernatant was removed. Cells were washed again with 5mL of PBS through pipetting up and down mixing the cell pellet and supernatant together. The sample was centrifuged again at 400 x g for 5 minutes. The cell pellet was stored at -20°C until required for further experimentation. The supernatant was kept as a control for numerous activation and drug treatment experiments.

4.3 *Image Analysis*

After each activation/drug treatment timepoint, images of the RAW 264.7 macrophages were taken with a 1SH500 eyepiece camera and IScapture (Tuscen Photonic Co., Ltd; version 3.6.9.3_N) software. The process of taking images using this software was used to monitor the morphological changes that occurred with activation and drug treatment of macrophages.

4.4 *Cell Activation*

RAW 264.7 cells seeded at 0.5 x 10^6 cells into 24 well culture plates were activated using 1 μg/ml of LPS and 1U of IFN-γ, unless otherwise stated. This activation mix was made in 10% (v/v) or 0.1% (v/v) heat inactivated FCS DMEM complete media. The term re-activated was used for cells that were re-suspended in the activation mix containing LPS and IFN-γ during the drug treatment. The 24 well plate was incubated for 12 hours (unless otherwise stated) at 37°C and 5 % CO_2. After the activation time points, the cell viability was tested using the Trypan blue assay (refer to section 4.7 for the method).

4.5 *Drug Treatment*

Cyclohexanone and oxalyldihydrazide was dissolved into a 5000 micromolar (μM) stock which was placed into 0.1% FCS DMEM complete media. RAW 264.7 macrophages were seeded at $0.5x10^6$ cells per well. The cells were either non-activated (no activation mix added), activated (not resuspended in activation mix during drug treatment) or re-activated (resuspended in 1μg/ml of LPS and 1U/ml of IFN-γ during drug treatment).

Serial dilutions were pipetted into the subsequent well. The stock solution was added to the first well 5000μM and a tenfold dilution was made to 500μM and the subsequent 2-fold serial dilutions were pipetted. The cells were collected at certain time points as indicated in the specific experiments, ranging from 12-18 hours after the cells were incubated with the breakdown products. Both the supernatant and cell pellet were used for further analysis.

The solubility of the drugs was assessed over a 24-hour period to ensure that the oxalyldihydrazide and cyclohexanone would not precipitate out of solution when conducting the cell culture drug treatment experiments. The most effective medium for dissolving oxalyldihydrazide was water, however, the powder form oxalyldihydrazide fell out of solution in 100% ethanol and acetic acid, shown left to right respectively, in Figure 10A. In Figure 10B, over a course of 24 hours, the cyclohexanone did not precipitate out of solution in de-ionised water.

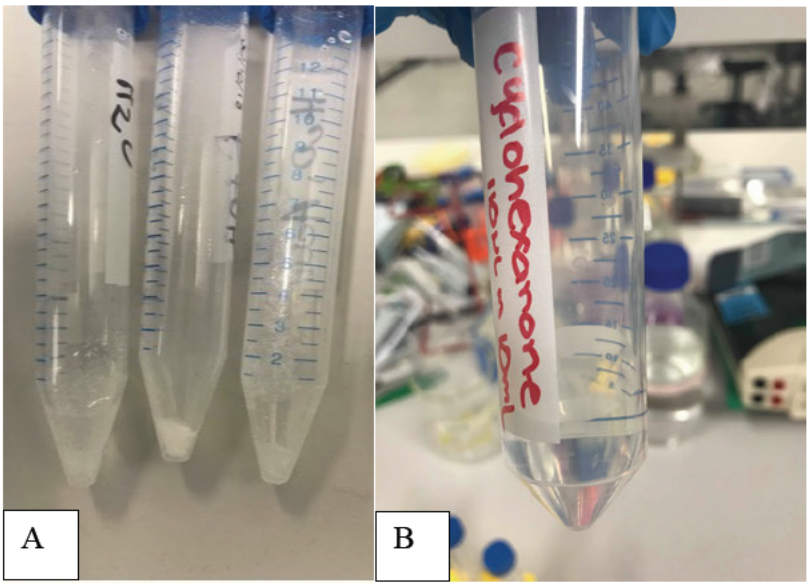

Figure 10: Images showing the solubility of oxalyldihydrazide and cyclohexanone.
A) Solubility of oxalyldihydrazide in water, ethanol, and acetic acid. B) The solubility of cyclohexanone in de-ionised water over 24 hours.

4.6 *Alamar Blue Assay*

Alamar blue is a dye that is used in an assay that utilises fluorometric detection to establish the metabolic mitochondrial activity of cells (Zachari et al. 2014). Resazurin is the blue dye utilised in this assay, which is water soluble, non-toxic to cells and can permeate through cell membranes (Kreft & Kreft 2009). Changes in this dye monitor the reducing environment of cells, in particular the reduction of the weakly fluorescent blue resazurin into highly fluorescent red resofurin (O' Brien et al. 2000). The change in colour from blue to pink is an indicator of microbial respiration and growing cells (Cox et al. 2009). Resazurin has the role of acting as an electron acceptor in the electron transport chain (ETC). Once resazurin accepts electrons it changes from an oxidized non-fluorescent blue state to its reduced fluorescence pink state. Alamar blue subsequently could indicate an impairment of cellular metabolism (Rampersad 2012). The mechanism by which the reduction occurs, includes entry of resazurin into the cytosol where it is reduced by mitochondrial enzymes including nicotinamide adenine dinucleotide phosphate, flavin adenine dinucleotide, flavin mononucleotide, nicotinamide adenine dinucleotide and cytochromes (Al-Nasiry & Geusens 2007). However, due to mitochondrial reductases not being the only enzymes having the ability to reduce resazurin, this pertains to the reduction of Alamar blue indicating impaired cellular metabolism may not only be confined to the mitochondria and ETC (Rampersad 2012). Other enzymes that have the potential to reduce Alamar blue include flavin reductases and diaphorases (Rampersad 2012). These fluorometric readings are sensitive and visible changes in colour are obvious (Rampersad 2012). The fluorescent reader is set at an excitation wavelength of 530-560 nanometres (nm) and the emission wavelength of 590nm (O' Brien et al. 2000).

4.6.1 **Alamar Blue Method**

To each of the 24 wells seeded with $0.5x10^6$ cells was 500µL of 1x Alamar blue solution (using 0.1% or 10% FCS DMEM complete media) was added. The optimisation of the incubation period was performed using numerous time points (shown in Figure 11). The plates were placed in the incubator set at 37°C and 5% CO_2 for 2 hours (as optimised after the analysis of data shown in Figure 12). After the two-hour incubation period, 100µL of each well were pipetted in triplicates into a flat bottom 96 well plate, with 3 blanks for each treatment (100 µL of the 1x Alamar blue solution) (as shown in Figure 11B). The plates were placed into the POLARstar omega microplate reader set at 544nm excitation and 590nm emission. The

analysis tool used the omega control program, which records the fluorescence intensity (FI) into a Microsoft Excel spreadsheet for further analysis.

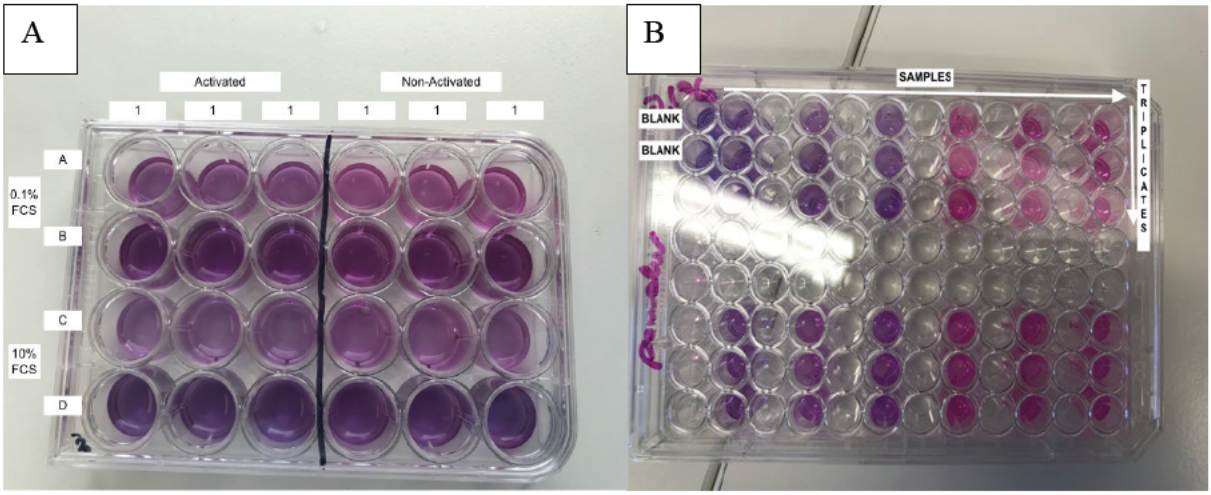

Figure 11: Photo of plates used for the Alamar blue assay.
A) Rows A and B are made up with 0.1% FCS DMEM complete media and rows C and D are made up with 10% FCS DMEM complete media. The left half of the 24 well plate contains activated cells and the right half of the 24 well plate contains non-activated cells. Rows A and C contain 500µL and rows B and D contain 1mL of the 1x Alamar blue. B) Example of supernatants removed from wells after incubation of the of the cells shown in (A) and transferred into the flat bottom 96 well plate for analysis of data using the POLARstar omega microplate reader.

Optimisation: As shown in Figure 11A, after 2 hours of incubation Rows B and D the large volume of resofurin (1mL) was not visually reduced. Whereas, rows A and C showed a pinker colour indicating reduction of 0.5mL of Alamar blue. Notable differences in reduction were observed between the activated (left) and non-activated (right) cells in 0.1% FCS (row A).

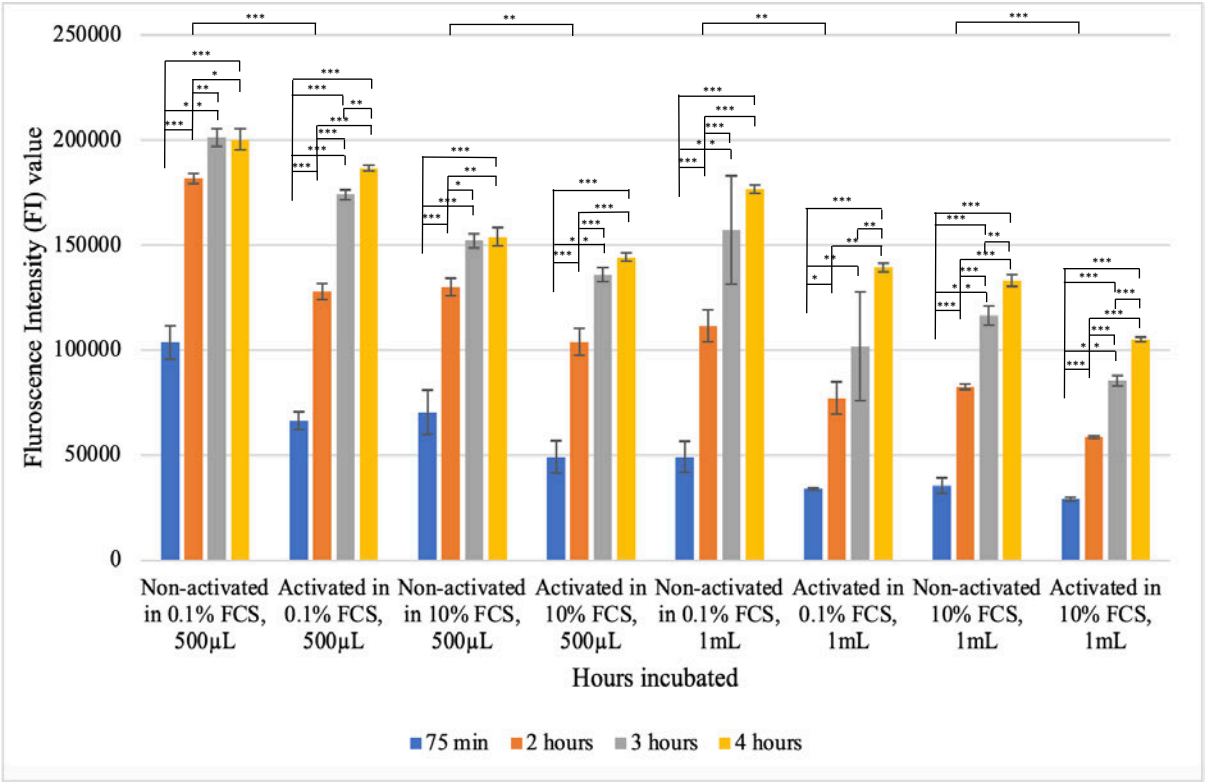

Figure 12: Graph illustrating different time points for the Alamar blue assay to optimise the incubation time.

Appendix 10.1.1 for blank corrected FI values. Statistical analysis shown in Appendix 10.1.2-10.1.29. (N=4).

Figure 12 illustrates the FI values for different concentrations of FCS and volumes of Alamar blue solution at varied incubation times: FI values plateaued between the 3 and 4-hour incubation. Before the plateau at the 2-hour time point significant differences between non-activated and activated RAW 264.7 macrophages were detected for cells grown in 0.1% FCS and 500µL of Alamar blue ($p= 0.000037$), 10% FCS and 500µL of Alamar blue ($p=0.0039$), 0.1% FCS with 1mL of Alamar blue ($p=0.0018$) and the cells in 10% FCS with 1mL of Alamar blue ($p=0.000015$). Based on these results and the optimising steps described in section 5.1.1, the RAW 264.7 macrophages were cultured in 0.1% FCS and the optimal amount of 1x Alamar solution was determined as 500µL into each well for all further experiments performed in thesis.

4.7 *Trypan Blue Assay*

The cells were removed from the cell flask/wells using a cell scraper. 20µL of the cell suspension and 20µL of Trypan blue, were mixed and 10µL was pipetted onto the hemocytometer. The live and dead cells were then counted on four quadrants of the hemocytometer at a 20x magnification to determine the cell viability (the borders of one quadrant is indicated by a red box in Figure 13A). Live and dead cells were determined by the colour of the cell, live/viable cells were indicated by a yellow shiny colour, whereas the dead cells were blue in colour (Figure 13B). Cells were counted blindly randomised (without knowing what sample they came from) in order to reduce bias.

The total number of cells were determined using the following equations:

$$C_{T/mL} = \frac{\sum_{n=1}^{n=4} HQ_n}{4} \times DF \times 10^4$$

where $C_{T/mL}$ is the total number of live and dead cells/mL, HQ_n is the live and dead cell count for respective quadrant n in the hemocytometer and DF is the dilution factor.

$$C_T = C_{T/mL} \times W_{mL}$$

where C_T is the total number of live and dead cells and W_{mL} is the total amount of mL in the cell culture flask/well.

The percentage of viable cells were determined using the following equation:

$$C_V = \frac{C_A}{C_T}$$

where C_V is the percentage of viable cells and C_A is the number of live cells.

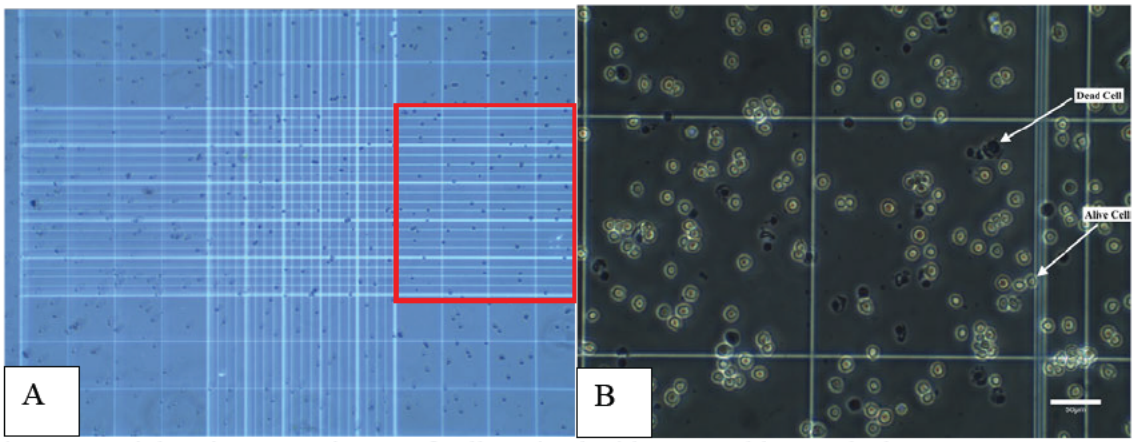

Figure 13: Light microscopy image of cells stained with Trypan blue on the hemocytometer. A) Light microscopy image (8x magnification) showing the grid layout of the hemocytometer. The red box is an example of one of the four quadrants used to count the cells. B) Light microscopy image (20x magnification) the white arrows are pointing to an example of a live and dead cell.

4.8 *Bicinchoninic Acid Assay*

Once the cells were cultured and harvested as described in section 4.1 and 4.2, the cell pellet was lysed using Pierce's lysis buffer and protease inhibitors (Halt protease inhibitor cocktail 100x). The volume was dependant on the size of the cell pellet (Appendix 10.1.31). Lysed cell pellets were incubated on ice for 10 minutes, then centrifuged at 15000 x g for 10 minutes to remove the insoluble fragments. The pellet was discarded, and the lysate was used for the bicinchoninic acid assay (BCA).

A total of 20µL of Bovine Serum Albumin (BSA) standards were pipetted into a flat bottom 96 well plate, with concentrations of 0.25, 0.50, 1.0, 2.0, 4.0, 6.0 and 8.0mg/ml into subsequent wells, plated in duplicates, as shown in Figure 14A. 20 µL of Pierce's lysis buffer was plated in duplicate as the blank. With a total volume of 20µL into each well, each of the samples were pipetted with different concentrations based on the dilution factor. 200µL of the BCA colour reagent was pipetted into each well. The colour reagent was made up in a 1:50 dilution 4% w/v Copper sulfate: BCA. This colour reagent turned the samples in the well to a different gradient of purple (Figure 14A). The 96 well plate was placed in an incubator set at 37°C for 10 minutes.

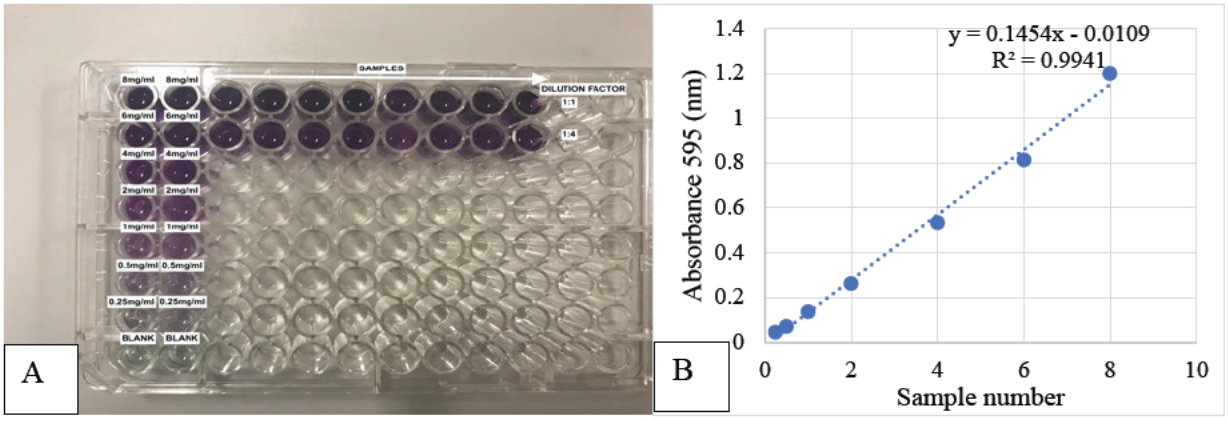

Figure 14: BCA assay performed and a Microsoft Excel graph of a standard curve.
A) Example of BCA plate layout, shown in Appendix 10.1.30. B) Example of BCA standard curve. Cell pellets used and raw absorbance values are shown in Appendix 10.1.31 and 10.1.32, respectively.

The flat bottom 96 well plate was placed in a plate reader at an absorbance set at 595nm and tabulated by BMG Labtech Fluostar Optima Software. A linear standard curve was produced in Microsoft Excel using $y = mx + b$, the total protein concentration x was used by rearranging the formula and substituting the protein's absorbance value for y (example shown in Figure 14B). All readings were corrected by subtracting the blank from all the values.

4.9 *Western Blots*

Western blotting, also known as immunoblotting, is a protein detection technique that is commonly used in research laboratories. This process involves the segregation of native proteins through gel electrophoresis. These proteins are then transferred to a protein binding membrane and are detected using specific antibodies (Burnette 1981). The transfer of proteins occurs onto a polyvinylidene difluoride (PVDF) absorbent membrane, this activated membrane allows for high protein binding. This forms a replica of the SDS polyacrylamide gel through electrophoresis (Kurien & Scofield 2006). WBs are used as a semiquantitative method of the expression of specific proteins in cells and tissues (Ghosh, Gilda & Gomes 2014). To ensure that the results were not from human error including loading and protein concentration calculation errors, Glyceraldehyde-3-phosphate dehydrogenase (GAPDH) was used as the house keeping protein at the beginning of this study. Cho et al. (2018) observed that GAPDH is induced by PRMT1 in a NO dependent manner. Therefore, GAPDH is not a good control protein for non-activated and activated RAW 264.7 cells. For the remainder of the study beta-tubulin was used as a loading control.

4.9.1 **SDS-PAGE and Transfer**

According to the protein concentration determined from the BCA assay, the samples were normalised to total protein concentration. The reducing sample buffer and Pierce's lysis buffer were pipetted into Eppendorf tubes. The samples were boiled for 10 minutes and placed immediately onto ice. In the Allegra X-30R centrifuge at max speed, the samples were centrifuged for 15 seconds to ensure that the condensed liquid on the side of the tube formed after cooling, will be spun down and combined with the sample to prevent change in the concentration and volume of the samples. Mini protean precast gradient gels (4-20%) were used for the experiments. 1x tris-glycine-SDS running buffer was poured into the chamber and filled to the appropriate volume, as shown on the outside of the Bio-Rad electrophoresis machine based on the number of gels being used. Carefully, the comb of the gel was removed and each of the wells was aspirated with the running buffer. Samples were pipetted into each of the wells (total volume depended on if a 10 well or 15 well gel was used), with a total of 4µL of PageRuler Plus ladder (Thermo Scientific) pipetted into the appropriate well/wells and the proteins were separated at 80V for 20 minutes then 120V for 1 hour until the blue line had reached the bottom of the electrophoresis chamber (as shown in Figure 15).

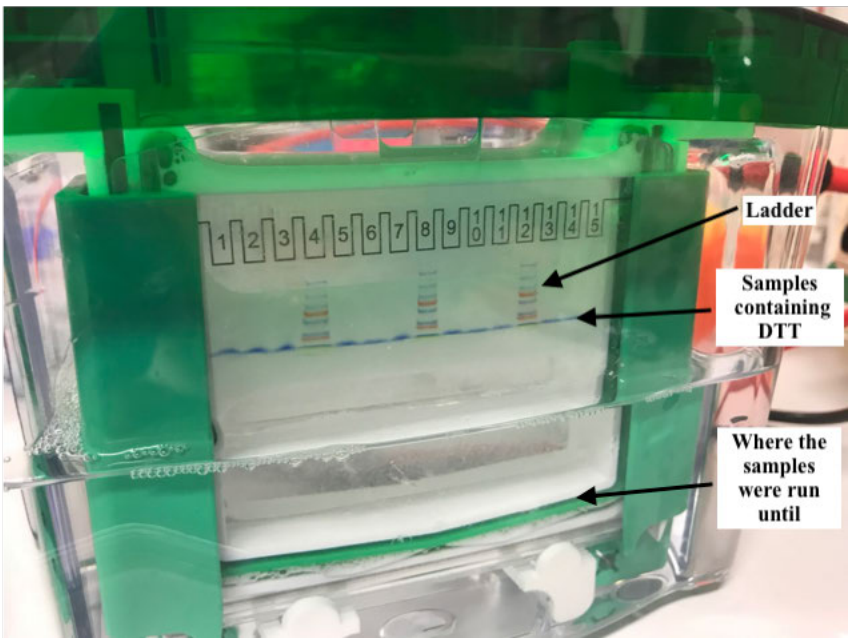

Figure 15: Photo showing an SDS-PAGE using a Bio-Rad electrophoresis chamber.

The running buffer was removed, and the gel plates were opened, and the gel was removed with the thicker parts of the gel being cut off. The gels were then placed into the container containing 1x tris glycine transfer buffer. The following were stacked onto the semi-dry blotter, from bottom to top (resembling Figure 16): 3x 2.5mm filter paper was soaked in 1x tris glycine transfer buffer, gel, the PVDF membrane was then activated in methanol for 1 minute and rinsed in the 1x tris glycine transfer buffer and another 3x 2.5mm filter paper was added on top of the PVDF membrane. A roller was used to remove the air bubbles in the stack. The lid and cables were attached and placed at 200mA per gel for 1 hour and 20 minutes.

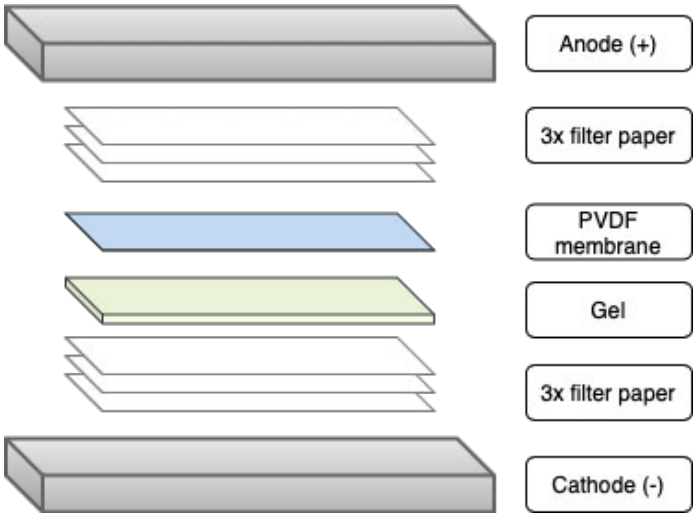

Figure 16: Diagram illustrating the assembly of the sandwich in a Western Blot. Created using Draw.io.

4.9.2 **Priming PVDF Membranes with Antibodies**

PVDF membranes were placed in a container containing 10mL of skim milk blocking buffer (5% w/v skim milk powder in PBS-T) for 2 hours on a rocking machine. The membranes were then washed using the following procedure, where they were washed three times with 10mL of PBS-T for 5 minutes each. The membranes were incubated in primary antibodies in PBS-T (see Table 4) for a minimum of 2 hours or overnight. Membranes were washed using the above washing procedure. The secondary antibody used was an anti-rabbit biotin antibody which was left on the membranes for 1 hour and 30 minutes. Membranes were washed using the above washing procedure. ExtraAvidin alkaline phosphatase (ExAP) at a concentration of 1:5000 was left on the membrane for 30 minutes and was washed 4x with 10mL of PBS-T for 5 minutes each. The alkaline phosphatase blue membrane solutions (substrate) in a 1:1 ratio were pipetted onto the membranes to observe the bands (1mL per membrane). The membranes were washed with MilliQ water and left to dry and were analysed using Adobe Photoshop version 20.0.2, to adjust the background after scanning them on a flatbed scanner.

4.9.3 **ImageJ Analysis of Western Blot Bands**

ImageJ software (National Institute of Health, USA, version 1.53a) was used for the densitometric analysis of the WB bands. The images from Adobe Photoshop (version 20.0.2) were changed to a type 8-bit image. Each of the bands were selected for analysis using the rectangular selection tool from the ImageJ toolbar (example shown in Appendix 10.8.3). The same profile was then applied to each band analysed. The straight-line tool was used from the selection tool on the ImageJ toolbar and used to remove the background from the profile plot (shown in in Appendix 10.8.2). The wand tracing tool was used to determine a numerical value for each of the peaks. The values were then exported into Microsoft Excel to determine the relative density of the peaks. The peak of one of the bands was used as the standard, and the relative density was calculated as one. For each of the bands the percentage was calculated by dividing by the peak from the sample by the control (shown in Appendix 10.8.1). Each of these relative density values were calculated as a percentage and depicted as a column graph using Microsoft Excel software.

4.10 *TNF-α ELISA*

4.10.1 **Preparation of the ELISA Microplate**

High covalent binding plates were coated with 100µL of primary 'capture' antibody at a concentration of 1µg/mL (polyclonal antibody). The plate was sealed using a film and incubated overnight at room temperature. The capture antibody was removed using the nunc-immuno 8 plate washer (Thermo Scientific). The wells were washed using a wash procedure which consisted of four washes with 300µL of wash buffer (0.05% Tween-20 in 1x PBS). After the four washes block buffer was pipetted into each well and was incubated for 1 hour at room temperature. The block buffer was removed using the nunc-immuno 8 plate washer and wells were washed using the above washing procedure.

4.10.2 **TNF-α ELISA Protocol**

Serial dilutions of the standards were prepared using a two-fold dilution, with standards being 2000pg/mL, 1000pg/mL, 500pg/mL, 250pg/mL, 125pg/mL, 62.5pg/mL and 31.25pg/mL of TNF-α. The Murine TNF-α standards were pipetted in duplicate. The supernatants from RAW 264.7 cells were diluted in the diluent (0.05% Tween-20 , 0.01% BSA in 1x PBS) with a dilution factor of 10, 100 or 1000 depending on activation status of the cells and the amount of LPS and IFN- γ used for activation of the cells, with differing amounts used as shown in Figure 17A. Dilutions were not required for the supernatants of the non-activated cells due to the low levels of TNF-α produced in non-activated RAW 264.7 cells. After the standards and samples were diluted, they were incubated at room temperature for a minimum of 2 hours. The plate was then washed using the washing procedure described above.

At a concentration of 0.5µg/mL, 100µL of the detection antibody was pipetted into each well and incubated at room temperature for 2 hours. The plate was washed using the same washing procedure as described earlier. Horseradish peroxidase (Avidin-HRP) was diluted 1:2000 in the diluent and 100µL was pipetted into each well and was left for 30 minutes at room temperature. The Avidin-HRP was removed using the nunc-immuno 8 plate washer and the plate was then washed using the above washing procedure. 100µL of the 2,2′-Azino-bis (3-ethylbenzthiazoline-6-sulfonic acid) (ABTS) liquid substrate was pipetted into each well. The plate was left for approximately 30 minutes incubating at room temperature, for colour to develop on the standards (Figure 17A). An ELISA plate reader set at 405nm with a wavelength

correction at 650nm was used to quantify the absorbance values. A standard curve was produced in Microsoft Excel using $y = mx + b$, the total protein concentration x was calculated by rearranging the formula and substituting the protein's absorbance value for y (example shown in Figure 17B). All readings were corrected by subtracting the blank from all the values and were multiplied by their dilution factor. This provided the total TNF-α concentration in pg/mL which was graphed and presented in results section 5.4.

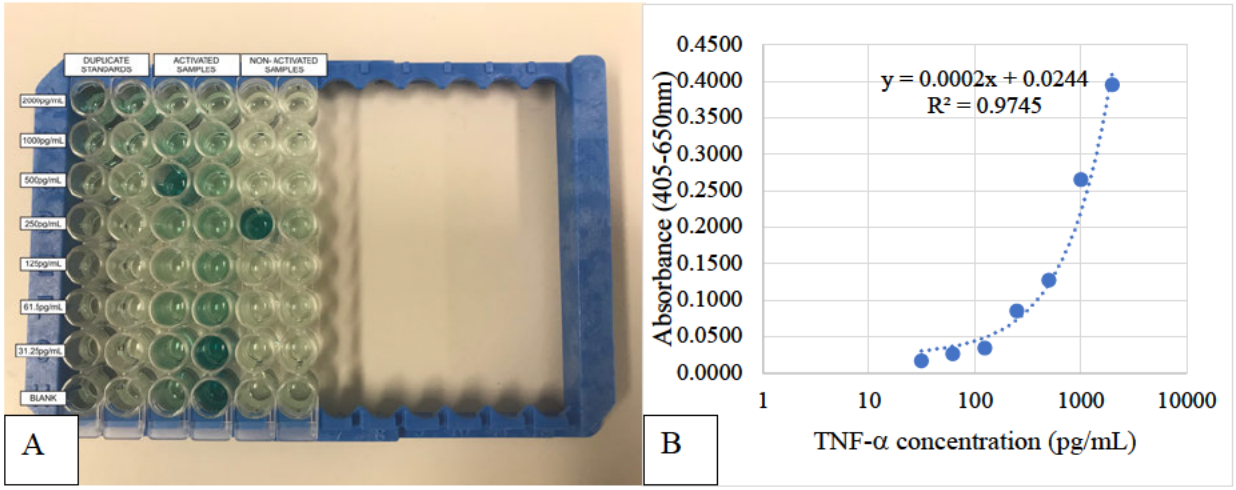

Figure 17: TNF-α ELISA plate layout and a Microsoft Excel graph of a standard curve.
A) Example of the layout of the TNF-α ELISA performed. B) Example of the TNF-α standard curve of the standard concentrations 2000pg/mL, 1000pg/mL, 500pg/mL, 250pg/mL,125pg/mL, 62.5pg/mL and 31.25pg/mL Raw absorbance values at 405-650nm and plate layout are shown in Appendix 10.1.33 and 10.1.34, respectively.

The non-activated samples had much lower TNF-α concentrations as expected (see results section 5.4.1) and Figure 17A contains an activated sample in the 4th well from the top in the first row of the samples labelled non-activated.

4.11 *IL-1β ELISA*

Pre-coated IL-1β wells were purchased from Invitrogen and 400µL of the 1x wash buffer (diluted from prepared 10x wash buffer using distilled water) was added to each well and was aspirated after around 10-15 seconds using the nunc-immuno 8 plate washer. This washing procedure was repeated twice. 100µL of sample diluent was pipetted into each well. Using serial dilutions prepared IL-1β standard at a concentration of 1000pg/mL was added to well A1. The contents of A1 were mixed and then 100µL was transferred to well A2. This procedure was repeated for the rest of the row to create concentrations of 500pg/mL, 250pg/mL, 125pg/mL, 62.5pg/mL, 31.25pg/mL, 15.625pg/mL, 7.8125pg/mL and a blank. Serial dilution procedure was repeated for row B. 100µL of each of the supernatants of the RAW 264.7 cells was pipetted into the well, or diluted, if necessary, in the diluent. 50µL of biotin conjugate was then pipetted into each well. The plate was covered using an adhesive film and was put onto a microplate rocker for 2 hours, incubated at room temperature. After two hours of incubation, the same wash procedure as described above was repeated four times. 100µL of diluted (1:200) streptavidin HRP was added to each well. The plate was covered using an adhesive film and was put onto a microplate rocker for 2 hours at room temperature.

After 1 hour of incubation, the same wash procedure as described above was repeated four times. 100µL of Tetramethyl-benzidine (TMB) substrate solution was pipetted to all the wells and was incubated at room temperature for approximately ten minutes away from direct sunlight. The stop solution (1M phosphoric acid) was added once the colour had developed, where the highest standard started to develop a dark blue colour. The addition of the stop solution caused the yellow colour of the wells shown in Figure 18A. A standard curve was produced in Microsoft Excel using $y = mx + b$, the total protein concentration x was calculated by rearranging the formula and substituting the protein's absorbance value for y (example shown in Figure 18B). All readings were corrected by subtracting the blank from all the values and were multiplied by their dilution factor. This provided the total IL-1β concentration in pg/mL which was graphed for further analysis.

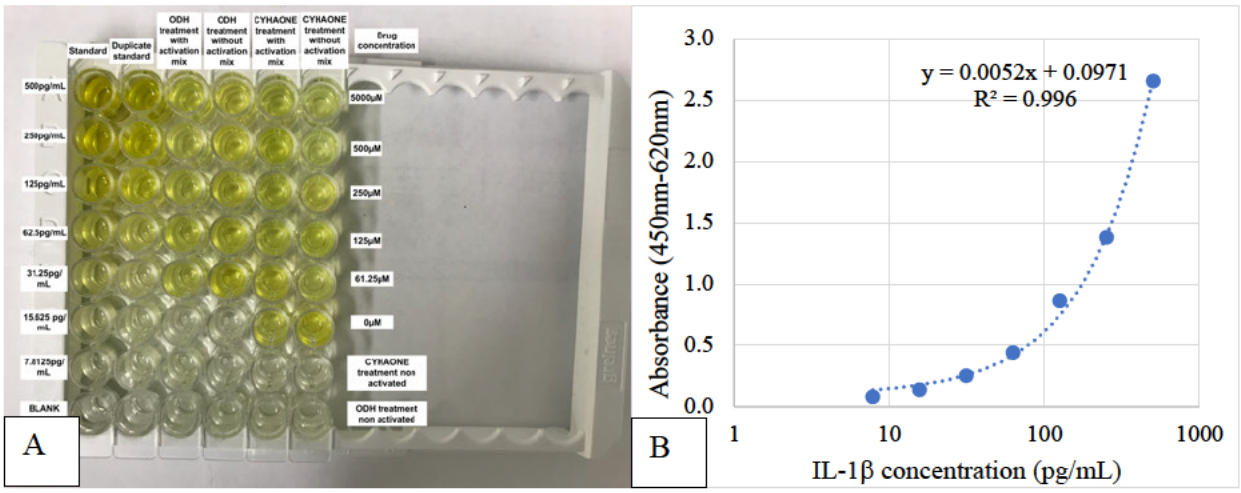

Figure 18: IL-1β ELISA plate layout and a Microsoft Excel graph of a standard curve.

A) IL-1β ELISA with the stop solution. B) Example of a standard curve for the IL-1β ELISA based on the standards and the curve was then used to calculate the IL-1β concentration of activated and non-activated cells (see results in section 5.5). Absorbance values and plate layout are shown in Appendices 10.1.35 and 10.1.36, respectively.

4.12 *Statistical Analysis*

Microsoft Excel (version 16.41) was utilised for the analysis of the distribution of data entries. Real statistics resource pack was the Microsoft Excel add-in used. One-way analysis of variance (ANOVA) with Tukey's HSD (honestly significant difference) post hoc test was used to compare various means. The level of significance was indicated as follows *$p<0.05$, ** $p<0.01$ and *** $p<0.001$. Note that only experiments with N equal to or greater than 3 were analysed for statistical significance and data analysed have error bars shown in the results section.

5.0 Results

5.1 *Activation of RAW 264.7 Macrophages*

5.1.1 Methodological Considerations of Activating RAW 264.7 Macrophages

In this experiment two different concentrations of FCS were tested (0.1% and 10%). Differing cell growth rates were evident within the different FCS concentrations as well as the non-activated versus activated RAW 264.7 macrophages. Williams et al. (2016) as discussed in section 4.1 showed mice macrophages incubated with LPS with no serum had a stronger pro-inflammatory response and are in the arrested phase of the cell cycle, which is consistent with the results shown in Figure 19. Optimisation of the activation protocol of the RAW 264.7 macrophages was necessary to predict the growth rate of the cells. Knowledge of the growth rate of the macrophages was essential in being able to effectively time the drug treatment and optimise the drug concentration per test drug. The lower concentration FCS (0.1%) was used to reduce the risk the confounding effects of contact inhibition occurring. Contact inhibition is the process in which the cells begin to arrest as soon as they contact one another. The close observation and optimal growth times should be accounted for to form a monolayer of cells in the culture flask, to ensure that the cells continue to proliferate and prevent contact inhibition from impinging on the cell culture results (Seluanov et al. 2009).

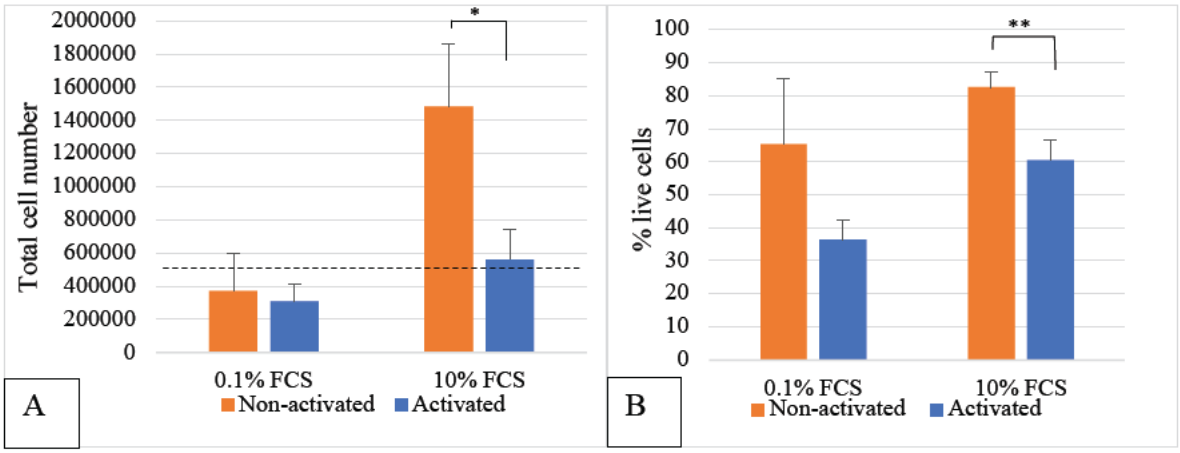

Figure 19: Optimisation of cell growth using different amounts of FCS.

A) Average total cell number in non-activated (orange) and activated cells (blue) with 2µg/mL of LPS and 2U/mL of IFN-γ for 24 hours. The broken line indicates the cell density seeded at the beginning of the experiment. B) Average percent of live cells in non-activated (orange) and activated cells (blue) with 2µg/mL of LPS and 2U/mL of IFN-γ for 24 hours. Raw cell counts and statistical analysis are shown in Appendix 10.2.1, 10.2.2-10.2.5 respectively. N=3. *= $p<0.05$ and ** =$p<0.01$ and statistical analysis was performed as per section 4.12.

Figure 19A illustrates the growth of RAW 264.7 cells incubated in 10% FCS compared to 0.1% FCS. There was no statistical difference between 0.1% FCS non-activated and activated RAW 264.7 cell number ($p=0.4$). Comparatively, there was a significant difference between the total number of cells non-activated to activated RAW 264.7 cells with 10% FCS ($p=0.018$). Furthermore, Figure 19B shows a larger proportion of live cells in non-activated RAW 264.7 cells compared to the activated cells obtained using the Trypan blue assay. There was no statistical significance between the percentage live cells in the non-activated and activated RAW 264.7 macrophages in 0.1% FCS ($p=0.14$). Whereas there was statistical significance between the % live cells in the non-activated and activated RAW 264.7 macrophages in 10% FCS ($p=0.0096$).

From these data, the rest of the experiments performed in this thesis used 0.1% FCS. Furthermore, due to the large change in the colour of the media, as well as the rapid growth in the non-activated cells grown in 10% FCS, growth shown in Figure 19A, mitosis of the cells was noted. To be able to optimise the protocols for activating the RAW 264.7 macrophages, routine observation under the light microscope and viability analysis via Trypan blue assay was conducted.

5.1.2 **Morphological Changes in Activated RAW 264.7 Macrophage Cells**

Distinct morphological changes were visible 6 and 24 hours after the activation of the RAW 264.7 cells with 1 µg/mL of LPS and 1U/mL of IFN-γ. For all further experiments the cells were seeded at $0.5x10^6$ cells per well, in order to prevent 'contact inhibition' from occuring. Cell seeded at densities of $1x10^6$ became largerly overconfluent, which could potentially affect the viability of the cells (shown in Figure 20). The lower cell density also allowed for easier observation of cell morphology in the drug treatment experiments (see section 5.2.2).

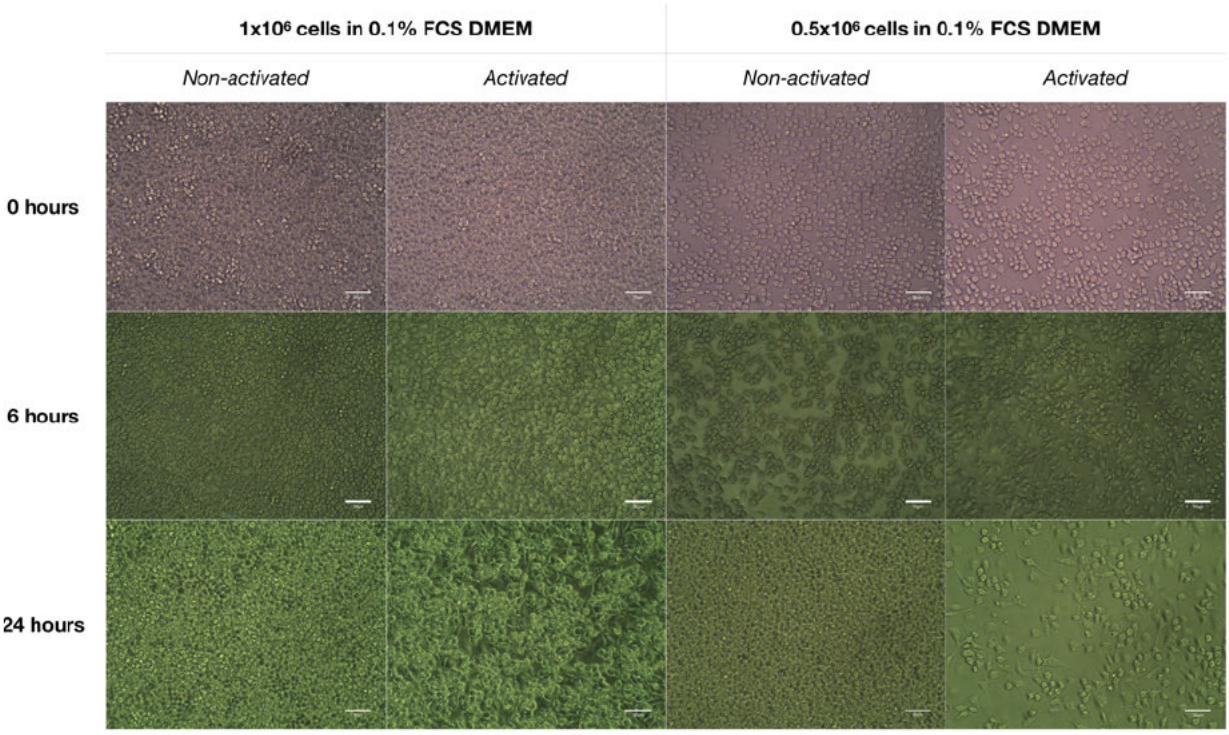

Figure 20: Light microscopy imaging (20x magnification) illustrating the morphological differences in non-activated and activated RAW 264.7 macrophages over time.

Comparison of RAW 264.7 macrophages activated with 1µg/ml of LPS and 1U/ml of IFN-γ for 6-24 hours, compared to non-activated 264.7 cells at different cell densities. Scale bar indicates 50µm.

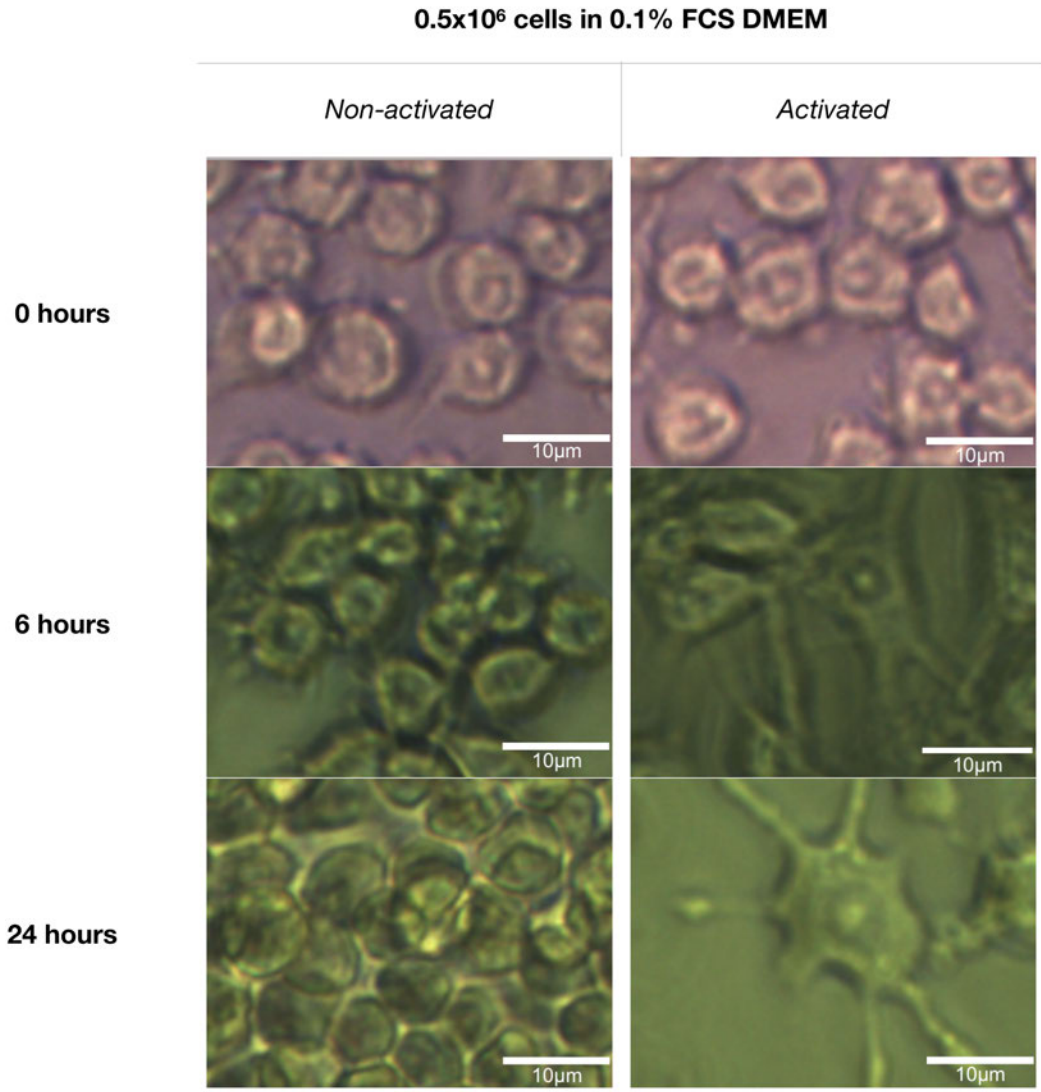

Figure 21: Morphological features of RAW 264.7 macrophages before activation, 6 hours activated, and 24 hours activated. Scale bar indicates 10µm.

Morphological features that were apparent in the RAW 264.7 macrophages before the activation mix (1µg/mL of LPS and 1U/mL of IFN-γ) was applied showed circular uniform cells when seeded at $0.5x10^6$ cells per well (Figure 21). When the RAW 264.7 macrophages were activated with 1µg/mL of LPS and 1U/ml of IFN-γ for 6 hours, there was pseudopodia like spreading. Comparatively, the cells that were non-activated for 6 hours showed little change in morphology compared to cellular morphology prior to activation. RAW 264.7 macrophages activated for 24 hours demonstrated an irregular morphology with prominent pseudopodia like processes. The control cells not activated with LPS or IFN-γ for 24 hours demonstrated a distinct and consistent round shape, with the cell's confluency being much larger than the 24 hour activated cells. The colour change in the images is due to the pH change of the phenol red of the DMEM due to the cell growth and nutrient uptake.

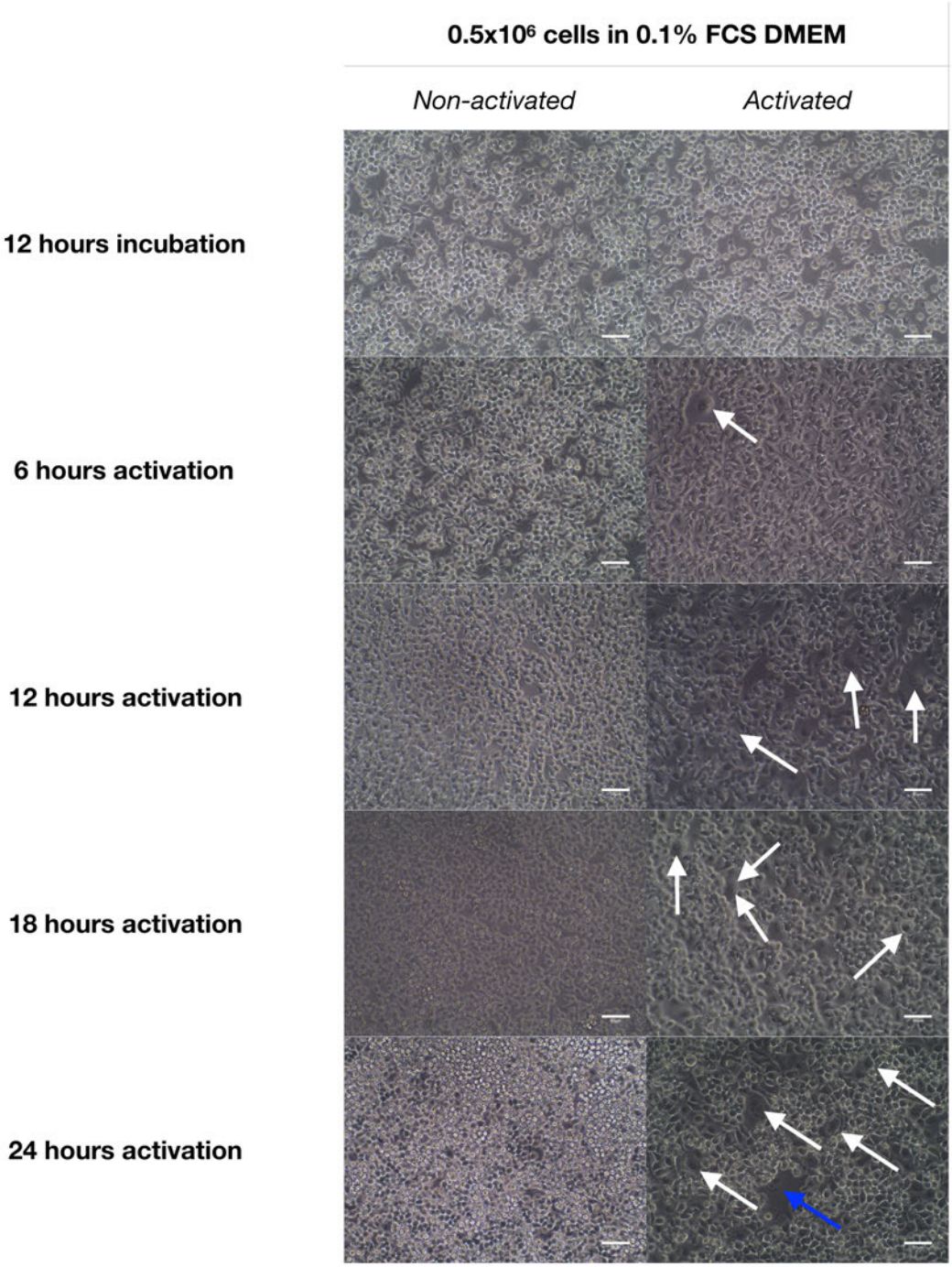

Figure 22: Light microscopy image (20x magnification) demonstrating cellular swelling.
Swelling was evident in the RAW 264.7 macrophages that were activated with 10µg/ml of LPS and 10U/ml of IFN-γ. The white arrows indicate cell swelling and the blue arrow indicates a potential lytic cell. Scale bar indicates 50µm.

A 24 well plate seeded at $0.5x10^6$ cells/well was incubated for 12 hours in 0.1% FCS DMEM. 0.1% FCS was heat inactivated to prevent the interference of complement protein (as discussed in section 4.1). After 12 hours, a subset of wells was treated with 10µg/mL of LPS and 10U/mL

of IFN-γ for four different time points, 6 hours, 12 hours, 18 hours and 24 hours. This tenfold increase in LPS and IFN-γ was used to exaggerate the effect of the activation on the cells, to see the change in morphology. The wells were in triplicates with half the plate being non-activated, which acted as the control. Photos were taken after each time point to illustrate the cell swelling that was occurring, as indicated by the white arrows (shown in Figure 22). There was a distinct morphological difference between the activated and non-activated cells, with no swelling seen in the non-activated RAW 264.7 cells. Comparatively, the activated cells showed increased swelling with each activation time point, as indicated by the white arrows. Shown in Figure 22, there was distinct cellular swelling observed even in the earlier time points. By the 24-hour activation time point, the majority of the swollen/flattened cells had presumably ruptured. The morphology of the RAW 264.7 cells in the 24-hour time point showed potential cell debris consistent with cell lysis, indicated by the white arrows in Figure 23.

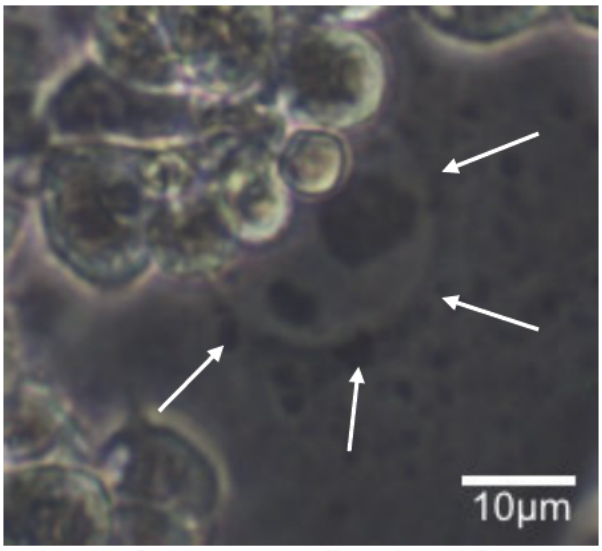

Figure 23: Light microscope image of RAW 264.7 cells activated for 24 hours. White arrows indicate blebbing around a cell. Scale bar indicates 10µm.

5.1.3 The Effect of LPS and IFN-γ on the Viability of the RAW 264.7 Macrophage Cells

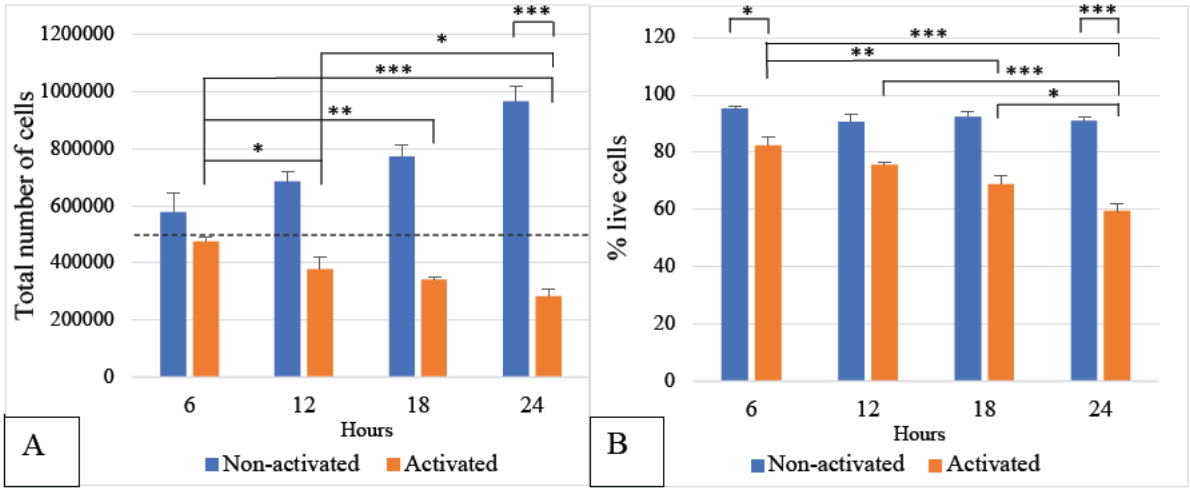

Figure 24: Graph demonstrating the effect of LPS and IFN-γ on the number and % live RAW 264.7 cells.

A) Average total number of cells at each time point showing activated and non-activated 264.7 cells. The dotted line indicates the cell density at which the experiment was seeded at. B) Average percentage of live cells in activated and non-activated 264.7 cells per time point using the Trypan blue assay. Cell counts are shown in Appendix 10.2.18. Statistical analysis shown in Appendix 10.2.6-10.2.17. N=3.

As shown in Figure 24A the number of non-activated (control) cells was not significantly different between the 6 and 12-hour incubation time point (p=0.18) before increasing significantly at 18 and 24 hours (p=0.013, p=0.0002 respectively). Please note these significant values have not been graphed in Figure 24A, statistical analysis is shown in Appendix 10.2.9. In contrast, within the number of activated RAW 264.7 macrophages, the total cell number reduced significantly at 6 and 12 hours (p=0.0295), 18 hours (p=0.0034) and 24 hours activation (p=0.0003). Statistical analysis shown in Appendix 10.2.11.

The non-activated RAW 264.7 macrophage viability (% live cells) remained at ~95% to 24 hours whereas, activated cell viability progressively declined to 60% over 24 hours (Figure 24 B). Significant differences in viability of non-activated and activated cells were observed at 6-hours (p=0.0339) and 24-hour time points (p=0.0123). Whereas the graded decline in viability of activated cells significantly differed between the 6 hour and 18-hour (p=0.0018) and 24 hours (p=0.00004), as well as between the 12 and 24 hour (p=0.0005) and 18 and 24-hour activation time point (0.0151). There were significant changes in the total cell number and viability of activated RAW 264.7 macrophages.

5.2 *Drug Treated RAW 264.7 Macrophages*

5.2.1 **Morphological Changes in Drug Treated RAW 264.7 Macrophage Cells**

The RAW 264.7 cells used for this experiment are classified as M1 macrophages as the cells were activated using LPS and IFN- γ, which are proinflammatory cells (Taciak et al. 2018; Williams et al. 2016). In Figure 25, the white arrows indicate the remnants of cells that were activated with LPS and IFN-γ and treated with 250µM of cyclohexanone. The red arrows in Figure 25 are pointing to a cell that is multi-nucleated, containing three nuclei. This could be an interruption to the cell division or could be macrophage fusion, see section 6.2.1 for further discussion. The white arrows show swollen cells, whereas the blue arrows are indicative of elongated pseudopodia like morphology of the cells.

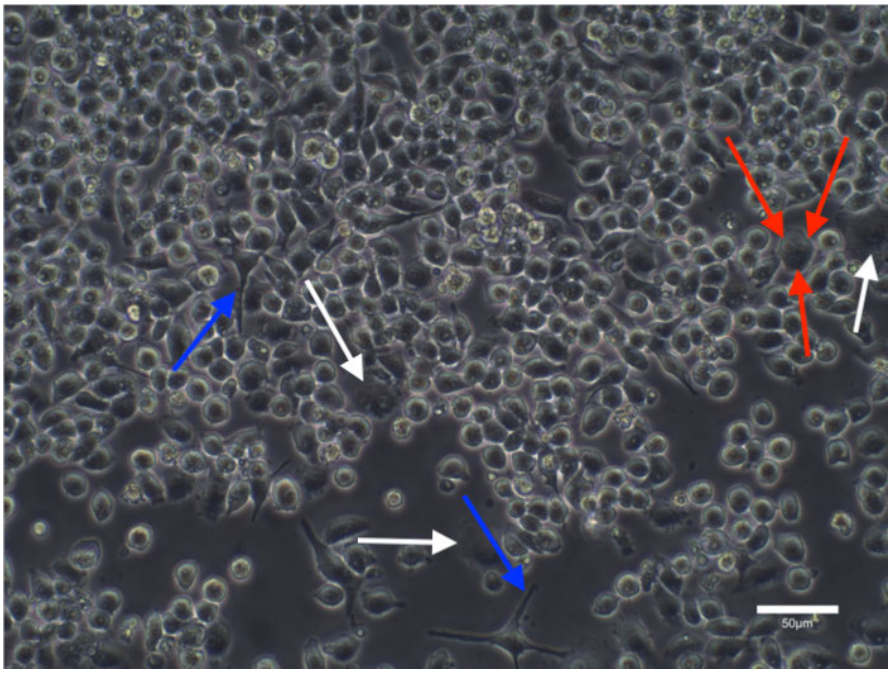

Figure 25: Light microscopy image (20x magnification) showing morphological changes in cyclohexanone treated RAW 264.7 cells.

Cells activated with 1µg/mL of LPS and 1U/mL of IFN-γ treated with 250µM of cyclohexanone in 0.1% FCS for 18 hours. The blue arrows show the distinct morphology of the activated cells, and the white arrows indicate swollen cells and the red arrow shows an example of a multi-nucleated RAW 264.7 cell. Scale bar indicates 50µm.

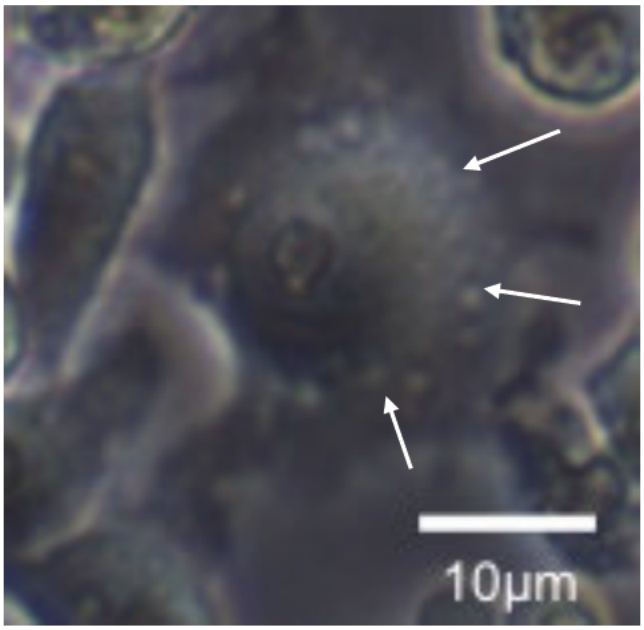

Figure 26: Light microscopy image (20x magnification) showing potential blebbing around macrophages. RAW 264.7 macrophages treated with 250µM of oxalyldihydrazide in 0.1% FCS. Scale bar indicates 10µm.

In Figure 26, the light microscopy image illustrates the presence of potential membrane blebbing, examples are indicated by the white arrows. This morphological change occurred with the presence of both CPZ breakdown products after 12 hours drug treatment in 0.1% FCS.

5.2.2 Morphological Changes in Drug Treated RAW 264.7 Cells

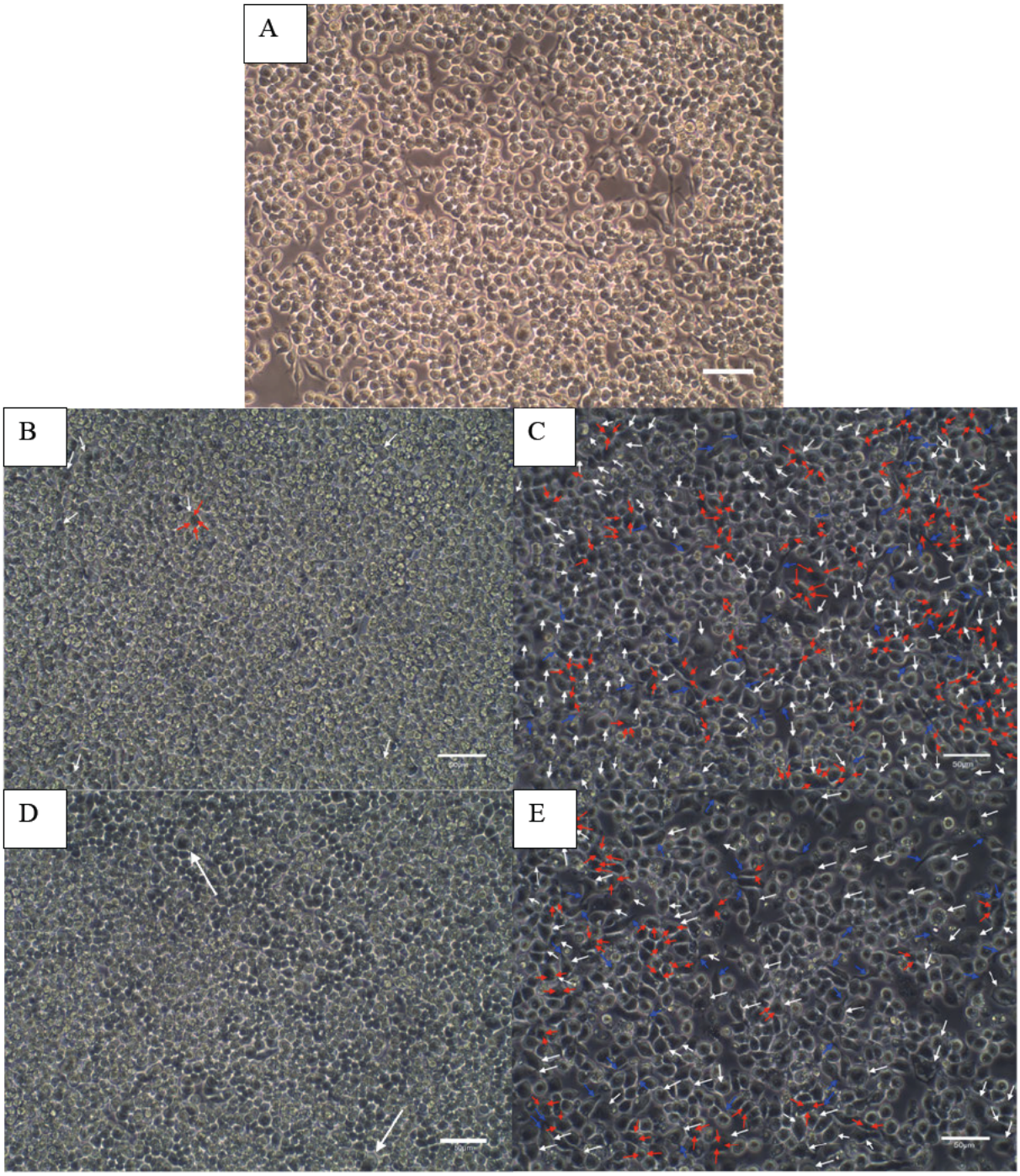

Figure 27: Light microscopy image (20x magnification) of RAW 264.7 cells treated with CPZ breakdown products.

A) Light microscopy image of non-activated RAW 264.7 cells after 12 hours incubation. B) Light microscopy image of non-activated RAW 264.7 cells after treatment with 125µM of cyclohexanone (D) and 125µM of oxalyldihydrazide (D). Light microscopy image (20x magnification) of activated RAW 264.7 cells after 12 hours of treatment with 125µM of cyclohexanone (C) and oxalyldihydrazide (E). Red arrows indicate examples of swollen/multi-nucleated cells. White arrows indicate swollen cells and the blue arrows indicate elongation of the RAW 264.7 macrophages. Scale bar indicates 50µm.

Figure 27A shows the cellular morphology of RAW 264.7 cells seeded at $0.5x10^6$ cells per mL, without activation or drug treatment. The morphology of the cells shows consistent cell size, with no swollen cells observed. Figure 27 (B and C) allow for the comparison between the morphology in RAW 264.7 cells treated with 125μM of cyclohexanone, that were either activated in 1μg/ml of LPS and 1U/ml of IFN-γ (C) or non-activated (B). The most notable observed change between the activated and non-activated RAW 264.7 macrophage cells is the number of cells. In Figure 27, non-activated, drug treated cells (B and D) microscopically showed larger cell numbers compared to the activated drug treated cells (C and E).

Furthermore, there was a distinguishable difference in the swollen-like cells identified between Figure 27 (B & C). Within Figure 27B the white arrows point to minimal swollen cells and the red arrow indicates one RAW 264.7 macrophage cell containing three nuclei. Whereas, in Figure 27C in the cyclohexanone activated RAW 264.7 macrophage cells, there are significantly more swollen cells, with examples shown by the white arrows. There is also an observable change in the morphology of the cells in terms of the shape, with the non-activated cells showing a more spherical shape, and the activated cells showing a more irregular shape, which is consistent with the activation of the RAW 264.7 macrophage cell line.

Figure 27D shows there was a low prevalence of swollen cells within the non-activated cells, treated with 125μM of oxalyldihydrazide. Figure 27E shows there was an increase in the prevalence of the swollen cellular morphology of the RAW 264.7 cells that were activated with 1μg/ml of LPS and 1U/ml of IFN-γ and treated with 125μM of oxalyldihydrazide. In Figure 27E, within the activated oxalyldihydrazide treated cells there are numerous multi-nucleated cells, indicated by the red arrows. Comparatively, there were more multi-nucleated cells in the cyclohexanone treated cells compared to oxalyldihydrazide treated cells, which is further shown in Figure 29.

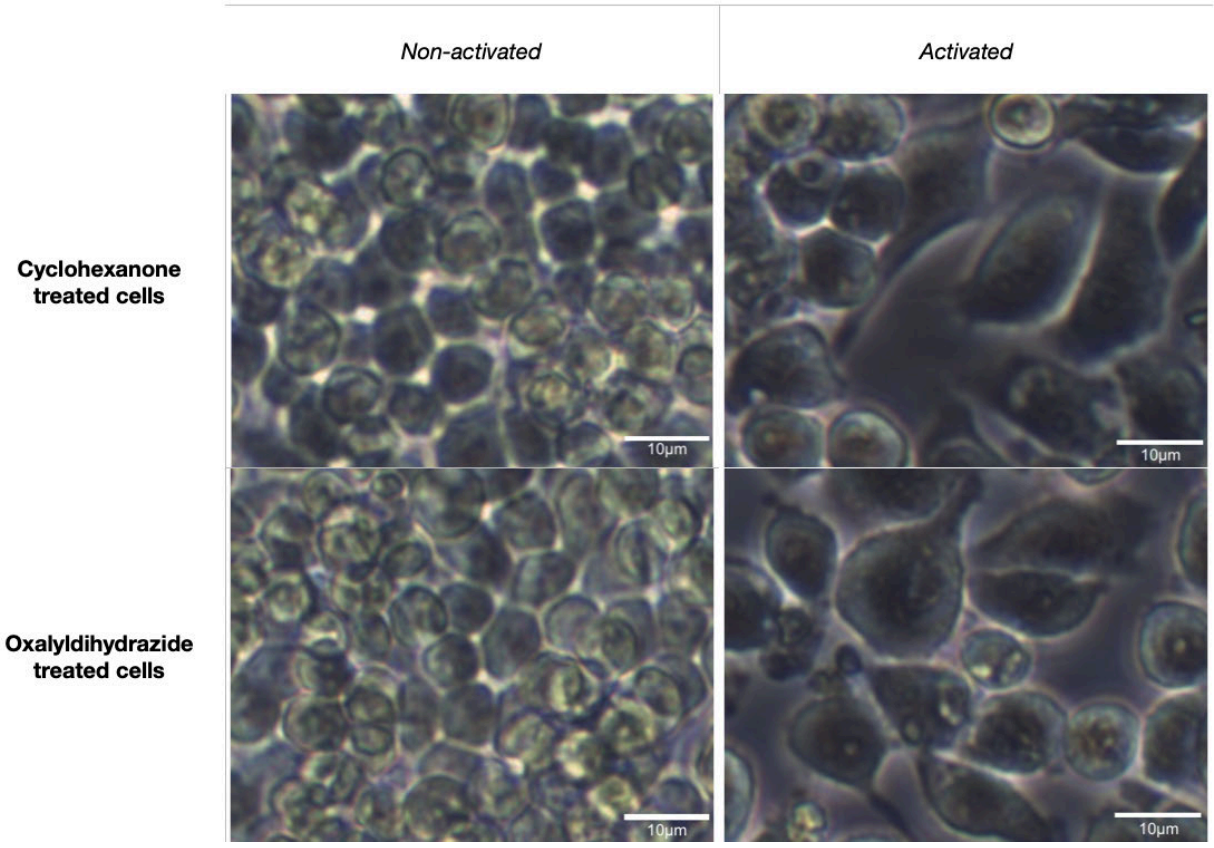

Figure 28: Light microscopy image of the morphology of RAW 264.7 cells treated with 125µM of cyclohexanone or oxalyldihydrazide. Scale bar indicates 10µm.

Figure 28 shows a close-up image of the RAW 264.7 macrophages that are either activated or non-activated and treated with cyclohexanone or oxalyldihydrazide. Consistent with previous experiments of non-activated RAW 264.7 macrophages (Figure 21) the morphology of the cells are circular and fairly consistent in shape and size. Whereas the cyclohexanone and oxalyldihydrazide treated cells that were activated with 1µg/mL of LPS and 1U/mL of IFN-γ show swollen and elongated cells. Amongst the cells treated with cyclohexanone are cells containing multiple nuclei. The different coloured cells that appear to be floating in the non-activated RAW 264.7 macrophages show that the cells are forming numerous layers of cells due to cell replication, which are no longer present in an optimal monolayer.

5.2.3 The Presence of Multinucleated Macrophages in RAW 264.7 Cells

Light microscopy was used in two different experiments of the cyclohexanone and oxalyldihydrazide treated RAW 264.7 macrophages and cells were photographed using the Luminoptic ISH500 eyepiece camera. The number of multinucleated cells were counted from the photographs manually. Figure 29 shows an increase in the number of multinucleated cells increasing with the increased concentration of drug treatment. These data suggest that the breakdown products of CPZ may be involved in the formation of MNGCs.

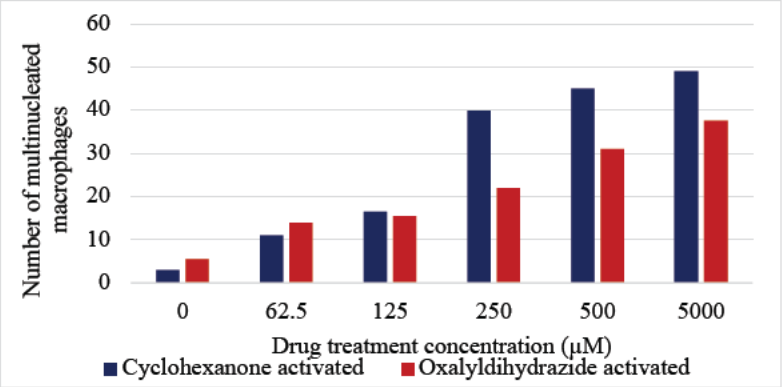

Figure 29: Average number of multi-nucleated cells in a sample of RAW 264.7 cells.
Cells treated with varying concentrations of cyclohexanone/oxalyldihydrazide for 16 hours (N=2). Raw counts shown in Appendix 10.2.19.

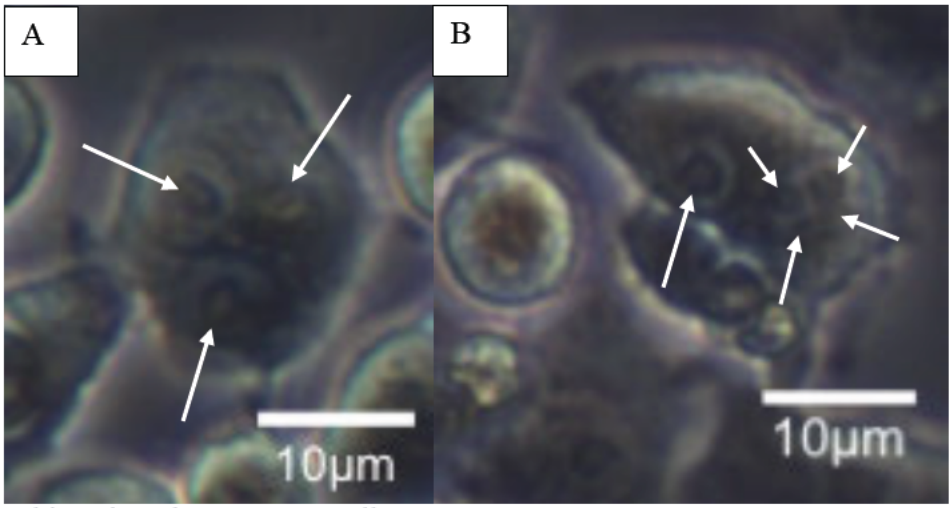

Figure 30: Multi-nucleated RAW 264.7 cells.
A) RAW 264.7 cell treated with 125µM of cyclohexanone showing multiple nuclei. B) RAW 264.7 cell treated with 125µM of oxalyldihydrazide showing multiple nuclei. White arrows indicate nuclei.

Shown in Figure 30 (A and B), multi-nucleated cells were evident in the drug treated RAW 264.7 cells. Figure 30A showing 3 nuclei and Figure 30B showing 4 nuclei and potentially a separate nucleus to the left. This could indicate an interruption to cytokinesis or potentially the formation of MNGCs.

5.3 *Cellular Analysis of Drug Treated RAW 264.7 Macrophages*

5.3.1 Cell Analysis of RAW 264.7 Macrophages Treated with Cyclohexanone or Oxalyldihydrazide with Trypan Blue

Optimisation of the protocols for the activation and drug treatment of RAW 264.7 macrophages was undertaken in order to determine the effects of CPZ breakdown products on non-activated (control), activated cells and re-activated cells (cells that were re-exposed to the activation mix when drug treated). Shown in Figure 31A, exposure of 1μg/mL of LPS and 1U/ml of IFN-γ with the drug treatment (indicated as the re-activated cells) to increasing concentrations of cyclohexanone resulted in reduced cell numbers. When the RAW 264.7 cells were not re-activated in 1μg/mL of LPS and 1U/ml of IFN-γ during drug treatment (termed activated cells), the increasing concentrations of cyclohexanone resulted in higher cell numbers. A similar trend was seen in the number of live cells of activated and re-activated RAW 264.7 macrophages treated with cyclohexanone (Figure 31C).

Illustrated in Figure 31B the re-activated RAW 264.7 macrophages treated with increasing concentrations of oxalyldihydrazide resulted in a progressive reduction in cell numbers. Whereas the effect on the activated cells treated with increasing amounts of oxalyldihydrazide was an increase in cell numbers. The number of live cells reduced with the subsequent increase of oxalyldihydrazide when the RAW 264.7 macrophages were re-activated with LPS and IFN-γ (Figure 31D). However, the trend was not so clear when the RAW 264.7 macrophages were not placed in the activation mix when treated with oxalyldihydrazide, this could pertain to the solubility issues of oxalyldihydrazide. Similarly, to the effects of cyclohexanone, this demonstrates that both breakdown products are ultimately dependent on the activation status of the macrophages.

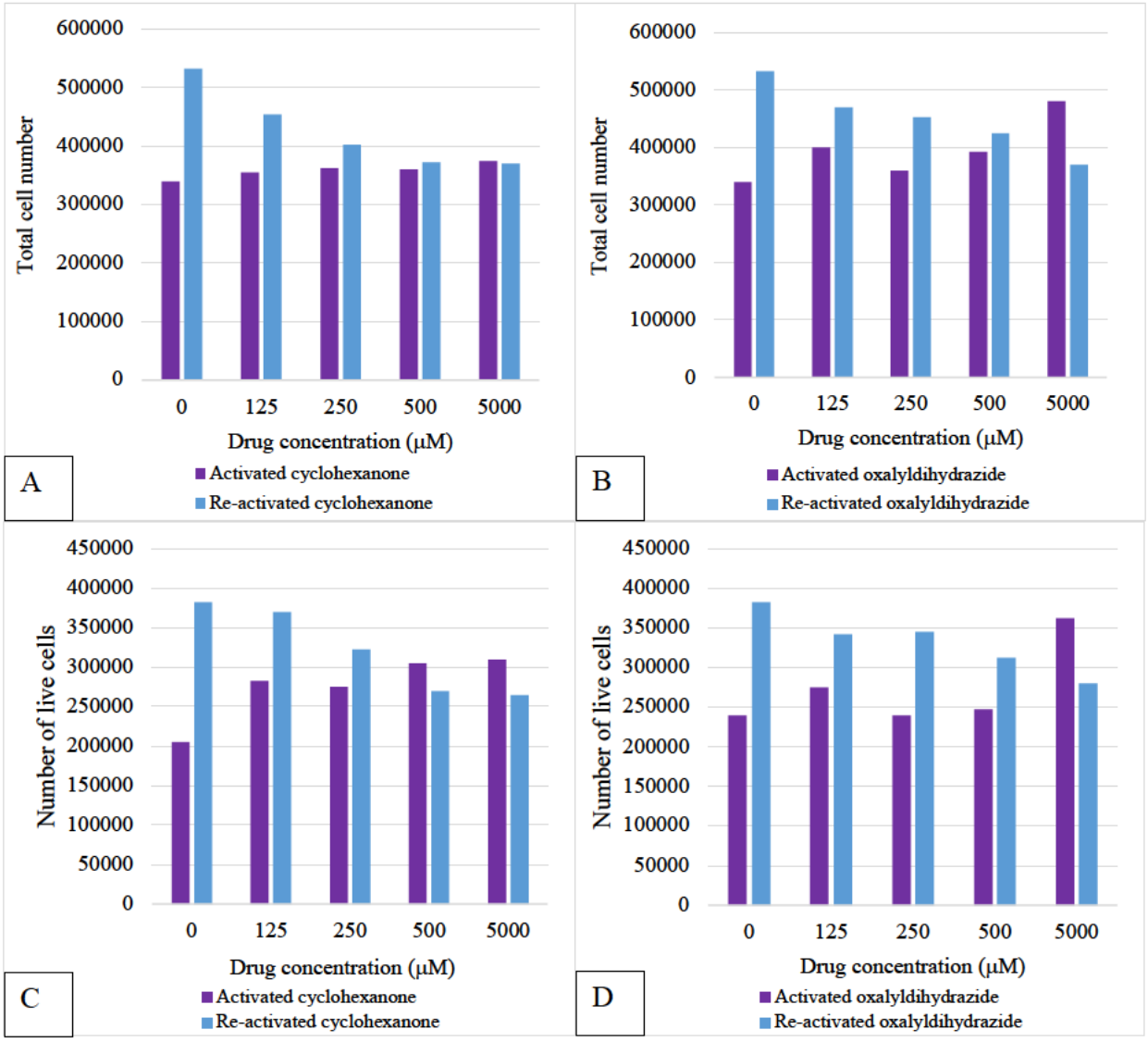

Figure 31: Total cell counts for activated and re-activated oxalyldihydrazide and cyclohexanone treated RAW 264.7 cells.

A) Total number of cells in the re-activated and activated cyclohexanone treated RAW 264.7 macrophages (16 hours) B) Total number of cells in the re-activated and activated oxalyldihydrazide treated RAW 264.7 macrophages. C) Number of live cells in the re-activated cyclohexanone treated RAW 264.7 macrophages. D) Number of live cells in the activated and re-activated oxalyldihydrazide treated RAW 264.7 macrophages. Cell counts are shown in Appendix 10.3.1-10.3.2. N=2.

5.3.2 Cell Analysis of RAW 264.7 Macrophages Treated with Cyclohexanone or Oxalyldihydrazide with Alamar Blue

In Figure 32 there were significantly higher FI values for all concentrations of cyclohexanone (A) and oxalyldihydrazide (B) in the non-activated cells compared to activated and re-activated RAW 264.7 macrophages. In Figure 32A there was not a clear trend in the activated cells treated with cyclohexanone. Overall, in comparison to the re-activated cyclohexanone treated cells, the activated cells had significantly lower FI values, with the exception of the cells treated with 125µM of cyclohexanone. However, in the oxalyldihydrazide treated cells the activated cells had significantly higher FI values compared to the re-activated drug treated RAW 264.7 macrophages. Interestingly, the highest FI value in the re-activated cyclohexanone treated cells was in the highest drug concentration (5000µM) (Figure 32A). This reinforces that the breakdown product, cyclohexanone, which may increase the pro-inflammatory response in the RAW 264.7 macrophages, which significantly increases the metabolic rate of the cells. This trend was not obvious within the oxalyldihydrazide treated cells, which appeared to have plateaued in the activated cells (Figure 32B), which may pertain to the solubility issues associated with the drug. Refer to Appendices for detailed statistical analysis.

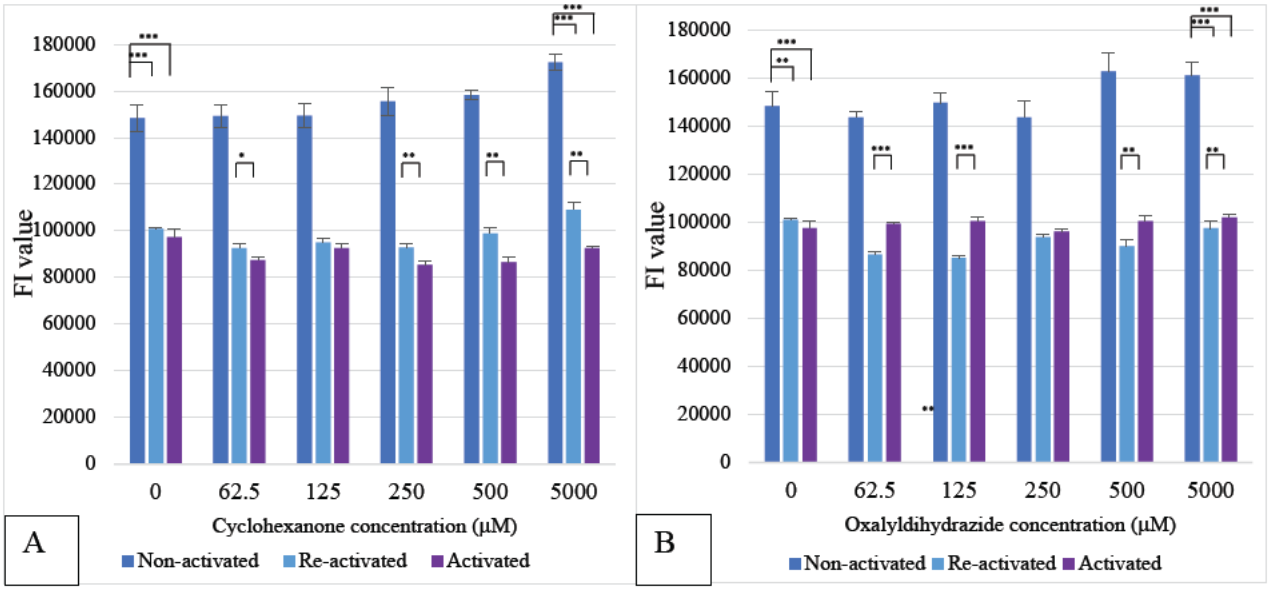

Figure 32: FI Values from Alamar blue assay of non-activated, re-activated and activated cells with 1µg/mL of LPS and 1U/mL of IFN-γ drug treated in 0.1% FCS.

A) FI values for cyclohexanone treated RAW 264.7 cells. Plate layout and absorbance values are shown in Appendix 10.4.1-10.4.4. Statistical analysis shown in Appendix 10.4.5-10.4.20. B) FI values for oxalyldihydrazide treated RAW 264.7 cells. Plate layout, absorbance values and statistical analysis are shown in Appendix 10.4.1-40.Cell counts shown in Appendix 10.3.1-10.3.2. N=3.

Due to the large influence of the measured FI values based on cell numbers, the data were analysed by dividing the raw FI values by either total cell numbers or live cell numbers. Shown in Figure 33A, when dividing the FI value by the live cells or total cell number when re-activated with cyclohexanone, similar to Figure 32, there was an increase in FI with the increased concentration of cyclohexanone. In Figure 33B this trend is not as clear, but it appears to have an increase in FI with the increased concentration of oxalyldihydrazide when the cells are re-activated. Figure 33C shows a decline in FI with the increased concentration of cyclohexanone when the cells are re-activated, with more of a plateau of FI values shown in the activated cells. In Figure 33D there was no clear trend which could allude to the solubility issues of oxalyldihydrazide. Based on this data, it is clear that the Alamar blue assay is largely reliant on the number of cells in each well.

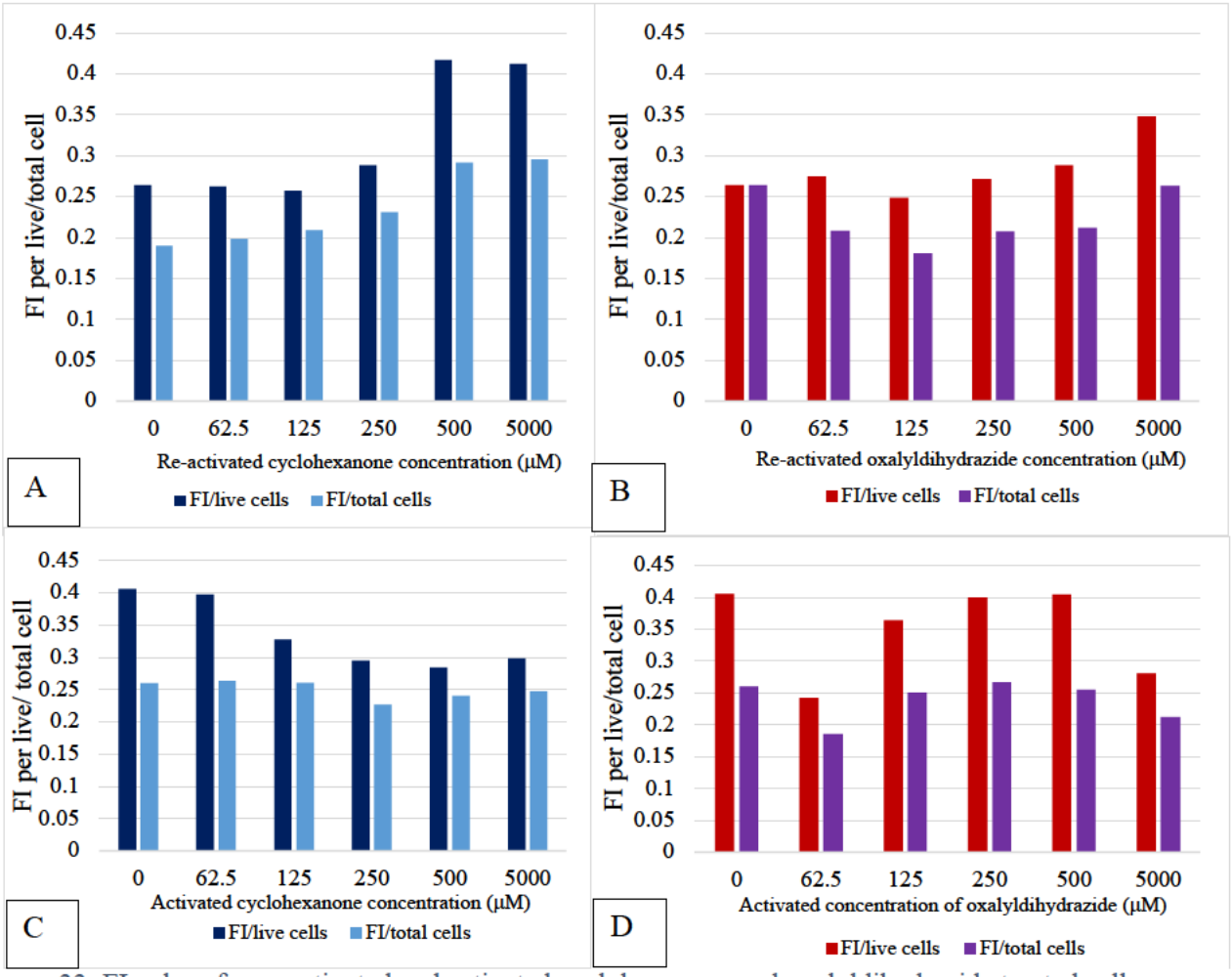

Figure 33: FI values for re-activated and activated cyclohexanone and oxalyldihydrazide treated cells. A) FI values per live and total cells from re-activated with 1µg/mL of LPS and 1U/mL of IFN-γ treated with cyclohexanone. B) FI values per live and total cells from re-activated oxalyldihydrazide treated cells. C) FI values per live and total cells from activated cyclohexanone treated cells. D) FI values per live and total cells from activated oxalyldihydrazide treated cells. Raw cell counts are shown in Appendix 10.3.1- 10.3.2. Plate layout and absorbance values are shown in Appendix 10.2.1-10.2.40.

Figure 33 can be compared to data of the breakdown products effect on total and live cell numbers, shown in Figure 31 which used the Trypan blue assay. The Trypan blue and Alamar blue assay showed opposing trends, however; collectively indicates an effect of the breakdown products of CPZ on cell number and metabolic activity and the consistent differences between activated and re-activated drug treated RAW 264.7 macrophages. Reiterating that the breakdown products have some effect on the macrophages that is dependent on activation status and may have to do with M1 to M2 continuum and/or some cellular pathway that is dependent on the activation state of the cell.

These were the only experiments where the Alamar blue assay was performed. This was because the assay analyses cell metabolism rather than cell viability. In order to get meaningful data, the cell counts were required which meant that the Trypan blue assay needed to be performed anyway and the FI data even when corrected for cell numbers (total or live) showed the opposite trend for drug treated cells than the cell numbers, see discussion section 6.8. Due to the gaps in knowledge on how CPZ impacts cellular metabolism and the mechanism of how Alamar blue is reduced; for the remaining experiments of cell viability after activation and drug treatments, the Trypan blue assay was used.

5.4 *Soluble TNF-α Release*

5.4.1 TNF-α Concentrations in Non-Activated and Activated RAW 264.7 Cells

The amount of soluble TNF-α present in supernatants increased over time (Figure 34). Interestingly, the large error bar at the 24-hour time point could be attributed to the cells overgrowing which may release TNF-α. Furthermore, the soluble TNF-α concentration was divided by the total number of cells to be able to analyse per cell how much soluble TNF-α was released. Cell supernatants were used for the TNF-α ELISA, and samples were run in triplicates.

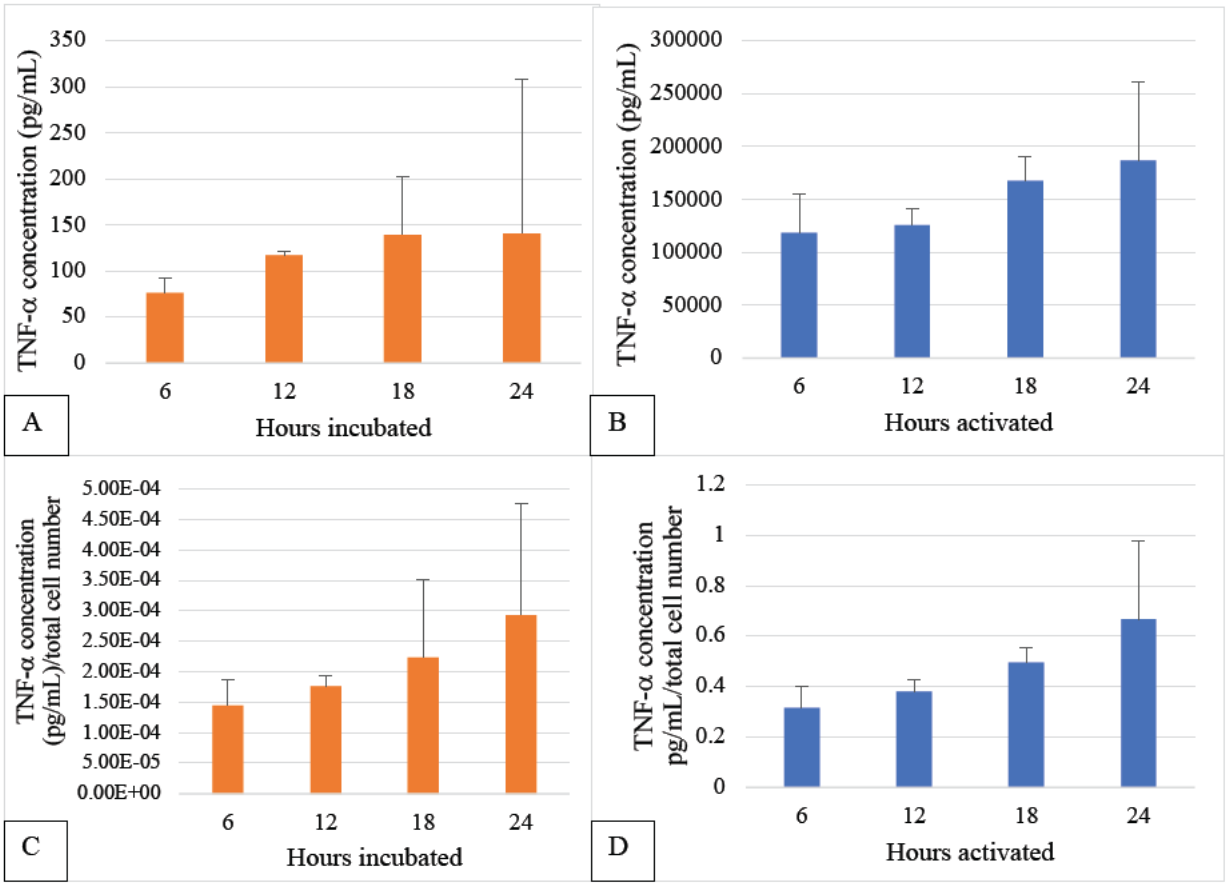

Figure 34: TNF-α concentrations in non-activated (orange) and activated (blue) RAW 264.7 macrophages.

A) TNF-α concentrations (pg/mL) at different time points in non-activated RAW 264.7 macrophages. B) TNF-α concentrations at different activation time points in activated RAW 264.7 macrophages. C) TNF-α concentrations (pg/mL) per total cell number in non-activated RAW 264.7 macrophages. D) TNF-α concentrations (pg/mL) per total cell number in activated RAW 264.7 macrophages. The raw cell counts are shown in Appendix 10.2.18 and statistical analysis is shown in Appendix 10.5.1-10.5.13. Absorbance values and plate layout are shown in Appendix 10.6.1 and 10.6.2, respectively. N=3.

TNF-α produced by non-activated RAW 264.7 macrophages, illustrated in Figure 34A, showed increased TNF-α concentration with each time point; however, this did not reach significance (p=0.169), shown in Appendix 10.5.1. TNF-α concentrations were analysed at 6, 12, 18 and 24-hour post activation. The TNF-α concentrations at any of the time points were not significantly different from each other (p=0.568), shown in Appendix 10.5.3. The RAW 264.7 macrophages were activated with 10μg/mL of LPS and 10U/mL of IFN-γ. Compared to Figure 34A, in Figure 34B the activated RAW 264.7 macrophages produced significantly higher amounts of TNF-α at the 6-hour time point (p=0.002). Similarly, at the 24-hour time point there was a significant difference between the TNF-α concentration between the non-activated and activated RAW 264.7 macrophages (p=0.0434). The error bar at the 24-hour activation time point is relatively large, this may be due to the variability in cell numbers contributing to different amounts of TNF-α produced after 24 hours activations 3 experiments. Based on these results, the protocol for the TNF-α measurements after drug treatment was adjusted to measure at 12 and 18 hours after activation.

The raw concentration of TNF-α was divided by the total cell number, where the cell count was obtained by the Trypan blue assay. In Figure 34C, the concentration of TNF-α per total cell number was the highest at the 24-hour time point in the non-activated RAW 264.7 cells. However, there was no significant difference between the TNF-α concentration per total cell across any of the time points (p=0.651). Furthermore, a similar pattern was shown in the activated RAW 264.7 macrophages shown in Figure 34D, where the TNF-α concentration per total cell number was not significantly different at any time point (p= 0.123).

5.4.2 TNF-α Concentrations in Response to Drug Treated RAW 264.7 Cells

Figure 35 illustrates the TNF-α concentrations after activating the cells for 12 hours with 1µg/mL of LPS and 1U/mL of IFN-γ, and then treating the RAW 264.7 cells with different concentrations of oxalyldihydrazide/cyclohexanone. Supernatants in this experiment were diluted 1:1000 due to the large amount of TNF-α produced. The raw values of TNF-α concentrations show very little differences in concentration of both cyclohexanone and oxalyldihydrazide treated 264.7 cells (Figure 35A).

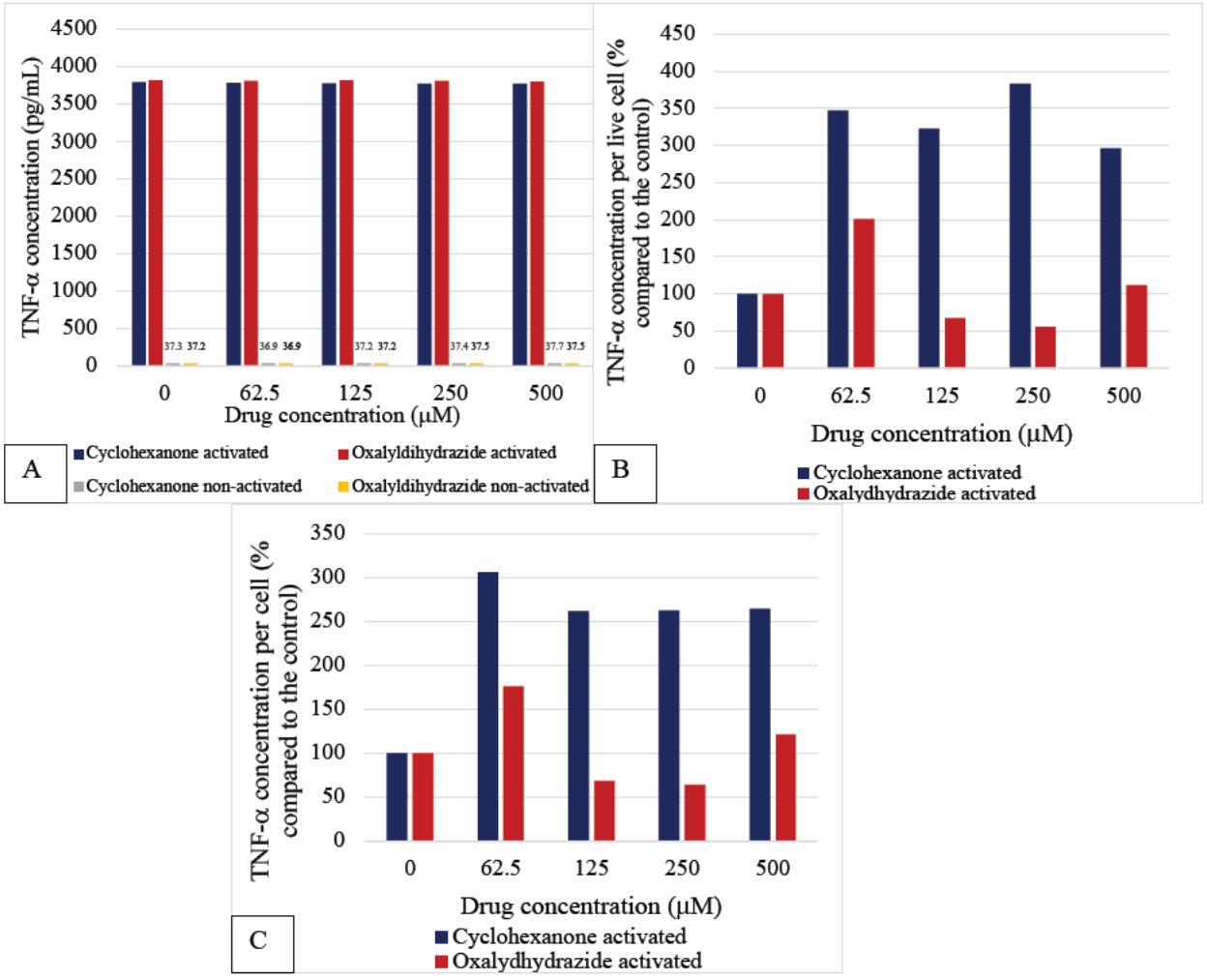

Figure 35: TNF-α concentrations in non-activated and activated cyclohexanone and oxalyldihydrazide treated RAW 264.7 macrophages.

A) TNF-α (pg/mL) in drug treated activated and non-activated RAW 264.7 cells. Absorbance values and plate layout are shown in Appendix 10.6.1-2. B) TNF-α concentration (pg/mL)/ number of live cells (%) in activated RAW 264.7 cells treated with cyclohexanone or oxalyldihydrazide. C) TNF-α concentration (pg/mL)/ total cells (%) in activated RAW 264.7 cells treated with cyclohexanone or oxalyldihydrazide. Cell counts are shown in Appendix 10.6.3-4.

In Figure 35A the TNF-α concentration in the non-activated cells showed virtually no change regardless of the cyclohexanone or oxalyldihydrazide concentration used to treat cells with. Cell supernatants were used for the TNF-α ELISA, the samples were diluted 1:10. Compared to the activated RAW 264.7 macrophages, the non-activated cells produced substantially lower concentrations of TNF-α. Furthermore, the activated RAW 264.7 macrophages produced similar concentrations of TNF-α when treated with cyclohexanone or oxalyldihydrazide (shown in Figure 35A).

When dividing the TNF-α concentration by the live cells, where the control was set at 100% (shown in Figure 35B), oxalyldihydrazide showed no clear trend, with a twofold spike in TNF-α occurring when the RAW 264.7 cells were treated with 65μM of cyclohexanone. This could be a result of the solubility issues with oxalyldihydrazide. In Figure 35B, compared to the control the TNF-α produced per live cells was at least three-fold higher with all the subsequent concentrations of cyclohexanone treated RAW 264.7 macrophages. Similar trends were evident when dividing the TNF-α by the total cells (shown in Figure 35C).

5.5 *IL-1β levels in Response to Activation and Drug Treatment*

This experiment was undertaken to analyse the differences in IL-1β production between non-activated, activated, and drug treated RAW 264.7 macrophages. The non-activated RAW 264.7 cells contained low concentrations of IL-1β. Interestingly, the cyclohexanone had a lower concentration compared to the control non-activated RAW 264.7 cells (as shown in Figure 36). Comparatively, the RAW 264.7 cells activated for 24 hours with 1ug/mL of LPS and 1U/ml produced more IL-1β relative to the non-activated drug treated cells. The RAW 264.7 macrophages treated with the breakdown products of CPZ, cyclohexanone and oxalyldihydrazide produced even larger levels of IL-1β, with oxalyldihydrazide producing more than cyclohexanone when treated for 24 hours. This experiment gave an overall profile of the cytokine production of different activated states and drug treatments for the RAW 264.7 macrophages.

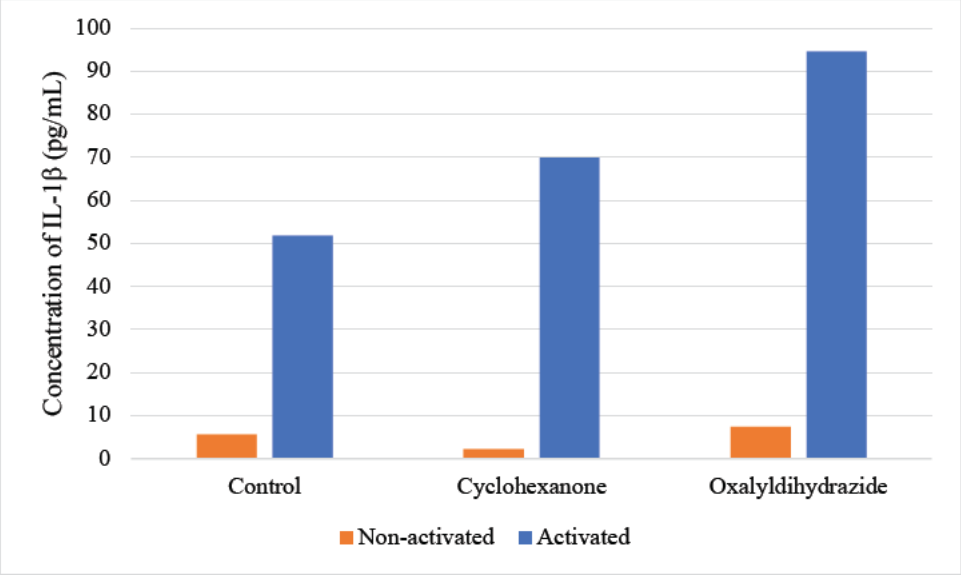

Figure 36: Concentration of IL-1β (pg/mL) in activated (1µg/mL of LPS and 1U/mL of IFN-γ for 24 hours) and non-activated RAW 264.7 macrophages, treated with cyclohexanone and oxalyldihydrazide (24 hours).

Raw absorbance values and plate layout are shown in Appendix 10.7.1 and 10.7.2, respectively.

5.5.1 IL-1β concentration in Cyclohexanone and Oxalyldihydrazide Treated RAW 264.7 Cells

In this experiment, optimisation of the activation of the RAW 264.7 macrophages was deemed valuable. Shown in Figure 36, there are differences in the IL-1β concentrations when treating the RAW 264.7 macrophages with cyclohexanone in activated versus non-activated states. The re-application of the activation mix when drug treating the cells was thought to be relevant due to the non-activated drug-treated cells producing IL-1β in very small concentrations (shown in Figure 36), highlighting the need for the application of the activation mix for the breakdown products of CPZ to take effect.

Figure 37A highlights the IL-1β produced by activated and re-activated RAW 264.7 macrophages treated with cyclohexanone. There was a considerable dose dependent response with the highest concentration of the IL-1β produced by the cells treated with the highest concentration (5000μM) of cyclohexanone re-suspended in the activation mix (1μg/mL of LPS and 1U/mL of IFN-γ). Whereas, in the activated RAW 264.7 cells where there was no activation mix reapplied, the highest concentration of IL-1β was found in control group with 0μM concentration of cyclohexanone. Figure 37A shows the concentrations of IL-1β in non-activated RAW 264.7 macrophages which was significantly lower than the activated and re-activated cells (ranging from 0-7.1pg/mL). Within the non-activated cells, the cells treated with the largest amount of cyclohexanone produced the largest concentration of IL-1β (7.1pg/mL).

Comparatively, shown in Figure 37B, the concentration of IL-1β does not follow a clear trend with the differing concentrations of oxalyldihydrazide when the RAW 264.7 macrophages were re-activated. In the activated oxalyldihydrazide treated cells there was a similar trend to cyclohexanone treated cells, with the highest concentration of IL-1β detected in the control group. Similar to the cyclohexanone treated RAW 264.7 cells, the cells not activated produced minimal amounts of IL-1β, ranging from 0-3.6pg/mL (shown in grey in Figure 37B).

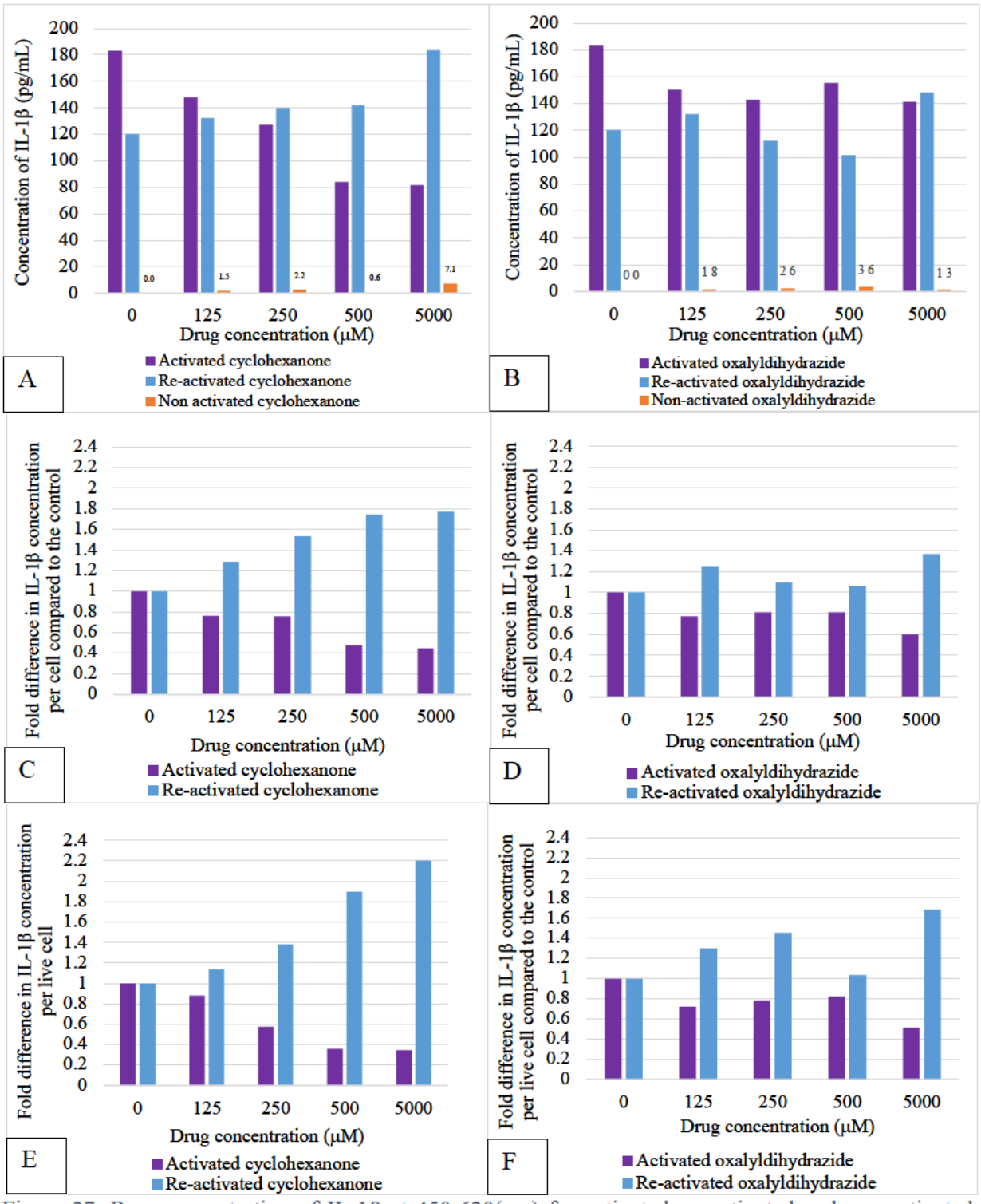

Figure 37: Raw concentration of IL-1β at 450-620(nm) for activated, re-activated and non-activated RAW 264.7 cells.

IL-1β concentration for RAW 264.7 cells treated with cyclohexanone (A) and oxalyldihydrazide (B). Absorbance values are shown in Appendix 10.7.3. Fold difference in IL-1β concentration (pg/mL) per total cell number in activated and re-activated cells treated with cyclohexanone (C) and oxalyldihydrazide (D). Fold difference in IL-1β concentration (pg/mL) per live cell number in activated and re-activated RAW 264.7 cells treated with cyclohexanone (E) and oxalyldihydrazide (F). Plate layout and cell counts are shown in Appendix 10.7.4 and 10.7.5-10.7.6, respectively.

To be able to analyse the IL-1β concentration data on a further level, the concentration of the IL-1β was divided by the total cell number, which was determined by the Trypan blue assay. In Figure 37C, the IL-1β concentrations per total cells treated with cyclohexanone are illustrated. In Figure 37C, in the re-activated cyclohexanone treated cells, the highest concentration of cyclohexanone (5000μM) produced almost a 1.77 fold higher concentrations of IL-1β. In the activated cells there was a 0.44 fold decrease of IL-1β concentration per total cells in the highest cyclohexanone treated cells (Figure 37C). In Figure 37E which illustrates the amount of IL-1β produced per live cells, the highest concentration of cyclohexanone (5000μM) produced more than 2.2 fold higher concentrations of IL-1β in the re-activated cells. Whereas, activated RAW 264.7 macrophages treated with 5000μM cyclohexanone contained 0.34 fold lower amounts of IL-1β, compared to the control (Figure 37E).

This opposing trend was also apparent in the oxalyldihydrazide treated cells in Figure 37D. In the re-activated cells treated with 5000μM of oxalyldihydrazide had 1.37 fold higher concentrations of IL-1β, compared to a 0.6 fold decline in the activated cells IL-1β concentration compared to the controls. This trend was not as obvious compared to the cyclohexanone treated cells. In Figure 37F the amount of IL-1β produced per live cells in the re-activated cells treated with 5000μM of oxalyldihydrazide there was a 1.68 fold higher concentrations of IL-1β, compared to the control. When the oxalyldihydrazide treated cells (5000μM) were activated there was a 0.51 fold lower concentration of IL-1β compared to the control (Figure 37F).

Similar to the IL-1β concentration per total cells with the breakdown products of CPZ, the IL-1β concentrations per lives cell shown in 37 (E and F) there was a similar trend in both breakdown products. However, in Figure 37F, there was a plateau in the activated cells after the control which may be due to the solubility issues of oxalyldihydrazide. There was also an outlier of IL-1β concentration in the re-activated cells treated with 500μM of oxalyldihydrazide which may be attributed to a pipetting error or solubility issue. Compared to oxalyldihydrazide, cyclohexanone treated re-activated RAW 264.7 macrophages had larger concentrations of IL-1β, denoting a stronger pro-inflammatory response in conjunction with the increased drug concentration.

5.6 *Protein Arginine Methylation in RAW 264.7 Cells*

5.6.1 **Protein Arginine Methylation in Non-Activated RAW 264.7 Cells**

Table 5 shows the cells that were used for the methylation experiments. The sample with the lowest cell passage number was the control and was set at 100% for the protein arginine methylation non-activated samples. When comparing the activated versus non-activated RAW 264.7 macrophages the non-activated samples were the control and set at 100%.

Table 5: RAW 264.7 cells used for Western Blots

Cell sample number	**Concentration**	**Activation Status**	**Passage number**	**Date**
4	$0.5x10^6$ cells from seeding	Non-activated in a T75 flask in 10% FCS	31	26/11/2019
7	$0.5x10^6$ cells from seeding	Non-activated in a T75 flask in 10% FCS	35	4/12/2019
9	$0.5x10^6$ cells from seeding	Non-activated in a T75 flask in 10% FCS	37	10/12/2019

5.6.2 Symmetrically Di-Methylated Proteins in Non-Activated RAW 264.7 Cells

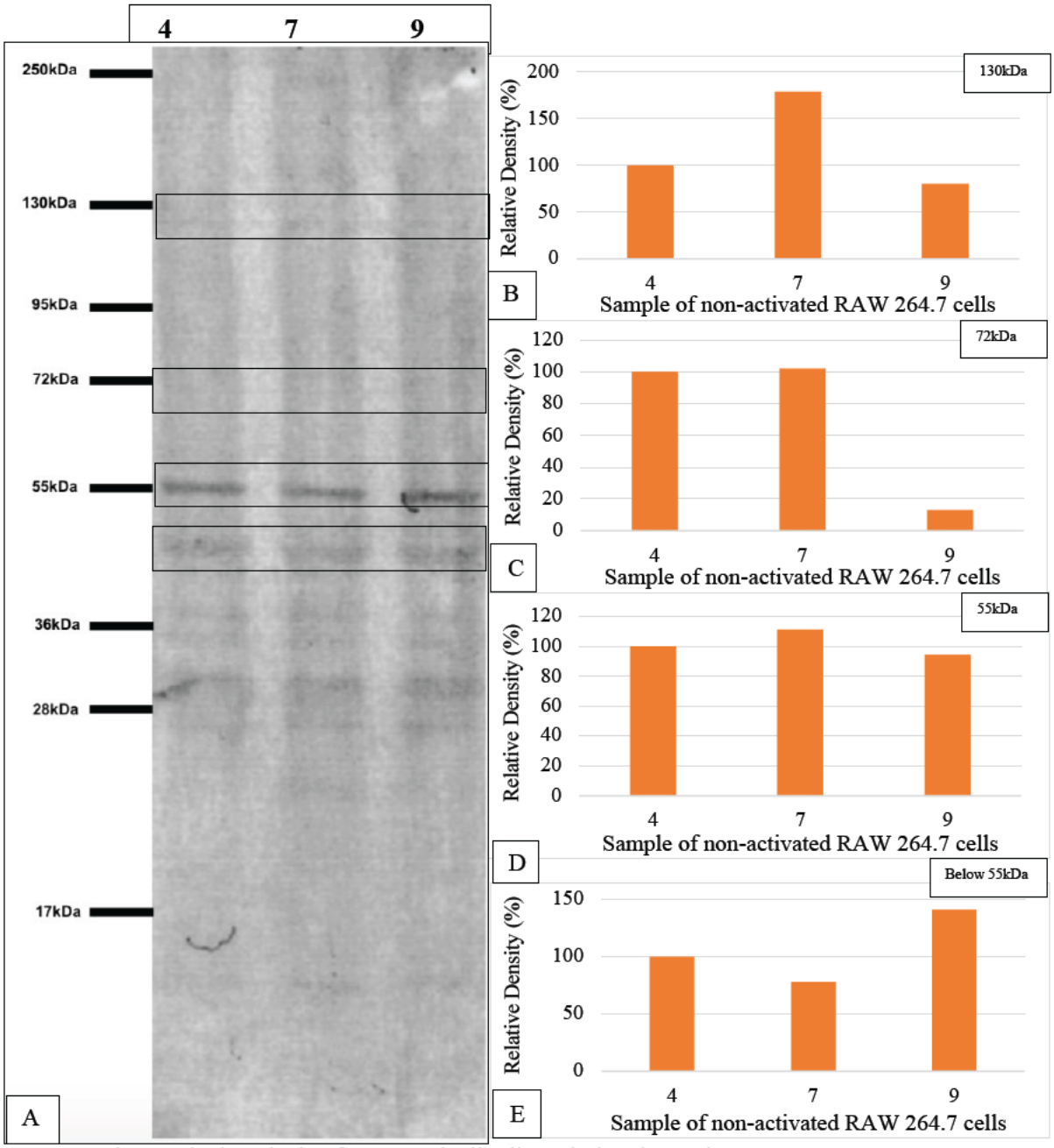

Figure 38: Densitometrical analysis of symmetrically di-methylated proteins.

A) Symmetrically di-methylated proteins within the non-activated RAW 264.7 cells. B) Relative density (%) of symmetrically di-methylated protein of ~130kDa MWT from 3 different passages of non-activated RAW 264.7 macrophages. Raw values and ImageJ analysis are shown in Appendix 10.8.1-3. C) Relative density (%) of symmetrically di-methylated protein of ~72kDa MWT from 3 different passages of non-activated RAW 264.7 macrophages. Raw values and ImageJ analysis are shown in Appendix 10.8.4-6. D) Relative density (%) of symmetrically di-methylated protein of ~55kDa MWT from 3 different passages of non-activated RAW 264.7 macrophages. Raw values and ImageJ analysis are shown in Appendix 10.8.7-9. E) Relative density (%) of symmetrically di-methylated protein of below 55kDa MWT from 3 different passages of non-activated RAW 264.7 macrophages. Raw values and ImageJ analysis are shown in Appendix 10.8.11-13.

Within Figure 38, symmetrical di-methylation (SDM) was evident in all four samples used from the non-activated RAW 264.7 cells (cells used in order from Table 5). These cells were from different passages and were pellets frozen and stored in the -80 °C freezer from different experiments (4,7,9). This experiment demonstrates the potential effect that time and passage number of the RAW 264.7 macrophages can have on SDM due to the band intensity changes. There were changes in band intensities shown at ~130kDa, ~72kDa, ~55kDa and below 55kDa. The control was set at 100% and was the earliest cell passage (4).

Figure 38B shows that there is a difference in the relative density of the SYM10 band with the MWT of approximately 130kDa. There is a significant spike (79% increase) in the band intensity in sample 7, which had a cell passage number of 35. With the intensity dropping 20% below the control (sample 4) in sample 9. The relative density of SYM10 band at approximately 72kDa was similar in sample 4 (the control) and sample 7. However, there was a drastic drop in band density in sample 9 (reduced to 12%), this may pertain to the protein/methylation being sensitive to the cell passage number (shown in Figure 38C). Figure 38D illustrates there is no dramatic change in band intensity at approximately 55kDa, with the relative density not deviating from the control by more than 10%. However, at the MWT below 55kDa (Figure 38E), there was a 20% drop in sample 7 and a 40% increase in band intensity in sample 7 compared to the control.

5.6.3 Asymmetrically Di-Methylated Proteins in Non-Activated RAW 264.7 Cells

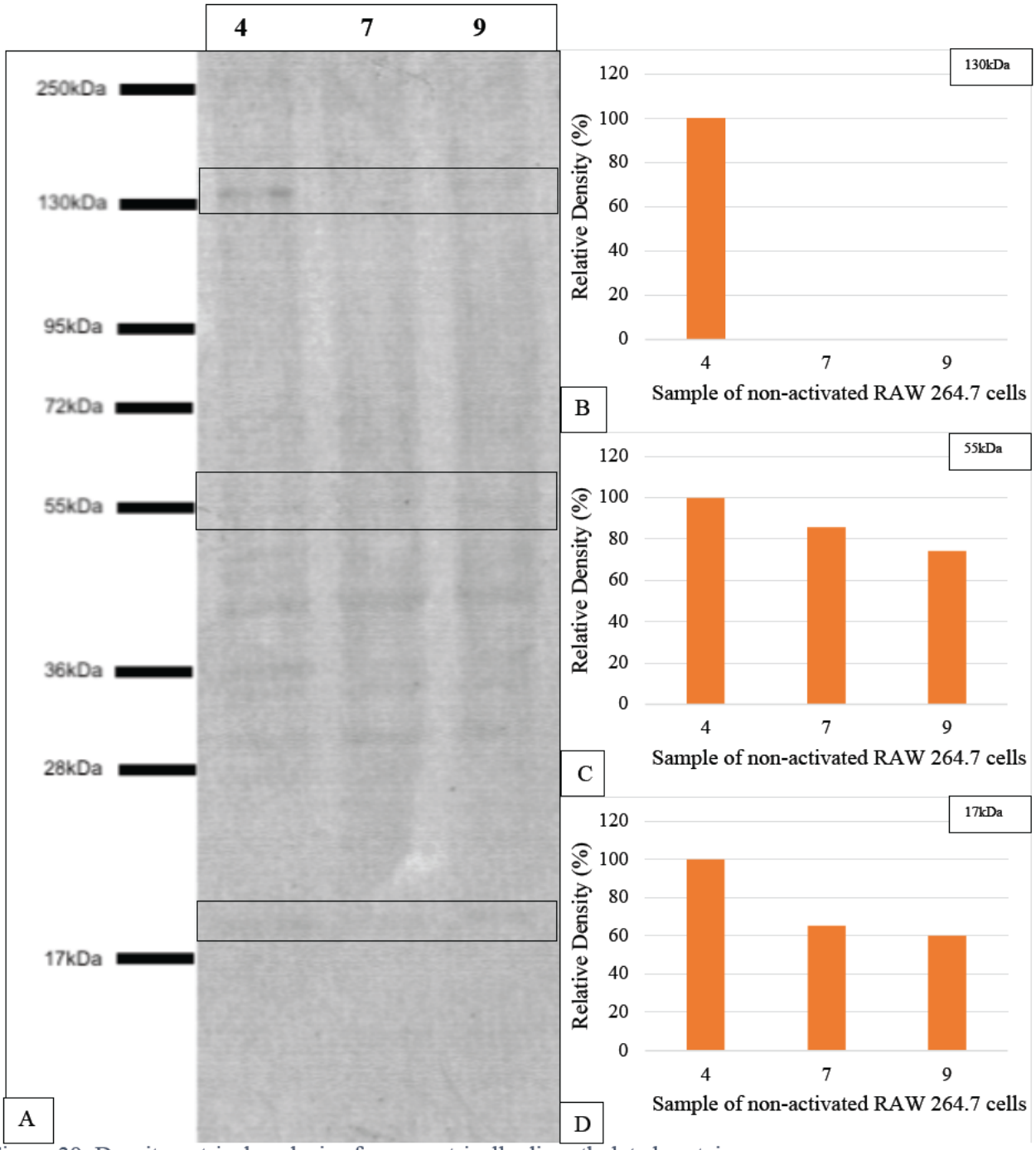

Figure 39: Densitometrical analysis of asymmetrically di-methylated proteins.

A) Asymmetrically di-methylated proteins within the non-activated RAW 264.7 cells. B) Relative density (%) an asymmetrically di-methylated protein of ~130kDa MWT from 3 different passages of non-activated RAW 264.7 macrophages. Raw values and ImageJ analysis are shown in Appendix 10.8.14-16. C) Relative density (%) an asymmetrically di-methylated protein of ~55 MWT from 3 different passages of non-activated RAW 264.7 macrophages. Raw values and ImageJ analysis are shown in Appendix 10.8.17-19. D) Relative density (%) an asymmetrically di-methylated protein above 17kDa MWT from 3 different passages of non-activated RAW 264.7 macrophages. Raw values and ImageJ analysis are shown in Appendix 10.8.20-22.

In Figure 39A there are distinct asymmetrically di-methylated bands at 130kDa, 55kDa and 17kDa, illustrated by the rectangles. As shown in Figure 39B, sample 4 (at passage number 31) was the only band to be detected by ImageJ analysis at the MWT of 130kDa. This stresses the importance of cell passage when analysing band intensities from WBs. In Figure 39C there was a gradual decline in relative density as the cell passage number increased at the bands at a MWT of 55kDa, which reduced to 74% of the control's density. This was also seen in the bands shown in Figure 39D at the MWT above 17kDa, where sample 9 band intensity reduced to 60% of the control's intensity.

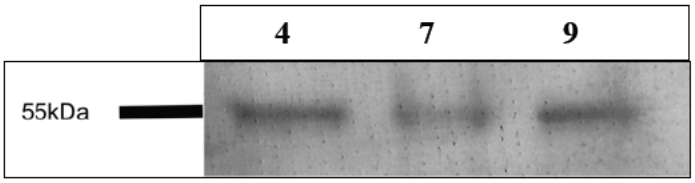

Figure 40: Beta tubulin, housekeeping protein.

Beta tubulin is a protein that is used as a house-keeping protein, it is detected at 55kDa (Cho et al. 2018). The band intensities for beta tubulin are shown in Figure 40. As can be clearly seen the amount of beta tubulin also seems to fluctuate over the passage number of cells with the lower intensity in sample 7 compared to 4 and 9. These variations in beta tubulin were seen even though the total protein concentration of the samples loaded was normalised according to a BCA assay, hence questioning the validity of this protein being a 'housekeeping' protein, as the amount of protein changed over the passage numbers.

5.6.4 PRMT1 Bands in Non-Activated RAW 264.7 Cells

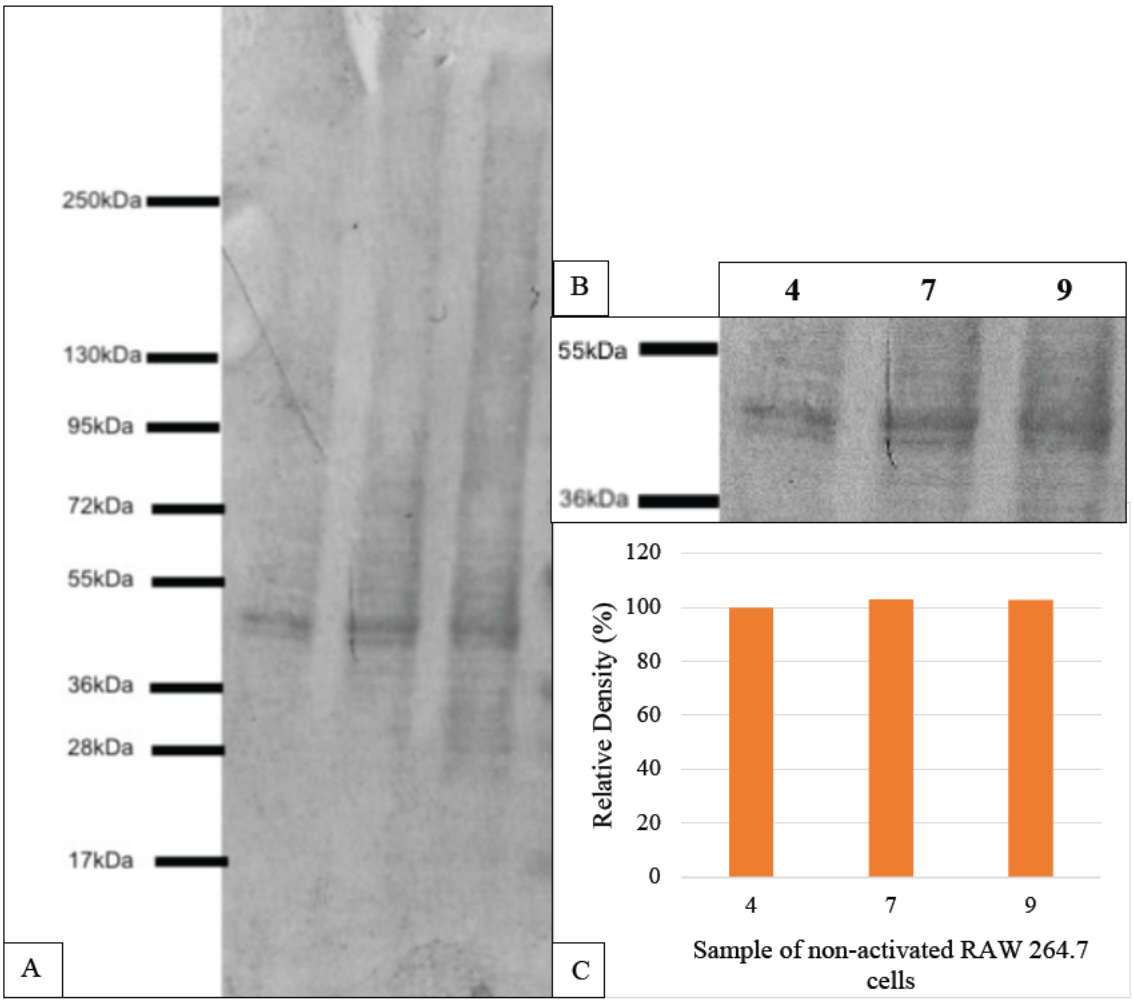

Figure 41: Densitometrical analysis of PRMT1 bands in non-activated RAW 264.7 macrophages. A) PRMT1 WB shows a 'duplet' double band at approximately 45kDa. B) Close up of PRMT1 duplet shown in A. C) Relative density (%) PRMT1 bands (~45kDa MWT) from 3 different passages of non-activated RAW 264.7 macrophages. Raw values and ImageJ analysis are shown in Appendix 10.8.23-25.

As shown in Figure 41 (A and B), PRMT1 was observed as a double band between 55kDa and 36kDa at approximately 45kDa, consistent with its MWT of 42kDa for the full lengths mouse PRMT1. However, PRMT1 is the most abundant type I PRMT in mammals and is involved in other important methylation vents not just activation and inflammation. In Figure 41C, there are no obvious differences in the density of the PRMT1 bands across all 3 samples. This unchanged relative density of the PRMT1 bands shown in the non-activated RAW 264.7 macrophages shows that the amount of PRMT1 is stable and is not altered with cell passage numbers.

5.6.5 **PRMT5 Bands in Non-Activated RAW 264.7 Cells**

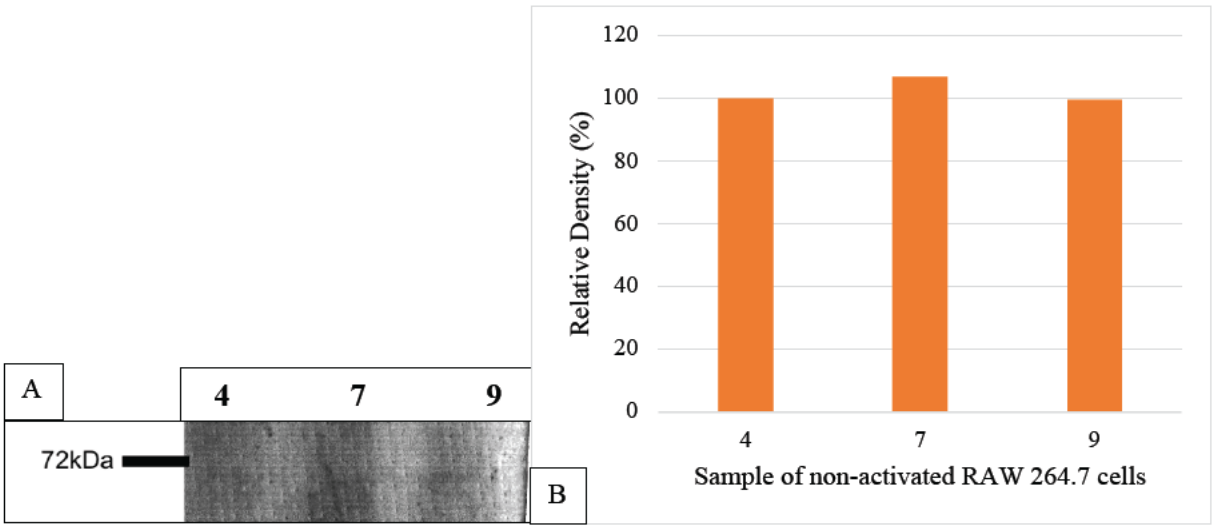

Figure 42: Densitometrical analysis of PRMT5 bands in non-activated RAW 264.7 macrophages. A) PRMT5 WB with bands shown below 72kDa. B) Relative density (%) of PRMT5 bands at ~72kDa MWT from 3 different passages of non-activated RAW 264.7 macrophages. Raw values and ImageJ analysis are shown in Appendix 10.8.26-28.

PRMT5 is a major PRMT type II facilitating symmetric di-methylation of arginine residues in proteins. Figure 42A shows PRMT5 as a faint band observed approximately at 72kDa, which is consistent with the calculated molecular weight of the mouse PRMT5 of 72.607kDa. Figure 42B, there is no large spike in relative density with any of the samples.

5.6.6 Symmetrically Di-Methylated Proteins in Activated Compared to Non-Activated RAW 264.7 Cells

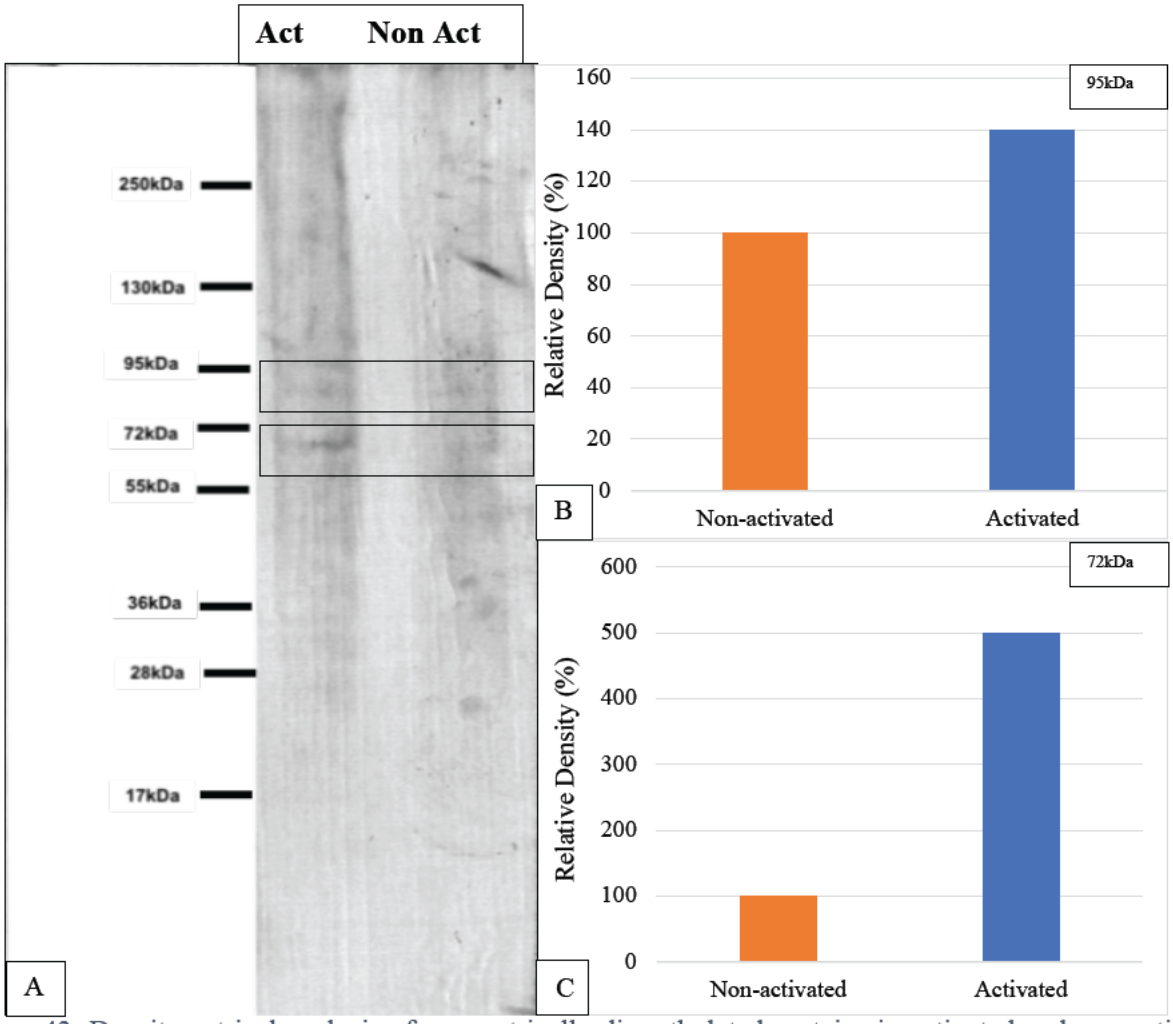

Figure 43: Densitometrical analysis of symmetrically di-methylated proteins in activated and non-activated RAW 264.7 macrophages.

(A) Symmetrically di-methylated protein bands in activated (1st lane) and non-activated (2nd lane) 264.7 cells. (B) Relative density (%) of symmetrically di-methylated protein of ~95kDa MWT from activated and non-activated RAW 264.7 macrophages. Raw values and ImageJ analysis are shown in Appendix 10.8.29-31. (C) Relative density (%) of symmetrically di-methylated protein of ~72kDa MWT from activated and non-activated RAW 264.7 macrophages. Raw values and ImageJ analysis are shown in Appendix 10.8.32-34.

In Figure 43A there were differences in band intensities in the symmetrically di-methylated duplet shown around 95kDa and another duplet shown around 55kDa. There are symmetrically di-methylated bands shown in the activated RAW 264.7 cells at approximately 95kDa that was 40% more intense than in the non-activated (Figure 43B). The ImageJ analysis in Figure 43C showed that there was a large increase in the band intensity of a symmetrically di-methylated protein at approximately 72kDa with a 5 fold increase in activated cells compared to the non-activated cells.

5.6.7 Asymmetrically Di-Methylated Proteins in Activated Compared to Non-Activated RAW 264.7 Cells

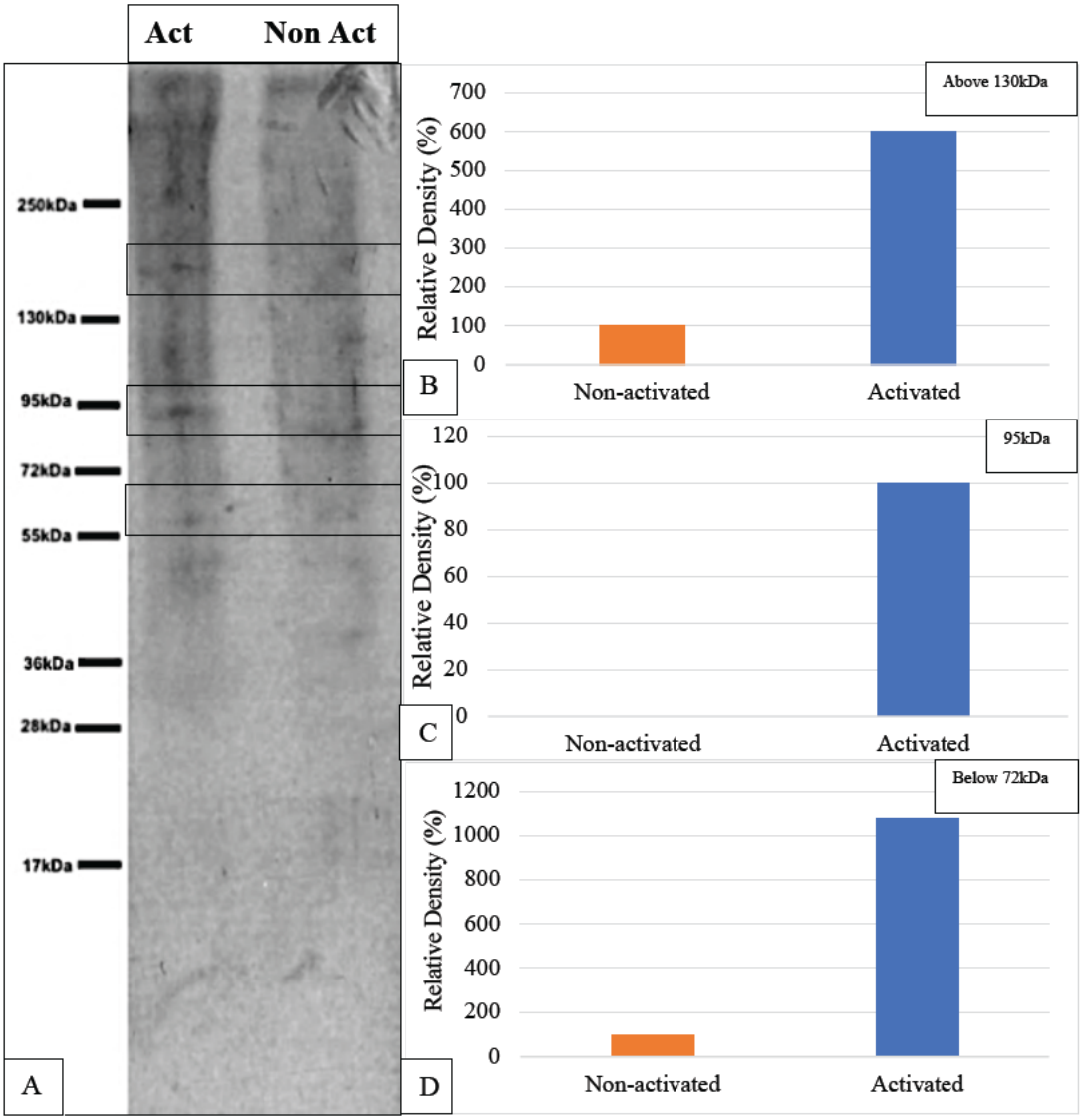

Figure 44: Densitometrical analysis of asymmetrically di-methylated proteins in activated and non-activated RAW 264.7 macrophages.

(A) Asymmetrically di-methylated protein bands in activated (1st lane) and non-activated (2nd lane) 264.7 cells. (B) Relative density (%) of an asymmetrically di-methylated protein of ~130kDa MWT from activated and non-activated RAW 264.7 macrophages. Raw values and ImageJ analysis are shown in Appendix 10.8.35-37. (C) Relative density (%) of an asymmetrically di-methylated protein of ~95kDa MWT from activated and non-activated RAW 264.7 macrophages. Raw values and ImageJ analysis are shown in Appendix 10.8.38-40. (D) Relative density (%) of an asymmetrically di-methylated protein of ~72kDa MWT from activated and non-activated RAW 264.7 macrophages. Raw values and ImageJ analysis are shown in Appendix 10.8.41-43.

In Figure 44A, there are asymmetrically di-methylated protein bands visible above 130kDa, at ~95kDa and below 72kDa. Shown in Figure 44B, there is a 6 fold increase in the relative ASYM24 band intensity of a protein above 130kDa MWT in the activated RAW 264.7 macrophages, compared to the control (non-activated sample). In Figure 44C at a MWT of ~95kDa, there was no detected band by ImageJ analysis in the non-activated cells compared to the clear band in the activated RAW 264.7 cells. The asymmetrically di-methylated protein bands below 72kDa in Figure 44D show a 10 fold increase in relative density in the activated RAW 264.7 macrophages compared to the non-activated cells.

5.6.8 PRMT1 Bands in Activated Compared to Non-Activated RAW 264.7 Cells

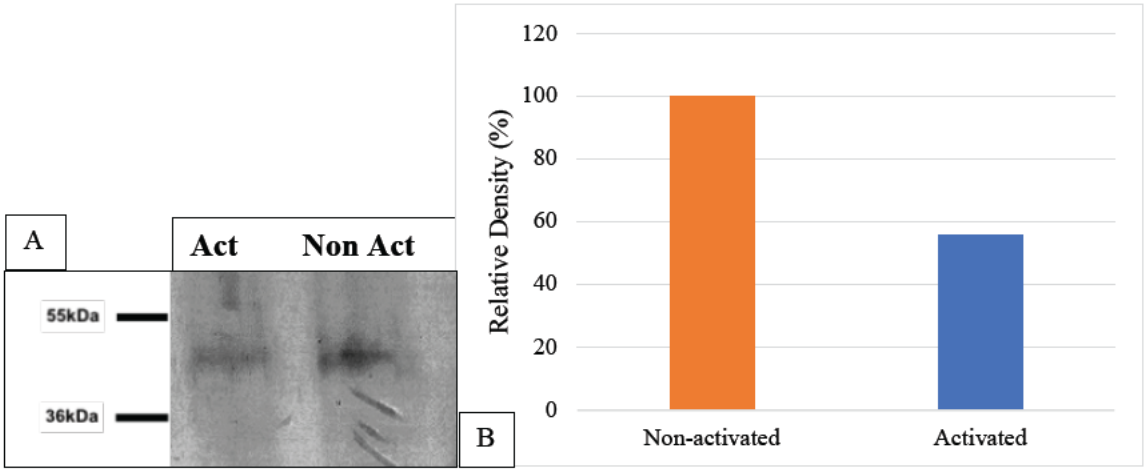

Figure 45: Densitometrical analysis of PRMT1 bands in non-activated RAW 264.7 macrophages. A) PRMT1 WB with bands shown below 72kDa PRMT1 in activated (1st lane) and non-activated (2nd Lane) RAW 264.7 cells. B) Relative density (%) of PRMT1 band from activated and non-activated macrophages. Raw values and ImageJ analysis are shown in Appendix 10.8.44-46.

In Figure 45A the density of PRMT1 protein band was lower in the activated compared with the non-activated RAW 264.7 macrophages. In Figure 45B, there relative density of the band decreased in the activated RAW 264.7 cells compared to the non-activated cells by 44%.

There is a growing interest of the role of protein arginine methylation in inflammatory related disorders. These experiments show that the activation of the immune system through LPS and IFN-γ causes change in the expression of PRMT1 within RAW 264.7 macrophage cells. This poses a pathway to further look at CPZ treated cells and the changes in PRMTs that may be influenced by the breakdown products of CPZ, which could act as diagnostic mechanisms and/or therapeutic targets. Tables 6 outlines the changes in relative density of asymmetrically di-methylated protein bands (ASYM24), symmetrically di-methylated protein bands (SYM10) PRMT1 and PRMT5 bands from activated and non-activated RAW 264.7 macrophages.

Table 6: Overview of the intensity of symmetrically di-methylated proteins, asymmetrically di-methylated proteins, PRMT1 and PRMT5 in non-activated and activated RAW 264.7 cells.

Sym bands (MWT)	**Passage**			**Activated**	**Non-activated**
	31 (4)	**35 (7)**	**37 (9)**		
130		+++	--	ND	ND
95	ND	ND	ND	+	
72			----	+++++	
55		NC	NC		
< 55		-	+		
Asym bands (MWT)	**Passage**			**Activated**	**Non-activated**
	31 (4)	**35 (7)**	**37 (9)**		
130		ND	ND	++++++	
95					ND
72				+++++++++	
55		-	-		
17		-	-		
PRMT bands	**Passage**			**Activated**	**Non-activated**
	31 (4)	**35 (7)**	**37 (9)**		
PRMT1	NC	NC	NC	--	
PRMT5	NC	NC	NC		

	Signficant decrease
	Moderate decrease
	Slight decrease
	Slight increase
	Moderate increase
	Signficant increase

NC = no change
ND = not detected

6.0 Discussion

In this thesis, visual morphological changes were identified in the non-activated, activated and drug treated RAW 264.7 macrophages. When the RAW 264.7 macrophages were activated with 1μg/mL of LPS and 1U/mL of IFN-γ, there was pseudopodia like spreading observed using light microscopy. When the cells were treated with either cyclohexanone or oxalyldihydrazide elongated, swollen and multi-nucleated cells were observed. It was hypothesised that the swollen cells and blebbing that occurred were due to a pyroptotic pathway. Future experiments involving PI staining, caspase-1 ELISA and Gasdermin D ELISA would assist in confirming that the pyroptotic pathway is involved in the effects of the CPZ breakdown products on RAW 264.7 macrophages.

There were significant differences in the total and live cell numbers between different activation time points when the RAW 264.7 macrophages were activated with 10μg/mL of LPS and 10U/mL of IFN-γ. Protocols were optimised to be able to ensure that the viability and cell numbers were not reducing significantly from the activation mix. This also provided a baseline to determine the effects of the breakdown products of CPZ. Previous studies have not conducted experiments on the effect of the breakdown products of CPZ on cultured cells. This experiment is important to investigate further the cellular mechanisms and potential toxicity or effects that are associated with each individual breakdown product.

It was hypothesised that oxalyldihydrazide would be cytotoxic to the RAW 264.7 macrophages compared to the other breakdown product of CPZ, cyclohexanone. Using the Trypan blue assay cyclohexanone appeared to reduce cell numbers with increased concentration of cyclohexanone when cells were re-activated during the drug exposure with LPS and IFN-γ. Re-activated cyclohexanone/oxalyldihydrazide treated cells incur a high metabolic demand to produce more TNF-α and IL-1β, which may contribute to toxicity as their pro-inflammatory state is enhanced. Conversely, the activated (not re-immersed in the activation mix during drug treatment) cells seemed to be less susceptible to the effects of cyclohexanone and oxalyldihydrazide. The differences in cell number and cytokine production between the activated and re-activated RAW 264.7 macrophages were hypothesised to be due to the activation of caspase-1 and caspase-11 pathways from the CPZ breakdown products and LPS respectively, which is explored in section 6.3.

For this hypothesis to be confirmed or rejected future work is required. This thesis aimed to identify the differences in protein arginine methylation in non-activated and activated RAW 264.7 macrophages. Although changes in protein/methylation were evident on the WBs, there were some bands in the WBs that were not clear, potentially attributed to the polyclonal antibodies used, as affinity towards methylated proteins differ. Replicates and mass spectrometry are required to identify the proteins that were differentially methylated.

6.1 *Activation of RAW 264.7 Macrophages*

6.1.1 **Morphological Changes in Activated RAW 264.7 Macrophages**

When carrying out the cell culture experiments, light microscopy images were used to monitor the cells and the notable morphological changes that occurred in non-activated, activated and drug-treated RAW 264.7 macrophages. The images allowed assessment of confluency, size and shape of the RAW 264.7 cells. A close observation of the fluctuating morphological features of the RAW 264.7 macrophages was deemed necessary, as the change in cell morphology and its impact on functioning of the macrophages has not been well documented (Frances et al. 2013).

The optimisation of the seeding density of the RAW 264.7 macrophages is shown in Figure 20. The RAW 264.7 macrophages seeded at a density of $1x10^6$ had largely become over-confluent making the morphology of individual cells hard to distinguish and enhancing the potential for contact inhibition to occur, described in section 5.1.2 (Seluanov et al. 2009). In contrast, a monolayer of cells formed when RAW 264.7 macrophages were seeded at a density of $0.5x10^6$ cells per well, which allowed morphological changes to be observed following activation and treatments with CPZ breakdown (drug) products. As shown in Figure 21, RAW 264.7 macrophages adopted elongated, irregular-shaped morphologies after 24 hours activation with 1μg/mL of LPS and 1U/ml of IFN-γ, compared to small, round uniform cells in the non-activated RAW 264.7 cultures. Consistent with the distinct changes in cellular size and morphology shown in Figure 21 others have reported that LPS and IFN-γ can increase cell size five to ten-fold (Duque & Descoteaux 2014; Sieweke & Allen 2013) and the adoption of flattened pancake shape morphologies (Frances et al. 2013). Dai et al. (2019) study with RAW 264.7 cells activated with LPS portrayed a spindle shaped pseudopodia morphology, which is consistent with the morphology observed in the experiments performed in this thesis.

6.1.2 **Effect of Activation on the Cell Number of RAW 264.7 Macrophages**

The optimisation experiments performed in Figure 24 showed that activation of the RAW 264.7 macrophages demonstrated that 10% FCS not only increased the total cell number and cell viability but also revealed marked differences between the non-activated and activated cells that were not seen with 0.1% FCS. This experiment was performed to standardise the total cell number for the drug treatment with either cyclohexanone or oxalyldihydrazide. Consequently,

in all subsequent experiments 0.1% FCS was used to prevent differences in drug effective concentration (i.e., drug availability per cell) as well as cell number variations based on the activation state of the RAW 264.7 macrophages. The viability of the cells that were treated with 10μg/mL of LPS and 10U/ml of IFN-γ was determined by the Trypan blue assay. Control/ non-activated cell counts doubled with the viability remaining stable at ~90% over the 24 hours, whereas activated cells reduced by half in their cell counts with the viability falling to less than 60% over the 24 hours activation time (Figure 24). For future experiments as there was no significant difference in the viability between the 6 hour and 12 hours for activated RAW 264.7 macrophages, the 12-hour time point is recommended for future experiments to avoid declining RAW 264.7 macrophage cell numbers at the 24-hour time point when assessing the impact of drug treatment.

6.2 *Morphological Changes in Drug Treated RAW 264.7 Cells*

6.2.1 **Formation of Multi-Nucleated Giant Cells**

In Figure 29, it is acknowledged that the actual cell numbers of MNGCs was low there was a positive correlation between the increasing number of multi-nucleated cells and the increasing concentration of cyclohexanone or oxalyldihydrazide is shown. There was a larger formation of multi-nucleated cells in activated RAW 264.7 macrophages treated with cyclohexanone (except at 62.5μM of cyclohexanone) than oxalyldihydrazide. This could pertain to cyclohexanone enhancing an inflammatory and immune response, due to the presence of increased numbers of multi-nucleated cells. In contrast, few multi-nucleated cells were observed in the non-activated drug treated RAW 264.7 cells, suggesting a differential effect based on activation state, warranting further investigation into the mechanisms behind the formation of multi-nucleated cells. Further understanding of this mechanism could provide further insight into how the drug interacts with RAW 264.7 macrophages and exerts its effects.

Two possible mechanisms are postulated that may explain the prescence of this change in morphology, cytokinesis and/or the formation of multi-nucleated giant cells (MNGCs). In Figure 30A RAW 264.7 macrophages treated with 125μM of cyclohexanone contained 3 nuclei within the one cell. However in Figure 30B, RAW 264.7 macrophages treated with 125μM of oxalyldihydrazide, a cell was observed to have 4 nuclei together and a separate nucleus to the left. However, it is not possible to conclude from morphological changes what process is causing these changes without further analysis and testing.

One of the postulated mechanisms for the presence of the multi-nucleated cells is by syncytia, which is the formation of multi-nucleated cells through cell fusion, or coenocytes, where of nuclear division proceeds but is not followed by cytokinesis. Cytokinesis is a highly complex final stage of cell division (Guertin, Trautmann & McCollum 2002). This process involves the division of the cell into two identical daughter cells, through the formation of an actomyosin contractile ring that chromosomally segregates the cell midway at the poles of the mitotic spindle (Straight & Field 2000). The trigger for this process is not well understood, however, the failure of this process has been found to predispose cells to become tumorigenic, due to the formation of aneuploidy and tetraploidy. It is possible for cells to undergo failure of cytokinesis but follow a normal mitotic process, which leads to the formation of bi-nucleated daughter cells. However, in the next cell cycle mitotic failure ensures the removal from the cycling

population (Hayashi & Karlseder 2013). The presence of 3 nuclei (Figure 30A) in RAW 264.7 macrophages treated with 125μM of cyclohexanone and multiple other uneven number of nuclei observed makes it unlikely that these changes were due to failed cytokinesis, as such failures result in an even number of nuclei. Mi et al. (2016) interestingly found the up-regulation of 16 genes and down-regulation of one gene related to the cell cycle regulation in the pre-frontal cortex in C57BL/6 mice treated with CPZ. This raises the question of whether the mode of action for cyclohexanone or oxalyldihydrazide is linked to the formation of MNGCs and the disruption to the cell cycling.

The observed presence of multiple nuclei in the RAW 264.7 cells could also be due to the formation of MNGCs, which occurs when macrophages fuse with each other in the event of chronic inflammation (McNally & Anderson 2011). The process of macrophage fusion is not well understood, in terms of the mechanism and role in the presence of infection (McNally & Anderson 2011). However, MNGCs have been indicated in a myriad of infectious and non-infectious diseases such as atherosclerosis, sarcoidosis and Langerhans cells histiocytosis. Whether the formation of MNGCs assists with the progression or resolution of these disease processes is currently unknown (Milde et al. 2015). The process by which macrophage fusion can occur is associated with soluble molecules including cytokines, growth factors, NADPH oxidase-generated reactive oxygen species, adhesion proteins and receptors (Quinn & Schepetkin 2009). It is postulated that the unique ability of macrophages to fuse is involved in the eradication of disease by increasing the capacity to engulf foreign bodies. Furthermore, the process of fusing of macrophages results in the loss of plasticity and mobility of macrophages (Vignery 2008).

Interestingly, as outlined in section 7.3.2 microglia are a cell line that should be used in future studies, in comparison to the data reported here in the RAW 264.7 macrophages. Microglia would provide a good comparison, as the formation of MNGCs has been observed in numerous pathological states including tuberculosis, autoimmune conditions including sarcoidosis, and infectious agents, as well as in HIV-infected cells of patients (Tambuyzer & Nouwen 2005). Similar to macrophages, the phenomenon of MNGCs in microglia is largely unknown, however, it is postulated, that when the fully activated microglia cannot perform their immunological function, they fuse together to eliminate the pathogen (Tambuyzer & Nouwen 2005).

6.2.2 **Elongated Morphology of RAW 264.7 Drug Treated Cells**

The oxalyldihydrazide treated RAW 264.7 macrophages (Figure 27E), displayed more prominent elongated cells with pseudopodia-like processes, than the cyclohexanone treated cells. This morphological change suggests oxalyldihydrazide may be able to produce an alternative pathway for RAW 264.7 macrophages to be activated. Frances et al. (2013) observed morphological changes within BMDM stimulated with LPS and IFN-γ, consistent with the elongation of the cells was mostly observed in this study and they were mostly observed in the BMDMs stimulated to M2 polarisation, by the addition of IL-4 and IL-10. Interestingly, the M2 polarized BMDM had a significantly higher degree of elongation compared to M1 or M0 (non-activated) cells (Frances et al. 2013). The relevance and significance of the elongated RAW 264.7 cells are uncertain; however, it may be attributed to the cell line, cell density, concentration of activation mix used or potentially have a role in the functioning of the macrophages. It is noteworthy that the two breakdown products appeared to have different effects on the morphology of the RAW 264.7 macrophages, which may reflect a role in influencing their function and their ability to act as M1 or M2 macrophages. It needs to be confirmed with future morphometric analysis if the elongation of the cells is consistent with the M2 phenotype.

6.3 *Changes in Morphology in RAW 264.7 Macrophages Consistent with Pyroptosis*

The large differences in the morphology between the re-activated, activated and non-activated treated RAW 264.7 cells could be attributed to cysteine-aspartic protease (caspase)-11, which could be one of the mechanisms that affects the reduced cell number in the activated RAW 264.7 macrophages, due to LPS being the main driving agent of non-canonical pyroptosis (He et al. 2015). The enlargement of the activated drug treated RAW 264.7 macrophages need to be further investigated to identify what process is occurring to cause this cellular morphological change, which could be partly attributed to an inflammatory cell death 'pyroptosis'.

6.3.1 **Background Information on Pyroptosis**

Pyroptosis 'fiery death', also known as caspase-1 dependent cell death, is the process where a pathological stimulus causes an inflammatory response (Bergsbaken, Fink & Cookson 2009; McKenzie et al. 2018). Caspases are a family of cysteine endoproteases that have an integral role in the maintenance of homeostasis, through the tight regulation of cell death and inflammation (McIlwain, Berger & Mak 2013). Caspases are produced as inactive zymogens that are catalytically activated through either dimerisation or cleavage to form the active caspase (McIlwain, Berger & Mak 2013; Shi 2004). Caspases 1, 4, 5 and 12 have inflammatory roles, whereas caspase-3 and 7 induce apoptosis (McIlwain, Berger & Mak 2013; Taabazuing, Okondo & Bachovchin 2017). Caspase-5 is absent within mice, as it is presumed to have developed in higher order species. Mice caspase-11 is said to be the ortholog of human caspase 4 (Scott & Saleh 2006). Inflammatory caspases are transcribed from the same locus and have a role in the regulation of inflammation through the activation of proinflammatory cytokines (Mosser & Zhang 2008; Sollberger et al. 2014). In humans, inflammatory caspases are clustered together on chromosome 11q22.2-q22.3 and in mice, inflammatory caspases are found in the chromosomal region 9A1 (Scott & Saleh 2006).

6.3.2 **Canonical Pyroptosis**

Canonical pyroptosis occurs within a specific subset of cells inclusive of monocytes, macrophages, and dendritic cells, in which an inflammasome activates caspase-1 which in turn cleaves Gasdermin D (GSDMD), IL-1β and IL-18 (Taabazuing, Okondo & Bachovchin 2017). This process differs from apoptosis, as it involves swelling following pore formation in the

plasma membrane. As shown in Figure 46, the pore formation markedly increases the net osmotic pressure, which subsequently results in the rupturing of the membrane and release of inflammatory contents into the extracellular space (Bergsbaken, Fink & Cookson 2009). Cytosolic contents that are released as a subsequent result of caspase-1 being activated by the inflammasome include IL-1β and IL-18 (Miao, Rajan & Aderem 2011). Components of the inflammasome complex include the binding of the receptor proteins and adapter protein apoptosis-associated speck-like protein (ASC) and the caspase activation and recruitment domain (CARD) (McIlwain, Berger & Mak 2013; Tunctan et al. 2017).

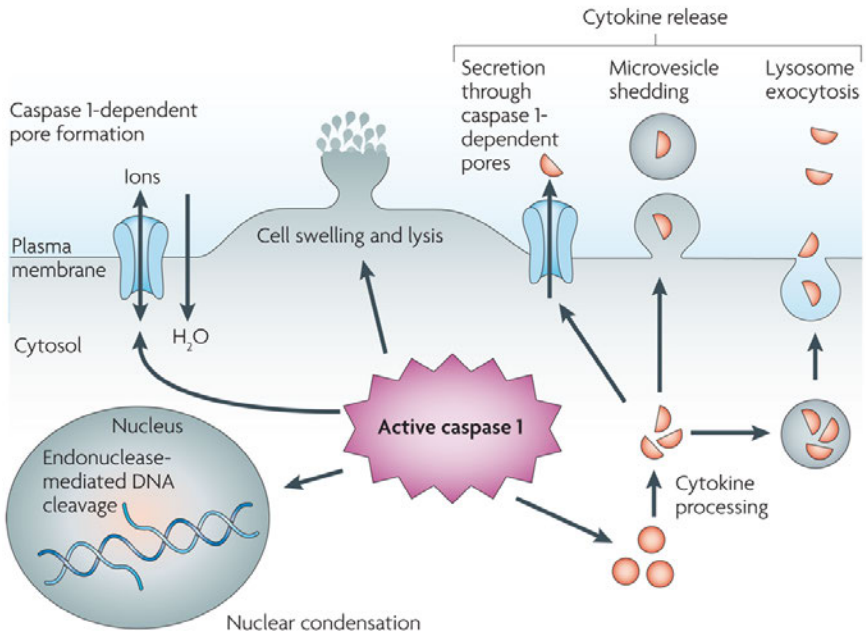

Figure 46: Illustration of the events that occur when cells undergo the process of pyroptosis (Bergsbaken, Fink & Cookson 2009).

6.3.3 Potential Pyroptotic Morphological Changes in Non-activated Drug-Treated RAW 264.7 Macrophages

Non-activated RAW 264.7 cells treated with cyclohexanone and oxalyldihydrazide (Figure 27 B and D), showed little change in morphology, compared to the control cells (Figure 27A). There was minimal cell swelling observed and very few multi-nucleated cells were seen. The minimal enlargement of the cells is postulated to be as a result of the activation of caspase-1 driven by cyclohexanone, due to the lack of LPS which has a role in activating caspase-11. However, due to the minimal impact of the drugs on the non-activated RAW 264.7 cells, this could suggest that the drugs only have a potent effect on cell morphology when the cells are activated with LPS and IFN-γ during drug treatment.

6.3.4 **Potential Pyroptotic Morphological Changes in Activated Drug-Treated RAW 264.7 Macrophages**

Activated RAW 264.7 cells treated with cyclohexanone produced more pronounced morphological changes (Figure 28) and had an increased number of multinucleated cells (Figure 29) than cells treated with oxalyldihydrazide. The morphological swelling apparent in the activated RAW 264.7 cells treated with cyclohexanone and oxalyldihydrazide is postulated to be at least partly a result of the inflammatory programmed cell death, pyroptosis. This change in morphology could be a direct result of the activation of non-canonical pyroptosis via LPS and canonical pyroptosis via the breakdown products of CPZ.

6.3.5 **Pyroptotic Bodies**

Morphological changes surrounding the cell (Figure 26) were apparent in activated RAW 264.7 macrophages treated with 250μM of oxalyldihydrazide. The observed blebbing of the membrane is consistent with the formation of pyroptotic bodies (Chen et al. 2016). Pyroptotic bodies are vesicles on the cell membrane occur early in pyroptosis, known to be of a similar size to apoptotic bodies (Huang et al. 2019). These are accompanied by pore formation, approximately 10-14nm in diameter in the later stages of pyroptosis (Huang et al. 2019). The formation of these pyroptotic bodies occurs before the rupturing of the plasma membrane (Chen et al. 2016). The remnants of pyroptotic cells have been described to look like a ‘fried egg’ (Chen et al. 2016). This morphology is evident in the light microscopy images Figure 27C and Figure 27E with RAW 264.7 cells treated with cyclohexanone or oxalyldihydrazide, respectively. Based on this interesting morphological finding under the light microscopy observation further investigation into the inflammatory cell death, pyroptosis was undertaken.

6.4 *IL-1β Production in Drug Treated RAW 264.7 Macrophages*

6.4.1 **IL-1β Production in Activated Drug Treated RAW 264.7 Macrophages**

The raw readings of the IL-1β concentration in the cyclohexanone treated cells, was highest in re-activated cells treated with 5000μM of cyclohexanone (shown in Figure 37A). Whereas, when the RAW 264.7 macrophages were not re-activated in the activation mix when treated with cyclohexanone the trend reversed and the highest concentration of IL-1β was in the cells treated with 0μM of cyclohexanone (Figure 37A). This trend was similar in the oxalyldihydrazide treated cells; however, the trend was not so definitive (Figure 37B). It was hypothesised that the non-activated cells could have potentially depleted the nutrients in the media, which could act as a mitochondrial insult, thereby stimulating IL-1β production. Interestingly, at the highest concentration of cyclohexanone or oxalyldihydrazide the IL-1β is the lowest in the activated RAW 264.7 macrophages.

The highest concentration of IL-1β per live cell was observed in the activated control cells (Figure 37E) with progressive reductions as cyclohexanone concentration increased (Figure 37C). In Figure 37F the effect of oxalyldihydrazide was less clear with IL-1β per live cell varying from dose to dose. When the cells were re-immersed during cyclohexanone or oxalyldihydrazide treatment, IL-1β production per live cell progressively increased with the highest levels quantified at 5000μM (shown in Figure 37E and Figure 37F, respectively). This enhanced IL-1β production following re-activation in the presence of the breakdown products of CPZ, may be indicative of what occurs within the pro-inflammatory environment when CPZ, and most clearly its breakdown product cyclohexanone, potentiate the inflammatory response including IL-1β production.

6.4.2 **Linkage of IL-1β to Pyroptosis**

Within a normal, healthy brain the expression of IL-1β is at low levels. However, IL-1β is largely increased in expression, in the presence of systemic inflammation, trauma, infections and excitotoxic brain damage (Prins et al. 2013). In the presence of MS, IL-1β has been found to play a role in the neurodegeneration and clinical progression. Yet, in terms of the inflammation driven neurodegeneration this process still remains unclear. This includes the processes of the increased synaptic transmission and neuronal damage through excitotoxic

processes (Rossi et al. 2014). The detrimental role of IL-1β may not be so clear, as it may have a dual role due to IL-1β assisting in the role of remyelination in the CPZ model.

Studies have also eluded to the presence of IL-1β in neurodegenerative diseases. Burm et al. (2016) using MS brain tissue staining detected IL-1β in the parenchyma of MS lesions and nodules of MHC class II+ microglia. Furthermore, a study by Seppi et al. (2014) reported CSF IL-1β levels had a high correlation with the number and volume of brain cortical demyelinating lesions. Peelen et al. (2015) postulated the potential pyroptosis event in neurodegenerative diseases, as he showed *IL-1β* and *CASP1* and *NLRP3* are more highly expressed in PBMC of MS patients compared to healthy controls.

Some treatments have emerged predicated on blocking IL-1β. Guarda et al. (2011) using bone derived macrophages showed that treatment of IFN-β was found to indirectly reduce pro IL-1β through increasing IL-10 expression. This complex mechanism by which IFN-β works via IL-1β also indirectly involved in repression of the NLRP3. Guarda et al. (2011) showed that there are numerous facets and positive and negative feedback regulatory mechanisms of different cytokines. It also poses the possibility that both pyroptosis alongside other forms of inflammatory processes and cell death, including apoptosis, are potentially interlinked and involved in the pathogenesis of MS.

6.4.3 **Non-Canonical Pyroptosis**

Non-canonical pyroptosis has been linked to caspase-4 and 5 activation by cytosolic LPS and goes through the same process as canonical pyroptosis. However, activated caspase 4 (caspase-11 in mice) and 5 do not cleave IL-1β and IL-18 (Taabazuing, Okondo & Bachovchin 2017). This is due to the maturation of the cytokines requiring the NLRP3-dependent activation of caspase-1 (Kayagaki et al. 2011). Cysteine aspartic protease 11 is known to be a non-canonical inflammasome, which is signalled by intracellular LPS as gram-negative bacteria are required for caspase-11 activation, resulting in pyroptosis. Studies have shown that caspase-11 KO mice are more resistant to endotoxic septic shock even in the presence of large amounts of LPS (Yi 2017). Furthermore, deficiency of caspase-11 is protective against LPS, whereas deficiencies in caspase-1 signalling has no protective effect (Kayagaki et al. 2011). Notably, some studies have shown that IFN is required for cytoplasmic sensing of LPS by caspase-11 (Pilla et al. 2014; Yi 2017). When cells are exposed to LPS, the accumulation of the NLRP3

inflammasome and activation of caspase-1 occurs (Sokolovska et al. 2013). A summary of non-canonical and canonical pyroptosis is shown in Figure 47.

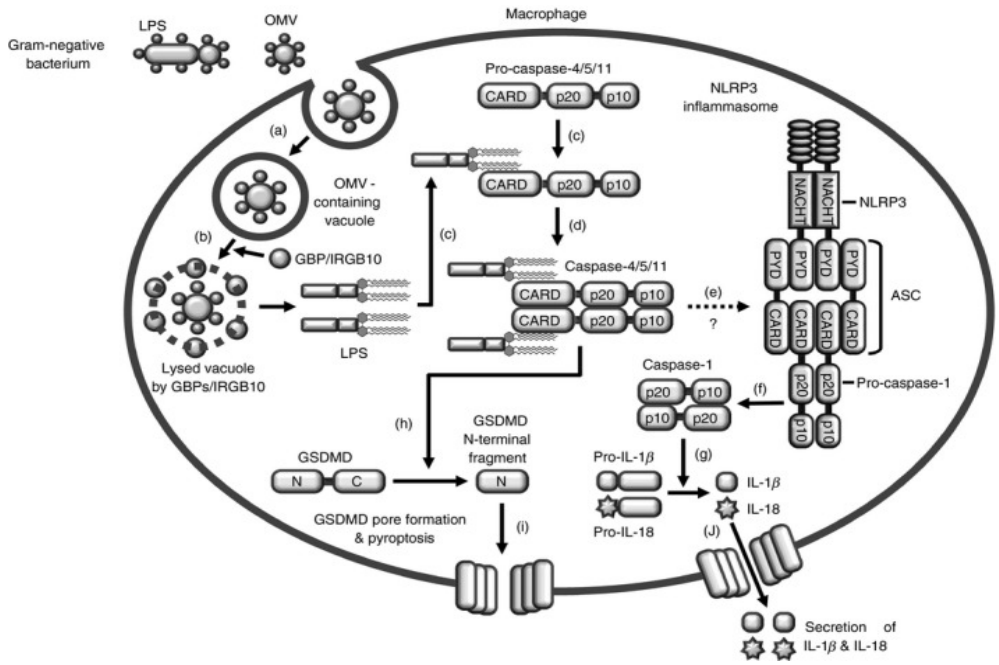

Figure 47: LPS induced canonical caspase pathway in macrophages (Yi 2017).

a) LPS penetrates the macrophage through endocytosis b) OMVs are secreted into the cytoplasm of the LPS-containing vacuole by GBP^{chr3} c) LPS binds to procaspase-11 through the CARD motifs. d) Formation of inflammasome with pro-caspase 11. e) Activated caspase-11 activates NLRP3 inflammasome-mechanism is still unclear. f) Maturation of pro-caspase 1 through proteolysis. g) Cleavage of caspase-1 induces maturation of Pro-IL-18 and Pro-IL-1β. h) N terminal fragments of GSDMD cleaved by active caspase-11. i) N-terminal fragments oligomerise with phosphoinositide to form pores within the cell membrane causing pyroptosis and cell lysis. j) Secretion of IL-1β and IL-18.

6.4.4 **Potential Pyroptotic Morphological changes in Activated RAW 264.7 Macrophages**

Using light microscopy images and larger concentrations of LPS (10µg/ml) and IFN-γ (10U/ml), observations were made on the enlarged nature of the cells at 6, 12, 18 and 24-hour time points to see if this morphology change was time related (Figure 22). Shown in Figure 23 is the presence of an enlarged RAW 264.7 cell, this is thought to be undergoing pyroptosis due to the non-canonical pyroptotic pathway (described in section 6.3), induced by LPS in a time dependent manner. Cellular swelling is characteristic of pyroptosis as the increased osmotic pressure results in swelling and eventually cell rupturing leading to the release of cytosolic

contents and the formation of apoptotic body-like cell protrusion (pyroptotic bodies) (Chen et al. 2016; Miao, Rajan & Aderem 2011). Chen et al. (2016) found that some of the morphological changes in pyroptosis included blebbing which became evident after 4 hours being primed with 1μg/mL of LPS and nigericin. The same concentration of LPS was used for this experiment and the cellular blebbing was similar as indicated by the white arrows in Figure 23. Morphological changes occur when macrophages are activated to assist in the phagocytic capacity and functioning of the cell to remove any pathogens (Duque & Descoteaux 2014; Sieweke & Allen 2013).

6.4.5 **Comparison of Apoptosis and Pyroptosis**

There is growing research on the distinguishing mechanisms behind the different forms of programmed cell death including apoptosis, necrosis and pyroptosis. There are factors that allow the comparative analysis of different types of cell deaths, with caspase-1 being the major distinguishing factor for pyroptosis. Furthermore, pyroptosis is a form of inflammatory cell death, which differs largely from apoptosis that has a role to inhibit inflammation (Fink & Cookson 2005). Further research on cell death will potentially unveil new therapeutic targets for numerous disease states.

GSDMD contains two domains that are 480 amino acids in length. It is a highly conserved protein within mammals: however, its' exact function within the body remains unclear (Yi 2017). GSDMD is seen to be a protagonist in the formation of the membrane pores, which facilitates the process of pyroptosis (Ramos-Junior & Morandini 2017). It has recently been discovered as a new member of cell death inducer-in particular pyroptosis (Ramos-Junior & Morandini 2017). GSDMD also serves as a distinguishing factor between pyroptosis and apoptosis; this is seen in Figure 48, as GSDMD is a substrate that induces pyroptosis through pore formation at the N-terminal p30 fragment of GSDMD (Taabazuing, Okondo & Bachovchin 2017). Taabazuing, Okondo and Bachovchin (2017) discovered Gsdmd $^{-/-}$ RAW 264.7 cells treated with Val-boroPro activated caspase-3 and 7 caused apoptosis to occur, whereas, the control mice underwent pyroptosis. Whereas, casp-1 $^{-/-}$ induced the cleavage of a p43 fragment of GSDMD which inhibits pyroptosis by inactivating the protein (Taabazuing, Okondo & Bachovchin 2017).

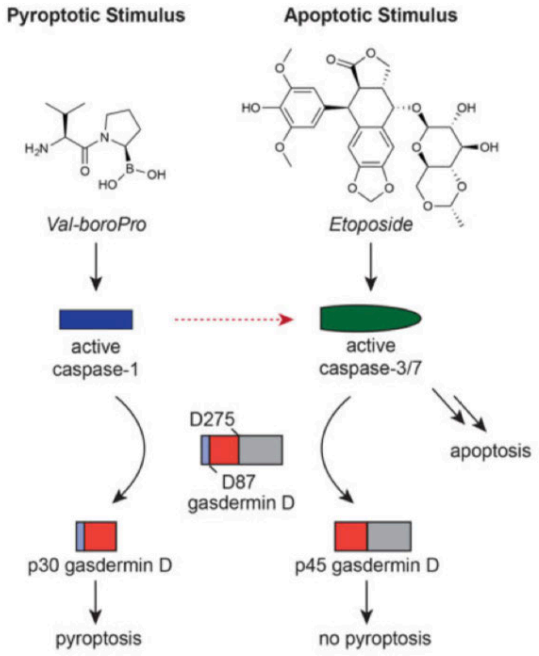

Figure 48: Graphical representation demonstrating differences between apoptosis and pyroptosis (Taabazuing, Okondo & Bachovchin 2017).

Caspase-1, also known as IL-1β converting enzyme (ICE), is not involved in the programmed cell death, apoptosis (Li et al. 1995). This is evident as Li et al. (1995) found that eleven ICE-deficient mice developed normally in terms of fertility, organ functionality, percentage of T cells and absence of gross abnormalities. Furthermore, ICE-deficient mice were able to undergo apoptosis, as studied through *in vitro* treatment of ATP, but were found to be defective in IL-1β secretion (Li et al. 1995).

6.5 *TNF-α Production in Drug Treated RAW 264.7 Macrophages*

6.5.1 TNF-α in Non-activated and Activated RAW 264.7 Cells

Within the non-activated RAW 264.7 cells, minimal amounts of TNF-α were detected (ranging from 76 to 302.5pg/mL) when the cells were incubated for 6, 12, 18 and 24 hours (Figure 32A). In contrast, high concentration of TNF-α were detected in the media of the activated cells, ranging from 109500-268000pg/mL. At the 24-hour time point each cell was producing close to 1pg/mL of TNF-α per total cell number. In another study by Reis et al. (2011) TNF-α levels rose to ~1pg/mL at 24 hours before declining at 36 hours following activation (10ng/mL of LPS and 50U/mL of IFN-γ). Although, the protocol in their experiment varied in terms of the cell density, which was seeded at 10^4 cells /100μL in each well and the concentrations of the activation mix were also different (Reis et al. 2011). The increase in the TNF-α concentrations over the time points is similar to the results in this thesis.

6.5.2 TNF-α in Non-Activated and Activated Drug Treated RAW 264.7 Cells

There was little change in the TNF-α concentrations in the non-activated cyclohexanone or oxalyldihydrazide treated cells (shown in Figure 35A). The activated drug-treated RAW 264.7 macrophages produced 100-fold higher amounts of TNF-α compared to non-activated cells. Shown in Figure 35B, the cells treated with all concentrations of cyclohexanone (62.5, 125, 250 and 500μM) had produced approximately 3 fold higher concentrations of TNF-α per live cell compared to the control. In Figure 35C the TNF-α per cell (live and dead) was at least 2.5 fold higher in all of the cells treated with cyclohexanone compared to the control. Comparatively, the cells treated with 125μM and 250μM of oxalyldihydrazide produced less TNF-α compared to the control, with the cells treated with 62.5μM and 500mM of cyclohexanone producing larger concentrations of TNF-α per live cell compared to the control. This trend was similar in the TNF-α concentration per cell treated with oxalyldihydrazide (see Figure 35C).

The highest cell count determined by the Trypan blue assay was in the highest drug treated cells and the lowest cell count was in the control cells. The more cells in the highest drug treated cells could explain the lower TNF-α produced in each cell, due to the similar amounts of TNF-α produced overall, as seen from the raw data (raw cell counts shown in Appendix

10.6.3-4). It is hypothesised that the control cells had overgrown and were dying due to the lack of nutrients in the media, which may indirectly increase the amount of TNF-α produced. Whereas in the drug treated cells the cyclohexanone may slow the growth of the cells, which inherently is protecting them from contact inhibition. Whereas, in the oxalyldihydrazide treated cells, there was no clear trend in the cell count, with increased drug concentration, either suggesting the drug is less toxic or that the actual concentration of oxalyldihydrazide was lower than calculated due to solubility issues discussed earlier. Unexpectedly, there was a lower number of cells when treated with 62.5μM oxalyldihydrazide which may explain the increase in TNF-α concentrations per live cell (Figure 35B). It is postulated that cyclohexanone treated RAW 264.7 cells produced larger amounts of TNF-α compared to oxalyldihydrazide, due to this breakdown product potentially driving the TNF-α accumulation which has been seen in MS patients (Sharief & Hentges 1991).

6.5.3 **Linkage of TNF-α to Pyroptosis**

The linkage between caspase-1 and caspase-11 in pyroptosis (see Figure 47) could be attributed to TNF-α. TNF-α and IFN- γ have been found to induce the caspase-1 gene expression. Jain, Sudhakar and Swarup (2007) found human lung carcinoma cell line A549 treated with 10-20ng/mL of TNF-α resulted in the increased expression of caspase-1 mRNA and protein levels.

McGeough et al. (2017) conveyed a link between TNF-α and Cryopyrin-Associated Periodic Syndromes (CAPS). The use of numerous KO backgrounds of mice including IL-1β / IL-18 caspase-1, caspase-11, Casp1/11- and TNF-α deficient strains of mice were used in the experiment. Using a knock in mouse model of *Nlrp3* inflammasomopathy, $Nlrp3^{A350V}$, showed with the treatment of TNF inhibitor etanercept allowed the pups to develop normally to adulthood. Similarly, $Nlrp3^{A350V}$ $Tnf^{-/-}$ mice conveyed similar phenotypic rescue, with a reduced expression of serum IL-1β and IL-18. Mice with a double KO $Nlrp3^{L351P}$ with $Ilr^{-/-}$ *and* $Il18^{-/-}$ resulted in better phenotypic rescue compared to mice with just the single cytokine KO. However, around 6 months of age there were observations of chronic inflammation compared to $Nlrp3^{L351P}$ $Casp^{1-/-}$ mice. Furthermore, 10μg/mL of LPS was injected into the mice, and by nine hours 80% of $Nlrp3^{L351P}$ with $Il1r^{-/-}$ and $Il18^{-/-}$ did not survive, whereas 100% of the control and $Nlrp3^{L351P}$ $Casp1/11^{-/-}$ survived. The above conveys that TNF-α plays a role in murine inflammasomopathy which mediates the progress of CAPS and potentially could play a role in

MS autoinflammation pathogenesis. It also suggests a potential link between TNF-α and pyroptosis, which could explain the cyclic nature of canonical and non-canonical pyroptosis.

6.6 *Medical Conditions Associated with Pyroptosis*

Numerous research has aimed to link pyroptosis to certain neurological conditions including MS, traumatic brain injury and Alzheimer's disease (McKenzie, Dixit & Power 2020). This form of programmed cell death differs from apoptosis (described in section 6.4.5). The growing research and interest in this inflammatory cell-death could provide more context in terms of therapeutic targets for neuroinflammation and neurodegeneration that occurs in the aforementioned diseases.

6.6.1 **Cryopyrin-Associated Periodic Syndromes**

CAPS is a mutative disorder where the threshold for the activation of NLRP3 is lowered, which increases the cytokine release, in particular, IL-1β, even without the presence of a stimulus (Jha & Ting 2009). This gain of function missense mutation is an autoinflammatory disease, that has demonstrated a link between neuroinflammatory diseases such as MS. For example, a study by Compeyrot-Lacassagne et al. (2009) showed that a 45 year old woman with muckle-wells syndrome (MWS), a form of CAPS, conveyed similar symptoms to MS. An MRI showed an anomaly in the fluid attenuation inversion recovery signal in the periventricular white matter, mainly residing in the temporal lobe and CC, which is consistent with demyelination that occurs in MS (Compeyrot-Lacassagne et al. 2009).

6.7 *Cell Numbers of Drug Treated RAW 264.7 Macrophages*

6.7.1 **Cell Numbers of RAW 264.7 Macrophages Treated with Cyclohexanone**

Cyclohexanone showed a cell reducing effect on RAW 264.7 macrophages that were re-activated in the activation mix, containing 1μg/mL of LPS and 1U/ml of IFN-γ (shown in Figure 31C). There was a decline in cell number with the increasing concentration of cyclohexanone. However, interestingly this trend was reversed in transiently activated RAW 264.7 macrophages (Figure 31C). There were differences in the total cell number between the activated and re-activated cells treated with cyclohexanone, shown in Figure 31A. Evidently showing that the effect of cyclohexanone on the cell number is dependent on the activation status of the RAW 264.7 macrophages.

6.7.2 **Cell Numbers of RAW 264.7 Macrophages Treated with Oxalyldihydrazide**

Similar to the cell numbers shown in the cyclohexanone treatment of RAW 264.7 macrophages, cells that were treated with oxalyldihydrazide in the presence of the activation mix (Figure 31B), 1μg/mL of LPS and 1U/mL of IFN-γ had a different amount of cells transiently activated: with the highest concentration of oxalyldihydrazide (5000μM) producing the highest cell counts in transiently activated cells but the lowest counts were observed following re-activation. This demonstrates the effect of oxalyldihydrazide on cell number is dependent on the activation status of the cells. When the cells were not re-activated with LPS and IFN-γ, no clear trend was discernible as the total live cells plateaued at the highest drug concentration (5000μM). This result may have been confounded by the poor solubility of oxalyldihydrazide, that may have limited the effective transfer of oxalyldihydrazide during serial dilutions, potentially impacting the cell numbers of the RAW 264.7 cells.

The differences in the cell numbers between the activated and re-activated RAW 264.7 cells, demonstrate the importance of the optimisation of the activation protocol and every study seems to be using different activation mixes (Chen et al. 2009; Reis et al. 2011). Overall, the data indicates that the breakdown products of CPZ appear to have a different effect in re-activated, activated and non-activated RAW 264.7 macrophages which is an important observation that has not been previously reported. This is an important finding as cells activated/primed with LPS and IFN-γ that were exposed to CPZ breakdown products may have

activated caspase-11 and caspase-1 respectively, resulting in the effects on cell numbers through the activation of the inflammatory pyroptotic pathway.

6.8 *Alamar Blue Assay*

The Alamar blue assay was used for activated and non-activated drug treated RAW 264.7 macrophages (see methods section 4.6). In the experiment there were significant differences between the FI in the non-activated, activated and re-activated macrophages treated with differing amounts of cyclohexanone shown in Figure 32A. The FI values were significantly larger in the non-activated cells compared to the activated and re-activated cells. This coincides with previous research shown in Figure 24B as the replication rate of cells of the non-activated cells remains consistently high, whereas, the activated RAW 264.7 macrophages reduced their cell numbers over the 24-hour activation time point.

The highest FI value was in the re-activated cells treated with 5000μM of cyclohexanone; whereas, the highest FI value in the activated cells was in the control cells. This does not correlate with the Trypan blue analysis in Figure 24A, as the highest cell number was in the control in the re-activated cells and highest in the 5000μM cyclohexanone treated activated RAW 264.7 cells. This inadvertently illustrates that the Alamar blue assay is not a reliable assay for measuring viability or number of live cells, but rather the metabolic status of the cells. This reverse trend in the re-activated and activated cyclohexanone treated cells was noted in the Trypan blue assay, further prompting the need to optimise the activation protocol when working with RAW 264.7 macrophages.

In Figure 32A, when comparing the FI value in the activated and re-activated cyclohexanone treated cells, the FI value was significantly higher when re-activated cells were treated with 500μM and 5000μM of cyclohexanone. This increase in FI correlates to the higher cell number shown in Figure 24B. This increase in FI when the cells are re-activated could be a result of the cells being placed back into the activation mix (1μg/mL of LPS and 1U/mL of IFN-γ), which could increase metabolic demand. Immunometabolism shows that the metabolic demands of immune cells are high, due to functional diversity (Kim 2018). In LPS-stimulated M1 macrophages there is a significant increase in aerobic glycolysis (Kim 2018). This is due to the demand of glucose being used for the biosynthesis of cytokines and chemokines (Kim 2018).

In Figure 32B, similar to the non-activated cyclohexanone treated cells, the oxalyldihydrazide treated cells showed increasing FI values with the increased oxalyldihydrazide concentration. There was also a significant difference in FI values between the non-activated, activated and re-activated oxalyldihydrazide treated cells shown in Figure 32B. There was not a clear trend in the activated oxalyldihydrazide treated cells with there not being no significant difference in FI values, with the exception of at 250μM and 5000μM. This could pertain to the solubility issues with oxalyldihydrazide. In the re-activated oxalyldihydrazide treated cells there was also an unclear trend occurring.

The metabolic activity was significantly decreased in both of the activated and re-activated RAW 264.7 macrophages treated with cyclohexanone and oxalyldihydrazide as shown in Figure 32 (A and B) compared to the non-activated cells. This could be attributed to CPZ breakdown products influencing the metabolism of the cells. Due to CPZ being a copper chelator, copper is an imperative aspect of the respiratory chain complex IV-cytochrome c oxidase in oligodendrocytes (Patergnani et al. 2017). This disruption with complex IV of the electron transport chain (ETC) in the cells is detrimental to oligodendrocytes, as myelin synthesis is an energy demanding process, posing oligodendrocytes as vulnerable to mitochondrial dysfunction when treated with CPZ (Bradl & Lassmann 2010). This damage is further accelerated through the simultaneous activation of oxidative stress and ROS production (Patergnani et al. 2017).

Shown in Figure 33 is the FI value divided by the total cell number and live cells. This data provided insight into how the highest drug concentration of cyclohexanone can have the highest FI, due to the lower number of cells in the well. This change in FI values when activating the RAW 264.7 cells could be attributed to the breakdown products of CPZ only exerting their interruption to the metabolic activity of the cells when they are activated with LPS and IFN-γ. However, the activated exhausted cells were revitalised when challenged by more LPS and IFN-γ and the breakdown products of CPZ, thereby sustaining a secondary metabolic response. Thus, facilitating the activation of caspases and inflammasomes required for pyroptosis to occur. However, due to the unknown nature of the exact mechanism in which CPZ impacts the metabolic activity of the cells and what metabolic activity the Alamar blue assay is detecting, the majority of the experiments in this thesis used Trypan blue assay to determine the number of live cells of the breakdown products of CPZ.

6.9 *Protein Arginine Methylation in RAW 264.7 Macrophages*

6.9.1 Protein Arginine Methylation in Non-Activated RAW 264.7 Macrophages

The optimisation of cell passage number was deemed important due to the differences in band intensity of WBs probed with anti-protein arginine methylation antibodies. The differences in band intensities based on differing cell passage numbers were evident in SYM10 at 130kDa, 72kDa and below 55kDa (shown in Figure 38). In the ASYM24 WB there was differences in relative densities in the non-activated cells at 130kDa, 55kDa and above 17kDa (shown in Figure 39). This change in relative density is evident in Figure 39B as the cells with the earliest passage number (4) had the only band identified by the ImageJ analysis at 130kDa MWT, not in the later passage numbers (7 and 9). It is speculated that this protein is an adhesion molecule, based on the molecular weight, which could explain why it isn't present in the later cell passages. Mass spectrometry would be required to confirm this finding.

6.9.2 Protein Arginine Methylation in Non-Activated and Activated RAW 264.7 Macrophages

The different bands detected on the WB of total cell lysates from activated versus non-activated RAW 264.7 cells could be due to different methylation of adhesion molecules. Within the activated and non-activated samples, in the ASYM24 WB, there was no identifiable band in the non-activated sample compared to the activated sample below 95kDa analysed by ImageJ (shown in Figure 44C). This could pertain to vascular cell adhesion molecule-1 (VCAM-1), which is a 90kDa glycoprotein induced by endothelial cells in conditions such as pro-inflammatory cytokines, TLR agonists and high levels of inflammation and stress (Kong et al. 2018). VCAM-1 is a major regulator of leukocyte adhesion (Kong et al. 2018). Elovaara et al. (2000) studied patients with RRMS and SPMS and found that there was an up regulation of adhesion molecules in the CSF and serum of these patients compared to the control. With patients with RRMS having a 4 fold higher expression of very late activation antigen 4 (VLA-4) and lymphocyte function associated antigen 1 (LFA-1) on CSF lymphocytes compared to the controls and SPMS having an approximately 3 fold higher expression of adhesion molecules compared to the controls, which could indicate more methylation or more of the protein. As well as vascular cell adhesion molecule 1(VCAM) being higher in serum of SPMS than in RRMS patients. Interestingly, intracellular adhesion molecule 1 (ICAM-1) was more upregulated in RRMS patients compared to the SPMS patients. To date no studies have been conducted to determine whether protein arginine methylation is different in MS patients or MS

models. Adhesion molecules have been detected in human serum and plasma in chronic inflammatory diseases. Future work into mass spectrometry to identify these adhesion molecules would be important when analysing WBs with RAW 264.7 macrophages treated with the breakdown products of CPZ.

6.9.3 **Heat Shock Proteins**

One of the potential proteins around 70kDa in the ASYM24 blots in the activated and non-activated RAW 264.7 macrophages could be a heat shock protein (HSP) (shown in Figure 44D). The increase in relative density in the activated cells was significantly higher than the non-activated cells. HSPs are conserved ubiquitous intracellular proteins. They are expressed in both micro-organisms and mammalian cells (Javid, Macary & Lehner 2007).

HSPs are known to be immunoregulatory agents that are molecular protein chaperones (Streicher 2019). HSP can be expressed in response to pathogen associated molecular patterns, including LPS (Wang et al. 2006). HSPs are subsequently released after cell lysis due to injury or infection. They have been found to have immunoactivity roles, as they bind to macrophage surface receptors and up regulate functions such as cytokine release and tumour rejection (Wang et al. 2006). They are expressed in all cell types and are found in the cytosol (HSP70 and HSP 90), nuclei, ER and mitochondria. The induction of HSPs can occur through heat shock, toxins, oxidative stress which causes cells lysis, subsequently resulting in large quantities of HSP in the extracellular fluid (Wang et al. 2006).

One of the potential therapeutic targets of HSP70 is evident as it is a protein that negatively regulates NLRP3 inflammasome activation (Martine et al. 2019). Martine et al. (2019) found the overexpression of HSP70 down-regulates the expression of caspase-1 activation and IL-1β. Conversely, when there was HSP70 deficiency, the IL-1β maturation and caspase-1 activation increased in BMDMs. Further research into protein arginine methylation in disease states could assist in reduction in symptoms and in the scenario of reduction of IL-1β and caspase-1 could reduce demyelination in MS through inducing HSP70.

6.9.4 **PRMT1 in Non-Activated and Activated RAW 264.7 Macrophages**

Furthermore, in Figure 45A the relative density of the PRMT1 band was lowered in the activated versus the non-activated RAW 264.7 macrophages. These results correlate with the data collected by Fan et al. (2017) who discovered using a quantitative polymerase chain reaction that RAW 264.7 cells demonstrated a down-regulated expression of PRMT1 mRNA levels as early as the 8 hours when activated with IFN-γ. Furthermore, WB revealed that RAW 264.7 cells treated with IFN-γ had reduced PRMT1 protein levels (Fan et al. 2017). This indicates that IFN-γ negatively regulates PRMT1 expression and potentially the function of activated macrophages.

7.0 Future Work

7.1 *Morphological Changes in Activated RAW 264.7 Macrophages*

Future work on the morphological changes in activated RAW 264.7 cells would be to repeat the experiments in triplicates and increase the sample size of light microscopy images for analysis. Furthermore, the use of lower cell passage number would be advisable to observe if the passage number impacts the morphology of the cells, to ensure this does not introduce a new variable when interpreting the drug treatment experiments. Additionally, due to the adherent nature of the cells, the use of an inverted phase contrast microscopy could be used to observe the morphology of the cells better, obtaining a different image of the cells adhered to the bottom of the flask.

7.2 *Viability changes in Activated RAW 264.7 Macrophages*

Future work focusing on RAW 264.7 macrophages would involve the activated and re-activated macrophages (1μg/mL of LPS and 1U/mL of IFN-γ). This experiment would replicate the drug treatment protocol; however, no drug will be applied to the cells. This will provide more controls to compare to the drug treatment experiment. This information on the total cell number and number of live cells for each of these timepoints in RAW 264.7 macrophages will determine how the activation status influences how the breakdown products of CPZ impact the macrophages.

7.3 *Morphological changes in Drug Treated RAW 264.7 Macrophages*

7.3.1 **Morphological changes in Activated Drug Treated RAW 264.7 Macrophages**

The morphological changes in the activated RAW 264.7 cells that would be of interest to further study would be the elongation of the cells after the activation and drug treatment and their alignment with M1 and M2 polarisation states. Morphometric analysis would be required to determine the significance of these findings. This may provide further insight into how the change in morphology of the RAW 264.7 macrophages affects the functioning and capacity of the cell to perform its immunological task, by quantifying and comparing the release of specific cytokines. These investigations could help unveil the mechanism behind the breakdown

products of CPZ and determine how this change in morphology correlates with a change in the function of the macrophages. To distinguish whether the elongated morphology of oxalyldihydrazide treated cells is consistent with activation of M2 macrophages detailed analysis of known M2 markers, namely the mannose receptor (CD206) and enzyme arginase receptor (Arg1), are proposed. In contrast, analysis of the surface markers CD86 and CD16/32, for M1 'classically' activated macrophages is proposed for cyclohexanone treated cells. A wider scale study on other cell types including, microglia and oligodendrocytes would be used to see whether similar morphological and functional changes are apparent when these cell lines are treated with cyclohexanone and oxalyldihydrazide.

7.3.2 **Multi Nucleated Giant Cells**

An investigation into the MNGCs, or potentially the effect of the drugs on cell replication would be an interesting and worthwhile experiment, as these aspects have not to date been investigated, despite MNGCs having been implicated in other diseases. Increasing the number of replicates and including CPZ testing in RAW 264.7 macrophages, as well as comparative studies on microglia and oligodendrocytes are required to observe the role of MNGCs formation in cell types typically associated with demyelinating diseases such as MS. Morphometric analysis is required to determine the significance of the size difference between these cells. This would help understand the destructive inflammatory pathway in MS and will also help denote the mechanism of action of CPZ and its breakdown products. Furthermore, an investigation into what cytokines may play a role in the formation of MNGCs in both the RAW 264.7 cells and microglia, especially IL-1β, IL-18, LPS, and TNF-α should be considered. If the results are consistent, MNGCs could potentially be a pathological hallmark and diagnostic/prognostic marker for MS or inflammatory diseases more broadly. The use of MS patient samples as a comparison, including peripheral blood and CSF, would be interesting future work to see if there is the presence of MNGCs and if it potentially only occurs in certain types of MS, which would especially assist patients with RRMS.

7.3.3 **Failure in Cytokinesis**

Future work into how CPZ and its breakdown products influence the cell cycle would provide knowledge on the formation of MNGCs, potentially due to the interruption in cytokinesis. Future work using flow cytometry with synchronised cells, could help explain the effects of CPZ breakdown products on macrophages. This would be of particular interest as systemic

CPZ is known to prevent oligodendrocytes from leaving the cell cycle and becoming mature oligodendrocytes (Mi et al. 2016). Future work on oligodendrocytes treated with the two separate breakdown products of CPZ would be of interest, to observe if there is a potent breakdown product accelerating this problematic state in the cell cycle, leading to defects in the myelination process associated with MS.

7.3.4 **Pyroptosis**

In this thesis an up-regulation of IL-1β and TNF-α in the activated, drug treated RAW 264.7 macrophages was observed. However, due to the complexity of the pyroptosis pathway further ELISA analysis on caspase-1 and the NLRP3 inflammasome would be required in order to gain a greater understanding on how cyclohexanone and oxalyldihydrazide affect the inflammatory pathways in macrophages. Furlan et al. (1999), studied the role of caspase-1 in MS. The study involved 12 participants, 7 with RRMS and 5 healthy controls. During the course of the experiment, PBMCs were collected every 15 days for a period of 1 year for the RRMS group and every 15 days for 2 months for the control group. Compared to the control's average, the mRNA levels of caspase-1 in PBMCs increased two to three-fold one week before an attack in the RRMS patients. Furthermore, there was a correlation between the caspase-1 PBMC mRNA and new lesions detected by MRI. This may pertain to caspase-1 being an immunological marker for repeated episodes.

Several studies have observed cytokines and inflammasomes associated with the pyroptotic pathway, but the connection as to how this form of cell death contributes to CPZ induced demyelination is a question that remains unsolved (Kang et al. 2012). NLRP3 is a regulator of CNS inflammation and demyelination which is characteristic of many neurological disorders and diseases. This regulation occurs through caspase-1 and IL-18 (Jha et al. 2010). This is evident as Jha et al. (2010) discovered that the *Nlrp3* gene was expressed 100 fold higher in the CPZ induced demyelination model, with 6-8 week old mice fed with 0.2% CPZ for 6 weeks. Mice lacking the *Nlrp3* gene, however, demonstrated delayed demyelination and neuroinflammation including microglial infiltration and astrogliosis and loss of oligodendrocytes compared to the WT mice (Jha et al. 2010). Prednisone has been shown to have a protective effect for individuals suffering from demyelinating diseases of the CNS and produce an inhibitory effect on the activation of the NLRP3 inflammasome and related chemokines including TNF-α in CPZ induced mice (Yu et al. 2018). As a future project, it

would be of great interest to have a comparative study of macrophages with microglia, to be able to determine the potential similarities and differences, which may underlie the immunological pathology associated with MS. Furthermore, the use of animal studies, injected with the breakdown products of CPZ, could help determine which part of CPZ is neurotoxic. Future experimental designs would include tissue culture, and investigation of the CPZ breakdown products in neuronal and Schwann cells.

7.3.5 **Pyroptotic Bodies**

Further investigation into the morphological changes that occurred in the RAW 264.7 macrophage cells in Figure 23 and 26 would be of interest. In particular, using a stain with propidium iodide (PI) of the blebbing occurring with the drug treatments, would help confirm the hypothesis of this change being pyroptotic bodies. Furthermore, the use of a larger sample size for the light microscopy images collected and higher magnification would be useful for future analysis. To be able to distinguish what form of cell death is occurring, the use of a GSDMD antibody, mixed linkage kinase domain like (MLKL) oligomers antibody will help determine if it is pyroptosis or necroptosis respectively as they are the executing proteins involved in these two different forms of cell death (Chen et al. 2016). Furthermore, the use of electron microscopy will help provide high resolution images of the cells to distinguish the morphological changes.

7.4 *Viability of RAW 264.7 Macrophages after Drug Treatment*

Future work on the breakdown product of CPZ would involve repeating the drug-treatment experiment in triplicate, to ensure the cell count is replicable and that the trends when activating and re-activating the RAW 264.7 macrophages are repeatable. Furthermore, as noted previously further optimisation of the cell culturing would involve the reduction in the time frame activating and treating the cells with the drugs to prevent the activation mix interfering with the viability of the cells. Furthermore, due to the plateau that was apparent in the live cells in Figure 31D when the cells were not re-activated when treated with oxalyldihydrazide further optimisation of the protocol to ensure the solubility of the drug will be required. For a comparative study, the Griess reagent could be used on the re-activated versus the non-reactivated RAW 264.7 cells treated with cyclohexanone and oxalyldihydrazide to evaluate the nitrite concentration, which indirectly measures activated cells through NO.

7.5 *Cytokine Production by Drug Treated RAW 264.7 Macrophages*

7.5.1 **TNF-α**

In relation to the non-drug treated cells, additional experiments on TNF-α ELISA would be undertaken to obtain a larger sample size. This experiment would be repeated, and the amount of the TNF-α would be reduced to 1μg/mL of LPS and 1U/mL of IFN-γ instead of 10μg/mL of LPS and 10U/mL of IFN-γ. This experiment will be repeated with earlier time points including 1,2,4 and 6-hour time points. Additionally, IL-10 concentration will be measured, as it is an anti-inflammatory cytokine that has a role in supressing TNF-α concentration, which is released from LPS activated macrophages.

Furthermore, due to time restraints and the uncertain nature of the COVID-19 pandemic, replicates could not be completed. Future work on TNF-α experiment should include what the effect of CPZ breakdown products is when it is re-activated when treating the RAW 264.7 macrophages with the drug, to see if it has a similar trend to the IL-1β. This is due to the TNF-α showing similar trend in the IL-1β amounts when the cells were not re-activated in the activation mix. Although the mouse model is a great way to help scientists understand complex pathological pathways in human diseases, there are definite discrepancies between mice and

humans. Insights into the pathological mechanisms within MS patients is necessary, this would require human MS samples including PBMC and CSF.

7.5.2 **IL-1β**

Replicates of the IL-1β assay on the cyclohexanone and oxalyldihydrazide drug experiment need to be performed, including both the activated and re-activated cells. Furthermore, due to the changes in the trends that occurred in the results when dividing the concentration of the cytokine by the total cell number, with the cell number largely influencing the trend. Further optimisation of the activation mix and drug treatment, needs to be done in the future. This would include simultaneously treating and activating the drugs or potentially activating the cells before the drug treatment for a shorter period, to ensure that the LPS and IFN-γ do not drastically reduce the cell number of the RAW 264.7 cells. To eliminate the solubility issue of oxalyldihydrazide, repeat experiments on CPZ could be used in the future. A potentially valuable future study would be using PBMCs from CPZ treated mice as a comparative study for the IL-1β concentrations.

7.5.3 **IL-18 and IL-6**

Although no IL-18 and IL-6 experiments were performed during this thesis, future work on cell cultures, using an ELISA when treating the RAW 264.7 cells with the breakdown product of CPZ should be performed. IL-6 is not a specific product of pyroptosis, however in terms of MS it is known to be a compelling cytokine that eventuates in the acute phase response in MS (Göbel, Ruck & Meuth 2018). One of the reasons that IL-6 is a cytokine of interest in MS, is that IL-6 knockout mice were observed to be fully resistant to the EAE model, suggesting that IL-6 is required for mice to be symptomatic of EAE (Samoilova et al. 1998). Future work regarding IL-6 would provide more input into the role of inflammatory cell death in demyelinating diseases.

7.6 ***Alamar Blue***

As a future project further experimentation into how variables influence the Alamar blue assay would be of interest. A repeat experiment on the re-activated RAW 264.7 macrophages as a comparison to the activated, non-activated and drug treated cells. This would hopefully provide more insight into how CPZ breakdown products and the activation status of the cells influences

the metabolism of the cells and how useful it is as a viability assay. Another comparative study will involve the RAW 264.7 macrophages being treated with CPZ and the Alamar blue assay results will be compared to the cells treated with each of the breakdown products of CPZ.

7.7 *Protein Arginine Methylation*

In terms of the protein arginine methylation, further studies using mass spectrometry would be required to gain knowledge of the identity of different methylated proteins that were observed in this thesis in activated versus non-activated RAW 264.7 cells. Furthermore, WBs on the cells treated with the breakdown products of CPZ would help investigate how CPZ breakdown products may initiate inflammation through PRMTs, which could provide information on the pathological process associated with demyelination. Specifically, looking at pyroptosis, potentially caspase-1 protein levels in MS patients, which may help uncover more information on the relevance of this inflammatory cell death in MS.

Replicates and mass spectrometry are required to identify the protein at 70kDa in Figure 44D. Adding to this experiment, WBs on the drug treated cells would be performed to see how HSP70 is affected, with the comparison to CPZ treated cells. To determine whether HSP70 inducers could be a potential drug treatment for neurological diseases mice overexpressing HSP70 would be treated with CPZ, and the macrophages/microglia will be tested against the control. Furthermore, investigation into adhesion molecules in the drug treated RAW 264.7 cells will help elucidate the potential involvement of MNGCs, the particular adhesion molecule of interest is VCAM-1. Furthermore, the downregulation of PRMT1 in activated RAW 264.7cells is hypothesised to be a result of IFN-γ which is one of the substances that was used to activate the cells, which has been previously recognised in this cell line (Fan et al. 2017). This would be repeated in triplicates and compared to the drug treated RAW 264.7 macrophages. Repeated experiments using the two breakdown products of CPZ to see the effect of the drugs on protein arginine methylation and PRMT1 as well as PRMT5 expression. An antibody to any protein of interest would be used to detect whether there is up-regulation of the protein or an increase in protein arginine methylation.

7.8 *Potential Future Therapeutic Targets for Demyelinating Diseases*

Despite numerous studies on the cytokines, inflammasome activation and the induction of pyroptosis via caspase-1 and caspase-11, further research is required to fill the gap in knowledge regarding the regulation of these cytokines as potential therapeutic agents (He et al. 2015). Cancer and inflammatory disorders flourish in an environment where a deregulation of caspases occurs. This further emphasises the need to understand the mechanism and regulation of these endoproteases (McIlwain, Berger & Mak 2013). Furthermore, understanding the mechanism of abnormally regulated protein-arginine methylation which may be because of pyroptosis or another pathway that is activated by the CPZ breakdown products may assist in the construction of therapeutic targets for demyelinating diseases.

A study conducted by Jha et al. (2010) showed IL-18 $^{-/-}$ mice displayed an increased rate of remyelination, suggesting that IL-18 may be a pharmacological target to increase remyelination (Jha et al. 2010). The treatment with IL-1 blockers has been largely successful for the treatment of CAPS (McGeough et al. 2017). Collectively, this provides a plausible link between NLRP3 and caspases with neuroinflammation and demyelination. NLRP3 is said to be involved in the aetiology of diseases including Alzheimer's, Parkinson's, Prion and Type 2 diabetes (Tunctan et al. 2017). Further studies are required to determine if NLRP3, caspases, and pyroptosis have a direct or indirect effect on neurological conditions (Jha et al. 2010).

Adding to this, Kang et al. (2012) discovered that mice deficient in IL-17A, IL-17RC and adaptor protein Act 1 had less demyelination, and microglial reactivity compared to the WT, despite all mice being fed 0.2% CPZ for 4 weeks. Lalor et al. (2011) observed that pyroptosis via caspase-1 in immune cells is vital for the T cell production of IL-17 for the production of autoimmunity including neuroinflammation and demyelination. This could potentially provide a link between the IL cytokines and MS.

Some theories of why TNF-α blockers may be ineffective in MS patients could pertain to the inability of the drugs to target the CNS (Pegoretti et al. 2018). In terms of the Lenercept study, negative effects could be attributed to the pleiotropic effects of TNF; blocking both the pro and anti-inflammatory functions of TNF-α may be the reason behind the ineffective results of the treatment (Dong et al. 2016). The specificity on the cytokine's receptor deems to be clinically

relevant. This is evident as TNFR1 silencing or TNFR2 activation appear to be potential pathways by which therapeutic targets for MS could emerge (Pegoretti et al. 2018).

Protein arginine methylation is a field of research that is emerging regarding demyelinating diseases such as MS. It has been suspected to play a role in the pathologic immune response evident in MS (Webb & Guerau-de-Arellano 2017). *In vivo* studies conducted on rats showed that the inhibition of methylation reactions with methylthioadenosine resulted in decreased inflammation and severity of the disease. This is evident as T lymphocytes are a cell that is sensitive to any changes in the arginine methylation of protein. This suggests that there could be a potential therapeutic target associated with altering the methylation in demyelinating and inflammatory diseases (Parry & Ward 2010).

8.0 Conclusions

In conclusion, there were visual changes in the cell morphology that occurred when the RAW 264.7 macrophages were activated, and drug treated with the breakdown products of CPZ. This thesis revealed changes within cell morphology that were hypothesised to pertain to the process of pyroptosis. The development of multinucleated giant RAW 264.7 cells was apparent when treating the cells with cyclohexanone and oxalyldihydrazide, which needs to be further investigated to determine if they are MNGCs or if there is a hindered process in cytokinesis. This could provide further insight into how CPZ interacts with the immune cells as well as identify possible diagnostic markers for demyelinating diseases such as MS.

Future work is required to understand the impact of CPZ breakdown products on the metabolism of the cells to be able to use the Alamar blue assay credibly in comparison to the Trypan blue assay. However, the drop in FI in the activated cyclohexanone treated RAW 264.7 macrophages may spark more interest into how CPZ influences the metabolism of macrophages. The Trypan blue assay showed a positive correlation between the live cell numbers and the cyclohexanone and oxalyldihydrazide concentration. This was only notable when the macrophages were re-activated in the activation mix (1μg/mL of LPS and 1U/mL of IFN-γ). Figure 49 summarises the results, observations, and future work derived from this thesis.

There were significant differences in activated versus non-activated cells in terms of protein arginine methylation, with future work involving the investigation of protein arginine methylation in drug treated RAW 264.7 macrophages. The observed changes in protein arginine methylation of proteins in WBs could allude to heat shock proteins and adhesion molecules. Furthermore, changes in the protein methylation in the activated versus non-activated RAW 264.7 macrophages provide a baseline for the changes in methylation, which future work could stem to analyse the changes in protein methylation after treatment with each of the two breakdown products of CPZ.

Using ELISA kits, the cytokine concentrations when the RAW 264.7 macrophages were activated, and drug treated using different protocols demonstrated alternating results. This revealed the importance of the optimisation of cell culture work and the numerous variables

that can occur. An interesting analysis was the different effects noted in RAW 264.7 cells that were placed in the activation mix when treated with the drugs (re-activated) and the cells not placed in activation mix when treated with the drugs (activated). The differences in cell numbers as well as IL-1β and TNF−α concentration in the drug treated cells is postulated to be an effect associated with the pyroptosis pathway and the M1/M2 status of the macrophages.

The cellular morphology, the effect of CPZ breakdown products on cell number and cytokine production in drug treated RAW 264.7 macrophages could provide further insight into the potential role of pyroptosis in the pathogenesis of demyelinating diseases which could allude to more diagnostic markers and potential therapeutic targets.

.

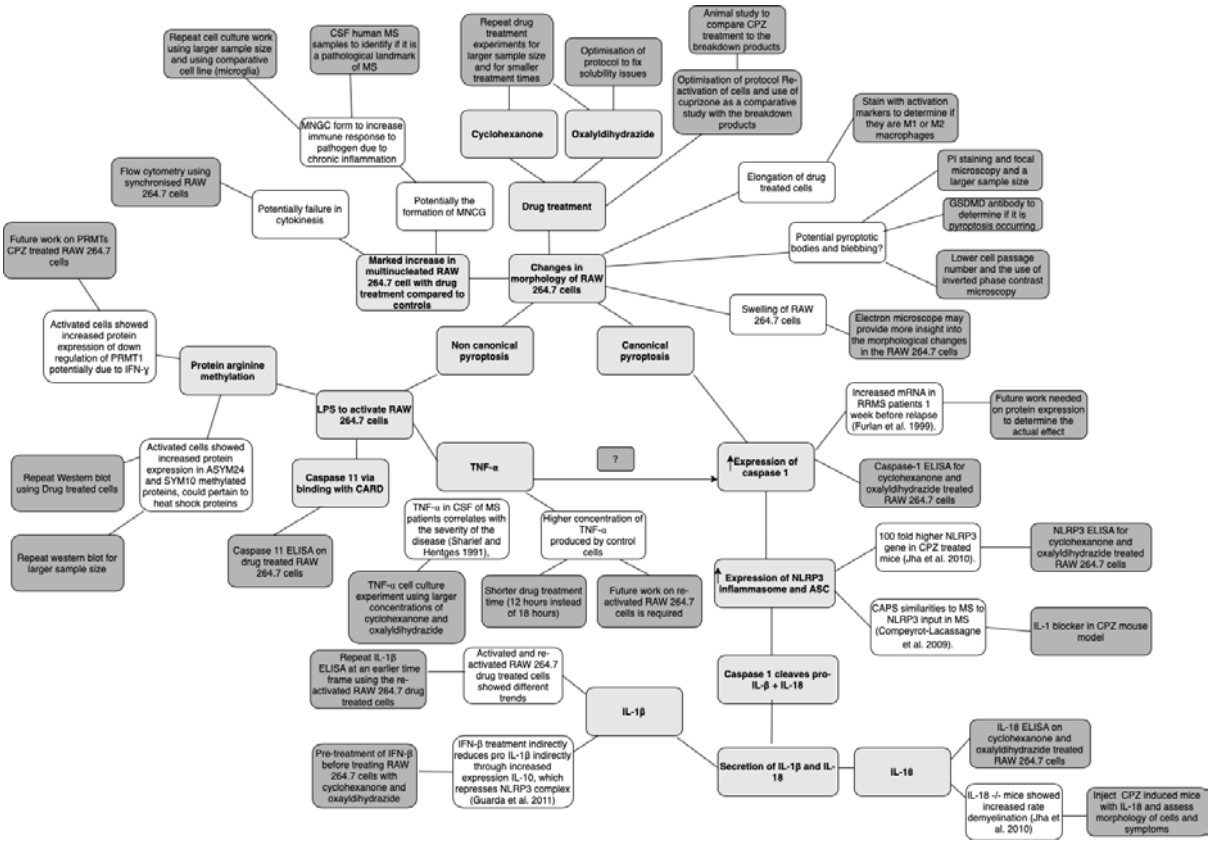

Figure 49: Summary of results, observations and suggested future work.
Light grey boxes indicate study areas of interest. White boxes indicate observations and results from this thesis (except for those with references). Dark grey boxes indicate future work (Mind map made using Draw.io).

9.0 References

Aguzzi, A, Barres, BA & Bennett, ML 2013, 'Microglia: Scapegoat, saboteur, or something else?', *Science*, vol. 339, no. 6116, pp. 156-61.

Akassoglou, K, Bauer, J, Kassiotis, G, Pasparakis, M, Lassmann, H, Kollias, G et al. 1998, 'Oligodendrocyte apoptosis and primary demyelination induced by local tnf/p55tnf receptor signaling in the central nervous system of transgenic mice', *The American Journal of Pathology*, vol. 153, no. 3, pp. 801-13.

Al-Nasiry, S & Geusens, N 2007, 'The use of alamar blue assay for quantitative analysis of viability, migration and invasion of choriocarcinoma cells', *Human Reproduction*, vol. 22, no. 5, pp. 1304-09.

Alliot, F, Godin, I & Pessac, B 1999, 'Microglia derive from progenitors, originating from the yolk sac, and which proliferate in the brain', *Developmental Brain Research*, vol. 117, no. 2, pp. 145-52.

Almuslehi, MSM, Sen, MK, Shortland, PJ, Mahns, DA & Coorssen, JR 2020, 'Cd8 t-cell recruitment into the central nervous system of cuprizone-fed mice: Relevance to modeling the etiology of multiple sclerosis', *Frontiers in Cellular Neuroscience*, vol. 14, no. 43, pp. 1-20.

Álvarez, S, van Der Goot, FG & Muñoz-Fernández, MÁ 2013, 'Tnf-α may mediate inflammasome activation in the absence of bacterial infection in more than one way', *PLoS ONE*, vol. 8, no. 8, p. e71477.

Arnett, HA, Mason, J, Marino, M, Suzuki, K, Matsushima, GK & Ting, JPY 2001, 'Tnfα promotes proliferation of oligodendrocyte progenitors and remyelination (book review)', *Nature Neuroscience*, vol. 4, no. 11, pp. 1116-22.

Arora, M 2013, 'Cell culture media: A review', *Mater Methods*, vol. 3, no. 175.

ATCC 2022, RAW 264.7, viewed 21 August 2022, < https://www.atcc.org/products/tib-71>.

Basavarajappa, BS & Subbanna, S 2021, 'Histone methylation regulation in neurodegenerative disorders', *International Journal of Molecular Sciences*, vol. 22, no. 9, p. 4654.

Bedford, MT 2007, 'Arginine methylation at a glance', *Journal of Cell Science*, vol. 120, no. Pt 24, pp. 4243-6.

Bergsbaken, T, Fink, S & Cookson, B 2009, 'Pyroptosis: Host cell death and inflammation', *Nature Reviews. Microbiology*, vol. 7, no. 2, pp. 99-109.

Beutler, B & Rietschel, ET 2003, 'Innate immune sensing and its roots: The story of endotoxin', *Nature Reviews Immunology*, vol. 3, pp. 169-76.

Beutler, BA 1999, 'The role of tumor necrosis factor in health and disease', *The Journal of Rheumatology*, vol. 57, pp. 16-21.

Biancotti, JC, Kumar, S & de Vellis, J 2008, 'Activation of inflammatory response by a combination of growth factors in cuprizone-induced demyelinated brain leads to myelin repair', *Neurochemical Research*, vol. 33, no. 12, pp. 2615-28.

Bjornevik, K, Cortese, M, Healy, BC, Kuhle, J, Mina, MJ, Leng, Y et al. 2022, 'Longitudinal analysis reveals high prevalence of epstein-barr virus associated with multiple sclerosis', *Science (American Association for the Advancement of Science)*, vol. 375, no. 6578, pp. 296-301.

Blanc, RS & Richard, S 2017, 'Arginine methylation: The coming of age', *Molecular Cell*, vol. 65, no. 1, pp. 8-24.

Boutilier, AJ & Elsawa, SF 2021, 'Macrophage polarization states in the tumor microenvironment', *International Journal of Molecular Sciences*, vol. 22, no. 13, p. 6995.

Bradl, M & Lassmann, H 2010, 'Oligodendrocytes: Biology and pathology', *Acta Neuropathologica*, vol. 119, no. 1, pp. 37-53.

Brown, MA, Wallace, CS, Anamelechi, CC, Clermont, E, Reichert, WM & Truskey, GA 2007, 'The use of mild trypsinization conditions in the detachment of endothelial cells to promote subsequent endothelialization on synthetic surfaces', *Biomaterials*, vol. 28, no. 27, pp. 3928-35.

Brownlee, WJ, Hardy, TA, Fazekas, F & Miller, DH 2017, 'Diagnosis of multiple sclerosis: Progress and challenges', *The Lancet*, vol. 389, no. 10076, pp. 1336-46.

Burm, SM, Peferoen, LAN, Zuiderwijk-Sick, EA, Haanstra, KG, t Hart, BA, van der Valk, P et al. 2016, 'Expression of il-1[beta] in rhesus eae and ms lesions is mainly induced in the cns itself.(report)', *Journal of Neuroinflammation*, vol. 13, no. 1, pp. 1-16.

Burnette, WN 1981, '"Western blotting": Electrophoretic transfer of proteins from sodium dodecyl sulfate-polyacrylamide gels to unmodified nitrocellulose and radiographic detection with antibody and radioiodinated protein a', *Analytical biochemistry*, vol. 112, no. 2, pp. 195-203.

Carlton, WW 1966, 'Response of mice to the chelating agents sodium diethyldithiocarbamate, α-benzoinoxime, and biscyclohexanone oxaldihydrazone', *Toxicology and Applied Pharmacology*, vol. 8, no. 3, pp. 512-21.

Casano, AM & Peri, F 2015, 'Microglia: Multitasking specialists of the brain', *Developmental Cell*, vol. 32, no. 4, pp. 469-77.

Centonze, D, Muzio, L, Rossi, S, Furlan, R, Bernardi, G & Martino, G 2009, 'The link between inflammation, synaptic transmission and neurodegeneration in multiple sclerosis', *Cell Death and Differentiation*, vol. 17, no. 7, pp. 1083-91.

Chastain, EML, Duncan, D, Amp, Apos, Anne, S, Rodgers, JM et al. 2011, 'The role of antigen presenting cells in multiple sclerosis', *Biochimica et Biophysica Acta (BBA) - Molecular Basis of Disease*, vol. 1812, no. 2, pp. 265-74.

Chen, D, Zeng, S, Huang, M, Xu, H, Liang, L & Yang, X 2017, 'Role of protein arginine methyltransferase 5 in inflammation and migration of fibroblast-like synoviocytes in rheumatoid arthritis', *Journal of Cellular and Molecular Medicine*, vol. 21, no. 4, pp. 781-90.

Chen, L, Deng, H, Cui, H, Fang, J, Zuo, Z, Deng, J et al. 2018, 'Inflammatory responses and inflammation-associated diseases in organs', *Oncotarget*, vol. 9, no. 6, pp. 7204-18.

Chen, T-L, Chang, C-C, Lin, Y-L, Ueng, Y-F & Chen, R-M 2009, 'Signal-transducing mechanisms of ketamine-caused inhibition of interleukin-1β gene expression in lipopolysaccharide-stimulated murine macrophage-like raw 264.7 cells', *Toxicology and Applied Pharmacology*, vol. 240, no. 1, pp. 15-25.

Chen, X, He, W-T, Hu, L, Li, J, Yuan, F, Wang, X et al. 2016, 'Pyroptosis is driven by non-selective gasdermin-d pore and its morphology is different from mlkl channel-mediated necroptosis', *Cell Research*, vol. 26, no. 9, pp. 1007-20.

Cho, J-H, Lee, R, Kim, E, Choi, YE & Choi, E-J 2018, 'Prmt1 negatively regulates activation-induced cell death in macrophages by arginine methylation of gapdh', *Experimental Cell Research*, vol. 368, no. 1, pp. 50-58.

Chu, F, Shi, M, Zheng, C, Shen, D, Zhu, J, Zheng, X et al. 2018, 'The roles of macrophages and microglia in multiple sclerosis and experimental autoimmune encephalomyelitis', *Journal of Neuroimmunology*, vol. 318, pp. 1-7.

Coggan, JS, Bittner, S, Stiefel, KM, Meuth, SG & Prescott, SA 2015, 'Physiological dynamics in demyelinating diseases: Unraveling complex relationships through computer modeling', *International Journal of Molecular Sciences*, vol. 16, no. 9, pp. 21215-36.

Compeyrot-Lacassagne, S, Tran, T-A, Guillaume-Czitrom, S, Marie, I & Koné-Paut, I 2009, 'Brain multiple sclerosis-like lesions in a patient with muckle–wells syndrome', *Rheumatology*, vol. 48, no. 12, pp. 1618-19.

Constantinescu, CS, Farooqi, N, O'Brien, K & Gran, B 2011, 'Experimental autoimmune encephalomyelitis (eae) as a model for multiple sclerosis (ms)', *British Journal of Pharmacology*, vol. 164, no. 4, pp. 1079-106.

Cox, K, Quello, K, Deford, R & Beckerman, J 2009, 'A rapid method to quantify fungicide sensitivity in the brown rot pathogen monilinia fructicola', *Plant Disease*, vol. 93, no. 4, pp. 328-31.

Dai, B, Wei, D, Zheng, N-n, Chi, Z-h, Xin, N, Ma, T-x et al. 2019, 'Coccomyxa gloeobotrydiformis polysaccharide inhibits lipopolysaccharide-induced inflammation in raw 264.7 macrophages', *Cellular Physiology and Biochemistry*, vol. 51, no. 6, pp. 2523-35.

David, S & Kroner, A 2011, 'Repertoire of microglial and macrophage responses after spinal cord injury', *Nature Reviews Neuroscience*, vol. 12, no. 7, pp. 388-99.

Dhananjaya, N, Nagabhushana, H, Nagabhushana, BM, Rudraswamy, B, Sharma, SC, Sunitha, DV et al. 2012, 'Effect of different fuels on structural, thermo and photoluminescent properties

of gd2o3 nanoparticles', *Spectrochimica Acta. Part A, Molecular and Biomolecular Spectroscopy*, vol. 96, pp. 532-40.

Dinarello, CA 2018, 'Overview of the interleukin-1 family in innate inflammation and acquired immunity', *Seminars in Immunology*, vol. 281, no. 1, pp. 8-27.

Dinarello, CA, Novick, D, Kim, S & Kaplanski, G 2013, 'Interleukin-18 and il-18 binding protein', *Frontiers in Immunology*, vol. 4, pp. 289-89.

Dong, Y, Fischer, R, Naudé, PJW, Maier, O, Nyakas, C, Duffey, M et al. 2016, 'Essential protective role of tumor necrosis factor receptor 2 in neurodegeneration', *Proceedings of the National Academy of Sciences of the United States of America*, vol. 113, no. 43, pp. 12304-09.

Duque, GA & Descoteaux, A 2014, 'Macrophage cytokines: Involvement in immunity and infectious diseases', *Frontiers in Immunology*, vol. 5, no. 491, pp. 491-91.

Elovaara, I, Ukkonen, M, Leppäkynnäs, M, Lehtimäki, T, Luomala, M, Peltola, J et al. 2000, 'Adhesion molecules in multiple sclerosis: Relation to subtypes of disease and methylprednisolone therapy', *Archives of Neurology*, vol. 57, no. 4, pp. 546-51.

Fan, Z, Li, Z, Li, P, Ye, Q, Xu, H, Wu, X et al. 2017, 'Protein arginine methyltransferase 1 (prmt1) represses mhc ii transcription in macrophages by methylating ciita', *Scientific Reports*, vol. 7, pp. 1-9.

Feldmann, M, Brennan, FM, Elliott, M, Katsikis, P & Maini, RN 1994, 'Tnf alpha as a therapeutic target in rheumatoid arthritis', *Circulatory Shock*, vol. 43, no. 4, pp. 179-84.

Fierz, W 2017, 'Multiple sclerosis: An example of pathogenic viral interaction?', *Virology Journal*, vol. 14, no. 1, pp. 42-42.

Fink, SL & Cookson, BT 2005, 'Apoptosis, pyroptosis, and necrosis: Mechanistic description of dead and dying eukaryotic cells', *Infection and Immunity*, vol. 73, no. 4, pp. 1907-16.

Flynn, JL, Goldstein, MM, Chan, J, Triebold, KJ, Pfeffer, K, Lowenstein, CJ et al. 1995, 'Tumor necrosis factor-alpha is required in the protective immune response against mycobacterium tuberculosis in mice', *Immunity*, vol. 2, no. 6, pp. 561-72.

Frances, YM, Tingting, W, Phoebe, N, Thanh, C & Wendy, FL 2013, 'Modulation of macrophage phenotype by cell shape', *Proceedings of the National Academy of Sciences of the United States of America*, vol. 110, no. 43, pp. 17253-58.

Furlan, R, Filippi, M, Bergami, A, Rocca, MA, Martinelli, V, Poliani, PL et al. 1999, 'Peripheral levels of caspase-1 mrna correlate with disease activity in patients with multiple sclerosis; a preliminary study', *Journal of Neurology, Neurosurgery & Psychiatry*, vol. 67, no. 6, pp. 785-88.

Gaudino, SJ & Kumar, P 2019, 'Cross-talk between antigen presenting cells and t cells impacts intestinal homeostasis, bacterial infections, and tumorigenesis', *Frontiers in Immunology*, vol. 10, pp. 360-60.

Geissmann, F, Manz, MG, Jung, S, Sieweke, MH, Merad, M & Ley, K 2010, 'Development of monocytes, macrophages, and dendritic cells', *Science (American Association for the Advancement of Science)*, vol. 327, no. 5966, pp. 656-61.

Ghasemi, N, Razavi, S & Nikzad, E 2017, 'Multiple sclerosis: Pathogenesis, symptoms, diagnoses and cell-based therapy', *Cell Journal*, vol. 19, no. 1, pp. 1-10.

Ghosh, R, Gilda, JE & Gomes, AV 2014, 'The necessity of and strategies for improving confidence in the accuracy of western blots', *Expert Review of Proteomics*, vol. 11, no. 5, pp. 549-60.

Ginhoux, F, Greter, M, Samokhvalov, IM, Merad, M, Leboeuf, M, Nandi, S et al. 2010, 'Fate mapping analysis reveals that adult microglia derive from primitive macrophages', *Science (American Association for the Advancement of Science)*, vol. 330, no. 6005, pp. 841-45.

Göbel, K, Ruck, T & Meuth, SG 2018, 'Cytokine signaling in multiple sclerosis: Lost in translation', *Multiple Sclerosis (Houndmills, Basingstoke, England)*, vol. 24, pp. 432-39.

Goldberg, J, Clarner, T, Beyer, C & Kipp, M 2015, 'Anatomical distribution of cuprizone-induced lesions in c57bl6 mice', *Journal of Molecular Neuroscience*, vol. 57, no. 2, pp. 166-75.

Goldenberg, MM 2012, 'Multiple sclerosis review', *P & T : A Peer-Reviewed Journal for Formulary Management*, vol. 37, no. 3, pp. 175-84.

Gonzalez-Perez, O & Alvarez-Buylla, A 2010, 'Oligodendrogenesis in the subventricular zone and the role of epidermal growth factor', *Brain Research Reviews*, vol. 67, no. 1, pp. 147-56.

Gordon, S & Taylor, P 2005, 'Monocyte and macrophage heterogeneity', *Nature Reviews Immunology*, vol. 5, no. 12, pp. 953-64.

Goverman, JM & Stromnes, IM 2006, 'Active induction of experimental allergic encephalomyelitis', *Nature protocols*, vol. 1, no. 4, pp. 1810-19.

Grell, M, Wajant, H, Zimmermann, G & Scheurich, P 1998, 'The type 1 receptor (cd120a) is the high-affinity receptor for soluble tumor necrosis factor', *Proceedings of the National Academy of Sciences - PNAS*, vol. 95, no. 2, pp. 570-75.

Guadagno, J, Xu, X, Karajgikar, M, Brown, A & Cregan, SP 2013, 'Microglia-derived tnfα induces apoptosis in neural precursor cells via transcriptional activation of the bcl-2 family member puma', *Cell Death and Disease*, vol. 4, no. 3, p. e538.

Guarda, G, Braun, M, Staehli, F, Tardivel, A, Mattmann, C, Förster, I et al. 2011, 'Type i interferon inhibits interleukin-1 production and inflammasome activation', *Immunity*, vol. 34, no. 2, pp. 213-23.

Guertin, D, Trautmann, S & McCollum, D 2002, 'Cytokinesis in eukaryotes', *Microbiology and Molecular Biology Reviews*, vol. 66, no. 2, pp. 155-78.

Hadjikyriacou, A, Yang, Y, Espejo, A, Bedford, MT & Clarke, SG 2015, 'Unique features of human protein arginine methyltransferase 9 (prmt9) and its substrate rna splicing factor sf3b2', *The Journal of Biological Chemistry*, vol. 290, no. 27, pp. 16723-43.

Hailman, E, Lichenstein, H, Wurfel, M, Miller, D, Johnson, D, Kelley, M et al. 1994, 'Lipopolysaccharide (lps)-binding protein accelerates the binding of lps to cd14', *Journal of Experimental Medicine*, vol. 179, no. 1, pp. 269-77.

Hamann, L, Stamme, C, Ulmer, AJ & Schumann, RR 2002, 'Inhibition of lps-induced activation of alveolar macrophages by high concentrations of lps-binding protein', *Biochemical and Biophysical Research Communications*, vol. 295, no. 2, pp. 553-60.

Hayashi, M & Karlseder, J 2013, 'DNA damage associated with mitosis and cytokinesis failure', *Oncogene*, vol. 32, no. 39, pp. 4593-601.

He, W-T, Wan, H, Hu, L, Chen, P, Wang, X, Huang, Z et al. 2015, 'Gasdermin d is an executor of pyroptosis and required for interleukin-1 beta secretion', *Cell Research*, vol. 25, no. 12, pp. 1285-98.

Hendriks, JJA, Teunissen, CE, de Vries, HE & Dijkstra, CD 2005, 'Macrophages and neurodegeneration', *Brain Research Reviews*, vol. 48, no. 2, pp. 185-95.

Hiltbrunner, A, Belanger, Oger, J, Gosselin, Bouchard, JP, Thibault et al. 1999, 'Tnf neutralization in ms: Results of a randomized, placebo-controlled multicenter study. The lenercept multiple sclerosis study group and the university of british columbia ms/mri analysis group', *Neurology*, vol. 53, no. 3, pp. 457-65.

Hirayama, D, Iida, T & Nakase, H 2017, 'The phagocytic function of macrophage-enforcing innate immunity and tissue homeostasis', *International Journal of Molecular Sciences*, vol. 19, no. 1, p. 92.

Hortelano, S, Castrillo, A, Alvarez, AM & Boscá, L 2000, 'Contribution of cyclopentenone prostaglandins to the resolution of inflammation through the potentiation of apoptosis in activated macrophages', *Journal of Immunology*, vol. 165, no. 11, pp. 6525-31.

Huang, X, Feng, Y, Xiong, G, Whyte, S, Duan, J, Yang, Y et al. 2019, 'Caspase-11, a specific sensor for intracellular lipopolysaccharide recognition, mediates the non-canonical inflammatory pathway of pyroptosis', *Cell & Bioscience*, vol. 9, no. 31.

Huitinga, van, R, de Groot, CJ, Uitdehaag, BM & Dijkstra, CD 1990, 'Suppression of experimental allergic encephalomyelitis in lewis rats after elimination of macrophages', *The Journal of Experimental Medicine*, vol. 172, no. 4, pp. 1025-33.

Ivanova, MV, Kolkova, NI, Morgunova, EY, Pashko, YP, Zigangirova, NA & Zakharova, MN 2015, 'Role of chlamydia in multiple sclerosis', *Bulletin of experimental biology and medicine*, vol. 159, no. 5, pp. 646-48.

Jain, N, Sudhakar, C & Swarup, G 2007, 'Tumor necrosis factor-α-induced caspase-1 gene expression', *FEBS Journal*, vol. 274, no. 17, pp. 4396-407.

Javid, B, Macary, PA & Lehner, PJ 2007, 'Structure and function: Heat shock proteins and adaptive immunity', *Journal of Immunology*, vol. 179, no. 4, pp. 2035-40.

Jha, S, Srivastava, SY, Brickey, WJ, Iocca, H, Toews, A, Morrison, JP et al. 2010, 'The inflammasome sensor, nlrp3, regulates cns inflammation and demyelination via caspase-1 and interleukin-18', *The Journal of Neuroscience*, vol. 30, no. 47, pp. 15811-20.

Jha, S & Ting, JPY 2009, 'Inflammasome-associated nucleotide-binding domain, leucine-rich repeat proteins and inflammatory diseases', *Journal of Immunology*, vol. 183, no. 12, pp. 7623-29.

Kagan, JC & Medzhitov, R 2006, 'Phosphoinositide- mediated adaptor recruitment controls toll- like receptor signaling', *Cell*, vol. 125, no. 5, pp. 943-55.

Kalyvas, A & David, S 2004, 'Cytosolic phospholipase a2 plays a key role in the pathogenesis of multiple sclerosis-like disease', *Neuron (Cambridge, Mass.)*, vol. 41, no. 3, pp. 323-35.

Kamil, K, Yazid, MD, Idrus, RBH, Das, S & Kumar, J 2019, 'Peripheral demyelinating diseases: From biology to translational medicine', *Frontiers in Neurology*, vol. 10, pp. 87-87.

Kang, Z, Liu, L, Spangler, R, Spear, C, Wang, C, Gulen, MF et al. 2012, 'Il-17-induced act1-mediated signaling is critical for cuprizone-induced demyelination', *The Journal of Neuroscience*, vol. 32, no. 24, pp. 8284-92.

Kayagaki, N, Warming, S, Lamkanfi, M, Walle, LV, Louie, S, Dong, J et al. 2011, 'Non-canonical inflammasome activation targets caspase-11', *Nature*, vol. 479, no. 7371, pp. 117-21.

Kemanetzoglou, E & Andreadou, E 2017, 'Cns demyelination with tnf-α blockers', *Current Neurology and Neuroscience Reports*, vol. 17, no. 4, pp. 1-15.

Kielian, T & Blecha, F 1995, 'Cd14 and other recognition molecules for lipopolysaccharide: A review', *Immunopharmacology*, vol. 29, no. 3, pp. 187-205.

Kim, J 2018, 'Regulation of immune cell functions by metabolic reprogramming', *Journal of Immunology Research*, vol. 2018, pp. 1-12.

Kim, JH, Yoo, BC, Yang, WS, Kim, E, Hong, S & Cho, JY 2016, 'The role of protein arginine methyltransferases in inflammatory responses', *Mediators of Inflammation*, vol. 2016, pp. 4028353-53.

Kim, S, Steelman, AJ, Koito, H & Li, J 2011, 'Astrocytes promote tnf-mediated toxicity to oligodendrocyte precursors.(report)', *Journal of Neurochemistry*, vol. 116, no. 1, p. 53.

Kirikae, T, Tamura, H, Hashizume, M, Kirikae, F, Uemura, Y, Tanaka, S et al. 1997, 'Endotoxin contamination in fetal bovine serum and its influence on tumor necrosis factor production by macrophage-like cells j774.1 cultured in the presence of the serum', *International Journal of Immunopharmacology*, vol. 19, no. 5, pp. 255-62.

Kong, D-H, Kim, YK, Kim, MR, Jang, JH & Lee, S 2018, 'Emerging roles of vascular cell adhesion molecule-1 (vcam-1) in immunological disorders and cancer', *International Journal of Molecular Sciences*, vol. 19, no. 4, p. 1057.

Koriem, KMM 2016, 'Multiple sclerosis: New insights and trends', *Asian Pacific Journal of Tropical Biomedicine*, vol. 6, no. 5, pp. 429-40.

Kreft, S & Kreft, M 2009, 'Quantification of dichromatism: A characteristic of color in transparent materials', *Journal of the Optical Society of America*, vol. 26, no. 7, pp. 1576-81.

Kurien, BT & Scofield, RH 2006, 'Western blotting', *Methods*, vol. 38, no. 4, pp. 283-93.

Lalor, SJ, Dungan, LS, Sutton, CE, Basdeo, SA, Fletcher, JM & Mills, KHG 2011, 'Caspase-1-processed cytokines il-1beta and il-18 promote il-17 production by gammadelta and cd4 t cells that mediate autoimmunity', *Journal of Immunology*, vol. 186, no. 10, pp. 5738-48.

Larsen, S, Sylvestersen, K, Mund, A, Lyon, D, Mullari, M, Madsen, M et al. 2016, 'Proteome-wide analysis of arginine monomethylation reveals widespread occurrence in human cells', *Science Signaling*, vol. 9, no. 443, pp. rs9-rs9.

Lassmann, H & Bradl, M 2017, 'Multiple sclerosis: Experimental models and reality', *Pathology and Mechanisms of Neurological Disease*, vol. 133, no. 2, pp. 223-44.

Li, P, Allen, H, Banerjee, S, Franklin, S, Herzog, L, Johnston, C et al. 1995, 'Mice deficient in il-1 beta-converting enzyme are defective in production of mature il-1 beta and resistant to endotoxic shock', *Cell*, vol. 80, no. 3, pp. 401-11.

Li, T, Chen, X, Zhang, C, Zhang, Y & Yao, W 2019, 'An update on reactive astrocytes in chronic pain', *Journal of Neuroinflammation*, vol. 16, no. 1, pp. 140-40.

Liu, X, Chen, B, Chen, L, Ren, W-T, Liu, J, Wang, G et al. 2013, 'U-shape suppressive effect of phenol red on the epileptiform burst activity via activation of estrogen receptors in primary hippocampal culture.(research article)(report)', *PLoS ONE*, vol. 8, no. 4, p. e60189.

Loma, I & Heyman, R 2011, 'Multiple sclerosis: Pathogenesis and treatment', *Current Neuropharmacology*, vol. 9, no. 3, pp. 409-16.

Love, S 2006, 'Demyelinating diseases', *Journal of Clinical Pathology*, vol. 59, no. 11, pp. 1151-59.

Lucchinetti, C, Brück, W, Parisi, J, Scheithauer, B, Rodriguez, M & Lassmann, H 2000, 'Heterogeneity of multiple sclerosis lesions: Implications for the pathogenesis of demyelination', *Annals of Neurology*, vol. 47, no. 6, pp. 707-17.

Mandel, W 1959, 'Pyridoxine and the isoniazid-induced neuropathy', *Diseases of the Chest*, vol. 36, no. 3, pp. 293-96.

Mannara, F, Valente, T, Saura, J, Graus, F, Saiz, A & Moreno, B 2012, 'Passive experimental autoimmune encephalomyelitis in c57bl/6 with mog: Evidence of involvement of b cells', *PLoS ONE*, vol. 7, no. 12, pp. e52361-e61.

Manoj, KM & Yong, VW 2016, 'Myeloid cells - targets of medication in multiple sclerosis', *Nature Reviews Neurology*, vol. 12, no. 9, pp. 539-51.

Marrodan, M, Alessandro, L, Farez, MF & Correale, J 2019, 'The role of infections in multiple sclerosis', *Multiple Sclerosis Journal*, vol. 25, no. 7, pp. 891-901.

Martine, P, Chevriaux, A, Derangère, V, Apetoh, L, Garrido, C, Ghiringhelli, F et al. 2019, 'Hsp70 is a negative regulator of nlrp3 inflammasome activation', *Cell Death & Disease*, vol. 10, no. 4, pp. 256-56.

Martinez, B & Peplow, P 2020, 'Protective effects of pharmacological therapies in animal models of multiple sclerosis: A review of studies 2014-2019', *Neural Regeneration Research*, vol. 15, no. 7, pp. 1220-34.

Mason, JL, Suzuki, K, Chaplin, DD & Matsushima, GK 2001, 'Interleukin-1β promotes repair of the cns', *The Journal of Neuroscience*, vol. 21, no. 18, pp. 7046-52.

Matsushima, GK & Morell, P 2001, 'The neurotoxicant, cuprizone, as a model to study demyelination and remyelination in the central nervous system', *Brain Pathology*, vol. 11, no. 1, pp. 107-16.

McGeough, MD, Wree, A, Inzaugarat, ME, Haimovich, A, Johnson, CD, Pena, C et al. 2017, 'Tnf regulates transcription of nlrp3 inflammasome components and inflammatory molecules in cryopyrinopathies', *The Journal of Clinical Investigation*, vol. 127, no. 12, pp. 4488-97.

McIlwain, DR, Berger, T & Mak, TW 2013, 'Caspase functions in cell death and disease', *Cold Spring Harbor Perspectives in Biology*, vol. 5, no. 4, p. a008656.

McKenzie, BA, Dixit, VM & Power, C 2020, 'Fiery cell death: Pyroptosis in the central nervous system', *Trends in Neurosciences*, vol. 43, no. 1, pp. 55-73.

McKenzie, BA, Mamik, MK, Saito, LB, Boghozian, R, Monaco, MC, Major, EO et al. 2018, 'Caspase-1 inhibition prevents glial inflammasome activation and pyroptosis in models of multiple sclerosis', *Proceedings of the National Academy of Sciences of the United States of America*, vol. 115, no. 26, pp. E6065-74.

McMahon, EJ, Suzuki, K & Matsushima, GK 2002, 'Peripheral macrophage recruitment in cuprizone-induced cns demyelination despite an intact blood–brain barrier', *Journal of Neuroimmunology*, vol. 130, no. 1, pp. 32-45.

McNally, AK & Anderson, JM 2011, 'Macrophage fusion and multinucleated giant cells of inflammation. ', *Advances in Experimental Medicine and Biology*, vol. 713, pp. 97-111.

Meca-Lallana, V, Berenguer-Ruiz, L, Carreres-Polo, J, Eichau-Madueño, S, Ferrer-Lozano, J, Forero, L et al. 2021, 'Deciphering multiple sclerosis progression', *Frontiers in Neurology*, vol. 11, no. 6.

Meng, F & Lowell, CA 1997, 'Lipopolysaccharide (lps)-induced macrophage activation and signal transduction in the absence of src- family kinases hck, fgr, and lyn', *The Journal of Experimental Medicine*, vol. 185, no. 9, pp. 1661-70.

Merly, L & Smith, SL 2017, 'Murine raw 264.7 cell line as an immune target: Are we missing something?', *Immunopharmacology and Immunotoxicology*, vol. 39, no. 2, pp. 55-58.

Meyer, N & Rinholm, JE 2021, 'Mitochondria in myelinating oligodendrocytes: Slow and out of breath?', *Metabolites*, vol. 11, no. 6, p. 359.

Mi, G, Gao, Y, Liu, S, Ye, E, Li, Y, Jin, X et al. 2016, 'Cyclin-dependent kinase inhibitor flavopiridol promotes remyelination in a cuprizone induced demyelination model', *Cell Cycle*, vol. 15, no. 20, pp. 2780-91.

Miao, EA, Rajan, JV & Aderem, A 2011, 'Caspase- 1- induced pyroptotic cell death (report)', *Immunological Reviews*, vol. 243, pp. 206-14.

Micheau, O & Tschopp, J 2003, 'Induction of tnf receptor i-mediated apoptosis via two sequential signaling complexes', *Cell*, vol. 114, no. 2, pp. 181-90.

Miclea, A, Bagnoud, M, Chan, A & Hoepner, R 2020, 'A brief review of the effects of vitamin d on multiple sclerosis', *Frontiers in Immunology*, vol. 11, pp. 781-81.

Milde, R, Ritter, J, Tennent, Glenys a, Loesch, A, Martinez, Fernando o, Gordon, S et al. 2015, 'Multinucleated giant cells are specialized for complement-mediated phagocytosis and large target destruction', *Cell Reports*, vol. 13, no. 9, pp. 1937-48.

Mosser, DM & Zhang, X 2008, 'Activation of murine macrophages', *Current Protocols in Immunology*, vol. 111, no. 1, pp. 1-9.

Muniz-Miranda, M, Pagliai, M, Cardini, G, Messori, L, Bruni, B, Casini, A et al. 2008, 'A multi-technique approach to predicting the molecular structure of cuprizone in the gas phase and in the crystalline state', *CrystEngComm*, vol. 111, no. 4, pp. 416-22.

Nahrendorf, M & Swirski, FK 2016, 'Abandoning m1/m2 for a network model of macrophage function', *Circulation Research*, vol. 119, no. 3, pp. 414-17.

Nakajima, K & Kohsaka, S 2001, 'Microglia: Activation and their significance in the central nervous system', *Journal of Biochemistry*, vol. 130, no. 2, pp. 169-75.

Nally, F, K., Santi, C, De. & Mccoy, C, E. 2019, 'Nanomodulation of macrophages in multiple sclerosis', *Cells*, vol. 8, no. 6, p. 543.

Nimmerjahn, A, Kirchhoff, F & Helmchen, F 2005, 'Resting microglial cells are highly dynamic surveillants of brain parenchyma in vivo', *Science*, vol. 308, no. 5726, pp. 1314-18.

O' Brien, J, Wilson, I, Orton, T & Pognan, F 2000, 'Investigation of the alamar blue (resazurin) fluorescent dye for the assessment of mammalian cell cytotoxicity', *European Journal of Biochemistry*, vol. 267, no. 17, pp. 5421-26.

Olsen, JV, Ong, S-E & Mann, M 2004, 'Trypsin cleaves exclusively c-terminal to arginine and lysine residues', *Molecular & Cellular Proteomics : MCP*, vol. 3, no. 6, pp. 608-14.

Palma, A, Jarrah, AS, Tieri, P, Cesareni, G & Castiglione, F 2018, 'Gene regulatory network modeling of macrophage differentiation corroborates the continuum hypothesis of polarization states', *Frontiers in Physiology*, vol. 9, pp. 1659-59.

Parameswaran, N & Patial, S 2010, 'Tumor necrosis factor-α signaling in macrophages', *Critical Reviews in Eukaryotic Gene Expression*, vol. 20, no. 2, pp. 87-103.

Parry, RV & Ward, SG 2010, 'Protein arginine methylation: A new handle on t lymphocytes?', *Trends in Immunology*, vol. 31, no. 4, pp. 164-69.

Patergnani, S, Fossati, V, Bonora, M, Giorgi, C, Marchi, S, Missiroli, S et al. 2017, 'Mitochondria in multiple sclerosis: Molecular mechanisms of pathogenesis', *International Review of Cell and Molecular Biology*, vol. 328, pp. 49-103.

Peelen, E, Damoiseaux, J, Muris, AH, Knippenberg, S, Smolders, J, Hupperts, R et al. 2015, 'Increased inflammasome related gene expression profile in pbmc may facilitate t helper 17 cell induction in multiple sclerosis', *Molecular Immunology*, vol. 63, no. 2, pp. 521-29.

Pegoretti, V, Baron, W, Laman, JD & Eisel, ULM 2018, 'Selective modulation of tnf-tnfrs signaling: Insights for multiple sclerosis treatment', *Frontiers in Immunology*, vol. 9, pp. 925-25.

Perez, C, Albert, I, Defay, K, Zachariades, N, Gooding, L & Kriegler, M 1990, 'A nonsecretable cell surface mutant of tumor necrosis factor (tnf) kills by cell-to-cell contact', *Cell*, vol. 63, no. 2, pp. 251-58.

Pilla, DM, Hagar, JA, Haldar, AK, Mason, AK, Degrandi, D, Pfeffer, K et al. 2014, 'Guanylate binding proteins promote caspase-11–dependent pyroptosis in response to cytoplasmic lps', *Proceedings of the National Academy of Sciences*, vol. 111, no. 16, p. 6046.

Płóciennikowska, A, Hromada-Judycka, A, Borzęcka, K & Kwiatkowska, K 2015, 'Co-operation of tlr4 and raft proteins in lps-induced pro-inflammatory signaling', *Cellular and Molecular Life Sciences*, vol. 72, no. 3, pp. 557-81.

Podbielska, M, Banik, N, Kurowska, E & Hogan, E 2013, 'Myelin recovery in multiple sclerosis: The challenge of remyelination', *Brain Sciences*, vol. 3, no. 3, pp. 1282-324.

Prat, A & Antel, J 2005, 'Pathogenesis of multiple sclerosis', *Current Opinion in Neurology*, vol. 18, no. 3, pp. 225-30.

Prins, M, Eriksson, C, Wierinckx, A, Bol, JGJM, Binnekade, R, Tilders, FJH et al. 2013, 'Interleukin-1β and interleukin-1 receptor antagonist appear in grey matter additionally to white matter lesions during experimental multiple sclerosis', *PLoS ONE*, vol. 8, no. 12.

Probert, L, Akassoglou, K, Pasparakis, M, Kontogeorgos, G & Kollias, G 1995, 'Spontaneous inflammatory demyelinating disease in transgenic mice showing central nervous system-

specific expression of tumor necrosis factor alpha', *Proceedings of the National Academy of Sciences, USA*, vol. 92, no. 24, pp. 11294-98.

Quinn, MT & Schepetkin, IA 2009, 'Role of nadph oxidase in formation and function of multinucleated giant cells', *Journal of Innate Immunity*, vol. 1, no. 6, pp. 509-26.

Raetz, CRH & Whitfield, C 2002, 'Lipopolysaccharide endotoxins', *Annual Review of Biochemistry*, vol. 71, p. 635.

Rahat, MA, Ebitterman, H & Elahat, N 2011, 'Molecular mechanisms regulating macrophage response to hypoxia', *Frontiers in Immunology*, vol. 2, no. 45, pp. 1-15.

Rahman, H, Qasim, M, Schultze, FC, Oellerich, M & R Asif, A 2011, 'Fetal calf serum heat inactivation and lipopolysaccharide contamination influence the human t lymphoblast proteome and phosphoproteome', *Proteome Science*, vol. 9, no. 1, pp. 71-71.

Ramagopalan, SV, Maugeri, NJ, Handunnetthi, L, Lincoln, MR, Orton, S-M, Dyment, DA et al. 2009, 'Expression of the multiple sclerosis-associated mhc class ii allele hla-drb11501 is regulated by vitamin d', *PLoS genetics*, vol. 5, no. 2, pp. e1000369-e69.

Ramos-Junior, ES & Morandini, AC 2017, 'Gasdermin: A new player to the inflammasome game', *Biomedical Journal*, vol. 40, no. 6, pp. 313-16.

Rampersad, SN 2012, 'Multiple applications of alamar blue as an indicator of metabolic function and cellular health in cell viability bioassays', *Sensors (Basel, Switzerland)*, vol. 12, no. 9, pp. 12347-60.

Raposo, AE & Piller, SC 2018, 'Protein arginine methylation: An emerging regulator of the cell cycle', *Cell Division*, vol. 13, no. 1, pp. 1-16.

Rawji, KS & Yong, VW 2013, 'The benefits and detriments of macrophages/microglia in models of multiple sclerosis', *Clinical & Developmental Immunology*, vol. 2013, pp. 1-13.

Reis, J, Guan, XQ, Kisselev, AF, Papasian, CJ, Qureshi, AA, Morrison, DC et al. 2011, 'Lps-induced formation of immunoproteasomes: Tnf-α and nitric oxide production are regulated by altered composition of proteasome-active sites', *Cell Biochemistry and Biophysics*, vol. 60, no. 1-2, pp. 77-88.

Rejdak, K, Jackson, S & Giovannoni, G 2010, 'Multiple sclerosis: A practical overview for clinicians', *British Medical Bulletin*, vol. 95, no. 1, pp. 79-104.

Rosko, L, Smith, VN, Yamazaki, R & Huang, JK 2019, 'Oligodendrocyte bioenergetics in health and disease', *The Neuroscientist*, vol. 25, no. 4, pp. 334-43.

Rossi, S, Motta, C, Studer, V, Macchiarulo, G, Volpe, E, Barbieri, F et al. 2014, 'Interleukin-1[beta] causes excitotoxic neurodegeneration and multiple sclerosis disease progression by activating the apoptotic protein p53', *Molecular Neurodegeneration*, vol. 9, no. 1, pp. 1-11.

Ryu, J-K, Kim, SJ, Rah, S-H, Kang, JI, Jung, HE, Lee, D et al. 2017, 'Reconstruction of lps transfer cascade reveals structural determinants within lbp, cd14, and tlr4-md2 for efficient lps recognition and transfer', *Immunity*, vol. 46, no. 1, pp. 38-50.

Samoilova, EB, Horton, JL, Hilliard, B, Liu, TS & Chen, Y 1998, 'Il-6-deficient mice are resistant to experimental autoimmune encephalomyelitis: Roles of il-6 in the activation and differentiation of autoreactive t cells', *Journal of Immunology*, vol. 161, no. 12, pp. 6480-86.

Sato, F, Martinez, NE, Stewart, EC, Omura, S, Alexander, JS & Tsunoda, I 2015, '"Microglial nodules" and "newly forming lesions" may be a janus face of early ms lesions; implications from virus-induced demyelination, the inside-out model', *BMC neurology*, vol. 15, no. 219, pp. 1-6.

Scott, A & Saleh, M 2006, 'The inflammatory caspases: Guardians against infections and sepsis', *Cell Death and Differentiation*, vol. 14, no. 1, pp. 23-31.

Seluanov, A, Hine, C, Azpurua, J, Feigenson, M, Bozzella, M, Mao, Z et al. 2009, 'Hypersensitivity to contact inhibition provides a clue to cancer resistance of naked mole-rat', *Proceedings of the National Academy of Sciences of the United States of America*, vol. 106, no. 46, pp. 19352-57.

Sen, MK, Almuslehi, MSM, Gyengesi, E, Myers, SJ, Shortland, PJ, Mahns, DA et al. 2019, 'Suppression of the peripheral immune system limits the central immune response following cuprizone-feeding: Relevance to modelling multiple sclerosis', *Cells (Basel, Switzerland)*, vol. 8, no. 11, p. 1314.

Seppi, D, Puthenparampil, M, Federle, L, Ruggero, S, Toffanin, E, Rinaldi, F et al. 2014, 'Cerebrospinal fluid il-1β correlates with cortical pathology load in multiple sclerosis at clinical onset', *Journal of Neuroimmunology*, vol. 270, no. 1-2, pp. 56-60.

Sharief, MK & Hentges, R 1991, 'Association between tumor necrosis factor-α and disease progression in patients with multiple sclerosis', *The New England Journal of Medicine*, vol. 325, no. 7, pp. 467-72.

Shen, X, Venero, JL, Joseph, B & Burguillos, MA 2018, 'Caspases orchestrate microglia instrumental functions', *Progress in Neurobiology*, vol. 171, pp. 50-71.

Shi, Y 2004, 'Caspase activation, inhibition, and reactivation: A mechanistic view', *Protein Science*, vol. 13, no. 8, pp. 1979-87.

Shigemoto-Mogami, Y, Hoshikawa, K, Goldman, JE, Sekino, Y & Sato, K 2014, 'Microglia enhance neurogenesis and oligodendrogenesis in the early postnatal subventricular zone', *The Journal of Neuroscience : The Official Journal of the Society for Neuroscience*, vol. 34, no. 6, pp. 2231-43.

Sieweke, MH & Allen, JE 2013, 'Beyond stem cells: Self-renewal of differentiated macrophages', *Science (New York, N.Y.)*, vol. 342, no. 6161, p. 1242974.

Singh, S, Metz, I, Amor, S, Valk, P, Stadelmann, C & Brück, W 2013, 'Microglial nodules in early multiple sclerosis white matter are associated with degenerating axons', *Pathology and Mechanisms of Neurological Disease*, vol. 125, no. 4, pp. 595-608.

Skripuletz, T, Lindner, M, Kotsiari, A, Garde, N, Fokuhl, J, Linsmeier, F et al. 2008, 'Cortical demyelination is prominent in the murine cuprizone model and is strain-dependent', *The American Journal of Pathology*, vol. 172, no. 4, pp. 1053-61.

Sokolovska, A, Becker, CE, Eddie Ip, W, Rathinam, VA, Brudner, M, Paquette, N et al. 2013, 'Activation of caspase-1 by the nlrp3 inflammasome regulates the nadph oxidase nox2 to control phagosome function', *Nature Immunology*, vol. 14, no. 6, pp. 543-53.

Sollberger, G, Strittmatter, GE, Garstkiewicz, M, Sand, J & Beer, H-D 2014, 'Caspase-1: The inflammasome and beyond', *Innate Immunity*, vol. 20, no. 2, pp. 115-25.

Sotelo, J & Corona, T 2011, 'Varicella zoster virus and relapsing remitting multiple sclerosis', *Multiple Sclerosis International*, vol. 2011, pp. 1-6.

Sotelo, J, Ordoñez, G & Pineda, B 2007, 'Varicella-zoster virus at relapses of multiple sclerosis', *Journal of Neurology*, vol. 254, no. 4, pp. 493-500.

Steinman, L 2014, 'Immunology of relapse and remission in multiple sclerosis', *Annual Review of Immunology*, vol. 32, no. 1, pp. 257-81.

Stiefel, KM, Torben-Nielsen, B & Coggan, JS 2013, 'Proposed evolutionary changes in the role of myelin', *Frontiers in Neuroscience*, vol. 7, no. 7, pp. 1-9.

Straight, AF & Field, CM 2000, 'Microtubules, membranes and cytokinesis', *Current Biology*, vol. 10, no. 20, pp. R760-R70.

Streicher, JM 2019, 'The role of heat shock proteins in regulating receptor signal transduction', *Molecular Pharmacology*, vol. 95, no. 5, pp. 468-74.

Stromnes, IM & Goverman, JM 2006, 'Passive induction of experimental allergic encephalomyelitis', *Nature protocols*, vol. 1, no. 4, pp. 1952-60.

Taabazuing, CY, Okondo, MC & Bachovchin, DA 2017, 'Pyroptosis and apoptosis pathways engage in bidirectional crosstalk in monocytes and macrophages', *Cell Chemical Biology*, vol. 24, no. 4, pp. 507-14.e4.

Taciak, B, Bialasek, M, Braniewska, A, Sas, Z, Sawicka, P, Kiraga, L et al. 2018, 'Evaluation of phenotypic and functional stability of raw 264.7 cell line through serial passages.(research article)', *PLoS ONE*, vol. 13, no. 6, p. e0198943.

Takeuchi, O & Akira, S 2010, 'Pattern recognition receptors and inflammation', *Cell*, vol. 140, no. 6, pp. 805-20.

Tambuyzer, BR & Nouwen, EJ 2005, 'Inhibition of microglia multinucleated giant cell formation and induction of differentiation by gm-csf using a porcine in vitro model', *Cytokine*, vol. 31, no. 4, pp. 270-79.

Tanaka, J 2020, 'Favorable and unfavorable roles of microglia and macrophages in the pathologic central nervous system', *Neuroimmunology and Neuroinflammation*, vol. 2020, no. 2, pp. 73-91.

Toomey, LM, Papini, M, Lins, B, Wright, AJ, Warnock, A, McGonigle, T et al. 2021, 'Cuprizone feed formulation influences the extent of demyelinating disease pathology', *Scientific Reports*, vol. 11, no. 1, pp. 22594-94.

Torkildsen, Ø, Brunborg, LA, Myhr, KM & Bø, L 2008, 'The cuprizone model for demyelination', *Acta Neurologica Scandinavica*, vol. 117, no. s188, pp. 72-76.

Traka, M, Podojil, JR, McCarthy, DP, Miller, SD & Popko, B 2015, 'Oligodendrocyte death results in immune-mediated cns demyelination', *Nature Neuroscience*, vol. 19, no. 1, pp. 65-74.

Triglia, RP & Linscott, WD 1980, 'Titers of nine complement components, conglutinin and c3b-inactivator in adult and fetal bovine sera', *Molecular Immunology*, vol. 17, no. 6, pp. 741-48.

Tunctan, B, Kucukkavruk, S, Temiz-Resitoglu, M, Guden, D, Sari, A, Sahan-Firat, S et al. 2017, 'Inhibition of nlrp3 inflammasome contributes to protective effect of 5,14-hedge against lipopolysaccharide-induced septic shock', *International Journal of Pharmacology*, vol. 13, no. 6, pp. 654-66.

van Munster, CEP, Jonkman, LE, Weinstein, HC, Uitdehaag, BMJ & Geurts, JJG 2015, 'Gray matter damage in multiple sclerosis: Impact on clinical symptoms', *Neuroscience*, vol. 303, p. 446.

Varhaug, KN, Kråkenes, T, Alme, MN, Vedeler, CA & Bindoff, LA 2020, 'Mitochondrial complex iv is lost in neurons in the cuprizone mouse model', *Mitochondrion*, vol. 50, pp. 58-62.

Vega-Riquer, JM, Mendez-Victoriano, G, Morales-Luckie, RA & Gonzalez-Perez, O 2019, 'Five decades of cuprizone, an updated model to replicate demyelinating diseases', *Current Neuropharmacology*, vol. 17, no. 2, pp. 129-41.

Venturini, G 1973, 'Enzymic activities and sodium, potassium and copper concentrations in mouse brain and liver after cuprizone treatment in vivo', *Journal of Neurochemistry*, vol. 21, no. 5, pp. 1147-51.

Vignery, A 2008, 'Macrophage fusion: Molecular mechanisms', *Methods in Molecular Biology (Clifton, N.J.)*, vol. 475, pp. 149-61.

Vogel, D, Vereyken, E, Glim, J, Heijnen, P, Moeton, M, van Der Valk, P et al. 2013, 'Macrophages in inflammatory multiple sclerosis lesions have an intermediate activation status', *Journal of Neuroinflammation*, vol. 10, no. 35, pp. 1-12.

Wang, J, Wang, J, Wang, J, Yang, B, Weng, Q & He, Q 2019, 'Targeting microglia and macrophages: A potential treatment strategy for multiple sclerosis', *Frontiers in Pharmacology*, vol. 10, pp. 286-86.

Wang, R, Kovalchin, JT, Muhlenkamp, P & Chandawarkar, RY 2006, 'Exogenous heat shock protein 70 binds macrophage lipid raft microdomain and stimulates phagocytosis, processing, and mhc-ii presentation of antigens', *Blood*, vol. 107, no. 4, pp. 1636-42.

Watanabe, S, Alexander, M, Misharin, AV & Budinger, GRS 2019, 'The role of macrophages in the resolution of inflammation', *The Journal of Clinical Investigation*, vol. 129, no. 7, pp. 2619-28.

Webb, LM, Amici, SA, Jablonski, KA, Savardekar, H, Panfil, AR, Li, L et al. 2017, 'Prmt5-selective inhibitors suppress inflammatory t cell responses and experimental autoimmune encephalomyelitis', *Journal of Immunology*, vol. 198, no. 4, pp. 1439-51.

Webb, LM & Guerau-de-Arellano, M 2017, 'Emerging role for methylation in multiple sclerosis: Beyond DNA', *Trends in Molecular Medicine*, vol. 23, no. 6, pp. 546-62.

Wei, H, Mundade, R, Lange, K & Lu, T 2014, 'Protein arginine methylation of non-histone proteins and its role in diseases', *Cell Cycle*, vol. 13, no. 1, pp. 32-41.

Williams, MR, Cauvi, DM, Rivera, I, Hawisher, D & De Maio, A 2016, 'Changes in macrophage function modulated by the lipid environment', *Innate immunity (London, England)*, vol. 22, no. 3, pp. 141-51.

Williams, TW & Granger, GA 1968, 'Lymphocyte in vitro cytotoxicity: Lymphotoxins of several mammalian species', *Nature (London)*, vol. 219, no. 5158, pp. 1076-77.

Wright, S, Ramos, R, Tobias, P, Ulevitch, R & Mathison, J 1990, 'Cd14, a receptor for complexes of lipopolysaccharide (lps) and lps binding protein', *Science*, vol. 249, no. 4975, pp. 1431-33.

Wynn, TA, Chawla, A & Pollard, JW 2013, 'Macrophage biology in development, homeostasis and disease', *Nature*, vol. 496, no. 7446, pp. 445-55.

Wypych, G 2008, *Cyclohexanone*, ChemTec Publishing.

Yang, Y & Bedford, MT 2012, 'Protein arginine methyltransferases and cancer', *Nature Reviews Cancer*, vol. 13, no. 1, pp. 37-50.

Yasuda, K, Nakanishi, K & Tsutsui, H 2019, 'Interleukin-18 in health and disease', *International Journal of Molecular Sciences*, vol. 20, no. 3, p. 649.

Yi, YS 2017, 'Caspase-11 non-canonical inflammasome: A critical sensor of intracellular lipopolysaccharide in macrophage-mediated inflammatory responses', *Immunology*, vol. 152, no. 2, pp. 207-17.

Yu, H, Wu, M, Lu, G, Cao, T, Chen, N, Zhang, Y et al. 2018, 'Prednisone alleviates demyelination through regulation of the nlrp3 inflammasome in a c57bl/6 mouse model of cuprizone-induced demyelination', *Brain Research*, vol. 1678, pp. 75-84.

Zachari, MA, Chondrou, PS, Pouliliou, SE, Mitrakas, AG, Abatzoglou, I, Zois, CE et al. 2014, 'Evaluation of the alamarblue assay for adherent cell irradiation experiments', *Dose-Response*, vol. 12, no. 2, pp. 246-58.

Zakrzewicz, D, Zakrzewicz, A, Preissner, K, Markart, P & Wygrecka, M 2012, 'Protein arginine methyltransferases (prmts): Promising targets for the treatment of pulmonary disorders', *International Journal of Molecular Sciences*, vol. 13, no. 10, pp. 12383-400.

Zhang, J-M & An, J 2007, 'Cytokines, inflammation, and pain', *International Anesthesiology Clinics*, vol. 45, no. 2, pp. 27-37.

Zhang, X, Goncalves, R & Mosser, DM 2008, 'The isolation and characterization of murine macrophages', *Current Protocols in Immunology*, vol. Chapter 14, no. 83, pp. 1-18.

Zhen, W, Liu, A, Lu, J, Zhang, W, Tattersall, D & Wang, J 2017, 'An alternative cuprizone-induced demyelination and remyelination mouse model', *ASN Neuro*, vol. 9, no. 4, pp. 1-9.

Zong, Y, Sun, L, Liu, B, Deng, Y-S, Zhan, D, Chen, Y-L et al. 2012, 'Resveratrol inhibits lps-induced mapks activation via activation of the phosphatidylinositol 3-kinase pathway in murine raw 264.7 macrophage cells.(research article)(lipopolysaccharides)(mitogen activated protein kinases)(report)', *PLoS ONE*, vol. 7, no. 8, pp. 1-13.

Zurita-Lopez, CI, Sandberg, T, Kelly, R & Clarke, SG 2012, 'Human protein arginine methyltransferase 7 (prmt7) is a type iii enzyme forming ω-ng-monomethylated arginine residues', *The Journal of Biological Chemistry*, vol. 287, no. 11, pp. 7859-70.

10.0 Appendices

10.1 *Methods and Materials Supporting Data*

10.1.1 **Raw blank corrected fluorescent intensities for Figure 12 Alamar blue assay**

Sample	Blank corrected values 75 min	Blank corrected values second reading 135 minutes	Blank corrected 2 hours	Blank corrected 3 hours	Blank corrected 4 hours
A1	67674	57952	126354.3	171519.7	185555.3
A2	69878	59228	132223.3	176068.7	188068.3
A3	61620	52713	124723.3	174596.7	186006.3
A4	108256	91193	183568.3	205658.7	204432.3
A5	108184	91582	179028.3	197469.7	194804.3
A6	94506	81360	182662.3	200336.7	201752.3
B1	33820	29065	85976.33	117653.7	141532.3
B2	34693	29428	72936.33	71931.67	138949.3
B3	33423	28580	72769.33	115814.7	137687.3
B4	53526	45825	113698.3	169803.7	183478.3
B5	53554	45265	112710.3	158157.7	178774.3
B6	40623	34826	108312.3	143517.7	167456.3
C1	41755.67	37228.67	97789.33	132187	144672.7
C2	48477.67	41327.67	103436.3	137220	146160.7
C3	57162.67	48878.67	110560.3	138474	142068.7
C4	79676.67	67611.67	131894.3	153892	153321.7
C5	72510.67	63038.67	133305.3	154073	158472.7
C6	59162.67	51654.67	125554.3	148216	149801.7
D1	28323.67	24797.67	58526.33	83457	106020.7
D2	30052.67	25615.67	59321.33	84448	103795.7
D3	28593.67	24281.67	58060.33	88188	105492.7
D4	36875.67	31224.67	82051.33	115093	132321.7
D5	38349.67	32281.67	81455.33	112564	130590.7
D6	31219.67	28176.67	84169.33	121300	136230.7

10.1.2 Single factor ANOVA for four different time points in the non-activated cells in 0.1% FCS and 500µL of Alamar blue in Figure 12.

ANOVA: Single Factor								
DESCRIPTION					Alpha	0.05		
Group	*Count*	*Sum*	*Mean*	*Variance*	*SS*	*Std Err*	*Lower*	*Upper*
75 min	3	310946	103648.667	62692561.3	125385122.7	3033.499	96653.41	110643.9
2 hours	3	545259	181753	5773065.33	11546130.67	3033.499	174757.7	188748.3
3 hours	3	603465	201155	17267182.3	34534364.67	3033.499	194159.7	208150.3
4 hours	3	600989	200329.667	24692581.3	49385162.67	3033.499	193334.4	207324.9
ANOVA								
Sources	*SS*	*df*	*MS*	*F*	*P value*	*Eta-sq*	*RMSSE*	*Omega Sq*
Between G	19257899258	3	6419299753	232.529846	4.0483E-08	0.988662	8.803973	0.983017
Within Grc	220850780.7	8	27606347.6					
Total	19478750038	11	1770795458					

10.1.3 Tukey HSD for four different time points in the non-activated cells in 0.1% FCS and 500µL of Alamar blue in Figure 12.

TUKEY HSD/KRAMER			alpha	0.05					
group	*mean*	*n*	*ss*	*df*	*q-crit*				
75 min	103648.7	3	125385122.7						
2 hours	181753	3	11546130.67						
3 hours	201155	3	34534364.67						
4 hours	200329.7	3	49385162.67						
		12	220850780.7	8	4.529				
Q TEST									
group 1	*group 2*	*mean*	*std err*	*q-stat*	*lower*	*upper*	*p-value*	*mean-crit*	*Cohen d*
75 min	2 hours	78104.33	3033.498947	25.74727557	64365.62	91843.05	0.0000***	13738.72	14.8652
75 min	3 hours	97506.33	3033.498947	32.1431901	83767.62	111245.1	0.0000***	13738.72	18.55788
75 min	4 hours	96681	3033.498947	31.87111705	82942.28	110419.7	0.0000***	13738.72	18.4008
2 hours	3 hours	19402	3033.498947	6.395914533	5663.283	33140.72	0.0084**	13738.72	3.692683
2 hours	4 hours	18576.67	3033.498947	6.123841475	4837.95	32315.38	0.0108*	13738.72	3.535602
3 hours	4 hours	825.3333	3033.498947	0.272073057	-12913.4	14564.05	0.9972636	13738.72	0.157081

10.1.4 Single factor ANOVA for four different time points in the activated cells in 0.1% FCS and 500µL of Alamar blue in Figure 12

ANOVA: Single Factor								
DESCRIPTION					Alpha	0.05		
Group	*Count*	*Sum*	*Mean*	*Variance*	*SS*	*Std Err*	*Lower*	*Upper*
75 min	3	199172	66390.6667	18283849.3	36567698.7	1849.012	62126.84	70654.49667
2 hours	3	383301	127767	15559220.3	31118440.7	1849.012	123503.2	132030.83
3 hours	3	522185	174061.667	5388019	10776038	1849.012	169797.8	178325.4967
4 hours	3	559630	186543.333	1795069	3590138	1849.012	182279.5	190807.1633
ANOVA								
Sources	*SS*	*df*	*MS*	*F*	*P value*	*Eta-sq*	*RMSSE*	*Omega Sq*
Between Groups	26662805525	3	8887601842	866.530267	2.1776E-10	0.996932	16.99539	0.995399815
Within Groups	82052315.33	8	10256539.4					
Total	26744857840	11	2431350713					

10.1.5 Tukey HSD for four different time points in the non-activated cells in 0.1% FCS and 500µL of Alamar blue in Figure 12.

TUKEY HSD/KRAMER			alpha	0.05					
group	*mean*	*n*	*ss*	*df*	*q-crit*				
75 min	66390.67	3	36567698.7						
2 hours	127767	3	31118440.7						
3 hours	174061.7	3	10776038						
4 hours	186543.3	3	3590138						
		12	82052315.3	8	4.529				
Q TEST									
group 1	*group 2*	*mean*	*std err*	*q-stat*	*lower*	*upper*	*p-value*	*mean-crit*	*Cohen d*
75 min	2 hours	61376.33	1849.0123	33.19412	53002.16	69750.51	0.0000***	8374.177	19.16463
75 min	3 hours	107671	1849.0123	58.23163	99296.82	116045.2	0.0000***	8374.177	33.62005
75 min	4 hours	120152.7	1849.0123	64.98208	111778.5	128526.8	0.0000***	8374.177	37.51742
2 hours	3 hours	46294.67	1849.0123	25.03751	37920.49	54668.84	0.0000***	8374.177	14.45541
2 hours	4 hours	58776.33	1849.0123	31.78796	50402.16	67150.51	0.0000***	8374.177	18.35279
3 hours	4 hours	12481.67	1849.0123	6.750451	4107.49	20855.84	0.0061**	8374.177	3.897375

10.1.6 Single factor ANOVA for four different time points in the non-activated cells in 10% FCS and 500µL of Alamar blue in Figure 12

ANOVA: Single Factor								
DESCRIPTION					Alpha	0.05		
Group	*Count*	*Sum*	*Mean*	*Variance*	*SS*	*Std Err*	*Lower*	*Upper*
75 min	3	211350	70450	108390809.3	216781618.7	3600.295	62147.7	78752.29548
2 hours	3	390754	130251.333	17044087	34088174	3600.295	121949	138553.6288
3 hours	3	456181	152060.333	11092364.33	22184728.67	3600.295	143758	160362.6288
4 hours	3	461596	153865.333	19018240.33	38036480.67	3600.295	145563	162167.6288
ANOVA								
Sources	*SS*	*df*	*MS*	*F*	*P value*	*Eta-sq*	*RMSSE*	*Omega Sq*
Between G	13673306484	3	4557768828	117.2073457	5.97276E-07	0.977754	6.250529	0.966724163
Within Gro	311091002	8	38886375.3					
Total	13984397486	11	1271308862					

10.1.7 Tukey HSD for four different time points in the non-activated cells in 0.1% FCS and 500µL of Alamar blue in Figure 12

TUKEY HSD/KRAMER			alpha	0.05					
group	*mean*	*n*	*ss*	*df*	*q-crit*				
75 min	70450	3	216781619						
2 hours	130251.3	3	34088174						
3 hours	152060.3	3	22184729						
4 hours	153865.3	3	38036481						
		12	311091002	8	4.529				
Q TEST									
group 1	*group 2*	*mean*	*std err*	*q-stat*	*lower*	*upper*	*p-value*	*mean-crit*	*Cohen d*
75 min	2 hours	59801.33	3600.2951	16.61011974	43495.6	76107.07	0.0000***	16305.74	9.589857
75 min	3 hours	81610.33	3600.2951	22.66767868	65304.6	97916.07	0.0000***	16305.74	13.08719
75 min	4 hours	83415.33	3600.2951	23.16902646	67109.6	99721.07	0.0000***	16305.74	13.37664
2 hours	3 hours	21809	3600.2951	6.057558939	5503.263	38114.74	0.0114*	16305.74	3.497333
2 hours	4 hours	23614	3600.2951	6.558906726	7308.263	39919.74	0.0073**	16305.74	3.786787
3 hours	4 hours	1805	3600.2951	0.501347787	-14500.7	18110.74	0.9836303	16305.74	0.289453

10.1.8 Single factor ANOVA for four different time points in the activated cells in 0.1% FCS and 500µL of Alamar blue in Figure 12

ANOVA: Single Factor								
DESCRIPTION					Alpha	0.05		
Group	*Count*	*Sum*	*Mean*	*Variance*	*SS*	*Std Err*	*Lower*	*Upper*
75 min	3	199172	66390.6667	18283849.3	36567698.7	1849.012	62126.84	70654.49667
2 hours	3	383301	127767	15559220.3	31118440.7	1849.012	123503.2	132030.83
3 hours	3	522185	174061.667	5388019	10776038	1849.012	169797.8	178325.4967
4 hours	3	559630	186543.333	1795069	3590138	1849.012	182279.5	190807.1633
ANOVA								
Sources	*SS*	*df*	*MS*	*F*	*P value*	*Eta-sq*	*RMSSE*	*Omega Sq*
Between Groups	26662805525	3	8887601842	866.530267	2.1776E-10	0.996932	16.99539	0.995399815
Within Groups	82052315.33	8	10256539.4					
Total	26744857840	11	2431350713					

10.1.9 Tukey HSD for four different time points in the activated in 0.1% FCS and 500µL of Alamar blue in Figure 12

TUKEY HSD/KRAMER			alpha	0.05					
group	*mean*	*n*	*ss*	*df*	*q-crit*				
75 min	66390.67	3	36567698.7						
2 hours	127767	3	31118440.7						
3 hours	174061.7	3	10776038						
4 hours	186543.3	3	3590138						
		12	82052315.3	8	4.529				
Q TEST									
group 1	*group 2*	*mean*	*std err*	*q-stat*	*lower*	*upper*	*p-value*	*mean-crit*	*Cohen d*
75 min	2 hours	61376.33	1849.0123	33.19412	53002.16	69750.51	0.0000***	8374.177	19.16463
75 min	3 hours	107671	1849.0123	58.23163	99296.82	116045.2	0.0000***	8374.177	33.62005
75 min	4 hours	120152.7	1849.0123	64.98208	111778.5	128526.8	0.0000***	8374.177	37.51742
2 hours	3 hours	46294.67	1849.0123	25.03751	37920.49	54668.84	0.0000***	8374.177	14.45541
2 hours	4 hours	58776.33	1849.0123	31.78796	50402.16	67150.51	0.0000***	8374.177	18.35279
3 hours	4 hours	12481.67	1849.0123	6.750451	4107.49	20855.84	0.0061**	8374.177	3.897375

10.1.10 Single factor ANOVA for four different time points in the non-activated cells in 10% FCS and 500µL of Alamar blue in Figure 12

ANOVA: Single Factor								
DESCRIPTION					Alpha	0.05		
Group	*Count*	*Sum*	*Mean*	*Variance*	*SS*	*Std Err*	*Lower*	*Upper*
75 min	3	211350	70450	108390809.3	216781618.7	3600.295	62147.7	78752.29548
2 hours	3	390754	130251.333	17044087	34088174	3600.295	121949	138553.6288
3 hours	3	456181	152060.333	11092364.33	22184728.67	3600.295	143758	160362.6288
4 hours	3	461596	153865.333	19018240.33	38036480.67	3600.295	145563	162167.6288
ANOVA								
Sources	*SS*	*df*	*MS*	*F*	*P value*	*Eta-sq*	*RMSSE*	*Omega Sq*
Between G	13673306484	3	4557768828	117.2073457	5.97276E-07	0.977754	6.250529	0.966724163
Within Gro	311091002	8	38886375.3					
Total	13984397486	11	1271308862					

10.1.11 Tukey HSD for four different time points in the non-activated in 10% FCS and 500µL of Alamar blue in Figure 12

TUKEY HSD/KRAMER			alpha	0.05					
group	*mean*	*n*	*ss*	*df*	*q-crit*				
75 min	70450	3	216781619						
2 hours	130251.3	3	34088174						
3 hours	152060.3	3	22184729						
4 hours	153865.3	3	38036481						
		12	311091002	8	4.529				
Q TEST									
group 1	*group 2*	*mean*	*std err*	*q-stat*	*lower*	*upper*	*p-value*	*mean-crit*	*Cohen d*
75 min	2 hours	59801.33	3600.2951	16.61011974	43495.6	76107.07	0.0000***	16305.74	9.589857
75 min	3 hours	81610.33	3600.2951	22.66767868	65304.6	97916.07	0.0000***	16305.74	13.08719
75 min	4 hours	83415.33	3600.2951	23.16902646	67109.6	99721.07	0.0000***	16305.74	13.37664
2 hours	3 hours	21809	3600.2951	6.057558939	5503.263	38114.74	0.0114*	16305.74	3.497333
2 hours	4 hours	23614	3600.2951	6.558906726	7308.263	39919.74	0.0073**	16305.74	3.786787
3 hours	4 hours	1805	3600.2951	0.501347787	-14500.7	18110.74	0.9836303	16305.74	0.289453

10.1.12 Single factor ANOVA for four different time points in the activated cells in 10% FCS and 500µL of Alamar blue in Figure 12

ANOVA: Single Factor								
DESCRIPTION					Alpha	0.05		
Group	*Count*	*Sum*	*Mean*	*Variance*	*SS*	*Std Err*	*Lower*	*Upper*
75 min	3	147396	49132	59665026.3	119330053	3108.898479	41962.87	56301.13
2 hours	3	311786	103928.667	40956404.3	81912808.7	3108.898479	96759.53	111097.8
3 hours	3	407881	135960.333	11071662.3	22143324.7	3108.898479	128791.2	143129.5
4 hours	3	432902	144300.667	4289904	8579808	3108.898479	137131.5	151469.8
ANOVA								
Sources	*SS*	*df*	*MS*	*F*	*P value*	*Eta-sq*	*RMSSE*	*Omega Sq*
Between G	16743297357	3	5581099119	192.479907	8.5338E-08	0.986335058	8.009992	0.979538
Within Gro	231965994	8	28995749.3					
Total	16975263351	11	1543205759					

10.1.13 Tukey HSD for four different time points in the activated in 10% FCS and 500µL of Alamar blue in Figure 12

TUKEY HSD/KRAMER			alpha	0.05					
group	*mean*	*n*	*ss*	*df*	*q-crit*				
75 min	49132	3	1.19E+08						
2 hours	103928.7	3	81912809						
3 hours	135960.3	3	22143325						
4 hours	144300.7	3	8579808						
		12	2.32E+08	8	4.529				
Q TEST									
group 1	*group 2*	*mean*	*std err*	*q-stat*	*lower*	*upper*	*p-value*	*mean-crit*	*Cohen d*
75 min	2 hours	54796.67	3108.898	17.62574978	40716.46546	68876.87	0.0000***	14080.201	10.17623
75 min	3 hours	86828.33	3108.898	27.92897032	72748.13212	100908.5	0.0000***	14080.201	16.1248
75 min	4 hours	95168.67	3108.898	30.61169971	81088.46546	109248.9	0.0000***	14080.201	17.67367
2 hours	3 hours	32031.67	3108.898	10.30322054	17951.46546	46111.87	0.0004***	14080.201	5.948567
2 hours	4 hours	40372	3108.898	12.98594994	26291.79879	54452.2	0.0001***	14080.201	7.497442
3 hours	4 hours	8340.333	3108.898	2.682729395	-5739.867876	22420.53	0.3011651	14080.201	1.548875

10.1.14 Single factor ANOVA for four different time points in the non-activated cells in 0.1% FCS and 1000µL of Alamar blue in Figure 12

ANOVA: Single Factor								
DESCRIPTION					Alpha	0.05		
Group	*Count*	*Sum*	*Mean*	*Variance*	*SS*	*Std Err*	*Lower*	*Upper*
75 min	3	147703	49234.3333	55616492.33	111232985	5042.691	37605.868	60862.8
2 hours	3	334721	111573.667	8221257.333	16442515	5042.691	99945.2013	123202.1
3 hours	3	471479	157159.667	173485452	346970904	5042.691	145531.201	168788.1
4 hours	3	529709	176569.667	67821537.33	135643075	5042.691	164941.201	188198.1
ANOVA								
Sources	*SS*	*df*	*MS*	*F*	*P value*	*Eta-sq*	*RMSSE*	*Omega Sq*
Between G	28820751512	3	9606917171	125.9325945	4.512E-07	0.979264	6.47900698	0.968976
Within Gro	610289478	8	76286184.8					
Total	29431040990	11	2675549181					

10.1.15 Tukey HSD for four different time points in the non-activated in 0.1% FCS and 1000µL of Alamar blue in Figure 12

TUKEY HSD/KRAMER			alpha	0.05					
group	*mean*	*n*	*ss*	*df*	*q-crit*				
75 min	49234.333	3	111232985						
2 hours	111573.67	3	16442515						
3 hours	157159.67	3	346970904						
4 hours	176569.67	3	135643075						
		12	610289478	8	4.529				
Q TEST									
group 1	*group 2*	*mean*	*std err*	*q-stat*	*lower*	*upper*	*p-value*	*mean-crit*	*Cohen d*
75 min	2 hours	62339.33	5042.6906	12.36232	39500.99	85177.68	0.0001***	22838.35	7.137386349
75 min	3 hours	107925.3	5042.6906	21.40233	85086.99	130763.7	0.0000***	22838.35	12.35664162
75 min	4 hours	127335.3	5042.6906	25.25147	104497	150173.7	0.0000***	22838.35	14.57894112
2 hours	3 hours	45586	5042.6906	9.040015	22747.65	68424.35	0.0010***	22838.35	5.219255271
2 hours	4 hours	64996	5042.6906	12.88915	42157.65	87834.35	0.0001***	22838.35	7.441554767
3 hours	4 hours	19410	5042.6906	3.849136	-3428.35	42248.35	0.0985196	22838.35	2.222299496

10.1.16 Single factor ANOVA for four different time points in the activated cells in 0.1% FCS and 1000µL of Alamar blue in Figure 12

ANOVA: Single Factor								
DESCRIPTION					Alpha	0.05		
Group	*Count*	*Sum*	*Mean*	*Variance*	*SS*	*Std Err*	*Lower*	*Upper*
75 min	3	101936	33978.6667	422106.333	844212.667	7808.18341	15972.96	51984.37
2 hours	3	231682	77227.3333	57415723	114831446	7808.18341	59221.63	95233.04
3 hours	3	305400	101800	669933482	1339866965	7808.18341	83794.3	119805.7
4 hours	3	418169	139389.667	3841426.33	7682852.67	7808.18341	121384	157395.4
ANOVA								
Sources	*SS*	*df*	*MS*	*F*	*P value*	*Eta-sq*	*RMSSE*	*Omega Sq*
Between G	17596960513	3	5865653504	32.0697178	8.2806E-05	0.923231312	3.269542	0.885941
Within Gro	1463225476	8	182903185					
Total	19060185989	11	1732744181					

10.1.17 Tukey HSD for four different time points in the activated in 0.1% FCS and 1000µL of Alamar blue in Figure 12

TUKEY HSD/KRAMER			alpha	0.05					
group	*mean*	*n*	*ss*	*df*	*q-crit*				
75 min	33978.67	3	844212.7						
2 hours	77227.33	3	1.15E+08						
3 hours	101800	3	1.34E+09						
4 hours	139389.7	3	7682853						
		12	1.46E+09	8	4.529				
Q TEST									
group 1	*group 2*	*mean*	*std err*	*q-stat*	*lower*	*upper*	*p-value*	*mean-crit*	*Cohen d*
75 min	2 hours	43248.67	7808.183	5.5388897	7885.404002	78611.93	0.0186*	35363.263	3.197879
75 min	3 hours	67821.33	7808.183	8.685929847	32458.07067	103184.6	0.0012**	35363.263	5.014824
75 min	4 hours	105411	7808.183	13.5000671	70047.73734	140774.3	0.0001***	35363.263	7.794267
2 hours	3 hours	24572.67	7808.183	3.147040147	-10790.596	59935.93	0.1959887	35363.263	1.816944
2 hours	4 hours	62162.33	7808.183	7.961177404	26799.07067	97525.6	0.0022**	35363.263	4.596388
3 hours	4 hours	37589.67	7808.183	4.814137257	2226.404002	72952.93	0.0377*	35363.263	2.779443

10.1.18 Single factor ANOVA for four different time points in the non-activated cells in 10% FCS and 1000µL of Alamar blue in Figure 12

ANOVA: Single Factor								
DESCRIPTION					Alpha	0.05		
Group	*Count*	*Sum*	*Mean*	*Variance*	*SS*	*Std Err*	*Lower*	*Upper*
75 min	3	106445	35481.6667	14166652	28333304	1931.225417	31028.25	39935.08
2 hours	3	247676	82558.6667	2034489.33	4068978.67	1931.225417	78105.25	87012.08
3 hours	3	348957	116319	20206731	40413462	1931.225417	111865.6	120772.4
4 hours	3	399143	133047.667	8347707	16695414	1931.225417	128594.3	137501.1
ANOVA								
Sources	*SS*	*df*	*MS*	*F*	*P value*	*Eta-sq*	*RMSSE*	*Omega Sq*
Between G	16679092696	3	5559697565	496.894255	1.9938E-09	0.994661979	12.86979	0.991998
Within Grc	89511158.67	8	11188894.8					
Total	16768603855	11	1524418532					

10.1.19 Tukey HSD for four different time points in the non-activated in 10% FCS and 1000µL of Alamar blue in Figure 12

TUKEY HSD/KRAMER			alpha	0.05					
group	*mean*	*n*	*ss*	*df*	*q-crit*				
75 min	35481.67	3	28333304						
2 hours	82558.67	3	4068979						
3 hours	116319	3	40413462						
4 hours	133047.7	3	16695414						
		12	89511159	8	4.529				
Q TEST									
group 1	*group 2*	*mean*	*std err*	*q-stat*	*lower*	*upper*	*p-value*	*mean-crit*	*Cohen d*
75 min	2 hours	47077	1931.225	24.37675042	38330.48009	55823.52	0.0000***	8746.5199	14.07392
75 min	3 hours	80837.33	1931.225	41.85805169	72090.81342	89583.85	0.0000***	8746.5199	24.16676
75 min	4 hours	97566	1931.225	50.52025473	88819.48009	106312.5	0.0000***	8746.5199	29.16788
2 hours	3 hours	33760.33	1931.225	17.48130127	25013.81342	42506.85	0.0000***	8746.5199	10.09283
2 hours	4 hours	50489	1931.225	26.1435043	41742.48009	59235.52	0.0000***	8746.5199	15.09396
3 hours	4 hours	16728.67	1931.225	8.662203034	7982.146753	25475.19	0.0013**	8746.5199	5.001125

10.1.20 Single factor ANOVA for four different time points in the activated cells in 10% FCS and 1000µL of Alamar blue in Figure 12

ANOVA: Single Factor								
DESCRIPTION					Alpha	0.05		
Group	*Count*	*Sum*	*Mean*	*Variance*	*SS*	*Std Err*	*Lower*	*Upper*
75 min	3	86970	28990	865170.333	1730340.667	858.7101	27009.81	30970.19
2 hours	3	175908	58636	406550.333	813100.6667	858.7101	56655.81	60616.19
3 hours	3	256093	85364.3333	6225340.33	12450680.67	858.7101	83384.14	87344.52
4 hours	3	315309	105103	1351536.33	2703072.667	858.7101	103122.8	107083.2
ANOVA								
Sources	*SS*	*df*	*MS*	*F*	*P value*	*Eta-sq*	*RMSSE*	*Omega Sq*
Between Group	9835005298	3	3278335099	1481.96826	2.55967E-11	0.998204	22.22587	0.997306
Within Groups	17697194.67	8	2212149.33					
Total	9852702493	11	895700227					

10.1.21 Tukey HSD for four different time points in the activated in 10% FCS and 1000µL of Alamar blue in Figure 12

TUKEY HSD/KRAMER			alpha	0.05					
group	*mean*	*n*	*ss*	*df*	*q-crit*				
75 min	28990	3	1730340.667						
2 hours	58636	3	813100.6667						
3 hours	85364.33	3	12450680.67						
4 hours	105103	3	2703072.667						
		12	17697194.67	8	4.529				
Q TEST									
group 1	*group 2*	*mean*	*std err*	*q-stat*	*lower*	*upper*	*p-value*	*mean-crit*	*Cohen d*
75 min	2 hours	29646	858.7101438	34.52387306	25756.9	33535.098	0.0000***	3889.098	19.93237
75 min	3 hours	56374.33	858.7101438	65.65001443	52485.24	60263.432	0.0000***	3889.098	37.90305
75 min	4 hours	76113	858.7101438	88.63642819	72223.9	80002.098	0.0000***	3889.098	51.17427
2 hours	3 hours	26728.33	858.7101438	31.12614137	22839.24	30617.432	0.0000***	3889.098	17.97069
2 hours	4 hours	46467	858.7101438	54.11255513	42577.9	50356.098	0.0000***	3889.098	31.2419
3 hours	4 hours	19738.67	858.7101438	22.98641376	15849.57	23627.765	0.0000***	3889.098	13.27121

10.1.22 Single factor ANOVA for the two-hour time point in the non-activated and activated cells in 0.1% FCS and 500µL of Alamar blue in Figure 12

ANOVA: Single Factor								
DESCRIPTION					Alpha	0.05		
Group	*Count*	*Sum*	*Mean*	*Variance*	*SS*	*Std Err*	*Lower*	*Upper*
Non-activated	3	334721	111573.667	8221257.33	16442514.67	1990.832	106046.2	117101.1
Activated	3	383301	127767	15559220.3	31118440.67	1990.832	122239.6	133294.4
ANOVA								
Sources	*SS*	*df*	*MS*	*F*	*P value*	*Eta-sq*	*RMSSE*	*Omega Sq*
Between Groups	393336066.7	1	393336067	33.0805859	0.004530906	0.892127	3.320672	0.842439
Within Groups	47560955.33	4	11890238.8					
Total	440897022	5	88179404.4					

10.1.23 Tukey HSD for four different time points in the non-activated and activated cells in 0.1% FCS and 500µL of Alamar blue in Figure 12

TUKEY HSD/KRAMER			alpha	0.05					
group	*mean*	*n*	*ss*	*df*	*q-crit*				
Non-activated	111573.7	3	16442514.67						
Activated	127767	3	31118440.67						
		6	47560955.33	4	3.926				
Q TEST									
group 1	*group 2*	*mean*	*std err*	*q-stat*	*lower*	*upper*	*p-value*	*mean-crit*	*Cohen d*
Non-activated	Activated	16193.33	1990.832224	8.13395179	8377.326	24009.341	0.0045**	7816.007	4.696139

10.1.24 Single factor ANOVA for the two-hour time point in the non-activated and activated cells in 10% FCS and 500µL of Alamar blue in Figure 12

ANOVA: Single Factor								
DESCRIPTION					Alpha	0.05		
Group	*Count*	*Sum*	*Mean*	*Variance*	*SS*	*Std Err*	*Lower*	*Upper*
Non-activated	3	390754	130251.333	17044087	34088174	3109.14	121619	138883.7
Activated	3	311786	103928.667	40956404.3	81912808.67	3109.14	95296.31	112561
ANOVA								
Sources	*SS*	*df*	*MS*	*F*	*P value*	*Eta-sq*	*RMSSE*	*Omega Sq*
Between Groups	1039324171	1	1039324171	35.8384609	0.003914662	0.899595	3.456321	0.85308
Within Groups	116000982.7	4	29000245.7					
Total	1155325153	5	231065031					

10.1.25 Tukey HSD for four different time points in the non-activated and activated cells in 10% FCS and 500µL of Alamar blue in Figure 12

TUKEY HSD/KRAMER			alpha	0 05					
group	*mean*	*n*	*ss*	*df*	*q-crit*				
Non-activated	130251 3	3	34088174						
Activated	103928 7	3	81912808 67						
		6	116000982 7	4	3 926				
Q TEST									
group 1	*group 2*	*mean*	*std err*	*q-stat*	*lower*	*upper*	*p-value*	*mean-crit*	*Cohen d*
Non-activated	Activated	26322 67	3109 13952	8 466222405	14116 18	38529 14842	0 0039**	12206 48	4 887976

10.1.26 Single factor ANOVA for the two-hour time point in the non-activated and activated cells in 0.1% FCS and 1000µL of Alamar blue in Figure 12

ANOVA: Single Factor								
DESCRIPTION					Alpha	0.05		
Group	*Count*	*Sum*	*Mean*	*Variance*	*SS*	*Std Err*	*Lower*	*Upper*
Non-activated	3	334721	111573.667	8221257.33	16442514.67	3307.491	102390.6	120756.7
Activated	3	231682	77227.3333	57415723	114831446	3307.491	68044.27	86410.4
ANOVA								
Sources	*SS*	*df*	*MS*	*F*	*P value*	*Eta-sq*	*RMSSE*	*Omega Sq*
Between Groups	1769505920	1	1769505920	53.9179563	0.001831501	0.930937	4.239416	0.898163
Within Groups	131273960.7	4	32818490.2					
Total	1900779881	5	380155976					

10.1.27 Tukey HSD for four different time points in the non-activated and activated cells in 0.1% FCS and 1000µL of Alamar blue in Figure 12

TUKEY HSD/KRAMER			alpha	0 05					
group	*mean*	*n*	*ss*	*df*	*q-crit*				
Non-activated	111573 7	3	16442514 67						
Activated	77227 33	3	114831446						
		6	131273960 7	4	3 926				
Q TEST									
group 1	*group 2*	*mean*	*std err*	*q-stat*	*lower*	*upper*	*p-value*	*mean-crit*	*Cohen d*
Non-activated	Activated	34346 33	3307 491001	10 38440719	21361 12	47331 543	0 0018**	12985 21	5 99544

10.1.28 Single factor ANOVA for the two-hour time point in the non-activated and activated cells in 10% FCS and 1000µL of Alamar blue in Figure 12

ANOVA: Single Factor								
DESCRIPTION					Alpha	0.05		
Group	*Count*	*Sum*	*Mean*	*Variance*	*SS*	*Std Err*	*Lower*	*Upper*
Non-activated	3	247676	82558.6667	2034489.33	4068978.667	637.8401	80787.74	84329.59
Activated	3	175908	58636	406550.333	813100.6667	637.8401	56865.07	60406.93
ANOVA								
Sources	*SS*	*df*	*MS*	*F*	*P value*	*Eta-sq*	*RMSSE*	*Omega Sq*
Between Groups	858440970.7	1	858440971	703.340452	1.20148E-05	0.994345	15.31166	0.991529
Within Groups	4882079.333	4	1220519.83					
Total	863323050	5	172664610					

10.1.29 Tukey HSD for four different time points in the non-activated and activated cells in 10% FCS and 1000µL of Alamar blue in Figure 12

TUKEY HSD/KRAMER			alpha	0 05					
group	*mean*	*n*	*ss*	*df*	*q-crit*				
Non-activated	82558 67	3	4068978 667						
Activated	58636	3	813100 6667						
		6	4882079 333	4	3 926				
Q TEST									
group 1	*group 2*	*mean*	*std err*	*q-stat*	*lower*	*upper*	*p-value*	*mean-crit*	*Cohen d*
Non-activated	Activated	23922 67	637 8400618	37 50574493	21418 51	26426 82675	0 0000***	2504 16	21 65395

10.1.30 **Plate layout for absorbance readings at 595nm for BCA assay in Figure 14**

	STANDARDS		SAMPLES									
	1	**2**	**3**	**4**	**5**	**6**	**7**	**8**	**9**	**10**	**11**	**12**
A	8mg/ml	8mg/ml	Non-act 1	Non-act 2	Non-act 3	Non-act 4	Non-act-6	Non-act 7	Non-act 8	Non-act 9	DF =1	
B	6mg/ml	6mg/ml	Non-act 1	Non-act 2	Non-act 3	Non-act 4	Non-act-6	Non-act 7	Non-act 8	Non-act 9	DF=5	
C	4mg/ml	4mg/ml										
D	2mg/ml	2mg/ml										
E	1mg/ml	1mg/ml										
F	0 5mg/ml	0 5mg/ml										
G	0 25mg/ml	0 25mg/ml										
H	BLANK	BLANK										

10.1.31 **Cell pellets used for BCA in Figure 14.**

Sample Number	Date Spun down	Where the cells came from	PBS Wash	Passage number	Lysis buffer
1	16/11/2018	T75 flask	10mL	30	300µL
2	19/11/2018	T75 flask	10mL	31	250µL
3	23/11/2018	T75 flask	10mL	32	250µL
4	26/11/2018	T75 flask and left-over cells from splitting	10mL	33	400µL
6	30/11/2018	T75 flask	10mL	34	250µL
7	4/12/2018	T75 flask	10mL	35	300µL
8	7/12/2018	T75 flask	10mL	36	250µL
9	10/12/2018	T75 Flask	10mL	37	250µL

10.1.32 **Raw absorbance readings at 595mm for BCA Assay in Figure 14**

	1	**2**	**3**	**4**	**5**	**6**	**7**	**8**	**9**	**10**	**11**	**12**
A	1 425	1 422	1 242	1 459	1 446	1 673	0 951	1 356	1 435	1 551		
B	0 981	1 094	0 736	0 856	0 854	0 953	0 557	0 786	0 816	0 856		
C	0 757	0 754										
D	0 491	0 481										
E	0 361	0 359										
F	0 307	0 28										
G	0 274	0 264										
H	0 229	0 211										

10.1.33 **Raw absorbance readings at 405nm-650nm for TNF-α standard in Figure 17**

	1	**2**	**3**	**4**	**5**	**6**	**7**	**8**	**9**	**10**	**11**	**12**
A	0 5994	0 5415	1 6293	0 0979								
B	0 3957	0 3685	1 9696	0 1051								
C	0 2568	0 2605	1 9806	0 1206								
D	0 2113	0 0000	2 0738	1 2774								
E	0 1676	0 0000	0 3498	0 0870								
F	0 0000	0 1377	0 6335	0 0945								
G	0 0000	0 1587	1 6492	0 1276								
H	0 1101	0 1883	0 6074	0 1985								

10.1.34 Plate layout for absorbance readings at 405nm-650nm for TNF-α standard curve in Figure 17

	STANDARDS		SAMPLES									
	1	2	3	4	5	6	7	8	9	10	11	12
A	2000pg/mL	2000pg/mL	Act 6hrs	Non-act 6hr								
B	1000pg/mL	1000pg/mL	Act 12 hrs	Non-act 12 hr								
C	500pg/mL	500pg/mL	Act 18 hrs	Non-act 18 hr								
D	250pg/mL	250pg/mL	Act 24 hrs	Non-act 24 hrs								
E	125pg/mL	125pg/mL	Act 6hrs	Non-act 6hrs								
F	62 5pg/mL	62 5pg/mL	Act 12 hrs	Non-act 12 hr								
G	31 25pg/mL	31 25pg/mL	Act 18 hrs	Non-act 18 hr								
H	Blank	Blank	Act 24 hrs	Non-act 24 hrs								

10.1.35 Raw absorbance values at 450nm and 620nm for IL-1β standard curve in Figure 18

Wavelength: 450 nm												
Abs	1	2	3	4	5	6	7	8	9	10	11	12
A	2.9577	2.5078	0.0806	0.0871	0.1188	0.1340						
B	1.6374	1.2723	0.0993	0.0949	0.1001	0.1049						
C	1.0337	0.8405	0.1344	0.1270	0.1156	0.1087						
D	0.5425	0.4893	0.2980	0.2178	0.1120	0.1063						
E	0.3748	0.2819	0.0880	0.0992	0.1198	0.1564						
F	0.2469	0.1736	0.0866	0.2779	0.1179	0.1213						
G	0.1550	0.1506	0.1531	0.1435	0.1334	0.4243						
H	0.0741	0.0745	0.3641	0.1435	0.1297	0.3447						
Wavelength: 620 nm												
Abs	1	2	3	4	5	6	7	8	9	10	11	12
A	0.0703	0.0651	0.0426	0.0428	0.0516	0.0448						
B	0.0620	0.0588	0.0431	0.0435	0.0426	0.0471						
C	0.0540	0.0506	0.0441	0.0435	0.0426	0.0433						
D	0.0473	0.0477	0.0482	0.0453	0.0442	0.0441						
E	0.0452	0.0449	0.0441	0.0430	0.0431	0.0443						
F	0.0448	0.0498	0.0426	0.0442	0.0435	0.0440						
G	0.0425	0.0482	0.0432	0.0454	0.0495	0.0492						
H	0.0426	0.0415	0.0551	0.0436	0.0428	0.0513						

10.1.36 Plate layout for absorbance readings for IL-1β standard curve in Figure 18

	STANDARDS		SAMPLES									
	1	2	3	4	5	6	7	8	9	10	11	12
A	500pg/ml	500pg/ml	6hrs 1/100	6hrs 1/100	6hrs nonact	Blank						
B	250pg/mL	250pg/mL	12hrs 1/100	12hrs 1/100	12 hrs nonac	12 hrs nonact						
C	125pg/mL	125pg/mL	18hrs 1/100	18hrs 1/100	18hrs nonact	18hrs nonact						
D	62 5pg/mL	62 5pg/mL	24hrs 1/100	24hrs 1/100	24 hrs nonac	24 hrs nonact						
E	31 25pg/mL	31 25pg/mL	6hrs 1/100	6 hrs 1/100	6hrs nonact	oxalyl nonact						
F	15 625pg/ml	15 625pg/ml	12hrs 1/100	24 hrs 1/100	12 hrs nonac	cyclo nonact						
G	7 8125pg/ml	7 8125pg/ml	18hrs 1/100	6 hrs 1/10	18hrs nonact	oxalyl act						
H	Blank	Blank	24hrs 1/100	24 hrs 1/10	24 hrs nonac	cyclo act						

10.2 *Activation Supporting Data*

10.2.1 Raw cell counts used for Figure 19.

	Well #	Quadrant 1 counts live	Quadrant 2 counts live	Quadrant 3 counts live	Quadrant 4 counts live	Quadrant 1 counts dead	Quadrant 2 counts dead	Quadrant 3 counts dead	Quadrant 4 counts dead
	B1	9	19	18	16	10	17	36	26
Activated in 0.1% FCS	B2	11	20	4	16	19	24	22	28
	B3	7	5	8	2	7	10	19	17
	B4	2	18	7	11	9	8	8	17
Non-activated in 0.1% FCS	B5	36	53	52	62	10	13	15	12
	B6	11	10	18	10	9	9	23	21
	D1	32	32	24	14	14	13	12	10
Activated in 10% FCS	D2	62	23	21	19	39	17	28	19
	D3	19	55	50	56	19	35	28	33
	D4	147	163	151	130	36	45	36	44
Non-activated in 10% FCS	D5	99	150	131	127	18	15	20	15
	D6	73	96	97	104	20	20	20	24

10.2.2 Statistical analysis ANOVA single factor 0.1% FCS non-activated and activated cells for Figure 19A.

ANOVA: Single Factor								
DESCRIPTION					Alpha	0.05		
Group	*Count*	*Sum*	*Mean*	*Variance*	*SS*	*Std Err*	*Lower*	*Upper*
Non-activated	3	1110000	370000	53181250000	1.06363E+11	108177.773	69650.3519	670349.648
Activated	3	692500	230833.3333	17033333333	34066666667	108177.773	-69516.315	531182.981
ANOVA								
Sources	*SS*	*df*	*MS*	*F*	*P value*	*Eta-sq*	*RMSSE*	*Omega Sq*
Between Groups	29051041667	1	29051041667	0.827493102	0.414454068	0.17141259	0.52519619	-0.0296022
Within Groups	1.40429E+11	4	35107291667					
Total	1.6948E+11	5	33896041667					

10.2.3 Statistical analysis ANOVA single factor 10% FCS non-activated and activated cells for Figure 19A.

ANOVA: Single Factor								
DESCRIPTION					Alpha	0.05		
Group	*Count*	*Sum*	*Mean*	*Variance*	*SS*	*Std Err*	*Lower*	*Upper*
Non-activated	3	4452500	1484166.667	1.4039E+11	2.80779E+11	169726.087	1012931.5	1955401.83
Activated	3	1685000	561666.6667	32452083333	64904166667	169726.087	90431.5045	1032901.83
ANOVA								
Sources	*SS*	*df*	*MS*	*F*	*P value*	*Eta-sq*	*RMSSE*	*Omega Sq*
Between Groups	1.27651E+12	1	1.27651E+12	14.77085242	0.0184*	0.78690366	2.21892259	0.69652295
Within Groups	3.45683E+11	4	86420833333					
Total	1.62219E+12	5	3.24439E+11					

10.2.4 Statistical analysis ANOVA single factor 0.1% FCS non-activated and activated % live cells for Figure 19B.

ANOVA: Single Factor								
DESCRIPTION					Alpha	0.05		
Group	*Count*	*Sum*	*Mean*	*Variance*	*SS*	*Std Err*	*Lower*	*Upper*
Non-activated	3	171.881298	57.2937661	397.6147336	795.2294672	8.48535252	33.7346506	80.8528816
Activated	3	105.809603	35.26986755	34.3925105	68.785021	8.48535252	11.7107521	58.828983
ANOVA								
Sources	*SS*	*df*	*MS*	*F*	*P value*	*Eta-sq*	*RMSSE*	*Omega Sq*
Between Groups	727.5781609	1	727.5781609	3.368360928	0.140360054	0.45713843	1.05961643	0.28301372
Within Groups	864.0144882	4	216.0036221					
Total	1591.592649	5	318.3185298					

10.2.5 Statistical analysis ANOVA single factor 10% FCS non-activated and activated cells % live cells Figure 19B.

ANOVA: Single Factor								
DESCRIPTION					Alpha	0.05		
Group	*Count*	*Sum*	*Mean*	*Variance*	*SS*	*Std Err*	*Lower*	*Upper*
Non-activated	3	248.2621359	82.75404531	24.14442741	48.28885482	3.28217838	73.6412572	91.8668334
Activated	3	183.3911794	61.13039314	40.49174219	80.98348438	3.28217838	52.017605	70.2431812
ANOVA								
Sources	*SS*	*df*	*MS*	*F*	*P value*	*Eta-sq*	*RMSSE*	*Omega Sq*
Between Groups	701.3734996	1	701.3734996	21.70219875	0.0096**	0.84437129	2.68962195	0.7752994
Within Groups	129.2723392	4	32.3180848					
Total	830.6458388	5	166.1291678					

10.2.6 Statistical analysis ANOVA single factor for 0.1% FCS non-activated and activated for 6 hours total cell number, Figure 24A.

ANOVA: Single Factor								
DESCRIPTION					Alpha	0.05		
Group	*Count*	*Sum*	*Mean*	*Variance*	*SS*	*Std Err*	*Lower*	*Upper*
Non-activated	2	1157500	578750	9453125000	9453125000	40498.1995	449866.654	707633.346
Activated	3	1425000	475000	193750000	387500000	33066.6415	369767.189	580232.811
ANOVA								
Sources	*SS*	*df*	*MS*	*F*	*P value*	*Eta-sq*	*RMSSE*	*Omega Sq*
Between Groups	12916875000	1	12916875000	3.937821531	0.141451921	0.56758761	1.28092114	0.37010426
Within Groups	9840625000	3	3280208333					
Total	22757500000	4	5689375000					

10.2.7 Statistical analysis ANOVA single factor for 0.1% FCS non-activated and activated for 24 hours total cell number, Figure 24A.

ANOVA: Single Factor								
DESCRIPTION					Alpha	0.05		
Group	*Count*	*Sum*	*Mean*	*Variance*	*SS*	*Std Err*	*Lower*	*Upper*
Non-activated	3	2900000	966666.6667	4133333333	8266666667	28382.3106	887864.739	1045468.59
Activated	3	855000	285000	700000000	1400000000	28382.3106	206198.073	363801.927
ANOVA								
Sources	*SS*	*df*	*MS*	*F*	*P value*	*Eta-sq*	*RMSSE*	*Omega Sq*
Between Groups	6.97004E+11	1	6.97004E+11	288.4155172	0.0001***	0.98632084	9.80502452	0.97955118
Within Groups	9666666667	4	2416666667					
Total	7.06671E+11	5	1.41334E+11					

10.2.8 Statistical analysis ANOVA single factor for 0.1% FCS non-activated for 6,12,18 and 24 hours, total cell number, Figure 24A.

ANOVA: Single Factor								
DESCRIPTION					Alpha	0.05		
Group	*Count*	*Sum*	*Mean*	*Variance*	*SS*	*Std Err*	*Lower*	*Upper*
6 hours	3	1736250	578750	4726562500	9453125000	33063.3598	502505.755	654994.245
12 hours	3	2055000	685000	1693750000	3387500000	33063.3598	608755.755	761244.245
18 hours	3	2322500	774166.6667	2564583333	5129166667	33063.3598	697922.422	850410.911
24 hours	3	2900000	966666.6667	4133333333	8266666667	33063.3598	890422.422	1042910.91
ANOVA								
Sources	*SS*	*df*	*MS*	*F*	*P value*	*Eta-sq*	*RMSSE*	*Omega Sq*
Between Groups	2.43224E+11	3	81074782986	24.72125832	0.0002***	0.90263349	2.87061308	0.85570641
Within Groups	26236458333	8	3279557292					
Total	2.69461E+11	11	24496437027					

10.2.9 Tukey's HSD (honestly significant difference) test for non-activated cells at 6,12,18 and 24-hours in Figure 24A.

TUKEY HSD/KRAMER			alpha	0.05					
group	*mean*	*n*	*ss*	*df*	*q-crit*				
6 hours	578750	3	9453125000						
12 hours	685000	3	3387500000						
18 hours	774166.667	3	5129166667						
24 hours	966666.667	3	8266666667						
		12	26236458333	8	4.529				
Q TEST									
group 1	*group 2*	*mean*	*std err*	*q-stat*	*lower*	*upper*	*p-value*	*mean-crit*	*Cohen d*
6 hours	12 hours	106250	33063.35984	3.21352701	-43493.957	255993.957	0.18389981	149743.957	1.85533069
6 hours	18 hours	195416.667	33063.35984	5.91036929	45672.71	345160.623	0.0131*	149743.957	3.4123533
6 hours	24 hours	387916.667	33063.35984	11.7325241	238172.71	537660.623	0.0002***	149743.957	6.77377596
12 hours	18 hours	89166.6667	33063.35984	2.69684228	-60577.29	238910.623	0.29739917	149743.957	1.55702262
12 hours	24 hours	281666.667	33063.35984	8.5189971	131922.71	431410.623	0.0014**	149743.957	4.91844527
18 hours	24 hours	192500	33063.35984	5.82215482	42756.0433	342243.957	0.0142*	149743.957	3.36142266

10.2.10 Statistical analysis ANOVA single factor for 0.1% FCS activated for 6,12,18 and 24 hours, total cell number, Figure 24A.

ANOVA: Single Factor								
DESCRIPTION					Alpha	0.05		
Group	*Count*	*Sum*	*Mean*	*Variance*	*SS*	*Std Err*	*Lower*	*Upper*
6 hours	3	1425000	475000	193750000	387500000	17613.7178	434382.694	515617.306
12 hours	3	1157500	385833.3333	2702083333	5404166667	17613.7178	345216.027	426450.639
18 hours	3	1032500	344166.6667	127083333.3	254166666.7	17613.7178	303549.361	384783.973
24 hours	3	855000	285000	700000000	1400000000	17613.7178	244382.694	325617.306
ANOVA								
Sources	*SS*	*df*	*MS*	*F*	*P value*	*Eta-sq*	*RMSSE*	*Omega Sq*
Between Groups	57429166667	3	19143055556	20.56780451	0.0004***	0.885228	2.61838401	0.83027694
Within Groups	7445833333	8	930729166.7					
Total	64875000000	11	5897727273					

10.2.11 Tukey's HSD (honestly significant difference) test for activated cells at 6,12,18 and 24-hour timepoint in Figure 24A.

TUKEY HSD/KRAMER			alpha	0.05					
group	*mean*	*n*	*ss*	*df*	*q-crit*				
6 hours	475000	3	387500000						
12 hours	385833.333	3	5404166667						
18 hours	344166.667	3	254166666.7						
24 hours	285000	3	1400000000						
		12	7445833333	8	4.529				
Q TEST									
group 1	*group 2*	*mean*	*std err*	*q-stat*	*lower*	*upper*	*p-value*	*mean-crit*	*Cohen d*
6 hours	12 hours	89166.6667	17613.71782	5.06234218	9394.13865	168939.195	0.0295*	79772.528	2.92274462
6 hours	18 hours	130833.333	17613.71782	7.42792264	51060.8053	210605.861	0.0034**	79772.528	4.28851313
6 hours	24 hours	190000	17613.71782	10.7870469	110227.472	269772.528	0.0003***	79772.528	6.22790442
12 hours	18 hours	41666.6667	17613.71782	2.36558046	-38105.861	121439.195	0.3954928	79772.528	1.36576851
12 hours	24 hours	100833.333	17613.71782	5.72470471	21060.8053	180605.861	0.0156*	79772.528	3.3051598
18 hours	24 hours	59166.6667	17613.71782	3.35912425	-20605.861	138939.195	0.15974787	79772.528	1.93939129

10.2.12 Statistical analysis ANOVA single factor for 0.1% FCS non-activated and activated for 6 hours % live, Figure 24B.

ANOVA: Single Factor								
DESCRIPTION					Alpha	0.05		
Group	*Count*	*Sum*	*Mean*	*Variance*	*SS*	*Std Err*	*Lower*	*Upper*
Non-activated	2	182.504353	91.25217655	1.636914237	1.636914237	1.86903211	85.3040822	97.2002709
Activated	3	246.864109	82.28803634	9.661386	19.322772	1.52605833	77.4314376	87.144635
ANOVA								
Sources	*SS*	*df*	*MS*	*F*	*P value*	*Eta-sq*	*RMSSE*	*Omega Sq*
Between Groups	96.42697166	1	96.42697166	13.80177698	0.0339*	0.82144746	2.39807014	0.71912916
Within Groups	20.95968624	3	6.986562079					
Total	117.3866579	4	29.34666447					

10.2.13 Statistical analysis ANOVA single factor for 0.1% FCS non-activated and activated for 24 hours % live cells, Figure 24B.

ANOVA: Single Factor								
DESCRIPTION					Alpha	0.05		
Group	*Count*	*Sum*	*Mean*	*Variance*	*SS*	*Std Err*	*Lower*	*Upper*
Non-activated	3	273.0611346	91.02037821	2.487696661	4.975393323	1.42297123	87.0695767	94.9711797
Activated	3	246.864109	82.28803634	9.661386	19.322772	1.42297123	78.3372348	86.2388378
ANOVA								
Sources	*SS*	*df*	*MS*	*F*	*P value*	*Eta-sq*	*RMSSE*	*Omega Sq*
Between Groups	114.3806919	1	114.3806919	18.82951909	0.0123*	0.82478825	2.50529566	0.74821145
Within Groups	24.29816532	4	6.074541331					
Total	138.6788573	5	27.73577145					

10.2.14 Statistical analysis ANOVA single factor for 0.1% FCS non-activated for 6,12,18 and 24 hours, % live cells, Figure 24B.

ANOVA: Single Factor								
DESCRIPTION					Alpha	0.05		
Group	*Count*	*Sum*	*Mean*	*Variance*	*SS*	*Std Err*	*Lower*	*Upper*
6 hours	2	182.5043531	91.25217655	1.636914237	1.636914237	1.56911464	87.54181	94.9625431
12 hours	3	271.8934894	90.63116313	9.417747737	18.83549547	1.28117674	87.6016615	93.6606647
18 hours	3	276.6395004	92.2131668	4.510943838	9.021887676	1.28117674	89.1836652	95.2426684
24 hours	3	273.0611346	91.02037821	2.487696661	4.975393323	1.28117674	87.9908766	94.0498798
ANOVA								
Sources	*SS*	*df*	*MS*	*F*	*P value*	*Eta-sq*	*RMSSE*	*Omega Sq*
Between Groups	4.079096356	3	1.359698785	0.276123496	0.84102701	0.10581646	0.30341254	-0.2459831
Within Groups	34.46969071	7	4.92424153					
Total	38.54878706	10	3.854878706					

10.2.15 Tukey's HSD test for non-activated cells at 6,12,18 and 24-hour timepoint, % live cells in Figure 24B.

TUKEY HSD/KRAMER			alpha	0.05					
group	*mean*	*n*	*ss*	*df*	*q-crit*				
6 hours	91.2521765	2	1.636914237						
12 hours	90.6311631	3	18.83549547						
18 hours	92.2131668	3	9.021887676						
24 hours	91.0203782	3	4.975393323						
		11	34.46969071	7	4.681				
Q TEST									
group 1	*group 2*	*mean*	*std err*	*q-stat*	*lower*	*upper*	*p-value*	*mean-crit*	*Cohen d*
6 hours	12 hours	0.62101342	1.432399143	0.43354774	-6.084047	7.3260738	0.98924376	6.70506039	0.27985386
6 hours	18 hours	0.96099025	1.432399143	0.67089558	-5.7440701	7.66605064	0.96265942	6.70506039	0.43306124
6 hours	24 hours	0.23179834	1.432399143	0.16182524	-6.4732621	6.93685872	0.99941711	6.70506039	0.10445774
12 hours	18 hours	1.58200367	1.281176742	1.23480517	-4.4151847	7.579192	0.81856031	5.99718833	0.7129151
12 hours	24 hours	0.38921508	1.281176742	0.30379499	-5.6079732	6.38640341	0.99620827	5.99718833	0.17539612
18 hours	24 hours	1.19278859	1.281176742	0.93101018	-4.8043997	7.18997692	0.90970664	5.99718833	0.53751898

10.2.16 Statistical analysis ANOVA single factor for 0.1% FCS activated for 6,12,18 and 24 hours, % live cells, Figure 24B.

ANOVA: Single Factor								
DESCRIPTION					Alpha	0.05		
Group	*Count*	*Sum*	*Mean*	*Variance*	*SS*	*Std Err*	*Lower*	*Upper*
6 hours	3	246.864109	82.28803634	9.661386	19.322772	1.64119797	78.503427	86.0726456
12 hours	3	226.4436934	75.48123115	1.327997689	2.655995378	1.64119797	71.6966218	79.2658404
18 hours	3	206.5004059	68.83346865	12.6142793	25.2285586	1.64119797	65.0488593	72.618078
24 hour	3	178.1515968	59.38386561	8.718706301	17.4374126	1.64119797	55.5992563	63.1684749
ANOVA								
Sources	*SS*	*df*	*MS*	*F*	*P value*	*Eta-sq*	*RMSSE*	*Omega Sq*
Between Groups	858.4289596	3	286.1429865	35.41114007	0.0001***	0.92996796	3.43565326	0.89586354
Within Groups	64.64473858	8	8.080592322					
Total	923.0736982	11	83.91579074					

10.2.17 Tukey's HSD (honestly significant difference) test for activated cells at 6,12,18 and 24-hour timepoint, % live cells in Figure 24B.

TUKEY HSD/KRAMER			alpha	0.05					
group	*mean*	*n*	*ss*	*df*	*q-crit*				
6 hours	82.2880363	3	19 322772						
12 hours	75.4812311	3	2.655995378						
18 hours	68.8334686	3	25.2285586						
24 hour	59.3838656	3	17.4374126						
		12	64.64473858	8	4.529				
Q TEST									
group 1	*group 2*	*mean*	*std err*	*q-stat*	*lower*	*upper*	*p-value*	*mean-crit*	*Cohen d*
6 hours	12 hours	6.80680519	1.641197969	4.147461378	-0.6261804	14.2397908	0.07314964	7.4329856	2.39453794
6 hours	18 hours	13.4545677	1.641197969	8.198016291	6.02158209	20.8875533	0.0018**	7.4329856	4.73312691
6 hours	24 hour	22.9041707	1.641197969	13.95576351	15.4711851	30.3371563	0.0000***	7.4329856	8.05736382
12 hours	18 hours	6.6477625	1.641197969	4.050554913	-0.7852231	14.0807481	0.08058578	7.4329856	2.33858897
12 hours	24 hour	16.0973655	1.641197969	9.808302129	8.66437993	23.5303511	0.0005***	7.4329856	5.66282587
18 hours	24 hour	9.44960304	1.641197969	5.757747216	2.01661744	16.8825886	0.0151*	7.4329856	3.32423691

10.2.18 Raw cell counts for Figure 24

	well #	Quadrant 1 counts live	Quadrant 2 counts live	Quadrant 3 counts live	Quadrant 4 counts live	Quadrant 1 counts dead	Quadrant 2 counts dead	Quadrant 3 counts dead	Quadrant 4 counts dead
	A1	38	32	41	38	10	11	11	8
	A2	35	43	33	52	7	9	10	7
Activated in 0.1% FCS 6 hours	A3	41	35	42	39	8	9	5	6
	A4	41	54	39	54	2	4	5	5
Non-activated in 0.1% FCS 6 hours	A5	57	60	62	55	6	7	7	5
	B1	31	24	22	29	13	9	7	4
	B2	36	22	23	30	7	7	9	12
Activated in 0.1% FCS 12 hours	B3	27	39	29	37	12	5	17	12
	B4	65	64	55	56	2	3	6	4
	B5	61	65	58	66	5	5	15	8
Non-activated in 0.1% FCS 12 hours	B6	63	55	69	67	4	6	8	12
	C1	28	24	14	26	13	13	11	9
	C2	19	19	20	37	11	10	8	18
Activated in 0.1% FCS 18 hours	C3	25	23	21	28	11	10	8	7
	C4	79	74	57	75	6	6	9	10
	C5	84	63	74	79	9	6	6	5
Non-activated in 0.1% FCS 18 hours	C6	74	66	59	72	6	6	2	2
	D1	9	20	17	16	14	12	9	13
	D2	16	20	12	18	11	8	11	10
Activated in 0.1% FCS 24 hours	D3	20	20	18	17	11	15	12	13
	D4	94	109	93	83	8	4	12	13
	D5	75	86	82	86	6	11	10	12
Non-activated in 0.1% FCS 24 hours	D6	90	77	83	98	5	6	9	8

10.2.19 Number of multinucleated cells in the drug treated RAW 264.7 cells per field of view (20x). Values were averaged and graphed in Figure 29.

Drug conc	Cyclohexanone activated		Oxalyldihydrazide activated		
5000uM	47	51	31	44	
500µM	41	49	27	35	
250µM	39	41	23	21	
125µM	14	19	16	15	
62.5µM	8	14	14	14	
0µM	3	3	6	5	

10.3 *Drug Treatment Supporting Data*

10.3.1 **Raw cell counts for Figure 31**

	well #	quadrant 1 counts live	quadrant 2 counts live	quadrant 3 counts live	quadrant 4 counts live	quadrant 1 counts dead	quadrant 2 counts dead	quadrant 3 counts dead	quadrant 4 counts dead
activated in 0.1% FCS cyclohexanone applied in activation mix	A1	24	26	29	27	11	9	5	17
	A2	27	28	25	28	6	11	12	12
	A3	35	36	29	29	4	13	10	5
	A4	46	38	33	31	7	8	13	6
	A5	34	32	42	33	14	10	7	15
	A6	38	45	36	34	14	18	17	11
activated in 0.1% FCS cyclohexanone applied without activation mix	B1	34	32	36	22	7	5	11	3
	B2	26	26	37	33	8	4	7	3
	B3	25	26	31	28	8	9	12	6
	B4	41	22	21	29	10	6	9	4
	B5	13	22	28	25	6	15	9	15
	B6	20	21	22	19	13	18	15	8

10.3.2 **Raw cell counts for Figure 31**

	well #	quadrant 1 counts live	quadrant 2 counts live	quadrant 3 counts live	quadrant 4 counts live	quadrant 1 counts dead	quadrant 2 counts dead	quadrant 3 counts dead	quadrant 4 counts dead
activated in 0.1% FCS, oxalyldihydrazide applied in activation mix	C1	25	34	28	25	12	8	8	8
	C2	39	32	28	26	13	9	8	15
	C3	31	41	38	28	9	14	12	8
	C4	36	30	40	31	9	13	16	13
	C5	32	33	35	26	10	4	7	19
	A6	38	45	36	34	14	18	17	11
activated in 0.1% FCS oxalyldihyrazide applied without activation mix	D1	37	36	46	26	12	13	10	12
	D2	24	32	23	20	16	11	18	13
	D3	24	22	26	24	10	5	21	12
	D4	29	28	23	30	7	10	16	17
	D5	42	45	42	35	11	16	10	13
	B6	34	21	22	19	13	18	15	8

10.4 *Supporting Data for Alamar Blue Assay*

10.4.1 Absorbance values for Alamar blue assay for activated and re-activated cyclohexanone treated RAW 264.7 cells in Figure 32.

Raw Data (544/590-10)											
1	**2**	**3**	**4**	**5**	**6**	**7**	**8**	**9**	**10**	**11**	**12**
9414	116357	2038	111094	2024	101199	1931	102309	2036	101109	2167	110916
9185	122476	2384	107778	2375	103949	2157	104896	2249	100915	2358	109574
9523	116796	2199	106317	2013	101655	2077	105994	2071	103969	2123	110210
305	1308	408	1063	392	1055	383	1075	361	1108	411	1067
304	1176	396	1060	382	1068	419	1092	379	1082	403	1084
1225	101121	1862	94525	1835	94513	1889	101305	1980	98381	2153	107856
1277	102300	2096	94570	1948	93372	2136	100673	2066	95589	2211	103180
1215	102605	1888	98860	1904	96762	1963	103981	1988	96753	2004	109355

Raw Data (544/590-10)											
1	**2**	**3**	**4**	**5**	**6**	**7**	**8**	**9**	**10**	**11**	**12**
9414	116357		111094		101199		102309		101109		110916
9185	122476		107778		103949		104896		100915		109574
9523	116796		106317		101655		105994		103969		110210
	101121		94525		94513		101305		98381		107856
	102300		94570		93372		100673		95589		103180
	102605		98860		96762		103981		96753		109355

10.4.2 Plate layout for Alamar blue assay for activated and re-activated cyclohexanone treated RAW 264.7 cells in Figure 32.

		3A1		**3A2**		**3A3**		**3A4**		**3A5**		**3A6**	
A		5000µM		500µM		250µM		125µM		62 5µM		0µM	
B		5000µM		500µM		250µM		125µM		62 5µM		0µM	
C		5000µM		500µM		250µM		125µM		62 5µM		0µM	
D	Re-activated cells treated with cyclohexanone												
E		**3B1**		**3B2**		**3B3**		**3B4**		**3B5**		**3B6**	
F		5000µM		500µM		250µM		125µM		62 5µM		0µM	
G		5000µM		500µM		250µM		125µM		62 5µM		0µM	
H		5000µM		500µM		250µM		125µM		62 5µM		0µM	
	Activated cells treated with cyclohexanone												

10.4.3 Plate layout for Alamar blue assay for activated and re-activated cyclohexanone treated RAW 264.7 cells in Figure 32.

		1A1		**1A2**		**1A3**		**1A4**		**1A5**		**1A6**	
A		5000µM		500µM		250µM		125µM		62 5µM		0µM	
B		5000µM		500µM		250µM		125µM		62 5µM		0µM	
C		5000µM		500µM		250µM		125µM		62 5µM		0µM	
D	Non-activated cells treated with cyclohexanone												
E		**1B1**		**1B2**		**1B3**		**1B4**		**1B5**		**B6**	
F		5000µM		500µM		250µM		125µM		62 5µM		0µM	
G		5000µM		500µM		250µM		125µM		62 5µM		0µM	
H		5000µM		500µM		250µM		125µM		62 5µM		0µM	
	Non-activated cells treated with cyclohexanone												

10.4.4 Absorbance values for Alamar blue assay for non-activated cyclohexanone treated RAW 264.7 cells in Figure 32.

	Raw Data (544/590-10)											
	1	**2**	**3**	**4**	**5**	**6**	**7**	**8**	**9**	**10**	**11**	**12**
A	10226	178358	3356	167432	3034	158798	2886	153378	3108	154118	3340	168210
B	9651	185317	3452	170573	3037	168415	3114	161748	3029	160395	3506	171301
C	10057	183230	3242	166751	2984	169556	2945	163407	2987	163111	3109	170758
	Raw Data (544/590-10)											
	1	**2**	**3**	**4**	**5**	**6**	**7**	**8**	**9**	**10**	**11**	**12**
A	10226	178358		167432		158798		153378		154118		168210
B	9651	185317		170573		168415		161748		160395		171301
C	10057	183230		166751		169556		163407		163111		170758

10.4.5 Statistical analysis ANOVA single factor for the FI in non-activated cyclohexanone treated RAW 264.7 macrophages shown in Figure 32A.

ANOVA: Single Factor								
DESCRIPTION					Alpha	0 05		
Group	*Count*	*Sum*	*Mean*	*Variance*	*SS*	*Std Err*	*Lower*	*Upper*
0	3	445163	148387 67	34402040 3	68804080 7	2752 833	142389 8	154385 6
62 5	3	447690	149230	21275239	42550478	2752 833	143232 1	155227 9
125	3	448599	149533	28898337	57796674	2752 833	143535 1	155530 9
250	3	466835	155611 67	34920522 3	69841044 7	2752 833	149613 8	161609 6
500	3	474822	158274	4156221	8312442	2752 833	152276 1	164271 9
5000	3	516971	172323 67	12753272 3	25506544 7	2752 833	166325 8	178321 6
ANOVA								
Sources	*SS*	*df*	*MS*	*F*	*P value*	*Eta-sq*	*RMSSE*	*Omega Sq*
Between Groups	1248674940	5	249734988	10 9849565	0 00037949	0 820694	1 913544	0 735001
Within Groups	272811264	12	22734272					
Total	1521486204	17	89499188					

10.4.6 Tukey HSD for FI in non-activated cyclohexanone treated RAW 264.7 macrophages shown in Figure 32A.

TUKEY HSD/KRAMER			alpha	0 05						
group	*mean*	*n*	*ss*	*df*	*q-crit*					
0	148387 7	3	68804081							
62 5	149230	3	42550478							
125	149533	3	57796674							
250	155611 7	3	69841045							
500	158274	3	8312442							
5000	172323 7	3	25506545							
		18	272811264	12	4 75					
Q TEST										
group 1	*group 2*	*mean*	*std err*	*q-stat*	*lower*	*upper*	*p-value*	*mean-crit*	*Cohen d*	
0	62 5	842 3333	2752 8332	0 305988	-12233 6	13918 29	0 9999151	13075 96	0 176662	
0	125	1145 333	2752 8332	0 416056	-11930 6	14221 29	0 9996174	13075 96	0 24021	
0	250	7224	2752 8332	2 624205	-5851 96	20299 96	0 469862	13075 96	1 515086	
0	500	9886 333	2752 8332	3 59133	-3189 62	22962 29	0 1870624	13075 96	2 073456	
0	5000	23936	2752 8332	8 695042	10860 04	37011 96	0 0005***	13075 96	5 020085	
62 5	125	303	2752 8332	0 110068	-12773	13378 96	0 9999995	13075 96	0 063548	
62 5	250	6381 667	2752 8332	2 318218	-6694 29	19457 62	0 5908921	13075 96	1 338424	
62 5	500	9044	2752 8332	3 285343	-4031 96	22119 96	0 2568764	13075 96	1 896793	
62 5	5000	23093 67	2752 8332	8 389054	10017 71	36169 62	0 0008***	13075 96	4 843423	
125	250	6078 667	2752 8332	2 208149	-6997 29	19154 62	0 635633	13075 96	1 274876	
125	500	8741	2752 8332	3 175274	-4334 96	21816 96	0 2864755	13075 96	1 833245	
125	5000	22790 67	2752 8332	8 278986	9714 709	35866 62	0 0008***	13075 96	4 779875	
250	500	2662 333	2752 8332	0 967125	-10413 6	15738 29	0 9804581	13075 96	0 55837	
250	5000	16712	2752 8332	6 070836	3636 042	29787 96	0 0104*	13075 96	3 504999	
500	5000	14049 67	2752 8332	5 103712	973 7089	27125 62	0 0328*	13075 96	2 946629	

10.4.7 Statistical analysis ANOVA single factor for the FI in re-activated and activated RAW 264.7 macrophages treated with 0µM of cyclohexanone shown in Figure 32A.

ANOVA: Single Factor								
DESCRIPTION					Alpha	0.05		
Group	*Count*	*Sum*	*Mean*	*Variance*	*SS*	*Std Err*	*Lower*	*Upper*
Re-activated	3	302578	100859.333	450649.3	901298.7	1343.157	97130.13	104588.5
Activated	3	292269	97423	10373767	20747534	1343.157	93693.8	101152.2
ANOVA								
Sources	*SS*	*df*	*MS*	*F*	*P value*	*Eta-sq*	*RMSSE*	*Omega Sq*
Between Groups	17712580.2	1	17712580.2	3.272709	0.144705	0.449999	1.044463	0.274724
Within Groups	21648832.7	4	5412208.17					
Total	39361412.8	5	7872282.57					

10.4.8 Statistical analysis ANOVA single factor for the FI in re-activated and activated RAW 264.7 macrophages treated with 62.5µM of cyclohexanone shown in Figure 32A.

ANOVA: Single Factor								
DESCRIPTION					Alpha	0.05		
Group	*Count*	*Sum*	*Mean*	*Variance*	*SS*	*Std Err*	*Lower*	*Upper*
Re-activated	3	277871	92623.67	2924025	5848051	902.8457	90116.97	95130.37
Activated	3	262601	87533.67	1966757	3933515	902.8457	85026.97	90040.37
ANOVA								
Sources	*SS*	*df*	*MS*	*F*	*P value*	*Eta-sq*	*RMSSE*	*Omega Sq*
Between Groups	38862150	1	38862150	15.892	0.0163*	0.798914	2.301593	0.712809
Within Groups	9781565.33	4	2445391					
Total	48643715.3	5	9728743					

10.4.9 Statistical analysis ANOVA single factor for the FI in re-activated and activated RAW 264.7 macrophages treated with 125µM of cyclohexanone shown in Figure 32A.

DESCRIPTION					Alpha	0.05		
Group	*Count*	*Sum*	*Mean*	*Variance*	*SS*	*Std Err*	*Lower*	*Upper*
Re-activated	3	285077	95025.67	3579566	7159133	1053.838	92099.74	97951.59
Activated	3	277837	92612.33	3083877	6167755	1053.838	89686.41	95538.26
ANOVA								
Sources	*SS*	*df*	*MS*	*F*	*P value*	*Eta-sq*	*RMSSE*	*Omega Sq*
Between Groups	8736266.67	1	8736267	2.622148	0.180695	0.395966	0.934906	0.21282
Within Groups	13326887.3	4	3331722					
Total	22063154	5	4412631					

10.4.10 **Statistical analysis ANOVA single factor for the FI in re-activated and activated RAW 264.7 macrophages treated with 250µM of cyclohexanone shown in Figure 32A.**

ANOVA: Single Factor								
DESCRIPTION					Alpha	0.05		
Group	*Count*	*Sum*	*Mean*	*Variance*	*SS*	*Std Err*	*Lower*	*Upper*
Re-activated	3	278681	92893.67	2172145	4344291	926.2357	90322.02	95465.31
Activated	3	256525	85508.33	2975330	5950661	926.2357	82936.69	88079.98
ANOVA								
Sources	*SS*	*df*	*MS*	*F*	*P value*	*Eta-sq*	*RMSSE*	*Omega Sq*
Between Groups	81814722.7	1	81814723	31.78829	0.0049**	0.888232	3.255165	0.836905
Within Groups	10294951.3	4	2573738					
Total	92109674	5	18421935					

10.4.11 **Statistical analysis ANOVA single factor for the FI in re-activated and activated RAW 264.7 macrophages treated with 500µM of cyclohexanone shown in Figure 32A.**

ANOVA: Single Factor								
DESCRIPTION					Alpha	0.05		
Group	*Count*	*Sum*	*Mean*	*Variance*	*SS*	*Std Err*	*Lower*	*Upper*
Re-activated	3	297067	99022.33333	5991684	11983369	1425.448	95064.66	102980
Activated	3	259833	86611	6199725	12399450	1425.448	82653.32	90568.68
ANOVA								
Sources	*SS*	*df*	*MS*	*F*	*P value*	*Eta-sq*	*RMSSE*	*Omega Sq*
Between Groups	231061793	1	231061792.7	37.90567	0.0035**	0.904548	3.554606	0.860158
Within Groups	24382818.7	4	6095704.667					
Total	255444611	5	51088922.27					

10.4.12 **Statistical analysis ANOVA single factor for the FI in re-activated and activated RAW 264.7 macrophages treated with 5000µM of cyclohexanone shown in Figure 32A.**

ANOVA: Single Factor								
DESCRIPTION					Alpha	0.05		
Group	*Count*	*Sum*	*Mean*	*Variance*	*SS*	*Std Err*	*Lower*	*Upper*
Re-activated	3	327507	109169	11649547	23299094	1429.672	105199.6	113138.4
Activated	3	277904	92634.66667	614220.3	1228441	1429.672	88665.26	96604.07
ANOVA								
Sources	*SS*	*df*	*MS*	*F*	*P value*	*Eta-sq*	*RMSSE*	*Omega Sq*
Between Groups	410076268	1	410076268.2	66.87607	0.0012**	0.943563	4.721443	0.916523
Within Groups	24527534.7	4	6131883.667					
Total	434603803	5	86920760.57					

10.4.13 Statistical analysis ANOVA single factor for the FI in re-activated RAW 264.7 macrophages treated with of cyclohexanone shown in Figure 32A.

ANOVA Single Factor								
DESCRIPTION					Alpha	0.05		
Group	*Count*	*Sum*	*Mean*	*Variance*	*SS*	*Std Err*	*Lower*	*Upper*
0	3	302578	100859.3333	450649.3	901298.7	1219.463	98202.35	103516.3
62.5	3	277871	92623.66667	2924025	5848051	1219.463	89966.69	95280.65
125	3	285077	95025.66667	3579566	7159133	1219.463	92368.69	97682.65
250	3	278681	92893.66667	2172145	4344291	1219.463	90236.69	95550.65
500	3	297067	99022.33333	5991684	11983369	1219.463	96365.35	101679.3
5000	3	327507	109169	11649547	23299094	1219.463	106512	111826
ANOVA								
Sources	*SS*	*df*	*MS*	*F*	*P value*	*Eta-sq*	*RMSSE*	*Omega Sq*
Between Groups	592111430.9	5	118422286.2	26.54453	4.27E-06	0.917083	2.974588	0.876478
Within Groups	53535235.33	12	4461269.611					
Total	645646666.3	17	37979215.66					

10.4.14 Tukey HSD for FI in the re-activated cyclohexanone treated RAW 264.7 macrophages shown in Figure 32A.

TUKEY HSD/KRAMER			alpha	0 05					
group	*mean*	*n*	*ss*	*df*	*q-crit*				
0	100859 3	3	901298 667						
62 5	92623 67	3	5848050 67						
125	95025 67	3	7159132 67						
250	92893 67	3	4344290 67						
500	99022 33	3	11983368 7						
5000	109169	3	23299094						
		18	53535235 3	12	4 75				
Q TEST									
group 1	*group 2*	*mean*	*std err*	*q-stat*	*lower*	*upper*	*p-value*	*mean-crit*	*Cohen d*
0	62 5	8235 667	1219 46294	6 753519	2443 218	14028 12	0 0047**	5792 449	3 899146
0	125	5833 667	1219 46294	4 7838	41 21769	11626 12	0 0481*	5792 449	2 761928
0	250	7965 667	1219 46294	6 53211	2173 218	13758 12	0 0060**	5792 449	3 771316
0	500	1837	1219 46294	1 506401	-3955 45	7629 449	0 885938	5792 449	0 869721
0	5000	8309 667	1219 46294	6 814202	2517 218	14102 12	0 0043**	5792 449	3 934181
62 5	125	2402	1219 46294	1 96972	-3390 45	8194 449	0 730667	5792 449	1 137218
62 5	250	270	1219 46294	0 221409	-5522 45	6062 449	0 999983	5792 449	0 127831
62 5	500	6398 667	1219 46294	5 247119	606 2177	12191 12	0 0277*	5792 449	3 029425
62 5	5000	16545 33	1219 46294	13 56772	10752 88	22337 78	0 0000***	5792 449	7 833328
125	250	2132	1219 46294	1 748311	-3660 45	7924 449	0 811684	5792 449	1 009388
125	500	3996 667	1219 46294	3 277399	-1795 78	9789 116	0 258931	5792 449	1 892207
125	5000	14143 33	1219 46294	11 598	8350 884	19935 78	0 0000***	5792 449	6 696109
250	500	6128 667	1219 46294	5 02571	336 2177	11921 12	0 0360*	5792 449	2 901595
250	5000	16275 33	1219 46294	13 34631	10482 88	22067 78	0 0000***	5792 449	7 705497
500	5000	10146 67	1219 46294	8 320603	4354 218	15939 12	0 0008***	5792 449	4 803902

10.4.15 Statistical analysis ANOVA single factor for the FI in activated RAW 264.7 macrophages treated with of cyclohexanone shown in Figure 32A.

ANOVA: Single Factor								
DESCRIPTION					Alpha	0 05		
Group	*Count*	*Sum*	*Mean*	*Variance*	*SS*	*Std Err*	*Lower*	*Upper*
0	3	292269	97423	10373767	20747534	1183 537	94844 29	100001 7
62 5	3	262601	87533 6667	1966757 3	3933515	1183 537	84954 96	90112 37
125	3	277837	92612 3333	3083877 3	6167755	1183 537	90033 63	95191 04
250	3	256525	85508 3333	2975330 3	5950661	1183 537	82929 63	88087 04
500	3	259833	86611	6199725	12399450	1183 537	84032 29	89189 71
5000	3	277904	92634 6667	614220 33	1228441	1183 537	90055 96	95213 37
ANOVA								
Sources	*SS*	*df*	*MS*	*F*	*P value*	*Eta-sq*	*RMSSE*	*Omega Sq*
Between Groups	317131455 8	5	63426291 2	15 093306	8 11E-05	0 862805	2 243012	0 796533
Within Groups	50427354 67	12	4202279 56					
Total	367558810 5	17	21621106 5					

10.4.16 **Tukey HSD for FI in the activated cyclohexanone treated RAW 264.7 macrophages shown in Figure 32A.**

TUKEY HSD/KRAMER			alpha	0.05					
group	*mean*	*n*	*ss*	*df*	*q-crit*				
0	97423	3	20747534						
62.5	87533.67	3	3933514.67						
125	92612.33	3	6167754.67						
250	85508.33	3	5950660.67						
500	86611	3	12399450						
5000	92634.67	3	1228440.67						
		18	50427354.7	12	4.75				
Q TEST									
group 1	*group 2*	*mean*	*std err*	*q-stat*	*lower*	*upper*	*p-value*	*mean-crit*	*Cohen d*
0	62.5	9889.333	1183.53701	8.355745	4267.533	15511.13	0.0008***	5621.801	4.824192
0	125	4810.667	1183.53701	4.064653	-811.134	10432.47	0.110988	5621.801	2.346728
0	250	11914.67	1183.53701	10.067	6292.866	17536.47	0.0001***	5621.801	5.812185
0	500	10812	1183.53701	9.135329	5190.199	16433.8	0.0003***	5621.801	5.274285
0	5000	4788.333	1183.53701	4.045783	-833.467	10410.13	0.113387	5621.801	2.335834
62.5	125	5078.667	1183.53701	4.291092	-543.134	10700.47	0.085629	5621.801	2.477463
62.5	250	2025.333	1183.53701	1.711255	-3596.47	7647.134	0.824164	5621.801	0.987993
62.5	500	922.6667	1183.53701	0.779584	-4699.13	6544.467	0.992505	5621.801	0.450093
62.5	5000	5101	1183.53701	4.309962	-520.801	10722.8	0.08378	5621.801	2.488358
125	250	7104	1183.53701	6.002347	1482.199	12725.8	0.0112*	5621.801	3.465457
125	500	6001.333	1183.53701	5.070677	379.5325	11623.13	0.0342*	5621.801	2.927556
125	5000	22.33333	1183.53701	0.01887	-5599.47	5644.134	1	5621.801	0.010895
250	500	1102.667	1183.53701	0.931671	-4519.13	6724.467	0.983389	5621.801	0.5379
250	5000	7126.333	1183.53701	6.021217	1504.533	12748.13	0.0110*	5621.801	3.476351
500	5000	6023.667	1183.53701	5.089547	401.8659	11645.47	0.0334*	5621.801	2.938451

10.4.17 **Statistical analysis ANOVA single factor for the FI in non-activated and re-activated RAW 264.7 macrophages treated with 0µM of cyclohexanone shown in Figure 32A.**

ANOVA: Single Factor								
DESCRIPTION					Alpha	0.05		
Group	*Count*	*Sum*	*Mean*	*Variance*	*SS*	*Std Err*	*Lower*	*Upper*
Non-activated	3	445163	148387.667	34402040.33	68804080.67	2410.141	141696	155079.3
Re-activated	3	302578	100859.333	450649.3333	901298.6667	2410.141	94167.71	107551
ANOVA								
Sources	*SS*	*df*	*MS*	*F*	*P value*	*Eta-sq*	*RMSSE*	*Omega Sq*
Between Groups	3388413704	1	3388413704	194.4420208	0.0002***	0.979843	8.050715	0.969916
Within Groups	69705379.3	4	17426344.8					
Total	3458119084	5	691623817					

10.4.18 **Statistical analysis ANOVA single factor for the FI in non-activated and re-activated RAW 264.7 macrophages treated with 5000µM of cyclohexanone shown in Figure 32A.**

ANOVA: Single Factor								
DESCRIPTION					Alpha	0.05		
Group	*Count*	*Sum*	*Mean*	*Variance*	*SS*	*Std Err*	*Lower*	*Upper*
Non-activated	3	516971	172323.667	12753272.33	25506544.67	2016.714	166724.4	177923
Re-activated	3	327507	109169	11649547	23299094	2016.714	103569.7	114768.3
ANOVA								
Sources	*SS*	*df*	*MS*	*F*	*P value*	*Eta-sq*	*RMSSE*	*Omega Sq*
Between Groups	5982767883	1	5982767883	490.3341537	0.0000***	0.991908	12.78455	0.987887
Within Groups	48805638.7	4	12201409.7					
Total	6031573521	5	1206314704					

10.4.19 **Statistical analysis ANOVA single factor for the FI in non-activated and activated RAW 264.7 macrophages treated with 0µM of cyclohexanone shown in Figure 32A.**

ANOVA: Single Factor								
DESCRIPTION					Alpha	0.05		
Group	*Count*	*Sum*	*Mean*	*Variance*	*SS*	*Std Err*	*Lower*	*Upper*
Non-activated	3	445163	148387.667	34402040.33	68804080.67	2731.782	140803	155972.3
Activated	3	292269	97423	10373767	20747534	2731.782	89838.36	105007.6
ANOVA								
Sources	*SS*	*df*	*MS*	*F*	*P value*	*Eta-sq*	*RMSSE*	*Omega Sq*
Between Groups	3896095873	1	3896095873	174.0268285	0.0002***	0.977531	7.61636	0.966485
Within Groups	89551614.7	4	22387903.7					
Total	3985647487	5	797129497					

10.4.20 **Statistical analysis ANOVA single factor for the FI in non-activated and activated RAW 264.7 macrophages treated with 5000µM of cyclohexanone shown in Figure 32A.**

ANOVA: Single Factor								
DESCRIPTION					Alpha	0.05		
Group	*Count*	*Sum*	*Mean*	*Variance*	*SS*	*Std Err*	*Lower*	*Upper*
Non-activated	3	516971	172323.667	12753272.33	25506544.67	1492.62	168179.5	176467.8
Activated	3	277904	92634.6667	614220.3333	1228440.667	1492.62	88490.49	96778.85
ANOVA								
Sources	*SS*	*df*	*MS*	*F*	*P value*	*Eta-sq*	*RMSSE*	*Omega Sq*
Between Groups	9525505082	1	9525505082	1425.174536	0.0000***	0.997201	21.79583	0.995805
Within Groups	26734985.3	4	6683746.33					
Total	9552240067	5	1910448013					

10.4.21 **Absorbance values for Alamar blue assay for activated and re-activated oxalyldihydrazide treated RAW 264.7 cells in Figure 32B.**

	Raw Data (544/590-10)											
	1	**2**	**3**	**4**	**5**	**6**	**7**	**8**	**9**	**10**	**11**	**12**
A	9489	104631	1826	102165	1979	103071	1843	93016	1883	94701	808	163
B	9182	110089	2133	99192	2247	104293	2084	95211	2045	95871	889	146
C	9506	105561	2122	96903	2004	102171	1980	95038	1903	96853	884	133
D	294	1178	376	1017	381	1038	380	991	330	1051	243	122
E	308	1226	421	1123	428	1134	441	1159	406	1144	240	128
F	1316	110257	2064	107737	2072	105100	2098	108094	2140	109163	1003	169
G	1392	112515	2344	108586	2202	104363	2305	109610	2294	108010	1051	164
H	1300	111032	2101	112587	2137	106650	2141	111329	2203	108683	876	171

	Raw Data (544/590-10)											
	1	**2**	**3**	**4**	**5**	**6**	**7**	**8**	**9**	**10**	**11**	**12**
A	9489	104631		102165		103071		93016		94701		
B	9182	110089		99192		104293		95211		95871		
C	9506	105561		96903		102171		95038		96853		
D												
E												
F		110257		107737		105100		108094		109163		
G		112515		108586		104363		109610		108010		
H		111032		112587		106650		111329		108683		

10.4.22 **Plate layout for Alamar blue assay for activated and re-activated oxalyldihydrazide treated RAW 264.7 cells in Figure 32B.**

		3C1		**3C2**		**3C3**		**3C4**		**3C5**		**3A6**	
A		5000µM		500µM		250µM		125µM		62 5µM		0µM	
B		5000µM		500µM		250µM		125µM		62 5µM		0µM	
C		5000µM		500µM		250µM		125µM		62 5µM		0µM	
D	Re-activated cells treated with oxalyldihydrazide												
E		**1D1**		**1D2**		**1D3**		**1D4**		**1D5**		**3B6**	
F		5000µM		500µM		250µM		125µM		62 5µM		0µM	
G		5000µM		500µM		250µM		125µM		62 5µM		0µM	
H		5000µM		500µM		250µM		125µM		62 5µM		0µM	
	Activated cells treated with oxalyldihydrazide												

10.4.23**Absorbance values for Alamar blue assay for non-activated oxalyldihydrazide treated RAW 264.7 cells in Figure 32B.**

	Raw Data (544/590-10)											
	1	**2**	**3**	**4**	**5**	**6**	**7**	**8**	**9**	**10**	**11**	**12**
A	10219	170150	2975	170197	2768	152706	2696	153454	2822	152049	1241	233
B	10046	173636	3331	169418	3321	161144	3042	157088	3168	149710	1327	166
C	10233	168329	3200	164509	3165	157041	2814	161667	2942	157782	1287	186
D	358	1784	545	1677	559	1518	472	1512	505	1550	308	134
E	375	1715	584	1512	492	1492	520	1487	538	1434	286	133
F	1932	165933	3263	165215	3036	149502	3010	157196	2995	154679	1282	179
G	2076	171473	3571	172701	3365	150083	3249	157622	3286	150826	1443	200
H	2164	176331	3328	180295	3216	161417	3167	164339	3367	155531	1273	209

	Raw Data (544/590-10)											
	1	**2**	**3**	**4**	**5**	**6**	**7**	**8**	**9**	**10**	**11**	**12**
A	10219	170150		170197		152706		153454		152049		
B	10046	173636		169418		161144		157088		149710		
C	10233	168329		164509		157041		161667		157782		
D												
E												
F		165933		165215		149502		157196		154679		
G		171473		172701		150083		157622		150826		
H		176331		180295		161417		164339		155531		

10.4.24 Plate layout for Alamar blue assay for non-activated oxalyldihydrazide treated RAW 264.7 cells in Figure 32B.

		1C1		**1C2**		**1C3**		**1C4**		**1C5**		**1A6**
A		5000µM		500µM		250µM		125µM		62 5µM		0µM
B		5000µM		500µM		250µM		125µM		62 5µM		0µM
C		5000µM		500µM		250µM		125µM		62 5µM		0µM
D	Non-activated cells treated with oxalyldihydrazide											
E		**1C1**		**1C2**		**1C3**		**1C4**		**1C5**		**1B6**
F		5000µM		500µM		250µM		125µM		62 5µM		0µM
G		5000µM		500µM		250µM		125µM		62 5µM		0µM
H		5000µM		500µM		250µM		125µM		62 5µM		0µM
	Non-activated cells treated with oxalyldihydrazide											

10.4.25 Statistical analysis ANOVA single factor for the FI in non-activated oxalyldihydrazide treated RAW 264.7 macrophages shown in Figure 32B.

ANOVA: Single Factor

DESCRIPTION — Alpha 0 05

Group	*Count*	*Sum*	*Mean*	*Variance*	*SS*	*Std Err*	*Lower*	*Upper*
0	3	445163	148387 6667	34402040	68804081	3212 725	141387 7	155387 6
62 5	3	430538	143512 6667	6284756	12569513	3212 725	136512 7	150512 6
125	3	448659	149553	16053669	32107338	3212 725	142553 1	156552 9
250	3	430504	143501 3333	45127390	90254781	3212 725	136501 4	150501 3
500	3	487713	162571	56852572	113705144	3212 725	155571 1	169570 9
5000	3	483239	161079 6667	27068361	54136723	3212 725	154079 7	168079 6

ANOVA

Sources	*SS*	*df*	*MS*	*F*	*P value*	*Eta-sq*	*RMSSE*	*Omega Sq*
Between Groups	1066694052	5	213338810 5	6 889721	0 002997	0 74165	1 515445	0 620642
Within Groups	371577579	12	30964798 22					
Total	1438271631	17	84604213 59					

10.4.26 Tukey HSD for FI in non-activated oxalyldihydrazide treated RAW 264.7 macrophages shown in Figure 32B.

TUKEY HSD/KRAMER — alpha 0 05

group	*mean*	*n*	*ss*	*df*	*q-crit*
0	148387 7	3	68804080 67		
62 5	143512 7	3	12569512 67		
125	149553	3	32107338		
250	143501 3	3	90254780 67		
500	162571	3	113705144		
5000	161079 7	3	54136722 67		
		18	371577578 7	12	4 75

Q TEST

group 1	*group 2*	*mean*	*std err*	*q-stat*	*lower*	*upper*	*p-value*	*mean-crit*	*Cohen d*
0	62 5	4875	3212 724608	1 517404	-10385 4	20135 44	0 882959	15260 44	0 876073
0	125	1165 333	3212 724608	0 362724	-14095 1	16425 78	0 999804	15260 44	0 209419
0	250	4886 333	3212 724608	1 520931	-10374 1	20146 78	0 881995	15260 44	0 87811
0	500	14183 33	3212 724608	4 414737	-1077 11	29443 78	0 074179	15260 44	2 548849
0	5000	12692	3212 724608	3 950541	-2568 44	27952 44	0 126227	15260 44	2 280846
62 5	125	6040 333	3212 724608	1 880128	-9220 11	21300 78	0 76462	15260 44	1 085492
62 5	250	11 33333	3212 724608	0 003528	-15249 1	15271 78	1	15260 44	0 002037
62 5	500	19058 33	3212 724608	5 93214	3797 891	34318 78	0 0122*	15260 44	3 424923
62 5	5000	17567	3212 724608	5 467945	2306 558	32827 44	0 0212*	15260 44	3 156919
125	250	6051 667	3212 724608	1 883656	-9208 78	21312 11	0 76331	15260 44	1 087529
125	500	13018	3212 724608	4 052012	-2242 44	28278 44	0 11259	15260 44	2 33943
125	5000	11526 67	3212 724608	3 587817	-3733 78	26787 11	0 187764	15260 44	2 071427
250	500	19069 67	3212 724608	5 935668	3809 225	34330 11	0 0122*	15260 44	3 42696
250	5000	17578 33	3212 724608	5 471472	2317 891	32838 78	0 0212*	15260 44	3 158956
500	5000	1491 333	3212 724608	0 464196	-13769 1	16751 78	0 999349	15260 44	0 268004

10.4.27 **Statistical analysis ANOVA single factor for the FI in the re-activated oxalyldihydrazide treated RAW 264.7 macrophages shown in Figure 32B.**

ANOVA: Single Factor								
DESCRIPTION					Alpha	0.05		
Group	*Count*	*Sum*	*Mean*	*Variance*	*SS*	*Std Err*	*Lower*	*Upper*
0	3	480335	160111.667	2723572.3	5447144.67	1105.427	157703.1	162520.2
62.5	3	259248	86416	1160721.3	2321442.67	1105.427	84007.48	88824.52
125	3	255088	85029.3333	1489406.3	2978812.67	1105.427	82620.81	87437.85
250	3	281358	93786	1134361.3	2268722.67	1105.427	91377.48	96194.52
500	3	270083	90027.6667	6961149	13922298	1105.427	87619.15	92436.19
5000	3	292104	97368	8526241.3	17052482.7	1105.427	94959.48	99776.52
ANOVA								
Sources	*SS*	*df*	*MS*	*F*	*P value*	*Eta-sq*	*RMSSE*	*Omega Sq*
Between Groups	12420004300	5	2484000860	677.59487	2.8215E-14	0.996471	15.0288	0.994707
Within Groups	43990903.33	12	3665908.61					
Total	12463995203	17	733176188					

10.4.28 **Tukey HSD for FI in the re-activated oxalyldihydrazide treated RAW 264.7 macrophages shown in Figure 32B.**

TUKEY HSD/KRAMER			alpha	0.05					
group	*mean*	*n*	*ss*	*df*	*q-crit*				
0	160111.7	3	5447144.67						
62.5	86416	3	2321442.67						
125	85029.33	3	2978812.67						
250	93786	3	2268722.67						
500	90027.67	3	13922298						
5000	97368	3	17052482.7						
		18	43990903.3	12	4.75				
Q TEST									
group 1	*group 2*	*mean*	*std err*	*q-stat*	*lower*	*upper*	*p-value*	*mean-crit*	*Cohen d*
0	62.5	73695.67	1105.42731	66.66713	68444.89	78946.45	0.0000***	5250.78	38.49029
0	125	75082.33	1105.42731	67.92155	69831.55	80333.11	0.0000***	5250.78	39.21452
0	250	66325.67	1105.42731	60.00003	61074.89	71576.45	0.0000***	5250.78	34.64103
0	500	70084	1105.42731	63.39992	64833.22	75334.78	0.0000***	5250.78	36.60396
0	5000	62743.67	1105.42731	56.75965	57492.89	67994.45	0.0000***	5250.78	32.7702
62.5	125	1386.667	1105.42731	1.254417	-3864.11	6637.446	0.9425848	5250.78	0.724238
62.5	250	7370	1105.42731	6.667105	2119.22	12620.78	0.0052**	5250.78	3.849255
62.5	500	3611.667	1105.42731	3.267213	-1639.11	8862.446	0.2615845	5250.78	1.886326
62.5	5000	10952	1105.42731	9.907481	5701.22	16202.78	0.0002***	5250.78	5.720087
125	250	8756.667	1105.42731	7.921522	3505.887	14007.45	0.0013**	5250.78	4.573493
125	500	4998.333	1105.42731	4.52163	-252.446	10249.11	0.0654637	5250.78	2.610564
125	5000	12338.67	1105.42731	11.1619	7087.887	17589.45	0.0000***	5250.78	6.444325
250	500	3758.333	1105.42731	3.399892	-1492.45	9009.113	0.2286349	5250.78	1.962928
250	5000	3582	1105.42731	3.240376	-1668.78	8832.78	0.2686747	5250.78	1.870832
500	5000	7340.333	1105.42731	6.640268	2089.554	12591.11	0.0053**	5250.78	3.83376

10.4.29 Statistical analysis ANOVA single factor for the FI in the activated oxalyldihydrazide treated RAW 264.7 macrophages shown in Figure 32B.

ANOVA: Single Factor								
DESCRIPTION					Alpha	0.05		
Group	*Count*	*Sum*	*Mean*	*Variance*	*SS*	*Std Err*	*Lower*	*Upper*
0	3	292269	97423	10373767	20747534	1123.40257	94975.32	99870.68393
62.5	3	297679	99226.33333	335456.333	670912.6667	1123.40257	96778.65	101674.0173
125	3	300856	100285.3333	2619740.33	5239480.667	1123.40257	97837.65	102733.0173
250	3	287936	95978.66667	1362673	2725346	1123.40257	93530.98	98426.3506
500	3	300733	100244.3333	6708550.33	13417100.67	1123.40257	97796.65	102692.0173
5000	3	305627	101875.6667	1316413	2632826	1123.40257	99427.98	104323.3506
ANOVA								
Sources	*SS*	*df*	*MS*	*F*	*P value*	*Eta-sq*	*RMSSE*	*Omega Sq*
Between Groups	68875661.78	5	13775132.36	3.63834351	0.031011456	0.60254	1.101263	0.42292373
Within Groups	45433200	12	3786100					
Total	114308861.8	17	6724050.693					

10.4.30 Tukey HSD for FI in the activated oxalyldihydrazide treated RAW 264.7 macrophages shown in Figure 32B.

TUKEY HSD/KRAMER			alpha	0.05					
group	*mean*	*n*	*ss*	*df*	*q-crit*				
0	97423	3	20747534						
62.5	99226.33	3	670912.6667						
125	100285.3	3	5239480.667						
250	95978.67	3	2725346						
500	100244.3	3	13417100.67						
5000	101875.7	3	2632826						
		18	45433200	12	4.75				
Q TEST									
group 1	*group 2*	*mean*	*std err*	*q-stat*	*lower*	*upper*	*p-value*	*mean-crit*	*Cohen d*
0	62.5	1803.333	1123.40257	1.605242	-3532.83	7139.496	0.8577493	5336.162	0.926787
0	125	2862.333	1123.40257	2.547914	-2473.83	8198.496	0.4992	5336.162	1.471039
0	250	1444.333	1123.40257	1.285677	-3891.83	6780.496	0.9367839	5336.162	0.742286
0	500	2821.333	1123.40257	2.511418	-2514.83	8157.496	0.5134764	5336.162	1.449968
0	5000	4452.667	1123.40257	3.963554	-883.496	9788.829	0.1243984	5336.162	2.288359
62.5	125	1059	1123.40257	0.942672	-4277.16	6395.162	0.9825152	5336.162	0.544252
62.5	250	3247.667	1123.40257	2.89092	-2088.5	8583.829	0.374141	5336.162	1.669073
62.5	500	1018	1123.40257	0.906176	-4318.16	6354.162	0.9852929	5336.162	0.523181
62.5	5000	2649.333	1123.40257	2.358312	-2686.83	7985.496	0.5746447	5336.162	1.361572
125	250	4306.667	1123.40257	3.833592	-1029.5	9642.829	0.143774	5336.162	2.213325
125	500	41	1123.40257	0.036496	-5295.16	5377.162	1	5336.162	0.021071
125	5000	1590.333	1123.40257	1.41564	-3745.83	6926.496	0.9089282	5336.162	0.81732
250	500	4265.667	1123.40257	3.797095	-1070.5	9601.829	0.1496764	5336.162	2.192254
250	5000	5897	1123.40257	5.249231	560.8378	11233.16	0.0276*	5336.162	3.030645
500	5000	1631.333	1123.40257	1.452136	-3704.83	6967.496	0.9000271	5336.162	0.838391

10.4.31 **Statistical analysis ANOVA single factor for the FI in re-activated and activated RAW 264.7 macrophages treated with 0µM of oxalyldihydrazide shown in Figure 32B.**

ANOVA: Single Factor								
DESCRIPTION					Alpha	0.05		
Group	*Count*	*Sum*	*Mean*	*Variance*	*SS*	*Std Err*	*Lower*	*Upper*
Re-activated	3	302578	100859.333	450649.3	901298.7	1343.157	97130.13	104588.5
Activated	3	292269	97423	10373767	20747534	1343.157	93693.8	101152.2
ANOVA								
Sources	*SS*	*df*	*MS*	*F*	*P value*	*Eta-sq*	*RMSSE*	*Omega Sq*
Between Groups	17712580	1	17712580.2	3.272709	0.144705	0.449999	1.044463	0.274724
Within Groups	21648833	4	5412208.17					
Total	39361413	5	7872282.57					

10.4.32 **Statistical analysis ANOVA single factor for the FI in re-activated and activated RAW 264.7 macrophages treated with 62.5µM of oxalyldihydrazide shown in Figure 32B.**

ANOVA: Single Factor								
DESCRIPTION					Alpha	0.05		
Group	*Count*	*Sum*	*Mean*	*Variance*	*SS*	*Std Err*	*Lower*	*Upper*
Re-activated	3	259248	86416	1160721	2321443	499.3625	85029.55	87802.45
Activated	3	297679	99226.3333	335456.3	670912.7	499.3625	97839.88	100612.8
ANOVA								
Sources	*SS*	*df*	*MS*	*F*	*P value*	*Eta-sq*	*RMSSE*	*Omega Sq*
Between Groups	246156960	1	246156960	329.0478	0.0001***	0.98799	10.47295	0.982038
Within Groups	2992355.33	4	748088.833					
Total	249149316	5	49829863.1					

10.4.33 **Statistical analysis ANOVA single factor for the FI in re-activated and activated RAW 264.7 macrophages treated with 125µM of oxalyldihydrazide shown in Figure 32B.**

ANOVA: Single Factor								
DESCRIPTION					Alpha	0.05		
Group	*Count*	*Sum*	*Mean*	*Variance*	*SS*	*Std Err*	*Lower*	*Upper*
Re-activated	3	255088	85029.3333	1489406	2978813	827.5613	82731.65	87327.01
Activated	3	300856	100285.333	2619740	5239481	827.5613	97987.65	102583
ANOVA								
Sources	*SS*	*df*	*MS*	*F*	*P value*	*Eta-sq*	*RMSSE*	*Omega Sq*
Between Groups	349118304	1	349118304	169.9225	0.0002***	0.977001	7.526011	0.965699
Within Groups	8218293.33	4	2054573.33					
Total	357336597	5	71467319.5					

10.4.34 **Statistical analysis ANOVA single factor for the FI in re-activated and activated RAW 264.7 macrophages treated with 250µM of oxalyldihydrazide shown in Figure 32B.**

ANOVA: Single Factor								
DESCRIPTION					Alpha	0.05		
Group	*Count*	*Sum*	*Mean*	*Variance*	*SS*	*Std Err*	*Lower*	*Upper*
Re-activated	3	281358	93786	1134361	2268723	645.1142	91994.88	95577.12
Activated	3	287936	95978.6667	1362673	2725346	645.1142	94187.54	97769.79
ANOVA								
Sources	*SS*	*df*	*MS*	*F*	*P value*	*Eta-sq*	*RMSSE*	*Omega Sq*
Between Groups	7211680.67	1	7211680.67	5.776197	0.074085	0.590843	1.387587	0.443217
Within Groups	4994068.67	4	1248517.17					
Total	12205749.3	5	2441149.87					

10.4.35 **Statistical analysis ANOVA single factor for the FI in re-activated and activated RAW 264.7 macrophages treated with 500µM of oxalyldihydrazide shown in Figure 32B.**

ANOVA: Single Factor								
DESCRIPTION					Alpha	0.05		
Group	*Count*	*Sum*	*Mean*	*Variance*	*SS*	*Std Err*	*Lower*	*Upper*
Re-activated	3	270083	90027.6667	6961149	13922298	1509.398	85836.91	94218.43
Activated	3	300733	100244.333	6708550	13417101	1509.398	96053.57	104435.1
ANOVA								
Sources	*SS*	*df*	*MS*	*F*	*P value*	*Eta-sq*	*RMSSE*	*Omega Sq*
Between Groups	156570417	1	156570417	22.90766	0.0087*	0.851343	2.763311	0.785005
Within Groups	27339398.7	4	6834849.67					
Total	183909815	5	36781963.1					

10.4.36 **Statistical analysis ANOVA single factor for the FI in re-activated and activated RAW 264.7 macrophages treated with 5000µM of oxalyldihydrazide shown in Figure 32B.**

ANOVA: Single Factor								
DESCRIPTION					Alpha	0.05		
Group	*Count*	*Sum*	*Mean*	*Variance*	*SS*	*Std Err*	*Lower*	*Upper*
Re-activated	3	292104	97368	8526241	17052483	1280.798	93811.94	100924.1
Activated	3	305627	101875.667	1316413	2632826	1280.798	98319.6	105431.7
ANOVA								
Sources	*SS*	*df*	*MS*	*F*	*P value*	*Eta-sq*	*RMSSE*	*Omega Sq*
Between Groups	30478588.2	1	30478588.2	6.193164	0.067585	0.60758	1.436798	0.463959
Within Groups	19685308.7	4	4921327.17					
Total	50163896.8	5	10032779.4					

10.4.37 **Statistical analysis ANOVA single factor for the FI in re-activated and non-activated RAW 264.7 macrophages treated with 0µM of oxalyldihydrazide shown in Figure 32B.**

ANOVA: Single Factor								
DESCRIPTION					Alpha	0.05		
Group	*Count*	*Sum*	*Mean*	*Variance*	*SS*	*Std Err*	*Lower*	*Upper*
Non-activated	3	445163	148387.667	34402040.3	68804080.7	2410.141	141696	155079.3
Re-activated	3	302578	100859.333	450649.333	901298.667	2410.141	94167.71	107551
ANOVA								
Sources	*SS*	*df*	*MS*	*F*	*P value*	*Eta-sq*	*RMSSE*	*Omega Sq*
Between Groups	3388413704	1	3388413704	194.442021	0.0002***	0.979843	8.050715	0.969916
Within Groups	69705379.3	4	17426344.8					
Total	3458119084	5	691623817					

10.4.38 **Statistical analysis ANOVA single factor for the FI in re-activated and non-activated RAW 264.7 macrophages treated with 5000µM of oxalyldihydrazide shown in Figure 32B.**

ANOVA: Single Factor								
DESCRIPTION					Alpha	0.05		
Group	*Count*	*Sum*	*Mean*	*Variance*	*SS*	*Std Err*	*Lower*	*Upper*
Non-activated	3	483239	161079.667	27068361.3	54136722.7	2435.659	154317.2	167842.1
Re-activated	3	292104	97368	8526241.33	17052482.7	2435.659	90605.53	104130.5
ANOVA								
Sources	*SS*	*df*	*MS*	*F*	*P value*	*Eta-sq*	*RMSSE*	*Omega Sq*
Between Groups	6088764704	1	6088764704	342.117301	0.0001***	0.988443	10.67891	0.982715
Within Groups	71189205.3	4	17797301.3					
Total	6159953910	5	1231990782					

10.4.39 **Statistical analysis ANOVA single factor for the FI in activated and non-activated RAW 264.7 macrophages treated with 0µM of oxalyldihydrazide shown in Figure 32B.**

ANOVA: Single Factor								
DESCRIPTION					Alpha	0.05		
Group	*Count*	*Sum*	*Mean*	*Variance*	*SS*	*Std Err*	*Lower*	*Upper*
Non-activated	3	445163	148387.667	34402040.3	68804080.7	2731.782	140803	155972.3
Activated	3	292269	97423	10373767	20747534	2731.782	89838.36	105007.6
ANOVA								
Sources	*SS*	*df*	*MS*	*F*	*P value*	*Eta-sq*	*RMSSE*	*Omega Sq*
Between Groups	3896095873	1	3896095873	174.026829	0.0002***	0.977531	7.61636	0.966485
Within Groups	89551614.7	4	22387903.7					
Total	3985647487	5	797129497					

10.4.40 **Statistical analysis ANOVA single factor for the FI in activated and non-activated RAW 264.7 macrophages treated with 5000μM of oxalyldihydrazide shown in Figure 32B.**

ANOVA: Single Factor								
DESCRIPTION					Alpha	0.05		
Group	*Count*	*Sum*	*Mean*	*Variance*	*SS*	*Std Err*	*Lower*	*Upper*
Non-activated	3	483239	161079.667	27068361.3	54136722.7	2175.039	155040.8	167118.5
Activated	3	305627	101875.667	1316413	2632826	2175.039	95836.79	107914.5
ANOVA								
Sources	*SS*	*df*	*MS*	*F*	*P value*	*Eta-sq*	*RMSSE*	*Omega Sq*
Between Groups	5257670424	1	5257670424	370.457088	0.0000***	0.989318	11.11241	0.984019
Within Groups	56769548.7	4	14192387.2					
Total	5314439973	5	1062887995					

10.5 *TNF-α concentration in Activated RAW 264.7 Macrophages*

10.5.1 Statistical analysis ANOVA single factor for the TNF-α concentration in non-activated for 6,12,18 and 24 hours in Figure 34A

ANOVA: Single Factor								
DESCRIPTION					Alpha	0.05		
Group	*Count*	*Sum*	*Mean*	*Variance*	*SS*	*Std Err*	*Lower*	*Upper*
6 hours	3	265.5	88.5	1116	2232	46.5174272	-21.496236	198.496236
12 hours	3	360	120	16.75	33.5	46.5174272	10.0037636	229.996236
18 hours	3	510.5	170.166667	7486.33333	14972.6667	46.5174272	60.1704302	280.162903
24 hours	2	539.5	269.75	28203.125	28203.125	56.9719804	135.032674	404.467326
ANOVA								
Sources	*SS*	*df*	*MS*	*F*	*P value*	*Eta-sq*	*RMSSE*	*Omega Sq*
Between Gro	43887.8447	3	14629.2816	2.25356646	0.16948064	0.49130493	0.98364336	0.25477786
Within Grou	45441.2917	7	6491.6131					
Total	89329.1364	10	8932.91364					

10.5.2 Tukey's HSD test for TNF-α concentration in non-activated cells at 6,12,18 and 24-hour timepoints in Figure 34A

TUKEY HSD/KRAMER			alpha	0.05					
group	*mean*	*n*	*ss*	*df*	*q-crit*				
6 hours	88.5	3	2232						
12 hours	120	3	33.5						
18 hours	170.166667	3	14972.6667						
24 hours	269.75	2	28203.125						
		11	45441.2917	7	4.681				
Q TEST									
group 1	*group 2*	*mean*	*std err*	*q-stat*	*lower*	*upper*	*p-value*	*mean-crit*	*Cohen d*
6 hours	12 hours	31.5	46.5174272	0.67716557	-186.24808	249.248077	0.96140912	217.748077	0.39096172
6 hours	18 hours	81.6666667	46.5174272	1.75561444	-136.08141	299.414743	0.62300334	217.748077	1.01360447
6 hours	24 hours	181.25	52.0080647	3.48503643	-62.199751	424.699751	0.15119515	243.449751	2.24958134
12 hours	18 hours	50.1666667	46.5174272	1.07844887	-167.58141	267.914743	0.86869679	217.748077	0.62264274
12 hours	24 hours	149.75	52.0080647	2.87936113	-93.699751	393.199751	0.26134091	243.449751	1.85861962
18 hours	24 hours	99.5833333	52.0080647	1.91476714	-143.86642	343.033084	0.5616417	243.449751	1.23597688

10.5.3 Statistical analysis ANOVA single factor for the TNF-α concentration in activated cells for 6,12,18 and 24 hours in Figure 34B

ANOVA: Single Factor								
DESCRIPTION					Alpha	0.05		
Group	*Count*	*Sum*	*Mean*	*Variance*	*SS*	*Std Err*	*Lower*	*Upper*
6 hours	3	446000	148666.6667	1353583333	2707166667	25086.9322	90816.0973	206517.236
12hours	3	414500	138166.6667	226583333.3	453166666.7	25086.9322	80316.0973	196017.236
18 hours	3	510500	170166.6667	534333333.3	1068666667	25086.9322	112316.097	228017.236
24 hours	3	556500	185500	5437750000	10875500000	25086.9322	127649.431	243350.569
ANOVA								
Sources	*SS*	*df*	*MS*	*F*	*P value*	*Eta-sq*	*RMSSE*	*Omega Sq*
Between Gro	4071562500	3	1357187500	0.718825516	0.568162925	0.21232526	0.48949822	-0.0756084
Within Grou	15104500000	8	1888062500					
Total	19176062500	11	1743278409					

10.5.4 Tukey HSD for TNF-α concentration in activated cells for 6,12,18 and 24 hours in Figure 34B

TUKEY HSD/KRAMER			alpha	0.05					
group	*mean*	*n*	*ss*	*df*	*q-crit*				
6 hours	148666.667	3	2707166667						
12hours	138166.667	3	453166666.7						
18 hours	170166.667	3	1068666667						
24 hours	185500	3	10875500000						
		12	15104500000	8	4.529				
Q TEST									
group 1	*group 2*	*mean*	*std err*	*q-stat*	*lower*	*upper*	*p-value*	*mean-crit*	*Cohen d*
6 hours	12hours	10500	25086.93219	0.4185446	-103118.72	124118.716	0.99029093	113618.716	0.24164684
6 hours	18 hours	21500	25086.93219	0.8570199	-92118.716	135118.716	0.92733167	113618.716	0.49480067
6 hours	24 hours	36833.3333	25086.93219	1.46822788	-76785.383	150452.049	0.73332269	113618.716	0.84768176
12hours	18 hours	32000	25086.93219	1.2755645	-81618.716	145618.716	0.80441343	113618.716	0.7364475
12hours	24 hours	47333.3333	25086.93219	1.88677248	-66285.383	160952.049	0.56883458	113618.716	1.0893286
18 hours	24 hours	15333.3333	25086.93219	0.61120799	-98285.383	128952.049	0.97122793	113618.716	0.3528811

10.5.5 Statistical analysis ANOVA single factor for the total cell number/ TNF-α concentration in non-activated for 6,12,18 and 24 hours in Figure 34C

ANOVA: Single Factor								
DESCRIPTION					Alpha	0.05		
Group	*Count*	*Sum*	*Mean*	*Variance*	*SS*	*Std Err*	*Lower*	*Upper*
6 hours	2	0.00030698	0.00015349	3.00872E-09	3.00872E-09	7.84583E-05	-3.84885E-05	0.00034547
12 hours	*3*	*0.0005276*	*0.0001759*	*2.85581E-10*	*5.71163E-10*	*6.40609E-05*	*1.91033E-05*	*0.0003326*
18 hours	3	0.00067218	0.00022406	1.59495E-08	3.1899E-08	6.40609E-05	6.73101E-05	0.00038081
24 hours	2	0.00056747	0.00028374	3.83895E-08	3.83895E-08	7.84583E-05	9.1757E-05	0.00047572
ANOVA								
Sources	*SS*	*df*	*MS*	*F*	*P value*	*Eta-sq*	*RMSSE*	*Omega Sq*
Between Groups	2.1285E-08	3	7.095E-09	0.576297845	0.651455972	0.223692244	0.520128986	-0.1456206
Within Groups	*7.387E-08*	*6*	*1.231E-08*					
Total	9.5154E-08	9	1.0573E-08					

10.5.6 Tukey HSD for total cell number/TNF-α concentration in non-activated cells for 6,12,18 and 24 hours in Figure 34C

TUKEY HSD/KRAMER			alpha	0.05					
group	*mean*	*n*	*ss*	*df*	*q-crit*				
6 hours	0.00015349	2	3.00872E-09						
12 hours	0.00017585	3	5.71163E-10						
18 hours	0.00022406	3	3.1899E-08						
24 hours	0.00028374	2	3.83895E-08						
		10	7.38684E-08	6	4.896				
Q TEST									
group 1	*group 2*	*mean*	*std err*	*q-stat*	*lower*	*upper*	*p-value*	*mean-crit*	*Cohen d*
6 hours	12 hours	2.2363E-05	7.16223E-05	0.31223177	-0.0003283	0.00037303	0.99578988	0.00035066	0.20154474
6 hours	18 hours	7.057E-05	7.16223E-05	0.98530131	-0.0002801	0.00042123	0.89478725	0.00035066	0.63600926
6 hours	24 hours	0.00013025	7.84583E-05	1.66006101	-0.0002539	0.00051438	0.6628088	0.00038413	1.1738404
12 hours	18 hours	4.8207E-05	6.40609E-05	0.75251463	-0.0002654	0.00036185	0.94804635	0.00031364	0.43446452
12 hours	24 hours	0.00010788	7.16223E-05	1.50627396	-0.0002428	0.00045855	0.72120129	0.00035066	0.97229566
18 hours	24 hours	5.9676E-05	7.16223E-05	0.83320441	-0.000291	0.00041034	0.9317757	0.00035066	0.53783114

10.5.7 Statistical analysis ANOVA single factor for the total cell number/ TNF-α concentration in activated for 6,12,18 and 24 hours in Figure 34D

ANOVA: Single Factor								
DESCRIPTION					Alpha	0.05		
Group	*Count*	*Sum*	*Mean*	*Variance*	*SS*	*Std Err*	*Lower*	*Upper*
6 hours	3	0.94398991	0.314663303	0.007416094	0.014832188	0.097495843	0.08983748	0.53948912
12 hours	3	1.09197626	0.363992088	0.005311815	0.010623631	0.097495843	0.13916627	0.58881791
18 hours	3	1.48208151	0.494027168	0.003519812	0.007039624	0.097495843	0.26920135	0.71885299
24 hours	3	2.00222985	0.667409949	0.097817552	0.195635104	0.097495843	0.44258413	0.89223577
ANOVA								
Sources	*SS*	*df*	*MS*	*F*	*P value*	*Eta-sq*	*RMSSE*	*Omega Sq*
Between Groups	0.22355102	3	0.074517008	2.61313562	0.123345529	0.494930582	0.93329803	0.28738583
Within Groups	0.22813055	8	0.028516318					
Total	0.45168157	11	0.041061961					

10.5.8 Tukey HSD for total cell number/TNF-α concentration in activated cells for 6,12,18 and 24 hours in Figure 34D

TUKEY HSD/KRAMER			alpha	0.05					
group	*mean*	*n*	*ss*	*df*	*q-crit*				
6 hours	0.3146633	3	0.01483219						
12 hours	0.36399209	3	0.01062363						
18 hours	0.49402717	3	0.00703962						
24 hours	0.66740995	3	0.1956351						
		12	0.22813055	8	4.529				
Q TEST									
group 1	*group 2*	*mean*	*std err*	*q-stat*	*lower*	*upper*	*p-value*	*mean-crit*	*Cohen d*
6 hours	12 hours	0.049328785	0.09749584	0.50595783	-0.3922299	0.49088746	0.98319412	0.44155868	0.29211489
6 hours	18 hours	0.179363866	0.09749584	1.83970782	-0.2621948	0.62092254	0.58725077	0.44155868	1.0621558
6 hours	24 hours	0.352746646	0.09749584	3.61806856	-0.088812	0.79430532	0.12391	0.44155868	2.08889286
12 hours	18 hours	0.130035081	0.09749584	1.33374999	-0.3115236	0.57159376	0.78361189	0.44155868	0.77004092
12 hours	24 hours	0.303417861	0.09749584	3.11211073	-0.1381408	0.74497654	0.20261885	0.44155868	1.79677797
18 hours	24 hours	0.17338278	0.09749584	1.77836074	-0.2681759	0.61494146	0.61143006	0.44155868	1.02673705

10.5.9 Statistical analysis ANOVA single factor for the TNF-α concentration in non-activated versus activated for 6 hours in Figure 34 A and B.

ANOVA: Single Factor								
DESCRIPTION					Alpha	0.05		
Group	*Count*	*Sum*	*Mean*	*Variance*	*SS*	*Std Err*	*Lower*	*Upper*
Non-activated	3	265.5	88.5	1116	2232	15019.9004	-41613.429	41790.429
Activated	3	446000	148666.6667	1353583333	2707166667	15019.9004	106964.738	190368.596
ANOVA								
Sources	*SS*	*df*	*MS*	*F*	*P value*	*Eta-sq*	*RMSSE*	*Omega Sq*
Between Groups	33113207415	1	33113207415	48.92669598	0.002198288	0.92442377	4.03842775	0.88873785
Within Groups	2707168899	4	676792224.7					
Total	35820376314	5	7164075263					

10.5.10 Tukey HSD for TNF-α concentration in non-activated versus activated for 6 hours in Figure 34 A and B.

TUKEY HSD/KRAMER			alpha	0.05					
group	*mean*	*n*	*ss*	*df*	*q-crit*				
Non-activate	88.5	3	2232						
Activated	148666.667	3	2707166667						
		6	2707168899	4	3.926				
Q TEST									
group 1	*group 2*	*mean*	*std err*	*q-stat*	*lower*	*upper*	*p-value*	*mean-crit*	*Cohen d*
Non-activate	Activated	148578.167	15019.90041	9.89208734	89610.0377	207546.296	0.0022**	58968.129	5.71119929

10.5.11 Statistical analysis ANOVA single factor for the TNF-α concentration in non-activated versus activated for 24 hours in Figure 33 A and B.

ANOVA: Single Factor								
DESCRIPTION					Alpha	0.05		
Group	*Count*	*Sum*	*Mean*	*Variance*	*SS*	*Std Err*	*Lower*	*Upper*
Non-activated	2	539.5	269.75	28203.125	28203.125	42574.4998	-135221.31	135760.81
Activated	3	556500	185500	5437750000	10875500000	34761.9335	74872.0131	296127.987
ANOVA								
Sources	*SS*	*df*	*MS*	*F*	*P value*	*Eta-sq*	*RMSSE*	*Omega Sq*
Between Groups	41172294618	1	41172294618	11.35732275	0.0434*	0.79104739	2.17536613	0.67442242
Within Groups	10875528203	3	3625176068					
Total	52047822821	4	13011955705					

10.5.12 Statistical analysis ANOVA single factor for the TNF-α concentration in non-activated versus activated for 6 hours in Figure 34 C and D.

ANOVA: Single Factor								
DESCRIPTION					Alpha	0.05		
Group	*Count*	*Sum*	*Mean*	*Variance*	*SS*	*Std Err*	*Lower*	*Upper*
Non-activated	2	0.00030698	0.00015349	3.00872E-09	3.00872E-09	0.049719532	-0.158076249	0.15838323
Activated	3	0.94398991	0.3146633	0.007416094	0.014832188	0.040595828	0.18546926	0.44385735
ANOVA								
Sources	*SS*	*df*	*MS*	*F*	*P value*	*Eta-sq*	*RMSSE*	*Omega Sq*
Between Groups	0 118699705	1	0.11869971	24.00853052	0.016268705	0.888923983	3.162839607	0.82148296
Within Groups	0.014832191	3	0.00494406					
Total	0 133531897	4	0.03338297					

10.5.13 Tukey HSD for TNF-α concentration in non-activated versus activated for 6 hours in Figure 34 C and D.

TUKEY HSD/KRAMER			alpha	0.05					
group	*mean*	*n*	*ss*	*df*	*q-crit*				
Non-activated	0.00015349	2	3.00872E-09						
Activated	0.3146633	3	0.014832188						
		5	0.014832191	3	4.501				
Q TEST									
group 1	*group 2*	*mean*	*std err*	*q-stat*	*lower*	*upper*	*p-value*	*mean-crit*	*Cohen d*
Non-activated	Activated	0.31450981	0.045387515	6.9294344	0.1102206	0.51879902	0.0163*	0.20428921	4.47293067

10.6 *TNF-α Supporting Data in Drug Treated RAW 264.7 Macrophages*

10.6.1 Absorbance values at 405nm and 650nm for TNF-α Assay in Figure 34 and 35

Wavelength: 405 nm												
Abs	**1**	**2**	**3**	**4**	**5**	**6**	**7**	**8**	**9**	**10**	**11**	**12**
A	0.5446	0.4398	0.1864	0.1799	0.1672	0.1481	0.1774	0.1493	0.1354	0.1615	0.1757	0.2419
B	0.7418	0.2941	0.1569	0.1745	0.1601	0.1588	0.1412	0.1675	0.1500	0.1724	0.1756	0.2445
C	0.2500	0.2211	0.1650	0.1757	0.1610	0.2051	0.1608	0.1568	0.1446	0.2089	0.1964	0.2572
D	0.1907	0.1917	0.1708	0.1589	1.7995	0.2497	0.1538	0.1477	0.1493	0.1736	0.2106	0.2563
E	0.1704	0.1401	0.1525	0.1807	0.1465	0.1893	0.1705	0.1459	0.1560	0.1676	0.2029	0.2598
F	0.1738	0.1634	0.1622	0.1928	0.1571	0.1982	0.1586	0.1549	0.1631	0.1748	0.2131	0.2572
G	0.1806	0.1707	0.1968	0.1517	0.1768	0.1904	0.1608	0.1685	0.1566	0.1712	0.1957	0.2502
H	0.2128	0.1656	0.2048	0.1470	0.1662	0.2682	0.1558	0.1644	0.2220	0.2033	0.1974	0.2856
Wavelength: 650 nm												
Abs	**1**	**2**	**3**	**4**	**5**	**6**	**7**	**8**	**9**	**10**	**11**	**12**
A	0.2466	0.2044	0.1081	0.0959	0.1080	0.0841	0.0956	0.0836	0.0763	0.0883	0.0952	0.1286
B	0.3260	0.1422	0.0842	0.0960	0.0877	0.0875	0.0793	0.0998	0.0827	0.0919	0.0920	0.1237
C	0.1239	0.1113	0.0878	0.0947	0.0868	0.1065	0.0877	0.0883	0.0798	0.1066	0.1016	0.1270
D	0.1010	0.1000	0.0908	0.0862	0.7384	0.1245	0.0840	0.0808	0.0814	0.0919	0.1081	0.1283
E	0.0916	0.0769	0.0831	0.0966	0.0813	0.1092	0.0937	0.0797	0.0849	0.0910	0.1048	0.1294
F	0.0929	0.0885	0.0880	0.1000	0.0863	0.1028	0.0874	0.0874	0.0887	0.0930	0.1089	0.1275
G	0.0936	0.0897	0.1104	0.0842	0.0948	0.1022	0.0872	0.0906	0.0854	0.0914	0.1012	0.1236
H	0.1075	0.0888	0.1037	0.0796	0.0885	0.1322	0.0854	0.0920	0.1123	0.1099	0.1002	0.1385

10.6.2 Plate layout for TNF-α ELISA in Figure 34 and 35

	1	2	3	4	5	6	7	8	9	10	11	12
A	St2000pg/mL	Standard 2000pg/mL	1:100 Activated 6hr (1)	1:100 Activated 6hr (3)orange	1:1 Non Act 6 hr (1) prev	1:1 BLANK	Cyclohexanone (1) Non activated 1:10 500µM	Oxalydihydrazide (1) Non activated 1:10 500 µM	Cyclohexanone (1) activated 1:1000 500 µM	Oxalydihydrazide (1) activated 1:1000 500 µM	Cyclohexanone (1) activated 1:100 500 µM	Oxalydihydrazide (1) activated 1:100 500 µM
B	Standard 1000pg/mL	Standard 1000pg/mL	1:100 Activated 12hr (1)	1:100 Activated 12hr (3)	1:1 Non Act 12 hr (1)prev	1:1 Non Act 12 hr (3)	Cyclohexanone (1) non activated 1:10 250 µM	OXalyldihydrazide(1) Non activated 1:10 250 µM	Cyclohexanone (1) activated 1:1000 250 µM	OXalyldihydrazide(1) activated 1:100 250 µM	Cyclohexanone (1) activated 1:100 250 µM	Oxalyldihydrazide(1) activated 1:100 250 µM
C	Standard 500pg/mL	Standard 500pg/mL	1:100 Activated 18hr (1)	1:100 Activated 18hr (3)	1:1 Non Act 18 hr (1)	1:1 Non Act 18 hr (3)	Cyclohexanone (1)non activated 1:10 125 µM	Oxalyldihydrazide(1) Non activated 1:10 125 µM	Cyclohexanone (1) activated 1:1000 125 µM	Oxalyldihydrazide(1) activated 1:1000 125 µM	Cyclohexanone (1) activated 1:100 125 µM	Oxalyldihydrazide(1) activated 1:100 125 µM
D	Standard 250pg/mL	Standard 250pg/mL	1:100 Activated 24hr (1)	1:100 Activated 24hr (3)	1:1 Non Act 24 hr (1)	1:1 Non Act 24 hr (3)	Cyclohexanone (1) non activated 1:10 62.5 µM	Oxalyldihydrazide(1) Non activated 1:10 62.5 µM	Cyclohexanone (1) activated 1:1000 62.5 µM	Oxalyldihydrazide(1) activated 1:1000 62.5 µM	Cyclohexanone (1) activated 1:100 62.5 µM	Oxalyldihydrazide(1) activated 1:100 62.5 µM
E	Standard 125pg/mL	Standard 125pg/mL	1:100 Activated 6hr (2)red	1:100 Activated 6 hours 1 ug/mL LPS and 1U/ml IFN-γ	1:1 Non Act 6 hr (2)	1:1 Non Activated 6 hour 1 ug/mL LPS and 1U/ml IFN-γ	Cyclohexanone (1) non activated 1:10 31.25 µM	Oxalyldihydrazide (1) Non activated 1:10 31.25 µM	Cyclohexanone (1) activated 1:1000 31.25 µM	Oxalyldihydrazide (1) activated 1:1000 31.25 µM	Cyclohexanone (1) activated 1:100 31.25 µM	Oxalyldihydrazide (1) activated 1:100 31.25 µM
F	Standard 62.5pg/mL	Standard 62.5pg/mL	1:100 Activated 12hr (2)	1:100 Activated 24 hours 1 ug/mL LPS and 1U/ml IFN-γ	1:1 Non Act 12 hr (2)	1:1 Non Act 24 hrs 1 ug/mL LPS and 1U/ml IFN-γ	Cyclohexanone (3)non activated 1:10 0 µM	Oxalyldihydrazide(3) Non activated 1:1000 0 µM	Cyclohexanone (3) activated 1:1000 0 µM	Oxalyldihydrazide(3) activated 1:1000 0 µM	Cyclohexanone (3) activated 1:100 0 µM	Oxalyldihydrazide(3) activated 1:100 0 µM
G	Standard 31.25pg/mL	Standard 31.25pg/mL	1:100 Activated 18hr (2)	BLANK	1:1 Non Act 18 hr (2)	1:1 Non Activated 6 hour 1 ug/mL LPS and 1U/ml IFN-γ	BLANK	BLANK	BLANK	BLANK	BLANK	BLANK
H	Blank	Blank	1:1000 Activated 24hr (2)	BLANK	1:1 Non Act 24 hr (2)	1:1 Non Activated 24 (hours 1 ug/mL LPS and 1U/ml IFN-γ	BLANK	BLANK	BLANK	BLANK/ml	BLANK	BLANK

10.6.3 **Cell count for TNF-α assay in Figure 35**

	well #	Quadrant 1 counts live	Quadrant 2 counts live	Quadrant 3 counts live	Quadrant 4 counts live	Quadrant 1 counts dead	Quadrant 2 counts dead	Quadrant 3 counts dead	Quadrant 4 counts dead
Oxalyldihydrazide Non-Activated in 0.1% FCS	**A1**	49	25	37	25	3	5	5	7
	A2	61	86	66	73	8	6	8	6
	A3	69	36	58	48	7	8	16	13
	A4	39	13	5	4	7	8	6	3
	A5								
	A6	27	46	30	37	10	6	8	8
Cyclohexanone Non-Activated in 0.1% FCS	**A1**	4	8	5	5	2	9	3	7
	A2	1	2	3	1	9	6	6	5
	A3	3	4	5	4	5	5	5	8
	A4	3	3	8	4	2	6	8	2
	A5								
	A6	10	29	8	31	9	7	19	13

10.6.4 **Cell count for TNF-α assay in Figure 35**

	well #	Quadrant 1 counts live	Quadrant 2 counts live	Quadrant 3 counts live	Quadrant 4 counts live	Quadrant 1 counts dead	Quadrant 2 counts dead	Quadrant 3 counts dead	Quadrant 4 counts dead
Oxalyldihydrazide Activated in 0.1% FCS	**A1**	5	6	9	6	23	18	14	20
	A2	4	10	8	5	8	13	5	14
	A3	2	4	2	3	19	12	11	11
	A4	0	5	6	5	11	13	14	15
	A5								
	A6	3	1	0	3	18	11	17	5
Cyclohexanone Activated in 0.1% FCS	**A1**	5	19	11	8	19	25	18	19
	A2	7	24	5	14	21	15	14	17
	A3	14	13	19	11	18	19	12	16
	A4	4	7	4	13	7	13	19	8
	A5								
	A6	1	0	3	18	11	17	5	5

10.7 *IL-1β Supporting Data in Drug Treated RAW 264.7 Macrophages*

10.7.1 Raw absorbance values at 450 and 620nm for IL-1β Assay in Figure 36.

Wavelength: 450 nm												
Abs	1	2	3	4	5	6	7	8	9	10	11	12
A	2 9577	2 5078	0 0806	0 0871	0 1188	0 1340						
B	1 6374	1 2723	0 0993	0 0949	0 1001	0 1049						
C	1 0337	0 8405	0 1344	0 1270	0 1156	0 1087						
D	0 5425	0 4893	0 2980	0 2178	0 1120	0 1063						
E	0 3748	0 2819	0 0880	0 0992	0 1198	0 1564						
F	0 2469	0 1736	0 0866	0 2779	0 1179	0 1213						
G	0 1550	0 1506	0 1531	0 1435	0 1334	0 4243						
H	0 0741	0 0745	0 3641	0 1435	0 1297	0 3447						
Wavelength: 620 nm												
Abs	1	2	3	4	5	6	7	8	9	10	11	12
A	0 0703	0 0651	0 0426	0 0428	0 0516	0 0448						
B	0 0620	0 0588	0 0431	0 0435	0 0426	0 0471						
C	0 0540	0 0506	0 0441	0 0435	0 0426	0 0433						
D	0 0473	0 0477	0 0482	0 0453	0 0442	0 0441						
E	0 0452	0 0449	0 0441	0 0430	0 0431	0 0443						
F	0 0448	0 0498	0 0426	0 0442	0 0435	0 0440						
G	0 0425	0 0482	0 0432	0 0454	0 0495	0 0492						
H	0 0426	0 0415	0 0551	0 0436	0 0428	0 0513						

	1	2	3	4	5	6
A	Standard 500pg/mL	Standard 500pg/mL	1:100 Activated 6hr (1)	1:100 Activated 6hrs (3)	1:1 Non Act 6 hrs (1)	1:1 BLANK
B	Standard 250pg/mL	Standard 250pg/mL	1:100 Activated 12hr (1)	1:100 Activated 12hrs (3)	1:1 Non Act 12 hr (1)	1:1 Non Act 12 hrs (3)
C	Standard 125pg/mL	Standard 125pg/mL	1:100 Activated 18hr (1)	1:100 Activated 18hrs (3)	1:1 Non Act 18 hr (1)	1:1 Non Act 18 hrs (3)
D	Standard 62.5pg/mL	Standard 62.5pg/mL	1:100 Activated 24hr (1)	1:100 Activated 24hrs (3)	1:1 Non Act 24 hr (1)	1:1 Non Act 24 hrs (3)
E	Standard 31.25pg/mL	Standard 31.25pg/mL	1:100 Activated 6hrs (2)red	1:100 Activated 6 hrs 1 ug/mL LPS and IU/mL of IFN-γ	1:1 Non Act 6 hrs (2)	Oxalyl non act 500uM
F	Standard 15.625pg/mL	Standard 15.625pg/mL	1:100 Activated 12hrs (2)	1:100 Activated 24 hours 1 ug/mL 2310	1:1 Non Act 12 hrs (2)	Cyclo non act 500uM
G	Standard 7.825pg/mL	Standard 7.825pg/mL	1:100 Activated 18hrs (2)	1:1 Non Activated 6 hrs	1:1 Non Act 18 hrs (2)	Oxalyl act 500uM (activation mix reapplied)
H	Blank	Blank	1:100 Activated 24hrs (2)	1:1 Non Activated 24 hrs	1:1 Non Act 24 hr s(2)	Cyclo act 500uM (no re activation mix)

10.7.2 **Plate layout for IL-1β Assay in Figure 36.**

10.7.3 **Raw absorbance values for IL-1β Assay in Figure 37.**

Wavelength: 450 nm												
Abs	1	2	3	4	5	6	7	8	9	10	11	12
A	2.3792	2.4776	0.5750	0.5421	0.5531	0.3685						
B	1.7007	1.4472	0.4341	0.5892	0.6892	0.3731						
C	1.0321	0.7638	0.4545	0.5487	0.5477	0.4957						
D	0.5440	0.4128	0.5185	0.5759	0.5224	0.5836						
E	0.3428	0.2386	0.4485	0.6647	0.5969	0.3730						
F	0.2214	0.1813	0.0998	0.0942	0.4817	0.6840						
G	0.1397	0.1268	0.1324	0.0914	0.1020	0.0967						
H	0.0755	0.0745	0.0946	0.1117	0.1054	0.0986						
Wavelength: 620 nm												
Abs	1	2	3	4	5	6	7	8	9	10	11	12
A	0.0635	0.0874	0.0551	0.0449	0.0541	0.0623						
B	0.0606	0.0684	0.0632	0.0466	0.0566	0.0589						
C	0.0507	0.0483	0.0499	0.0459	0.0551	0.0430						
D	0.0406	0.0389	0.0498	0.0486	0.0537	0.0643						
E	0.0463	0.0461	0.0523	0.0493	0.0475	0.0593						
F	0.0453	0.0475	0.0423	0.0417	0.0513	0.0521						
G	0.0444	0.0410	0.0415	0.0423	0.0426	0.0417						
H	0.0432	0.0417	0.0413	0.0434	0.0436	0.0421						

10.7.4 **Plate layout for IL-1β assay in Figures 37.**

	1	**2**	**3**	**4**	**5**	**6**
A	Standard 500pg/mL	Standard 500pg/mL	5000uM oxalyldihydrazide Activation mix	5000uM oxalyldihydrazide Not-reactivated	5000uM cyclohexanone Activation mix	5000uM cyclohexanone Not re-activated
B	standard 250g/mL	standard 250g/mL	500uM oxalyldihydrazide Activation mix	500uM oxalyl oxalyldihydrazide Not-reactivated	500uM cyclohexanone Activation mix	500uM cyclohexanone Not re-activated
C	Standard 125pg/mL	Standard 125pg/mL	250uM oxalyldihydrazide Activation mix	250uM oxalyldihydrazide Not-reactivated	250uM cyclohexanone Activation mix	250uM cyclohexanone Not re-activated
D	Standard 62 5pg/mL	Standard 62 5pg/mL	125uM oxalyldihydrazide Activation mix	125uM oxalyldihydrazide Not-reactivated	125uM cyclohexanone Activation mix	125uM cyclohexanone Not re-activated
E	Standard 31 25pg/mL	Standard 31 25pg/mL	62 5uM oxalyldihydrazide Activation mix	62 5uM oxalyldihydrazide Not-reactivated	62 5uM cyclohexanone Activation mix	62 5uM cyclohexanone Not re-activated
F	Standard 15 625pg/mL	Standard 15 625pg/mL	0uM oxalyldihydrazide	0uM oxalyldihydrazide Not-reactivated	0uM cyclohexanone Activation mix	0uM cyclohexanone Not re-activated
G	Standard 7 8pg/mL	Standard 7 8pg/mL	5000uM cyclohexanone Non-activated	500uM cyclohexanone Non-activated	250uM cyclohexanone Non activated	125uM cyclohexanone Non activated
H	BLANK	BLANK	5000uM oxalyldihydrazide Non-activated	500uM oxalyldihydrazide Non-activated	250uM oxalyldihydrazide Non-activated	125uM oxalyldihydrazide Non-activated

10.7.5 **Raw cell counts for IL-1β Assay in Figure 37.**

	well #	quadrant 1 counts live	quadrant 2 counts live	quadrant 3 counts live	quadrant 4 counts live	quadrant 1 counts dead	quadrant 2 counts dead	quadrant 3 counts dead	quadrant 4 counts dead
activated in 0.1% FCS cyclohexanone applied in activation mix	A1	24	26	29	27	11	9	5	17
	A2	27	28	25	28	6	11	12	12
	A3	35	36	29	29	4	13	10	5
	A4	46	38	33	31	7	8	13	6
	A5	34	32	42	33	14	10	7	15
	A6	38	45	36	34	14	18	17	11
activated in 0.1% FCS cyclohexanone applied without activation mix	B1	34	32	36	22	7	5	11	3
	B2	26	26	37	33	8	4	7	3
	B3	25	26	31	28	8	9	12	6
	B4	41	22	21	29	10	6	9	4
	B5	13	22	28	25	6	15	9	15
	B6	20	21	22	19	13	18	15	8

10.7.6 **Raw cell counts for IL-1β Assay in Figure 37.**

	well #	quadrant 1 counts live	quadrant 2 counts live	quadrant 3 counts live	quadrant 4 counts live	quadrant 1 counts dead	quadrant 2 counts dead	quadrant 3 counts dead	quadrant 4 counts dead
activated in 0.1% FCS, oxalyldihydrazide applied in activation mix	C1	25	34	28	25	12	8	8	8
	C2	39	32	28	26	13	9	8	15
	C3	31	41	38	28	9	14	12	8
	C4	36	30	40	31	9	13	16	13
	C5	32	33	35	26	10	4	7	19
	A6	38	45	36	34	14	18	17	11
activated in 0.1% FCS oxalyldihyrazide applied without activation mix	D1	37	36	46	26	12	13	10	12
	D2	24	32	23	20	16	11	18	13
	D3	24	22	26	24	10	5	21	12
	D4	29	28	23	30	7	10	16	17
	D5	42	45	42	35	11	16	10	13
	B6	34	21	22	19	13	18	15	8

10.8 *Protein Arginine Methylation Supporting Data*

10.8.1 ImageJ Raw values for SYM10 band at ~ 130kDa in non-activated RAW 264.7 cells

Sample	Area	Percent	Relative Density
4	4490.64	27.821	1
7	8041.267	49.818	1.79066173
9	3609.447	22.361	0.80374537

10.8.2 ImageJ figure showing the peaks of the bands in the samples

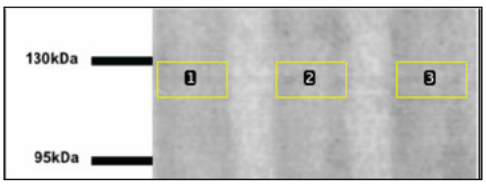

10.8.3 Boundaries of the Western blot bands measured using ImageJ

10.8.4 **ImageJ Raw values for SYM10 band at ~ 72kDa in non-activated RAW 264.7 cells**

Sample	Area	Percent	Relative Density
4	3554.853	46.473	1
7	3634.276	47.511	1.02233555
9	460.184	6.016	0.12945151

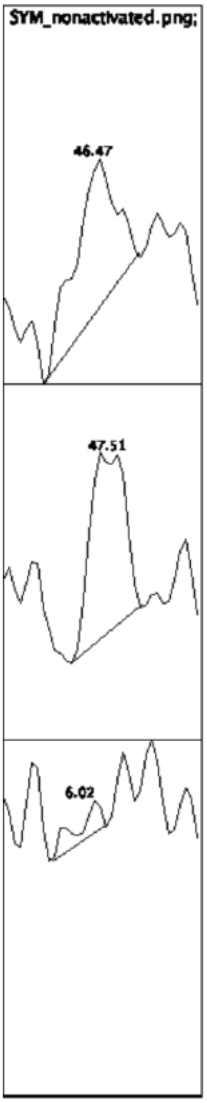

10.8.5 **ImageJ figure showing the peaks of the bands in the samples**

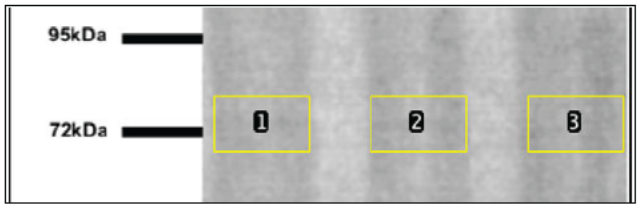

10.8.6 **Boundaries of the Western blot bands measured using ImageJ**

10.8.7 **ImageJ Raw values for SYM10 band at ~ 55kDa in non-activated RAW 264.7 cells**

Sample	Area	Percent	Relative Density
4	6553.175	32.711	1
7	7297.296	36.425	1.11353979
9	6183.347	30.865	0.94356638

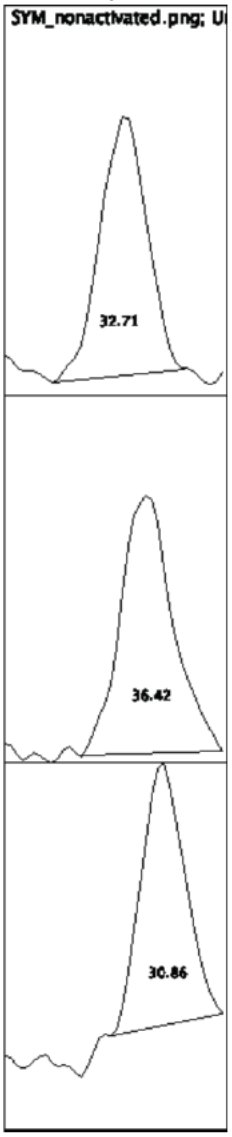

10.8.8 **ImageJ figure showing the peaks of the bands in the samples**

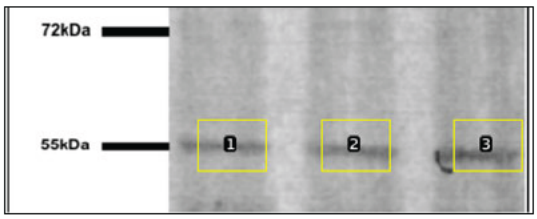

10.8.9 **Boundaries of the Western blot bands measured using ImageJ**

10.8.11 **ImageJ Raw values for SYM10 band below 55kDa in non-activated RAW 264.7 cells**

Sample	Area	Percent	Relative Density
4	8386.246	31.338	1
7	6528.296	24.395	0.77844789
9	11845.803	44.266	1.4125343

10.8.12 **ImageJ figure showing the peaks of the bands in the samples**

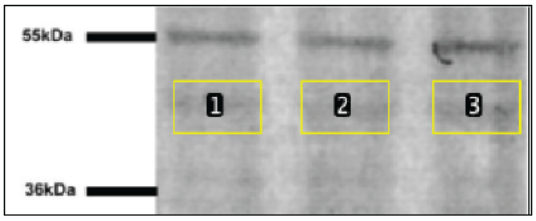

10.8.13 **Boundaries of the Western blot bands measured using ImageJ**

10.8.14 **ImageJ Raw values for ASYM24 band around 130kDa in non-activated RAW 264.7 cells**

Sample	Area	Percent	Relative Density
4	9588.095	29.005	1
7	0	0	0
9	0	0	0

10.8.15 **ImageJ figure showing the peak and corrected background noise for the non-activated bands in at 130kDa in ASYM24**

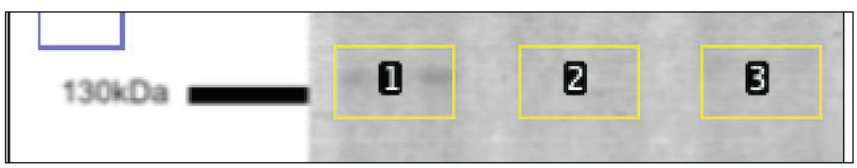

10.8.16 **Boundaries of the Western blot bands measured using ImageJ**

10.8.17 **ImageJ Raw values for ASYM24 band around 55kDa in non-activated RAW 264.7 cells**

Sample	Area	Percent	Relative Density	
4	4906.79	38.469	1	
7	4210.782	33.013	0.85817151	
9	3637.518	28.518	0.74132418	

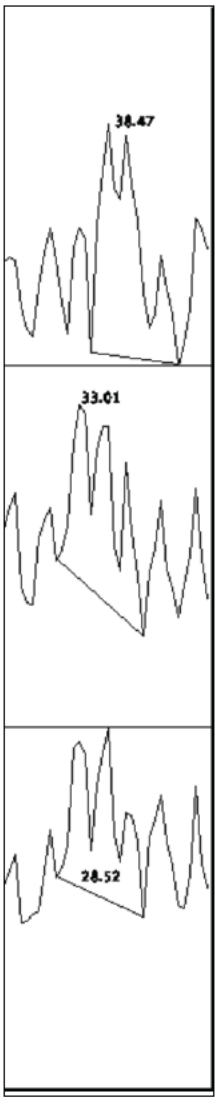

10.8.18 **ImageJ figure showing the peak and corrected background noise for the non-activated bands in at 55kDa in ASYM24**

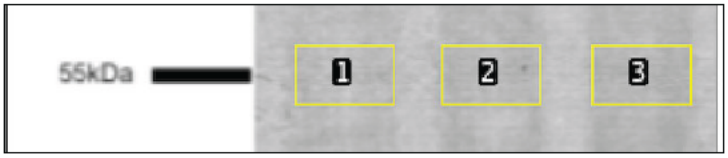

10.8.19 **Boundaries of the Western blot bands measured using ImageJ**

10.8.20 **ImageJ Raw values for ASYM24 band above 17kDa in non-activated RAW 264.7 cells**

Sample	Area	Percent	Relative Density
4	12351.731	34.425	1
7	8060.075	22.464	0.65254902
9	7408.439	20.648	0.59979666

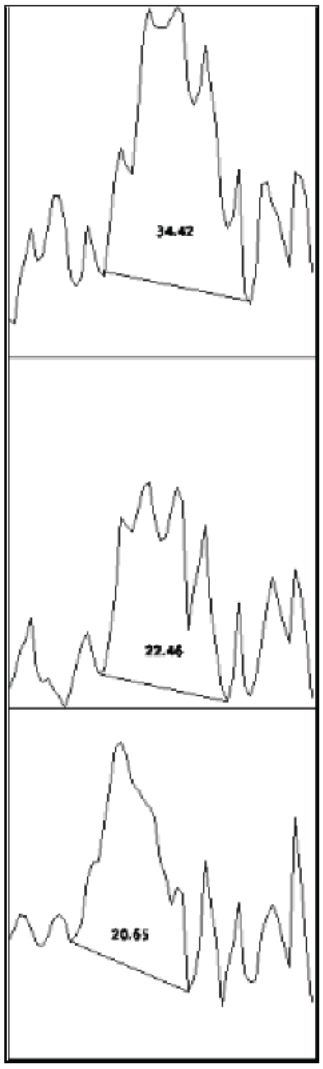

10.8.21 **ImageJ figure showing the peak and corrected background noise for the non-activated bands in at 17kDa in ASYM24**

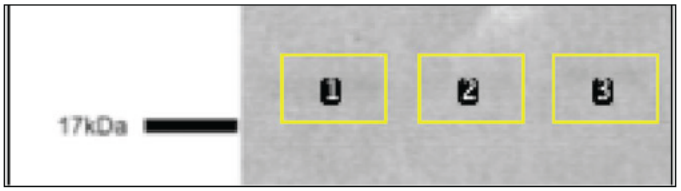

10.8.22**Boundaries of the Western blot bands measured using ImageJ above 17kDa**

10.8.23 **ImageJ Raw values for PRMT1 non-activated RAW 264.7 cells**

Sample	Area	Percent	Relative Density	
4	36625.517	32.705	1	
7	37739.153	33.699	1.03039291	
9	37623.91	33.596	1.02724354	

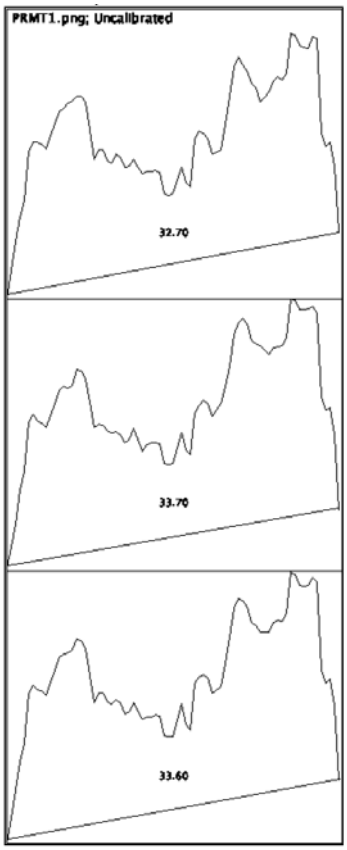

10.8.24 **ImageJ figure showing the two peaks and corrected background noise for the non-activated bands**

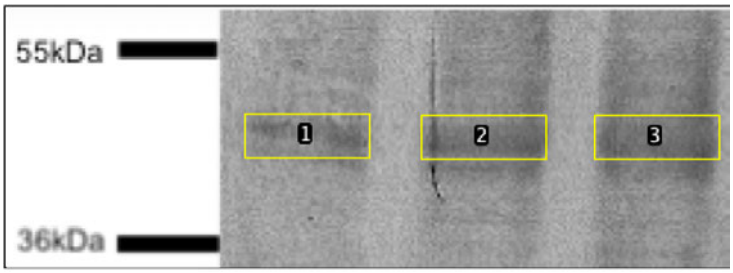

10.8.25 **Boundaries of the Western blot bands measured using ImageJ**

10.8.26 **ImageJ Raw values for PRMT5 non-activated RAW 264.7 cells**

Sample	Area	Percent	Relative Density	
4	17898.721	32.629	1	
7	19137.6	34.888	1.06923289	
9	17818.721	32.483	0.99552545	

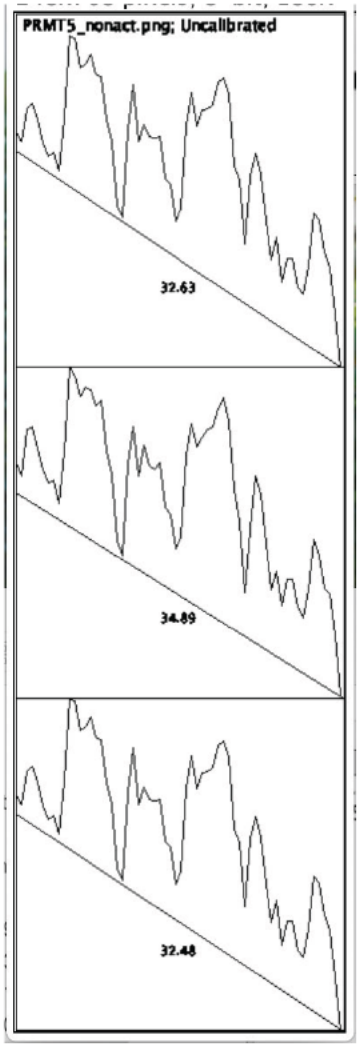

10.8.27 **ImageJ figure showing the two peaks and corrected background noise for the non-activated bands**

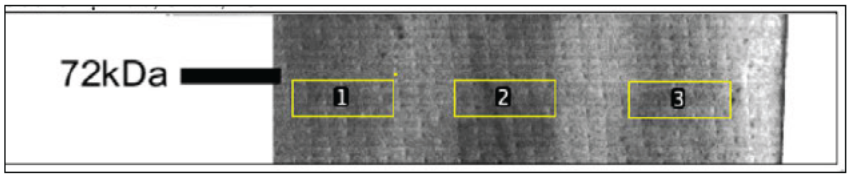

10.8.28 **Boundaries of the Western blot bands measured using ImageJ**

10.8.29 **ImageJ Raw values for SYM10 band below 95kDa in activated and non-activated RAW 264.7 cells**

Sample	Area	Percent	Relative Density	
Act	6249.024	58.274	1.39658726	
Non-act	4474.489	41.726	1	

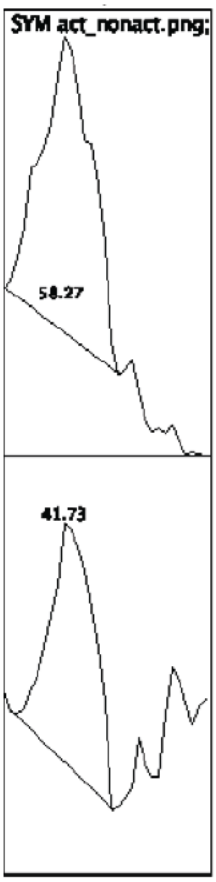

10.8.30 **ImageJ figure showing the peak and corrected background noise for the activated and non-activated bands below 95kDa in SYM10**

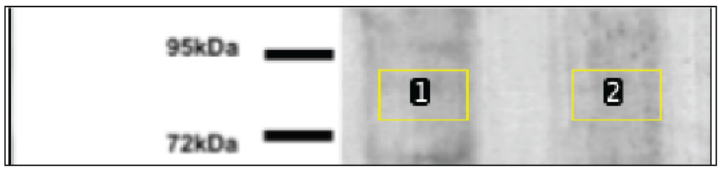

10.8.31 **Boundaries of the Western blot bands measured using ImageJ below 95kDa in SYM10 activated and non-activated RAW 264.7 cells.**

10.8.32 **ImageJ Raw values for SYM10 band ~ 72kDa in activated and non-activated RAW 264.7 cells**

Sample	Area	Percent	Relative Density	
Act	9749.004	83.313	4.99268892	
Non-act	1952.648	16.687	1	

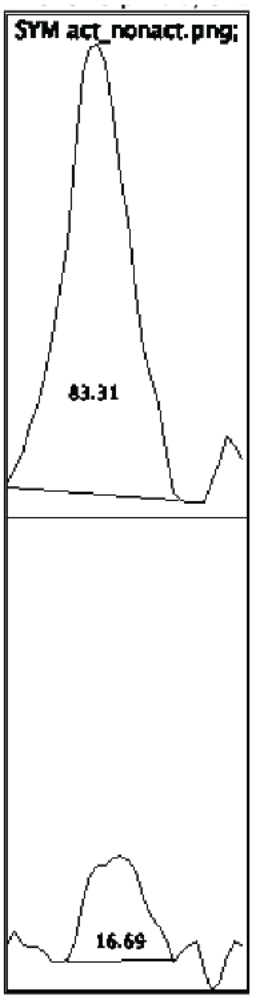

10.8.33 **ImageJ figure showing the peak and corrected background noise for the activated and non-activated bands ~72kDa in SYM10**

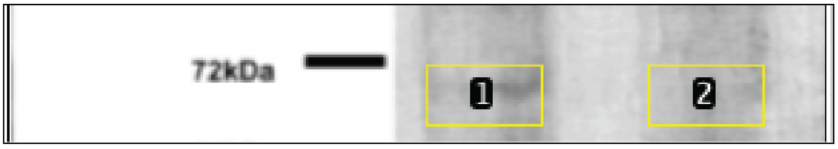

10.8.34 **Boundaries of the Western blot bands measured using ImageJ ~72kDa in SYM10 activated and non-activated RAW 264.7 cells.**

10.8.35 **ImageJ Raw values for ASYM24 band above 130kDa in activated and non-activated RAW 264.7 cells**

Sample	Area	Percent	Relative Density	
Act	3184.347	85.765	6.02493853	
Non-act	528.527	14.235	1	

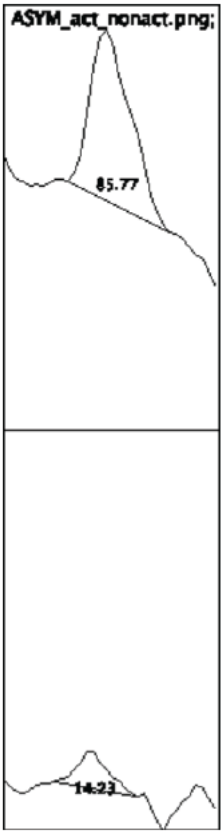

10.8.36 **ImageJ figure showing the peak and corrected background noise for the activated and non-activated bands below 130kDa**

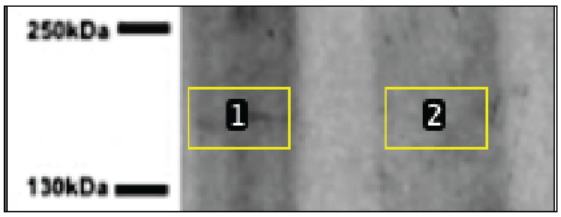

10.8.37 **Boundaries of the Western blot bands measured using ImageJ above 130kDa in ASYM24 activated and non-activated RAW 264.7 cells.**

10.8.38 **ImageJ Raw values for ASYM24 band ~ 95kDa in activated and non-activated RAW 264.7 cells**

Sample	Area	Percent	Relative Density	
Act	8941.125	100	1	
Non-act	0	0	0	

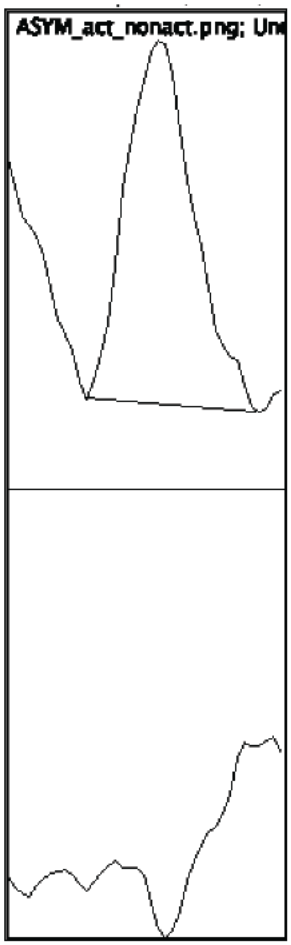

10.8.39 **ImageJ figure showing the peak and corrected background noise for the activated and non-activated band at ~95kDa in ASYM24**

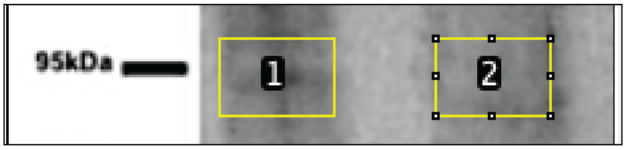

10.8.40 **Boundaries of the Western blot bands measured using ImageJ at ~ 95kDa.**

10.8.41 **ImageJ Raw values for ASYM24 band below 72kDa in activated and non-activated RAW 264.7 cells**

Sample	Area	Percent	Relative Density	
Activated	3908.983	91.506	10.7730162	
Non-activated	362.87	8.494	1	

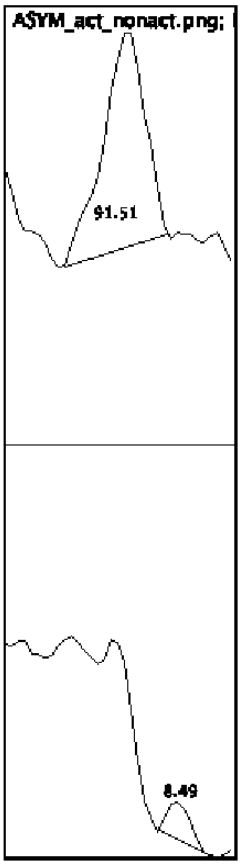

10.8.42 **ImageJ figure showing the peak and corrected background noise for the activated and non-activated band below 72kDa in ASYM24**

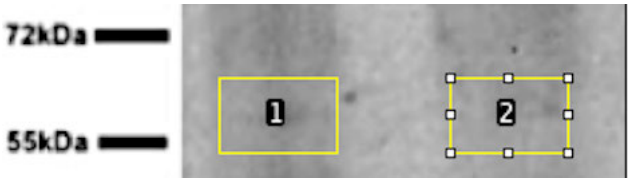

10.8.43 **Boundaries of the Western blot bands measured using ImageJ below 72kDa**

10.8.44 **ImageJ Raw values for PRMT1 activated and non-activated RAW 264.7 cells**

Sample	Area	Percent	Relative Density	
Act	7867.016	17.92	0.55860349	
Non-act	14085.472	32.08	1	

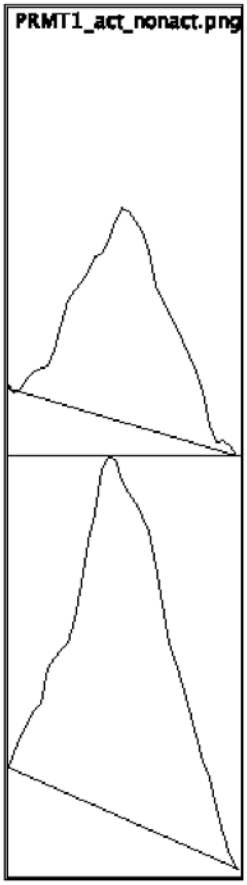

10.8.45 **ImageJ figure showing the two peaks and corrected background noise for the activated and non-activated bands**

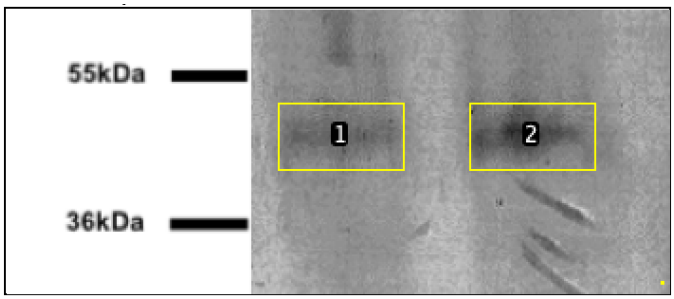

10.8.46 **Boundaries of the Western blot bands measured using ImageJ**